U.PORTO

FEUP FACULDADE DE ENGENHARIA
UNIVERSIDADE DO PORTO

Proteins Separation by Expanded Bed Chromatography Technology

Dissertation presented to *Faculdade de Engenharia da Universidade do Porto* for the degree of Ph.D. in Chemical and Biological Engineering

by

Pedro Sousa Ferreira Gomes

Supervised by Professor Alírio Egídio Rodrigues

And co-supervised by Professor José Miguel Loureiro

SRE CM

ASSOCIATE LABORATORY
LABORATORY OF SEPARATION AND REACTION ENGINEERING
LABORATORY OF CATALYSIS AND MATERIALS

Laboratory of Separation and Reaction Engineering, Associated Laboratory LSRE/LCM, Department of Chemical Engineering, Faculty of Engineering, University of Porto

September 2018

This work was financially supported by: Project POCI-01-0145-FEDER-006984 – Associate Laboratory LSRE-LCM funded by FEDER through COMPETE2020 - *Programa Operacional Competitividade e Internacionalização* (POCI) – and by national funds through FCT - *Fundação para a Ciência e a Tecnologia*; Project "Cyclic Adsorption Processes", with the reference NORTE-07-0124-FEDER-000006, funded by QREN and ON2 through the *European Regional Development Fund* (ERDF).

Laboratory of Separation and Reaction Engineering

University of Porto – Faculty of Engineering

Rua Dr. Roberto Frias s/n, 4200-465 Porto

Portugal

Acknowledgments

The true education becomes complete when we achieve our goals in life.

The following lines intend to refer a special thanks to all who have made this work possible.

To **Professor Alírio E. Rodrigues**, Ph.D. thesis supervisor, whose valuable *Curriculum Vitae,* needless to refer, made possible the realization of this life objective. His knowledge together with his vast professional experience, as well as his constant availability and work methodology have become an invaluable asset in this process. His personal and professional ethics, as well as his passion for science were an additional motivation, becoming an example to follow.

To **Professor José M. Loureiro**, Ph.D. thesis co-supervisor, with a professional career of excellence, always being present and receptive to teaching, sharing knowledge and experience, contribute effectively to my academic development. The constant conversations and encouragement kept me motivated.

To all the **Professors**, **colleagues** and **staff** from *LSRE* laboratory and Faculty for their willingness to help me during this work period.

To my **friends**.

Finally to my **family**, specially my **parents** for the constant love and support.

To all,

Thank you,

Pedro Ferreira Gomes

Abstract

Efficient separation and purification of proteins to the desired level of purity is one bottleneck in pharmaceutical industries. The work done has the purpose to study the purification of Human Serum Albumin (HSA) and human Immunoglobulin G (IgG) using expanded bed adsorption (EBA) over a new second generation adsorbent.

MabDirect MM is a new cation exchanger mixed mode adsorbent. Mixed Mode Chromatography (MMC) is a method of separation that uses more than one form of interactions (hydrophobic, electrostatic, thiophilic interactions and hydrogen bonds) between the stationary phase and the solutes in a feed stream.

Batch experiments are conducted in order to determine the adsorption equilibrium isotherms and, at the same time, estimate the diffusivity of the target protein in different conditions. The effects of salt and pH are assessed. The maximum adsorptions of HSA and IgG are observed for a buffer pH 5.0, without salt, i.e. near the target protein isoelectric point, either for HSA and IgG (36.0 ± 3.5 and 149.7 ± 7.1 mg·g_{dry}^{-1}, respectively). In the other hand, increasing salt concentration (up to 1M NaCl for HSA and 0.4M NaCl for IgG) in a pH 5.0 buffer solution decreases the adsorption capacity to 13.4 ± 2.5 and 16.3 ± 8.0 mg·g_{dry}^{-1} (63 and 89% of lost capacity) for HSA and IgG, respectively.

The adsorption kinetics, including film mass transfer and intra-particle diffusion resistances, are modelled with the aim of understanding the mass transfer phenomena. Experiments are carried out in a fixed bed column with the aim to understand the kinetics and hydrodynamics. In addition, these experiments validate the batch adsorption results, previously obtained. The influence of several operating parameters, such as flow rate, feed concentration and salt concentration are assessed.

A complete model of the EBA system is performed, using the data previously determined, to predict its dynamic behaviour. The mathematical simulation model fitted well with the EBA breakthrough experiments. Also, In order to estimate the liquid axial dispersion coefficient, residence time distribution experiments in three different expanded bed columns (Streamline 50, Omnifit 66/20 and XK 16/20) are performed.

Furthermore, the co-adsorption of HSA and IgG are performed in order to analyse the effects of competitive adsorption by batch, fixed bed and expanded bed adsorption experiments. Also, displacement experiments are carried out and showed that some amount of protein is released when other protein is being fed to the column.

Resumo

A separação e purificação de proteínas de forma eficiente até o nível desejado de pureza constitui um passo limitante nas indústrias farmacêuticas. O trabalho realizado tem por objetivo estudar a purificação da Albumina de Soro Humano (HSA) e da Imunoglobulina G (IgG) humana, utilizando adsorção em leito expandido (EBA) com um novo adsorvente de segunda geração.

O MabDirect MM é um novo adsorvente "mixed mode" com permuta catiónica. A Cromatografia de Mixed Mode (MMC) é um método de separação que usa mais de uma forma de interação (interações hidrofóbicas, eletrostáticas, tiofílicas e ligações de hidrogênio) entre a fase estacionária e os solutos numa corrente de alimentação.

Foram conduzidas experiências em sistema fechado para determinar as isotérmicas de equilíbrio de adsorção e, ao mesmo tempo, estimar a difusão da proteína alvo em diferentes condições. São avaliados os efeitos de sal e de pH. A adsorção máxima de HSA e IgG é observada para pH 5.0 sem sal, isto é, perto do ponto isoelétrico da proteína alvo; para HSA e IgG são obtidos 36.0 ± 3.5 e 149.7 ± 7.1 $mg \cdot g_{dry}^{-1}$, respetivamente. Por outro lado, aumentando a concentração de sal (até 1M NaCl para HSA e 0.4M NaCl para IgG) em pH 5.0 há um decréscimo da capacidade de adsorção para 13.4 ± 2.5 e 16.3 ± 8.0 $mg \cdot g_{dry}^{-1}$ (63 e 89% de perda de capacidade) para HSA e IgG, respetivamente.

São modeladas a cinética de adsorção, incluindo a resistência à transferência de massa externa e a resistência à difusão intraparticular, com o objetivo de compreender os fenômenos de transferência de massa. São realizadas experiências em coluna de leito fixo com o objetivo de compreender a cinética e a hidrodinâmica. Além disso, essas experiências validam os resultados de adsorção em sistema fechado, obtidos anteriormente. São avaliadas a influência de vários parâmetros operacionais, como caudal, concentração de entrada e concentração de sal.

É usado um modelo completo do sistema EBA, utilizando os dados previamente determinados, para prever o seu comportamento dinâmico. Os resultados da solução do modelo ajustam-se bem com os resultados experimentais obtidos pela operação da unidade EBA experimental. Também foram realizadas experiências de distribuição de tempos de residência em três colunas de leito expandido diferentes (Streamline 50, Omnifit 66/20 e XK 16/20) para estimar o coeficiente de dispersão axial do líquido. Além disso, foi realizada a co-adsorção de HSA e IgG com o objetivo de analisar os efeitos da adsorção competitiva por meio de experiências em sistema fechado, leito fixo e em leito expandido. São conduzidas experiências de adsorção competitiva numa coluna de leito fixo que mostraram que alguma quantidade de proteína é libertada quando outra proteína é alimentada à coluna.

Table of Contents

List of Figures

List of Tables

Chapter 1: Introduction

"We must remember that intelligence is not enough. Intelligence plus character – that is the goal of true education."

- Dr. Martin Luther King Jr.

The first chapter presents the motivation and relevance of the work done in this time period. Also, three methodologies used (Batch, fixed bed and expanded bed adsorption) are briefly summarized. Furthermore, the main objective is stated and each chapter of the thesis is described.

1.1. Relevance and motivation

Proteins have great importance in a wide range of applications; this is why several companies manifest their interest on these biological components, namely food companies, pharmaceutical and therapeutics industries. The main distinctive properties of proteins are their enzyme activity, specific recognition interactions and other therapeutic actions. Proteins are also the main focus of biotechnological industry [1]. Either for academic or industrial purposes, drug discovery initiatives, or high-throughput screening, proteins are the object of study of many researchers worldwide. In 2012, there were 200 approved recombinant proteins-based biopharmaceutical products for human therapeutic and diagnostic use, and already 350 in late stage clinical trials. *United States Food and Drug Administration* (US FDA) approved, in January 2012, 30 therapeutically complete monoclonal antibodies (mAb) and 3 antibody fragments for distinctive diseases treatment, such as thrombosis, neo-vascular age-related macular degeneration and Crohn disease [2-4]. By the end of December 2017, the new monoclonal antibody drug approvals hit record levels (Figure 1.1.), with 10 monoclonal antibody globally and the total number of mAb drugs (including drugs withdrawn for various reasons after approval, excluding fragment crystallisable fusion protein) reached 73. Figure 1.2. shows the impact area for the mAbs approved so far [5].

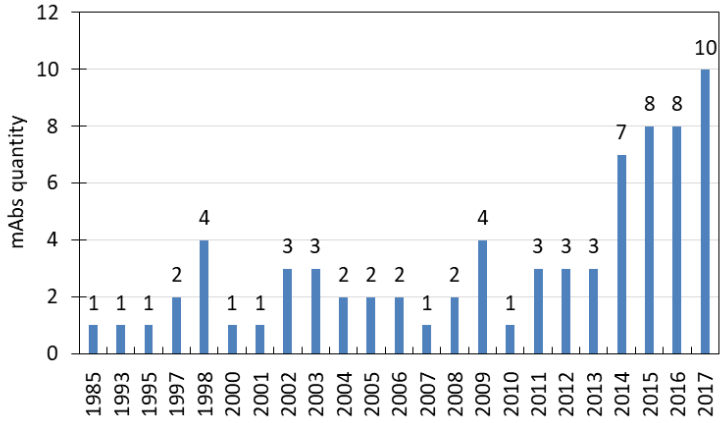

Figure 1.1 – Number of approved mAbs by year [5].

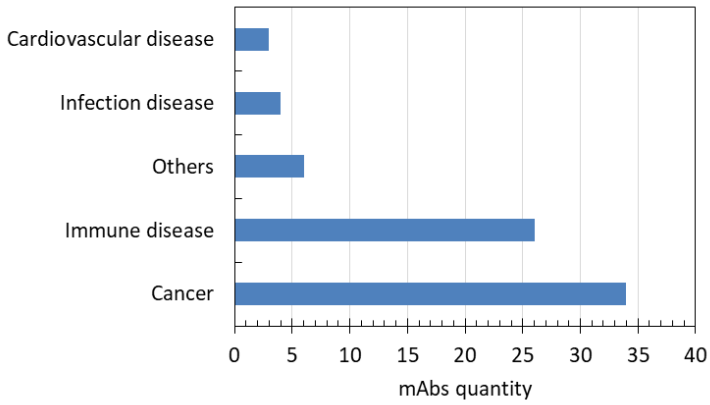

Figure 1.2 – Impact area of the 73 mAbs approved until the end of year 2017 [5].

1.1.1. Proteins on Human Plasma

Human Serum Albumin (HSA) and Immunoglobulin G (IgG) are the main protein components of Human plasma. Their importance to the scientific community is undeniable, since HSA is widely used clinically to treat several diseases, being a valuable product in the bio-market, and IgG is the only class of Immunoglobulin that can cross the placenta in humans, playing a crucial role in the protection of the newborns during the first months of life [6, 7].

1.1.2. The Need of Purification

Recombinant protein production is itself a complex process. Proteins are encoded by deoxyribonucleic acid (DNA). The desired protein DNA is introduced in a vector, usually a plasmid (small DNA molecule that has the ability to replicate automatically and independently from chromosomal DNA) which is introduced in a suitable host. Production of recombinant protein in the host cell is achieved by cells growth in shake flask cultures or fermentation broths [8-11]. The host cells can be yeasts, bacteria, molds, mammals, or *via* transgenic plants and animals [12]. *Escherichia coli* is the most applied of the bacterial expressions systems and the most commonly used for laboratory investigations, commercial activities or for comparison among various expression systems. This might be explained by its high growth rate with high cell densities and minimum nutrient requirements, high yields, ease of culture and genome modifications, and low manufacturing costs and availability to produce large quantities of recombinant protein [12-14]. *Escherichia coli* is not the only bacterial system used, there are others such as *Lactoccocus lactis* and *Pseudomonas* [13], while the two most utilized yeasts are *Saccharomyces cerevisiae* and *Pichia pastoris* [12]. The complexity of recombinant protein production depends on the cell growth characteristics, expression levels (intra-cellular or extra-cellular), and the inherent biodiversity in the peptide sequences [13-15].

Besides the proteins, at the end of recombinant proteins production processes there are several contaminants (dissolved or particulates) [16]. In terms of application purposes, protein purity is of utmost priority. There are separation methods that allow the target protein separation and purification from raw materials by downstream processing. The majority of protein purification schemes involve liquids that contain suspended particulates (whole or broken cells in fermentation broths), which are the result of cell breakage due to the necessity to release the intracellular products [1]. However, there is a need to ensure that all impurities are removed and sufficient amounts of highly purified protein is obtained efficiently to reduce the production costs. Protein separation and purification become a fundamental prerequisite for any pharmaceutical industry [3].

1.1.3. Methods of Separation

Adsorption techniques are a commonly used method for protein recovery. Adsorption can be carried out in batch or continuous stirred tanks for feedstocks containing particulates, or using fixed bed technology. Batch adsorption presents an easy setup and it has the capacity to handle particulate contaminants; however, it usually promotes the abrasion of the adsorption particles and it has poor adsorption and elution efficiency [17-19]. Fixed bed adsorption is another conventional operating mode. However, this method is not suitable for processing feedstocks that contain particulate material since it becomes trapped in the voids of the bed. Blockage is a common result by the formation of a plug of trapped solids near the bed inlet, increasing, this way, the pressure drop across the bed, which becomes unacceptable and lead to deformation and compression of non-rigid adsorbents [2]. The removal of these particulates is a lengthy process in which the time taken can result in future losses through denaturation [2].

Expanded bed adsorption (EBA) emerged as a hybrid technology, combining the benefits of both, batch and fixed bed, adsorption systems. EBA brings the advantage of an efficient hydrodynamics (similar to a fixed bed column) and avoids the blockage and high pressure drops (similar to batch). The concept of expanded bed comes from an upward flow through the column causing the expansion of suspended adsorbent particles where the cell, cell debris, unwanted similar proteins, contaminants and particulate matter pass through the column unhindered, while the target protein is adsorbed by a special adsorbent [20, 21]. This process involves different stages: after loading and washing, there are an elution stage where the bound protein is eluted from the adsorbent being captured and concentrated in a small amount of elution solution, and a regeneration stage, where the adsorbent will regain its capacity for another expanded bed cycle [2].

The main disadvantage of EBA is the need of specialized adsorbents. MabDirect is a new line of second generation adsorbents from *Rhobust Fastline Series* from *Upfront Chromatography*. Generally the adsorbents from this series are composed by a base matrix of 6% cross-linked agarose with tungsten carbide particles, which gives the appropriate density for expanded bed adsorption. This line is composed by MabDirect MM and MabDirect Protein A. MabDirect MM is a mixed mode adsorbent using a ligand that contains hydrophobic and electrostatic interaction groups. In turn, MabDirect Protein A contains a single polypeptide chain and specific interaction with Immunoglobulin G making this a very effective ligand (Protein A) for affinity chromatography from the serum of many species.

In conclusion, protein purification is usually the bottleneck in the cost of protein production and has put pressure to the development and improvement of purification methods. Expanded bed adsorption is the methodology of choice since it has been applied by some pharmaceutical companies (*DSM Biologics* and *Mucos Pharma GmbH & Co. KG*).

1.2. Objective and Methodology

The objective of the present work is to study the purification of HSA and IgG through EBA over second generation adsorbent, MabDirect MM. In order to reach this main goal, the work will be divided into three main supporting studies:

1.2.1. Batch Adsorption

Batch adsorption experiments are conducted in order to determine the adsorption equilibrium isotherms and at the same time estimate the diffusivity of the target protein in different conditions. The effects of ionic strength (by addition of salt) and of pH are assessed, since they are the main relevant physical properties that affect the protein adsorption. The interaction of these conditions with the target protein will be useful for understanding the adsorption phenomena. Furthermore, the co-adsorption of HSA and IgG are performed in order to analyse the effect of competitive adsorption. In addition, the kinetics are modelled with the aim of understanding the mass transfer phenomena.

This study helps us to understand the complex mechanism of protein adsorption, which is used for the design and optimization of the expanded bed adsorption process.

1.2.2. Fixed bed Adsorption

Fixed bed operation is usually used for cleaning and regeneration of the adsorbent, since at these stages, the particulates were already removed and it shows higher efficiency than EBA. Therefore, several experiments are carried out in a fixed bed column with the aim to understand the kinetics and hydrodynamics and to optimize these stages. In addition, these experiments serve to validate the Batch adsorption results, previously obtained.

The experiments are carried out by changing several parameters, such as, flow rate, feed concentration, pH and salt concentration. Moreover, tracer experiments are conducted in order to assess the hydrodynamics.

1.2.3. Expanded bed Adsorption

The main goal of the expanded bed adsorption experiments is the enhancement of the protein separation and purification; based on a mathematical model that is developed in order to better study the parameters that can affect the adsorption outcome. First, tracer experiments are

conducted in order to characterize the system hydrodynamics, together with protein adsorption experiments to validate the developed mathematical model: Adsorption/Desorption of the target proteins at different flow rates, pH, salt concentration, among others.

After validating, the optimum conditions will be computed based on the process simulation. Then, a final experiment will be conducted at the optimal conditions to confirm the results. In addition, binary mixture will be fed in order to analyse the effect of competitive adsorption.

1.3. Outline

The thesis is divided in seven chapters in order to better explain the work done. It starts with **Chapter 1**, Introduction where relevance and motivation are presented as well as the objectives of the thesis.

Chapter 2 consists on the state-of-the-art of the work. Relevance and brief characterization of the Human Serum Albumin and Immunoglobulin G are showed. Techniques of protein separation and purification since early ages are referred with the aim to guide the reader to the development and improvement through the history until now. Mixed-mode chromatography is introduced for a better understanding of the work theme, where the importance of the adsorbent ligand, conditions to be tested, and methodologies are pointed out. To finalize this chapter Expanded Bed Adsorption technology is referred, where procedures, case studies, scale-up, inappropriate situation for its use, the specificity of the adsorbents and the connection of this technology with protein separation and purification are addressed.

In **Chapter 3** are presented the adsorption equilibrium isotherms and kinetics of Human Serum Albumin (HSA) onto a novel high particle density multimodal adsorbent (MabDirect MM) studied by batch adsorption experiments. The effects of ionic strength (by addition of salt) and of pH are assessed. Langmuir isotherm parameters are obtained along with effective pore diffusivity values by fitting the batch experiments using a pore diffusion model. Furthermore, several experiments were carried out in a fixed bed column with the aim to understand the kinetics and hydrodynamics, and to validate the batch adsorption results.

Chapter 4 presents the adsorption equilibrium isotherms and the adsorption kinetics of Human Immunoglobulin G (IgG) onto the novel second generation high particle density multimodal adsorbent (MabDirect MM) by batch adsorption experiments. The effects of ionic strength (by addition of NaCl) and of pH are assessed. Langmuir isotherm parameters are obtained along with effective pore diffusivity values by fitting the batch experiments using a pore diffusion model that took into account the intraparticle effective diffusion and film mass transfer.

Furthermore, several experiments were carried out in a fixed bed column with the aim to understand the kinetics and hydrodynamics, and to validate the batch adsorption results. Dynamic binding capacity is also presented.

Chapter 5 presents expanded bed breakthrough experiments carried out for both target proteins (HSA and IgG separately) in different columns with different operating conditions and compared to the batch adsorption from previous experiments and literature. Residence time distribution experiments are conducted in order to characterize the hydrodynamics for three different columns used in EBA experiments. To finalize this chapter, the experimental EBA breakthrough results are compared to the mathematical model.

Chapter 6 demonstrate the adsorption equilibrium isotherm of a binary mixture (HSA and IgG) in order to analyse the effects of competitive adsorption. Fixed bed and expanded bed breakthrough experiments are also conducted for this binary mixture. Furthermore, displacement experiments performed in a fixed bed column are presented.

Finally, **Chapter 7** presents the conclusions of work done and recommendation for future work.

1.4. Nomenclature

DNA	–	Deoxyribonucleic acid
EBA	–	Expanded bed adsorption
HSA	–	Human Serum Albumin
Ig	–	Immunoglobulin
IgG	–	Immunoglobulin G
mAb	–	Monoclonal antibody
MM	–	Mixed-mode
US FDA	–	United States Food and Drug Administration

1.5. References

[1] H.A. Chase, Purification of Proteins by Adsorption Chromatography in Expanded Beds, Trends in Biotechnology, 12 (1994) 296-303.

[2] P. Li, Protein Separation and Purification by Expanded Bed Chromatography and Simulated Moving Bed Technology, in: Ph.D. Thesis, Department of Chemical Engineering, Faculty of Engineering University of Porto, Portugal, 2006.

[3] M. Saraswat, L. Musante, A. Ravida, B. Shortt, B. Byrne, H. Holthofer, Preparative purification of recombinant proteins: current status and future trends, BioMed research international, (2013) 1-18.

[4] P.A. Marichal-Gallardo, M.M. Alvarez, State-of-the-art in downstream processing of monoclonal antibodies: process trends in design and validation, Biotechnology Progress, 28 (2012) 899-916.

[5] Creative-Biolabs, New Monoclonal Antibody Drug Approvals Hit Record Levels in 2017, https://www.creative-biolabs.com/blog/index.php/new-monoclonal-antibody-drug-approvals-in-2017/. (Accessed 30.07.2018)

[6] Antibody Production and Purification Technical Handbook, in, Thermo Scientific Pierce 2010.

[7] G. Fanali, A. di Masi, V. Trezza, M. Marino, M. Fasano, P. Ascenzi, Human serum albumin: From bench to bedside, Molecular Aspects of Medicine, 33 (2012) 209-290.

[8] T. Makino, G. Skretas, G. Georgiou, Strain engineering for improved expression of recombinant proteins in bacteria, Microbial Cell Factories, 10 (2011) 1-10.

[9] A. de Marco, Biotechnological applications of recombinant single-domain antibody fragments, Microbial Cell Factories, 10 (2011) 1-14.

[10] L. Palomares, S. Estrada-Moncada, O. Ramírez, Production of Recombinant Proteins, Recombinant Gene Expression, 267 (2004) 15-51.

[11] A. Bernard, M. Payton, Fermentation and growth of Escherichia coli for optimal protein production, Current Protocols in Protein Science, Chapter 5 (2001) Unit 5.3.

[12] A.L. Demain, P. Vaishnav, Production of recombinant proteins by microbes and higher organisms, Biotechnology advances, 27 (2009) 297-306.

[13] R. Chen, Bacterial expression systems for recombinant protein production: E. coli and beyond, Biotechnology advances, 30 (2012) 1102-1107.

[14] S.C. Makrides, Strategies for achieving high-level expression of genes in Escherichia coli, Microbiological Reviews, 60 (1996) 512-538.

[15] Strategies for protein Purification handbook, in, GE Healthcare Bio-Science AB, Sweden, 2010.

[16] Protein production and purification, Nature Methods, 5 (2008) 135-146.

[17] M.A. Fernandez, G. Carta, Characterization of protein adsorption by composite silica-polyacrylamide gel anion exchangers I. Equilibrium and mass transfer in agitated contactors, Journal of Chromatography A, 746 (1996) 169-183.

[18] G. Garke, R. Hartmann, N. Papamichael, W.-D. Deckwer, F.B. Anspach, The Influence of Protein Size on Adsorption Kinetics and Equilibria in Ion-Exchange Chromatography, Separation Science and Technology, 34 (1999) 2521-2538.

[19] A.K. Hunter, G. Carta, Protein adsorption on novel acrylamido-based polymeric ion-exchangers: IV. Effects of protein size on adsorption capacity and rate, Journal of Chromatography A, 971 (2002) 105-116.

[20] F.X. McGarvey, R. Kunin, Mixed bed deionization. US2578937A (1951).

[21] H.A. Chase, N.M. Draeger, Expanded-Bed Adsorption of Proteins Using Ion-Exchangers, Separation Science and Technology, 27 (1992) 2021-2039.

Chapter 2: State-of-the-Art

"Our lives begin to end the day we become silent about things that matter."

- Dr. Martin Luther King Jr.

In this chapter it is presented the state-of-the-art of the work done. Relevance and brief characterization of the Human Serum Albumin and Immunoglobulin G are showed. Techniques of protein separation and purification since early ages are referred with the aim to guide the reader to the development and improvement through the history until now. Mixed-mode chromatography is introduced for a better understanding of the work theme, where the importance of the adsorbent ligand, conditions to be tested, and methodologies are pointed out. To finalize this chapter Expanded Bed Adsorption technology is referred, where procedures, case studies, scale-up, inappropriate situation for its use, the specificity of the adsorbents and the connection of this technology with protein separation and purification are addressed.

This chapter is partially based on the following book chapter:

Li, P., Gomes, P. F., Loureiro, J. M., Rodrigues, A. E. 2014. "Proteins Separation and Purification by Expanded Bed Adsorption and Simulated Moving Bed Technology" in "Continuous Processing in Pharmaceutical Manufacturing", Ganapathy Subramanian, Editor, John Wiley & Sons, Inc.

2.1. Proteins

Protein, word derived from the Greek language (*Proteios*), which means "*standing in front*" was introduced by Jöns Jacob Berzelius in 1838 who state the importance of this biological group of organic compounds. From that time until 1930, researchers tried to classify proteins as macromolecules or colloidal aggregates [1, 2]. In 1901, Hermann Emil Fischer [3, 4] was able to synthetize a dipeptide, showing the possibility to aggregate amino acids, and in the following year, 1902, Franz Hofmeister [5] suggested that amino acids could be linked by peptide bonds forming proteins [2]. Later on, in 1926, James B. Sumner [6] was able to crystallize an enzyme and showed by chemical analysis that the substance was in fact a protein, the first proof that enzymes are proteins. Chemistry Nobel Prize winner Linus Pauling and co-workers [7-9], in 1951, proposed the division of the primary structures of proteins in α and β sheets. In 1957, Christian B. Anfinsen and co-workers [10] showed that bovine pancreatic ribonuclease could be refolded to its native structure and regain its activity by reductive cleavage of its four disulfide bonds. Later on, Anfinsen [11] suggested that the native structure of a protein is the most thermodynamically stable structure and presented the amino acid sequence of bovine pancreatic ribonuclease; subsequently, Max Perutz and John Kendrew determined the structure of myoglobin [12, 13].

Proteins have a high relevance and a significant impact on our life, since they are not only an important biological compound present in every living organism but they are also a resource with a wide range of diverse applications, such as in pharmaceutical and therapeutical industries, food companies, textiles and leather materials, detergents, among others. This diverse biological compound can be found in raw source of feedstock material together with different contaminants and unwanted materials, so the efficient separation and purification become a key-factor for an economical and viable application for achieving this product [1].

2.1.1. Relevance

In modern times, the financial market of purified proteins has been increasing gradually (Figure 2.1); this is a consequence of their use on therapeutic and nutritional fields as mentioned before. Antibodies, blood factors, interferons and erythropoietins are the major pharmaceutical products that dominate the market. Antibodies are one of the current products of interest of researchers due to their potential for cancer treatment, autoimmune diseases and gene therapy. Early generations of researchers in the field of biotechnology have been focusing on developing techniques and methods to reach the highest protein purity possible, i.e., without specific impurities such as endotoxins in the antibody case [14, 15].

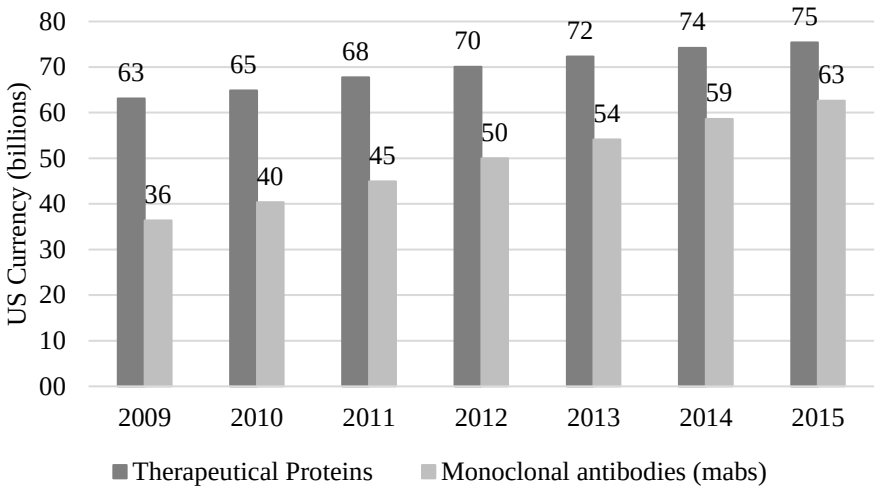

Figure 2.1 – Global therapeutic protein and monoclonal antibodies sales [16].

According to new report, global monoclonal antibody therapeutics market was valued at approximately 108.01 US billion dollars in 2017 and is expected to generate revenue of around 218.97 US billion by the end of 2023, growing at a CAGR (Compound Annual Growth Rate) of 12.5% between 2017 and 2023 [17].

Human Serum Albumin and Immunoglobulin G represent the major part of proteins in the Human plasma and since their importance is undeniable they are the target model proteins tested. The following sections (2.1.2. and 2.1.3.) will report the major advantages and characteristics of these two proteins.

2.1.2. Human Serum Albumin

Human Serum Albumin (*HSA* – Figure 2.2) is a globular protein of 585 amino acids with a molecular weight of 66 kDa, which accounts for 60% of the total protein in blood serum; it can be found in tissues and bodily secretions throughout the body. In a normal Human adult, the concentration of this protein is approximately 40 g/L. *HSA* has binding capacity for a wide range of endogenous and exogenous ligands, and its abundance makes it an important reference of the pharmacokinetic behaviour of many drugs [18-22]. *HSA* contributes significantly to the colloid osmotic blood pressure and aids in the transport, distribution and metabolism of the wide range ligands which represent several

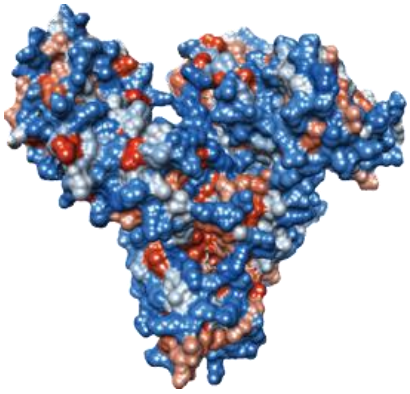

Figure 2.2 – Surface rendering of the atomic structure of Human Serum Albumin, illustrating charge distribution [18].

chemical molecules, such as fatty acids, amino acids (tryptophan and cysteine), steroids and metals (such as calcium, copper and zinc) [23].

HSA is a valuable bio-marker of many diseases (such as rheumatoid arthritis, ischemia, post-menopausal obesity, and cancer) and diseases that need monitoring of the glycemic levels [21]. Also, this protein is used clinically to treatments like in burns, shocks, surgical blood losses (since it is the major component of Human blood), hemorrhages, cardiopulmonary bypasses, and hemodialysis among others [21].

2.1.3. Immunoglobulin G

Immunoglobulin G (*IgG* – Figure 2.3) is a complex antibody composed by four peptide chains (with quaternary structure) with two heavy chains and two identical light chains arranged in a Y-shape typical of antibody monomers. *IgG* represents approximately 75% of immunoglobulins present in human serum. This protein has important functions on the immune system since it is the main antibody found in blood and extracellular fluid, having the function of controlling infection of body tissues. *IgG* antibodies have the molecular weight of 153 kDa and present four subclasses in humans (*IgG1*, *IgG2*, *IgG3* and *IgG4*). Regarding the importance of this protein, *IgG* can be used for diagnostic purposes, where the measured *IgG* levels are generally considered to be indicative of an individual immune status to a particular pathogen. Also, this protein can be used in therapy, where it is extracted from donated blood plasma and used to treat immune deficiencies, autoimmune disorders and infections [24, 25].

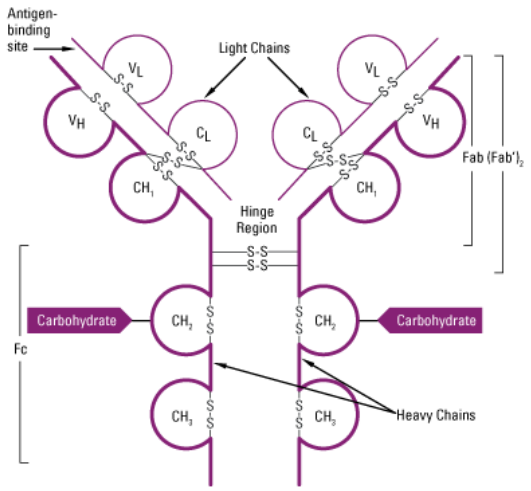

Figure 2.3 – Immunoglobulin G generalized structure [25]. Two heavy chains at the bottom and two light chains on the top arranged in a Y-shape.

This antibody is the only class of *Ig* that can cross the placenta in humans, and therefore is the main protein responsible for protection of the newborn during the first months of life. Considering its abundance and the good specificity toward antigens, *IgG* became the main antibody used in immunological research and clinical diagnostics [25].

2.2. Techniques of protein separation and purification

Protein purification has been performed for a long time. In 1789, Antoine Fourcroy prepared substances from plants that had properties similar to the egg white (mainly albumin) [26]. Early in the 20th century, protein separation procedures were only filtration, precipitation and crystallization. In 1840, Felix Hoppe-Seyler prepared the first crystal of hemoglobin [27], which, in 1889 was repeated by Hofmeister for ovalbumin [28]. The interest in albumin and other blood proteins peaked between 1939 and 1945 (Second World War). Cohn was probably the first to perform the fractionation of plasma for the purification of albumin and other proteins [29]. His method was based on multiple precipitation stages where pH, ethanol concentration, temperature, and protein concentration varied each step. Ammonium sulfate precipitation, for example, is still used today (2018). In 1906, the botanist Mikhail Tswett worked on the separation of plant pigments on a column of calcium carbonate [30]. Later, this botanist introduced the term chromatography. In 1924, Theodor Svedberg stated that proteins could also be separated by centrifugation [31]. Later in the 20th century more protein separation methods were developed: electrophoresis and affinity chromatography (AC) in the 1930s and ion exchange chromatography (IEX) in the 1940s. Arne Tiselius and co-workers, in 1956, developed a mixed mode ion exchanger known by the name of Hydroxyapatite [32]. The first chromatography matrices were invented for hydrophilic chromatography during the 1950s and 1960s. Nowadays, hydrophobic and ion-exchange chromatography are the most common used methods in purification of proteins [2, 33-35].

In 1955, starch was used to separate protein based on size differences. Later, in 1959, researchers Jerker Porath, Per Flodin and Bjorn Ingelman developed cross-linked dextran [36]. Hydrophilic materials, such as agarose (commonly used as matrices support, Table 2.2 on section 2.4.5.), porous silica, methacrylate and polyacrylamide were developed during the 1960s for electrophoresis and chromatography, which allowed the development of sodium dodecyl sulfate polyacrylamide gel electrophoresis (SDS-PAGE) and capillary zone electrophoresis (CZE) later on [2, 34, 37].

The foundation of modern affinity chromatography (AC) was enabled by Rolf Axén and co-workers, in 1967, with the introduction of cyanogen bromide activation which allowed ligand coupling to polysaccharides (agarose, for example) [38]. However, affinity chromatography method was attributed by Pedro Cuatrecasas and co-workers, who described the method one year later [39-41].

Between the 1960s and the 1970s, reverse phase liquid chromatography (RPLC), hydrophobic interaction chromatography (HIC), and immobilized metal ion affinity

chromatography (IMAC) were developed. These methods are based on different separation properties, such as charge or hydrophobicity. Also important is to add the high-performance liquid chromatography (HPLC), a high power separation method based on chromatography studied in 1941 and 1966 by researchers Martin and Synge, and still used today [42].

During the 1970s and 1980s there was an increase in the development of chromatography media and protein purification. The 1970s were the era of recombinant DNA technology. Molecular cloning allowed the overexpression of a target protein, which permitted the upcoming developments in the following decades, among them the affinity tagging of proteins which allowed efficient AC purification. Monoclonal antibody technology appears in 1975, involving the establishment of stable cell lines producing a single selected protein. This technique, in association with highly selective chromatography media based on Protein A and G ligands made possible the conception of large number of applications in research and pharmaceuticals later on. In 1972, Hjelm and co-workers studied the Immunoglobulin G purification by Protein A adsorbent [2, 25, 43, 44]. In 1982, *Pharmacia* (now *GE Healthcare*) introduced a chromatography system called Fast Protein Liquid Chromatography (FPLC) [2].

In 1990 was initiated the determination of many protein structures; the Human Genome Project and deoxyribonucleic acid (DNA) sequencing made available complete genome sequences. From a biological point of view, this technology is associated with gene expression information which will translate in messenger ribonucleic acid (mRNA) and finally in proteins. During this time it was developed the peptide mass fingerprint, where mass spectrometry of peptide fragments combine with a large library of known protein sequences, making possible the identification of a certain protein in a sample [45].

Also, in the 1990s, the term Proteomics is introduced, meaning all that involves the study of proteins, its structure and function in a given organism. Since proteins are the common components of physiological metabolic pathways of cells, their importance had researchers' attention, more specifically the attention of Marc Wilkins in 1994, at the time a PhD student, who suggested the term *proteome* to make an analogy with the term genomics (study of genome). *Proteome* became, by definition, the term that is used when referring to the entire assemblage of proteins [46].

Protein purification and separation became an easy procedure thanks to affinity tagging of the target protein; however, its efficiency is not always sufficient and further methods are necessary, such as gel filtration, HIC and IEX. Also, different proteins have different challenges for their purification, such as integral membrane protein and protein with a specific post translation modification.

There are other techniques regarding the separation and purification of proteins, such as size-exclusion chromatography (SEC), Immune-affinity chromatography and Microarrays. The following Table 2.1 shows some examples and on which phenomenon they base the separation.

Table 2.1 – Some protein separation examples and on which phenomenon they base the separation.

Techniques	**Phenomenon**						
	Isoelectric point (pI)	Electrostatic	Hydrophobicity	Affinity	Size	Charge	Metal ion binding
HPLC / RPLC			✓				
IMAC				✓			✓
SEC					✓		
SDS-PAGE / CZE					✓	✓	
IEX						✓	
Microarray				✓			
Gel filtration					✓		
Chromatofocusing	✓						
MMC	✓	✓	✓			✓	

2.3. Mixed-mode Chromatography

Mixed mode chromatography (MMC) is a method of separation that uses more than one form of interactions between the stationary phase and the solutes in a feed stream. Dye-ligand, histidine and peptide affinity adsorbents can be classified as mixed mode or multimodal adsorbents. Hydrophobic-ion-exchange chromatography studies showed up in 1972, at the same time as hydrophobic interaction chromatography. The different combination of interactions can lead to a unique selectivity and facilitate the separation process. In 1977, it was discovered that the charge repulsion in hydrophobic interaction chromatography can reduce the level of adsorption. In 1982, it was stated by Crowther and Hartwick that mixed mode interactions can enhance the resolution in high-performance liquid chromatography; also in 1982, Crowther and Hartwick [47] and again in 1984 by Bischoff and McLaughlin [48] reverse phase ion exchange chromatography was studied; in 1992, Zhu and co-workers [49] studied hydrophilic ion exchange chromatography (HIC); in 1997 and 2000, it was found that mixed mode interaction allowed the target protein to be adsorbed at a wide range of ionic strength thus eliminating the need of prior salt addition or removal from the feedstock. In 1998, hydrophobic charge induction chromatography (HCIC) was studied by Burton and Harding. The pKa of the ligand for HCIC is carefully considered since it is desired a ligand uncharged at neutral pH. If this condition is accepted, the only interactions on the adsorption stage are the hydrophobic interactions while elution is achieved by electrostatic repulsion [33, 50-55].

In ion exchange chromatography, proteins are separated by difference in surface charge; it is a reversible interaction between a charged protein and an oppositely charged chromatography medium (or adsorbent). The target protein is concentrated during the binding stage and collected in a purified form. It is known that the net charge of proteins varies according to the surrounding pH. For example, for a positively charged anion exchanger, the protein will bind when above its isoelectric point; however, below its isoelectric point, it will bind to a negatively charged cation exchanger. Nevertheless, even when the net charge of the protein is negative, there are several positive regions that can interact with negative charged ligands.

Also, unexpected or absence of binding can occur due to pH changes in the microenvironment inside the beads compared with the bulk buffer (Donnan effect). Elution of the bound protein is commonly performed by increasing salt concentration or changing the solution pH. Normally, NaCl is used as reference, although other salts can be used as well. Usually IEX is used to bind the target protein and let the impurities pass through the column; however the opposite is possible, the ion exchange media binding the impurities and letting the target protein flow freely [33, 56].

In hydrophobic interaction chromatography (HIC), the protein separation is, as the name suggests, by hydrophobicity. This method is based on the reversible interaction between the target protein and the hydrophobic surface of a chromatography medium (or adsorbent). The best results are achieved when using a high ionic strength buffer; then, conditions are altered for elution purposes. This stage is usually performed by decreasing the salt concentration. The target protein is concentrated during the binding stage and is collected in purified and concentrated form (same as in ion exchange chromatography). Other elution methods are reducing eluent polarity, changing the pH or temperature [33, 57, 58].

Mixed mode consists in complementary charge ligands with additional functional groups that will introduce new cooperative interactions (hydrophobic interactions, van der Waals interactions and hydrogen bonds). In most cases, the multiple interactions will simultaneously influence the adsorption. Being able to understand this interaction is a both complex and difficult task, although not an impossible one.

2.3.1. Ligands for mixed mode protein chromatography

Between 1972 and 1975, Yon and co-workers were perhaps the first group working with mixed mode ligands for protein chromatography. They divided the hydrophobic interaction ligands in two groups, i.e., hydrocarbon groups and other with mixed hydrocarbon and ionic groups. Important to refer is that the ligands developed by Yon et al. adsorbed proteins by the

effect of hydrophobic interaction and electrostatic repulsion. Nowadays these ligands are different. The mixed mode ligand usually have an aliphatic or aromatic group as the hydrophobic moiety and an amino, carboxyl or sulfonic group as the ionic moiety. Heterocyclic groups are good ligands due to their unique hydrophobicity and dissociation property compared with the common aliphatic and aromatic compounds [33]. In 1998, Burton and Harding tested a number of heterocyclic mixed mode ligands; a commercially available adsorbent, Mercapto-Ethyl-Pyridine Hypercel (MEP), was later produced based on this type of ligands. Some researchers, between 2001 and 2006 observed that MEP was un-charged at physiological conditions, so adsorption is achieved mainly by hydrophobic interactions and, later, protein recovery could be achieved when the ligand is positively charged. The premise that proteins are adsorbed by hydrophobic interaction and dissociated by charge repulsion are the basic principles developed by Burton and Harding in 1998 [33].

On some industrial ligands (hexylamine and phenylpropylamine hypercel) amine groups are the positively charged groups for electrostatic repulsion while carboxyl and sulfonic acids compose the negatively charged groups. In 2003, Johansson and co-workers stated that the introduction of hydrogen bond groups in the proximity of the ionic groups in mixed mode ligand would be beneficial for protein binding at high salt concentration [59].

2.3.2. Salt and pH variation on protein/adsorbent system

The dissociation of the adsorbed proteins can be achieved by both increasing salt gradient and pH. However, these variations are not as simple since they are not directly related, i.e., increase in pH will not, in some cases, increase the dissociation of the adsorbed protein.

2.3.2.1. Salt variation

Mixed mode chromatography possesses the advantage of salt-independent adsorption, facile elution by charge repulsion and unique selectivity proving beneficial for proteins separation [33]. “Salt-tolerant adsorbents” is an expression given to the adsorbents that have high dynamic binding capacities in a wide range of salt concentration, but not all mixed mode adsorbents possess this property.

Addition of salt affects the efficiency of adsorption/desorption processes. Li and co-workers, as the majority of the scientific community, stated that for adsorption purposes, the gradual increase of salt concentration will entrain a decrease in the adsorbent capacity [1, 60, 61]. However, different conditions were tested by Nfor and co-workers (2010), where they state that, for some particular cases, this association does not apply [62]. Also, Nfor reported a U-shape

curve for adsorption capacity as function of salt concentration. Since the target protein and the adsorbent form a unique system, when dealing with a system not yet mentioned in the literature, it is always advisable to study this parameter.

2.3.2.2. pH variation

Another well studied parameter is the pH, not only for the optimization of the adsorption conditions but to increase the efficiency of the elution stage as well. The isoelectric point of the target protein is a way to explain the protein retention on the ionic surface of the adsorbent. The second generation adsorbents (Section 2.4.5.) take this factor in consideration, as they also take advantage of hydrogen bond interactions and hydrophobic interactions to achieve a higher binding capacity in high ionic strength and salt concentrations. Following the example of a case study by Li et al [63], the target protein Bovine Serum Albumin (BSA) with a isoelectric point of 4.7 (same as the HSA) has negative charges, when working at pH between 5 and 7, so the adsorption takes advantage of the hydrogen interaction between protein and the ligand instead of the typical charge-charge interaction. Li suggested that multi-modal ligands are designed in such a way that the hydrogen bond interactions are greater in acid conditions, so it is expected an increase on the binding capacity of the protein when the pH value is reduced below 5. When the pH is lower than the isoelectric point of the protein, such as 4, the adsorption takes advantage of the charge-charge and the hydrogen bond interactions; however the maximum binding capacity takes place at a pH 5 that is near the isoelectric point proving that there is contribution of the hydrophobic interaction [1, 60, 63, 64]. Nonetheless, according to Nfor and co-workers [62], the adsorption dependency is a complex factor. The authors studied the thermodynamic modelling of protein adsorption on a mixed mode adsorbent functionalized with ligands carrying both hydrophobic and electrostatic groups for different proteins (widely different molecular masses and isoelectric points) on four mixed mode adsorbents. The solution pH affects the charge states of the protein and the adsorbent; the parameters of interest are the isoelectric point of the protein and the pKa of the charged group on the adsorbent ligand. Nfor et al. reported a good graphical representation of this complex parameter, where they show the binding strength dependency of pH solution varying with charge on ligand and on protein [62].

Also it is stated by Nfor et al. that at pH values below the isoelectric point, the protein and the ligand become similarly charged and so experience electrostatic charge repulsion, a phenomenon that is commonly exploited for desorption purposes. The variation of these conditions and the nature of different adsorbents used will determine the binding capacity [62].

2.3.3. Principles for mixed mode ligand design

Hydrophobic-ion-exchange ligand should possess at least one hydrophobic group and one ionic group. Regarding the hydrophobic choice, the butyl, phenyl or hexyl groups serve as examples to achieve this characteristic. Also, aromatic ligands have higher hydrophobicity than short alkyl chains. In 2003, Johansson and co-workers found that, for mixed mode anion exchange chromatography, the non-aromatic ligands with amine groups are preferred to ease the elution, while aromatic ligands with carboxyl groups are needed for mixed mode cation exchange conditions. However, long alkyl chains should be avoided since they can cause protein denaturation [33, 65, 66].

Ionic groups for ion exchange chromatography are also adaptable for mixed mode ligands. They are classified in two different types: strong (sulfonic and quaternary ammonium groups) and weak (carboxyl and amino groups). Strong groups can maintain their charge in a wide range of pH which is an advantage for selectivity. Weak groups have the advantage to be able to suppress its charge by pH adjustment. pKa of the ionic groups is essential for the performance of the ligand and should be estimated in ligand screening and design [33, 59].

Hydrophobic and electrostatic are not the only interactions involved in this mechanism. Also there is hydrogen bonding as a second type of interaction, which can participate in protein-protein binding. Introduction of the hydrogen bonding interaction gives the possibility to develop salt-tolerant chromatography. Introducing hydrogen donors to anion exchange ligands or hydrogen acceptors to cation ligands are the ways to exploit the hydrogen bonding [33, 59, 66, 67].

The ligand should also contain a reactive site (usually amino or mercapto) for coupling. It is also a common strategy to introduce a “spacer arm” between the ligand and the matrix in the affinity chromatography to avoid the hindrance in protein binding. The spacer arm should not interfere with the binding of proteins to the ligand and also should be chemically stable, biocompatible and inexpensive [33, 67].

Usually, the manufacture of this type of ligand involves the attachment of different kinds to a solid medium and examination of their respective adsorption and elution performances. However, with the development of bioinformatics and combinatorial chemistry, the design of ligands passes through 3 phases: library establishment, which contains all the possible candidate compounds that may bind with the desired target protein; library screening, where the ligands are screened by chromatographic evaluation (there are limitations to this method and therefore a high-throughput screening strategy was developed) and finally chromatography verification [33, 67].

2.3.4. Adsorption

Adsorption/Desorption is a surface phenomenon where attachment and detachment of chemical species onto or from the surface occur [68].

Adsorption equilibrium isotherms define the quantity of sorbate retained by the adsorbent at the equilibrium, and the final concentration of the adsorbate in the solution is measured at defined conditions (temperature, pH, salt and/or ionic strength). Equilibrium occurs when the adsorbent has been in contact with the adsorbate for the necessary period of time.

Adsorption kinetics define the behaviour (rate) of adsorbate/adsorbent systems to reach the equilibrium. Like adsorption equilibrium isotherms, different conditions (temperature, pH, salt and/or ionic strength) will result in a distinctive result. The interactions between the solute and the adsorbent can be explained by theoretical models. Linear, Langmuir, Freundlich, Brunauer-Emmet-Teller Isotherms are the most commonly used; however, others can be utilized as well, such as Sips, Toth and Myers. Typically, Langmuir model is the most used for protein separation purposes.

Adsorption can be performed in different formats. Namely, in batch, packed bed, fluidized bed and expanded bed technology [69].

2.3.5. Batch, Fixed-bed, Fluidized and Expanded-bed adsorption

2.3.5.1. Batch adsorption

Batch processes were commonly used for protein purification [70-74], due to their simplicity and ability to avoid the blockage of the adsorbent particles by the particulates (solid debris) that are present in the feedstock. The major drawbacks are the poor adsorption and elution efficiency and the adsorbent abrasion due to the stirring [69].

2.3.5.2. Fixed bed chromatography

In fixed bed adsorption, the fluid stream is forced to pass through the adsorbent packed in a column [69]. Fixed bed process allows a good adsorption, elution efficiency, cleaning, and regeneration of the adsorbent; therefore it is widely used in industry. However, contrarily to the batch process, the particulates commonly present in the feedstock lead to a blockage of the adsorbent, and consequently increase the pressure drop and decrease the adsorption capacity. Other major disadvantage of fixed bed operation is the eventual blockage occurring during the process; to solve this issue was developed an operation where the particles would be allowed to

move inside the column (fluidized and expanded bed) therefore preventing any blockage of the column. Years after this idea was implemented, researchers have been and are trying better ways to achieve the highest product quality possible [69, 75, 76]. Fixed bed chromatography is a common operating mode for proteins separation [77-80].

2.3.5.3. Fluidized bed chromatography

Fluidized bed adsorption consists in the passage of fluid through a column, in an upward direction, with suspended adsorbent, where there is a strong adsorbent mixing. This process comprises the characteristics of previously described technologies and expanded bed adsorption, and has the ability to solve any blockage and pressure related issues that are common in fixed beds, and also presents the ability to operate with particulates in the feedstock. However, this technology results in a poor product capture and, therefore, there is a need of recycling the feedstock. Also, it presents a poor adsorption and a fair elution efficiency [2, 81]. Albeit the referred disadvantages, this technology has been tested on proteins separation [82, 83].

2.3.5.4. Expanded bed chromatography

Expanded bed adsorption (EBA) technology has been successfully applied as an efficient technique for directly capture, separate and purify various protein products from unclarified source material, such as antibodies, enzymes, mammalian cell culture, milk, animal tissue extracts and yeasts [69, 76, 84, 85]. *Mucos Pharma GmbH & Co. KG* (Germany), founded in 1949 is a pharmaceutical company that produces enzymes which are used in vascular diseases, rheumatism, inflammations, immune system, viral infection and cancers. This company uses EBA technology as part of an integrated fermentation and purification process for the isolation of human chymotrypsinogen B expressed in *P. pastoris [86]*. In December 2013, *Therapure Biopharma Inc*. issued a press release stating that they acquired a plasma protein purification technology from Upfront Chromatography A/S related to human plasma fractionation (PlasmaCap EBA). Upfront had already divested their pharmaceutical business to *DSM Biologics* in April 2010. In 2014, Patheon acquired DSM pharmaceutical products adding small and large molecule drug substance capabilities in Europe as well as North America. Another company worthy of mention is XENDO, a ProPharma Group company, that provide consultancy and project management in the area of pharmaceutical product development, manufacturing, validation and engineering sustainable solutions for their customers. By the end of 2017, beginning of the year 2018, XENDO designed and built a custom-made continuous chromatography systems, naming them XPure. In this XPure Systems, they have XPure-E (Expanded bed adsorption system), XPure-S (SMB static system) and XPure-C (SMB carousel system).

This new technology (EBA) consists in suspending the adsorbent particles by passing an upwards stream on a column, therefore increasing void fraction, where the unwanted material and contaminants pass through the column unhindered without the risk of any blockage, thus minimizing the pressure drop problems commonly encountered in fixed bed reactors [75, 76]. Also, the adsorbent present in the column does not mix as in fluidized bed technology [2].

Mixed mode adsorbents are also designed for expanded bed purposes, in which the use of salt tolerant ligands eliminates the need of dilution of the feed to lower its ionic strength, making the method more adaptable for practical processes. Expanded bed is a much more flexible system than fixed bed. While the adsorbent in packed bed is immobilized, fixed, and/or packed, thus the name, in an expanded bed the adsorbent flows "freely" in the column. However, some restrictions have to be met so that the adsorbent do not leave the column while the non-desired compounds can pass through. These restrictions spurred the exploration of new types of adsorbents [77, 87-91]. EBA avoids the shortcoming of small voidage of the bed; with this type it is possible to work at high flow rate with a dense adsorbent allowing the cell debris to pass through without blocking the bed [92, 93]. This technology gives us the ability to operate with the particulates in the feedstock and has a good adsorption and elution efficiency [69, 94]. However, like everything, EBA has disadvantages since there is the need of specialized adsorbent and there is a shortage of industrial application data [69, 94]. In the following section (Section 2.4), this "new" technology will be discussed in detail.

2.4. Expanded Bed Adsorption Technology

To the author knowledge, the first experiments using fluidized and expanded bed technologies were around 1949. In this date, experiments were conducted by Leroy K. McCune and Richard H. Wilhelm, from Princeton University, in which they studied the mass transfer between an upward stream of liquid and solid particles in consolidated and in expanded, fluidized beds. The solid particles were 2-naphthol and the liquid was water [95].

In 1951, Francis X. McGarvey and Robert Kunin registered a patent (US2578937A) where it is described that an upward flow of water through a bed will cause the bed to expand. The expansion degree will increase as the upward flow increases until eventually the particular resin is completely carried out by water, herein referred to as the rate for resin fluidization [96]. In 1994, Howard Chase stated that modelling and optimization protocols developed for the operation of packed-beds may be modified to describe expanded bed protocols [69, 97].

Since then, the technology has evolved. The upward flow is now used with optimized solutions that will enable a good efficiency throughout the process, and with special adsorbents responsible for the separation of the target protein. Also, there are now efficient models of expanded bed adsorption [60, 62, 98-103].

2.4.1. Expanded bed procedures

2.4.1.1. Expanded bed stages

EBA consists on different stages: **Expansion/Equilibration** is the first stage, during which the column (Figure 2.4) will be expanded with an equilibration buffer that is going to be pumped in an upward flow during a time period, starting with at a low flow rate and steadily increasing it until the bed is stable. The primary goal of this stage is to achieve a stable expansion degree. Also important is to adjust the superior piston to a position above the height to which the bed expands, allowing this way to reduce the dead volume in the expanded bed [1, 69].

Figure 2.4 – Expanded bed system set-up.

Then, when all the preparation requirements are dealt with, the **adsorption stage** begins. In this stage, the feed stream enters at the bottom of the column and the adsorption can take place. It is expected in some cases that the expanded bed height gradually drops, especially if the bed is expanded with a low density adsorbent, which then steadily increases due to the protein adsorption on the adsorbent; so the liquid flow velocity has to be increased proportionally to maintain a constant degree of bed expansion. The average liquid velocity is calculated on this stage from the ratio between the total feed volume supplied to the column and the operating time in the loading process. Also, if the physical properties of the feedstock are different from those of the buffer used to expand the bed initially, it is common to observe that if the flow rate is not decreased properly the bed expansion will increase, so, if one wishes to maintain the original bed expansion constant it is a common procedure to reduce progressively the flow rate at which the feedstock is applied. There are two possibilities regarding the protocol to follow, either it is kept a constant degree of expansion thus necessitating an increase in the flow rate, or it is run at constant flow rate resulting in changes of the height of the expanded bed [1, 60, 63, 69, 104-107].

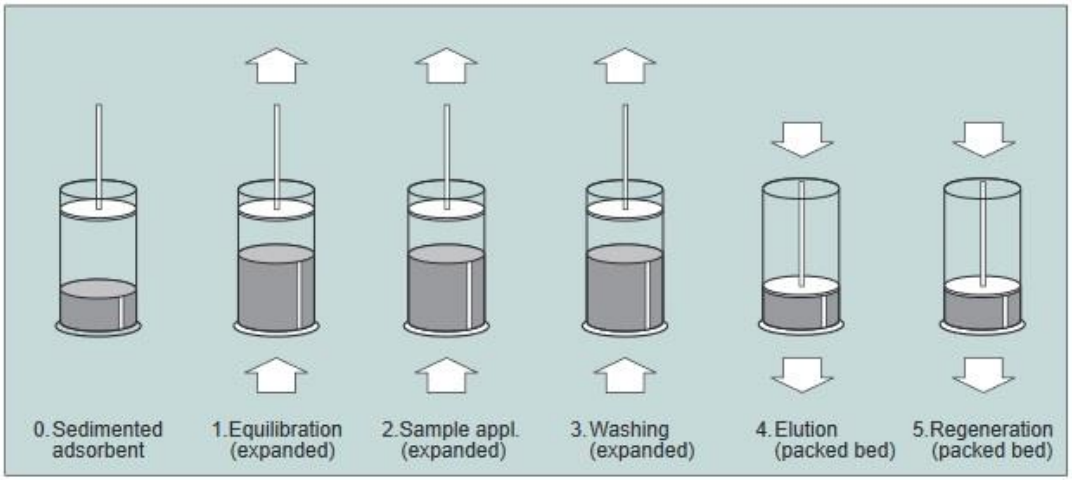

Figure 2.5 – Schematic presentation of the different expanded bed adsorption stages and configurations [108].

The **washing stage** begins when the measurement of the breakthrough curve has been completed by switching to the washing buffer; this is going to clean the unbound protein within the inter- and intra-particular voids of adsorbent, other loosely bound material and particulates from the column in the expanded mode until the effluent absorbance reaches a relative stable value. It order to remove the remaining particulates, it is essential to carry out at least the first stages of the washing with the bed in the expanded mode. Washing can be carried out with simple buffer, although there is evidence that the use of viscous wash buffers may reduce the number of column volumes needed to clear unwanted particulates from the bed [1, 60, 63, 69, 104, 105, 107].

Once all particulate material has been removed from the expanded bed, **further washing** may be continued with the bed in either expanded or packed configuration. If the bed would be on the packed configuration, since there is no need to be expanded, the flow rate could be chosen at will. The volumes of washing will be less when the height of the bed has been reduced to the packed configuration [60, 63, 69].

Afterwards, an **elution stage** takes place, where the bounded target protein can be eluted by an elution buffer and concentrated in a small amount of elution solution; apart from the bulk impurities and contaminants in the source materials, this is the final product where we want to achieve the highest purity. Although there are no factors that prevent the elution stage to be conducted on expanded mode, for more efficiency it is suggested the packed mode for this stage. Also, working with the bed in packed configuration will reduce the volume of eluent used and will result in the product being eluted in a higher concentration. In addition, the flow rate for elution can be chosen regarding the bed expansion characteristics or the direction in which the bed is loaded. However, reversing the direction of flow will give more efficient removal of adsorbed components by step procedures [1, 60, 63, 69].

Finally, it becomes necessary to perform a **clean-in-place procedure**. Re-using adsorbent in multiple cycles allows a minimization of overall process costs. Clean-in-place for expanded beds needs to be more severe than performed in packed beds, since the adsorbent has been in contact with cruder feedstock. There are different procedures to achieve this goal. Firstly, pass through the column a solution containing 1M NaCl and 1M NaOH and then the solution where the adsorbent is being stored (0.2M sodium acetate with 14% of NaCl in case of MabDirect MM). There are other types of solutions that achieve similar effects such as 1M NaOH, 2M NaCl, distilled water at neutral pH, 7% ethanol, 6M urea or 30% isopropanol. If there is an efficient clean-in-place procedure, the adsorbent will regain bed-expansion and adsorption characteristics that were typical of those of the fresh adsorbent [1, 60, 63]. Figure 2.5 shows a schematic presentation of the different expanded bed adsorption stages and possible configurations.

2.4.1.2. Residence time distribution

In order to characterize the hydrodynamics of a column, the residence time distribution (*RTD*) is measured. The residence time distribution measurement procedure starts by packing the column with the adsorbent; the settled bed height and above empty space are registered at this stage and the bed is expanded until a stable expansion. Then an inert tracer (such as acetone or Blue Dextran 2000) is injected at the bottom of the column, which means that this tracer will pass through the flow-cell on the top of the column, where the tracer concentrations are monitored by UV detector at 280 nm wavelength and the absorbance signal is sent by the data-acquisition software to a personal computer [1, 60, 63].

RTD is a method commonly used to study the flow characteristics; then, using the experimental data and fitting by dispersive plug flow model, it is possible to estimate distinctive parameters (mean residence time and Péclet) that characterize the bed hydrodynamics properties [93, 109-111].

2.4.2. Case studies

In 1994, applications of expanded bed for the purification of proteins from crude feedstocks were rather scarse, although there was considerable industrial interest. First experiments in this field were based on the same conditions and used primarily adsorbents developed for packed beds.

Examples of these works, include the adsorption of bovine serum albumin (BSA) onto ion-exchanger columns [94]; affinity systems that focused on the adsorption of human immunoglobulin G onto adsorbents derivatized with protein A [105], or an affinity adsorbent

with immobilized biomimetic dyes used to purify the enzyme phosphofructokinase from non-clarified homogenates of *S. cerivisae* [94]. All of these experiments enable different stages (clarification, concentration and purification) to be achieved in a single step.

Matrices are the solid (often porous) material to which functional group ligands are coupled to obtain a chromatography medium or adsorbent [2]. Section 2.4.5 shows the differences between homemade and commercialized adsorbents for expanded bed adsorption. In that section (2.4.5.), Tables 2.2 and 2.3 show some examples.

Besides *HSA* and *IgG* that can be used as model proteins in the expanded bed adsorption technology, there are other components of equal importance that could be used in expanded bed operation, *e.g. Bovine Serum Albumin* (*BSA*) [60, 63, 112, 113], *Myoglobin* [63, 114], *lysozyme* [62, 110, 114], *Chymosin* [29], *α-lactalbumin* (ALA) [90], *Ovalbumin* (OVA) [63], *Amyloglucosidase* (AMY) [63], *α-Chymotrypsin* (CHY) [63], and others [87, 88].

2.4.3. Scale-up

Similarities between expanded bed and packed bed processes are encountered when considering scale-up. Regarding the adsorbent used, the height of adsorbent in the column should not be changed while the cross-section of the bed and the volumetric flow through the column should be increased in proportion in order to keep the same interstitial velocity [69].

The expanded bed columns are most likely to be developed with a few centimeters as diameter. Then, subsequent scale-up would pass on pilot stage using columns with diameter in order of 20 cm and only then, increasing to a size production of 1 meter or more. Due to the similarities between expanded and packed beds, stages like adsorption, washing and elution can be optimized by feeding a pre-clarified feedstock to small, laboratory-scale packed beds [69].

2.4.4. Inappropriate situations for expanded bed adsorption

There will be certain conditions where this technology will show inappropriate. Expanded bed adsorption will show up to be inefficient if there are no sufficient differences in the physical properties of the particulates (size, density) and the adsorbent beads to allow separation of these compounds in the column. Also, the linear velocity of the flow should be between the minimum fluidization velocity and the terminal velocity of the adsorbent beads, while being higher than the terminal velocity of the particulates allowing this way the possibility of the particulate material to pass through the bed while the adsorbent beads are retained within it [69].

In the specific case of great resemblance of physical properties, the separation of two types of solids can be difficult. The same happens if cells grow as large as mycelia with diameters equal or greater than the adsorbent beads. However, this could be avoided by installing in the column a mesh-screen filter prior to the expanded bed. In addition, for processing fermentation broths with very high biomass content or disrupted cell preparations of high viscosity would be unfavorable if used in expanded bed. Nonetheless, dilution of the feedstock before its application should avoid this problem. Although the consequent increase in the volume of liquid will reduce the efficiency of the expanded bed [69, 106].

Also, biomass-adsorbent adhesion promotes impaired hydrodynamics as well as adsorbent fouling, a phenomenon that is being studied by the scientific community [115].

2.4.5. Expanded bed adsorbents

The first adsorbents tested in an expanded bed column were, naturally, the adsorbents used in fixed bed adsorption. However, there were problems of separation efficiency when this kind of material was used.

The design of an adsorbent is a key factor to enhance the efficiency of expanded bed adsorption. Some parameters of the adsorbent must be taken into account, such as size, density, ligand and adsorption capacity [30]. Normally, the matrices in the adsorbent have regular spherical shape, high density, proper size and size distribution allowing this way a high operating velocity and a short processing time. Also, the adsorbent must present a high surface area, good mechanical strength and chemical stability [93, 116-118].

The manufacture of a new adsorbent is a complex task; the target molecule and the specific expanded bed system have a strong influence on the design of both the matrix and ligand.

Regarding the matrix of the adsorbent, different types have been developed. First, a single or multi-core type with low density particles as the core covered with the gel layer, then, a dispersing type with densified-powder uniformly dispersed in the polymers or gels and finally a matrix with high-density rigid porous microspheres without the polymer-coated layer designated as integrity type matrices, where the microspheres show a high mechanical strength and good chemical stability. This last type is designated as second generation adsorbent.

The *EBA* process will be more effective for those adsorbents that have both high-density base matrix and salt-tolerant ligand. The high-density matrix enables minimizing dilution of biomass or coping with viscosity in feedstock and reducing dilution buffer consumption; the lack of sensitivity of the ligand to ionic strength and salt concentration means that there is no need for dilution of feedstock [93, 119, 120].

'Homemade' adsorbents are commonly used for research purposes. Agarose and cellulose are the major components utilized on the tailoring of adsorbents. Table 2.2 shows a list of such adsorbents.

Table 2.2 – Examples of "Homemade" adsorbents.

Year	Core	Adsorbent	Reference
1994	Crystalline Quartz	6% Agarose	[106]
1994	Perfluorocarbon	Poly Vinyl Alcohol - Perfluorodecalin	[121]
1995	Crystalline Quartz - Red H-E7B	6% Agarose	[122]
1995	Perfluorocarbon	Poly Vinyl Alcohol - Perfluoropolymer	[123]
1996	Crystalline Quartz - Cibacron blue (3GA)	6% Agarose	[124]
1997	Fluoride-modified porous zirconium oxide core		[125]
1999	Polyacrylamide gel	Silica	[126]
1999	Glass	Agarose	[127]
2000	Celbeads*	Cellulose	[117]
2000	Stainless Steel	Agarose	[93]
2001	Celbeads*	Cellulose	[128]
2001	Nd-Fe-B alloy Powder	Agarose	[129]
2002	Stainless Steel	6% Agarose	[130]
2002	Stainless Steel	6% Agarose	[131]
2002	Crystalline Quartz	6% Agarose (Streamline DEAE) modified with a layer of polyacrylic acid (PAA)	[132]
2002	Nd-Fe-B with Cibacron Blue 3GA (CB)	4% Agarose	[133]
2002	Zirconia-silica (ZSA)	4% Agarose	[61]
	ZSA - Cibracron Blue (CB)	4% Agarose	
2003	Zirconia-silica (ZSA)	Agarose	[134]
2003	CB-6AS	Cellulose	[135]
2003	Titanium Oxide	Cellulose	[112]
2004	Glass	4% Agarose	[136]
2005	Titanium Oxide	Cellulose	[137]
2005	Stainless Steel Powder	Cellulose	[138]
2006	Stainless Steel Powder	Cellulose	[139]
2007	Nickel Powder	Cellulose	[140]
2007	Tungsten Carbide	Cellulose	[141]

2008	Tungsten Carbide	Cellulose	[142]
2008	Stainless Steel Powder with benzyl amine (Mixed Mode)	Cellulose	[143]
2008	Zirconia-Silica	Agarose	[144]
2009	Zirconium Dioxide	Poly glycidyl methacrylate β-cyclodextrin	[145]
2009	Tungsten Carbide	β-cyclodextrin polymer	[146]
2010	Tungsten Carbide	β-cyclodextrin polymer	[147]
2010	Tungsten Carbide	Agarose	[148]
2011	Tungsten Carbide	Cellulose	[149]
2012	Nickel (Nanoporous)	Agarose	[120]
2012	Zinc (Nanoporous)	Agarose	[119]
2013	Tungsten Carbide	3% Agarose	[150]
2013	Titanium Dioxide	Polyacrylamide based Cryogel	[151]
2014	Nickel	Agarose	[152]
2015	Tungsten Carbide	Agarose	[153]
2017	Tungsten Carbide	Agarose	[154]
2018	Nickel	Agarose	[155]

* Celbeads = Rigid spherical macroporous adsorbent beads with surface of hydroxyl groups.

The drawback of agarose/cellulose based adsorbents is their low density. Therefore, EBA adsorbents were developed by incorporating a dense solid material in the beads. Table 2.3 shows a list of commercial adsorbents tested by different researchers through the years.

Table 2.3 – Examples of commercialized adsorbents.

Year	Core	Adsorbent	Commercialized Series	Reference
1995	Crystalline Quartz	6% cross-linked agarose	Streamline DEAE	[156]
1995	Crystalline Quartz	6% cross-linked agarose	Streamline SP	[157]
1996	Crystalline Quartz	6% cross-linked agarose	Streamline DEAE	[158]
1996	Crystalline Quartz	6% cross-linked agarose	Streamline SP	[114]
1996	Crystalline Quartz	4% cross-linked agarose	Streamline r-Protein A	[111]
1997	Crystalline Quartz	6% cross-linked agarose	Streamline DEAE	[159]
1997	Crystalline Quartz	6% cross-linked agarose	Streamline Phenyl	[160]
1998			DEAE Spherodex LS	[161]
1999	Crystalline Quartz	Agarose	Streamline DEAE DEAE Spherodex LS	[162]
1999	Crystalline Quartz	Agarose	Streamline DEAE	[163]
1999	Crystalline Quartz	6% cross-linked agarose	Streamline SP	[164]

Year	Core	Adsorbent	Commercialized Series	Reference
	Crystalline Quartz	6% cross-linked agarose	Streamline DEAE	
	Crystalline Quartz	6% cross-linked agarose	Streamline Chelating	
1999	Crystalline Quartz	6% cross-linked agarose	Streamline SP	[165]
	Crystalline Quartz	6% cross-linked agarose	Streamline Q XL	
2000	Crystalline Quartz	6% cross-linked agarose	Streamline Phenyl	[76]
2000	Crystalline Quartz	6% cross-linked agarose	Streamline Chelating	[166]
2001	Crystalline Quartz	6% cross-linked agarose	Streamline SP	[167]
	Porous Ceramic	Hydrogel	S Ceramic HyperD LS	
2001	Crystalline Quartz	6% cross-linked agarose	Streamline DEAE	[168]
			DEAE Spharose FF	
2001	Crystalline Quartz	6% cross-linked agarose	Streamline DEAE	[128]
	Crystalline Quartz	6% cross-linked agarose	Streamline SP	
2001	Crystalline Quartz	6% cross-linked agarose	Streamline SP	[129]
2001	Crystalline Quartz	6% cross-linked agarose	Streamline Q XL	[169]
2001	Crystalline Quartz	6% cross-linked agarose	Streamline SP	[110]
	Crystalline Quartz	6% cross-linked agarose	Streamline DEAE	
2002	Crystalline Quartz	6% cross-linked agarose	Streamline SP	[170]
	Crystalline Quartz	6% cross-linked agarose	Streamline DEAE	
2002	Crystalline Quartz	6% cross-linked agarose	Streamline	[131]
2002	Crystalline Quartz	6% cross-linked agarose	Streamline SP	[171]
	Crystalline Quartz	6% cross-linked agarose	Streamline Q XL	
2002	Crystalline Quartz	6% cross-linked agarose	Streamline DEAE	[130]
	Crystalline Quartz	6% cross-linked agarose	Streamline Q XL	
	Glass	6% cross-linked agarose	UFC DEAE/PEI	
2002	Crystalline Quartz	6% cross-linked agarose	Streamline	[61]
	Kieselguhr particles	4% cross-linked agarose	Macrosorb K4AX	
2003			DEAE Spherodex M	[172]
2003	Crystalline Quartz	6% cross-linked agarose	Streamline DEAE	[99]
2003			DEAE Spharose FF	[173]
	Crystalline Quartz	6% cross-linked agarose	Streamline DEAE	
2004	Crystalline Quartz	6% cross-linked agarose	Streamline SP	[101]
2004	Crystalline Quartz	6% cross-linked agarose	Streamline SP	[174]
2004	Tungsten Carbide	Agarose	Rhobust Fastline SP	[175]
2004	Tungsten Carbide	Agarose	Rhobust Fastline SP	[176]

Year	Core	Adsorbent	Commercialized Series	Reference
2005	Stainless Steel	4% cross-linked agarose	Streamline Direct CST-I	[60]
	Crystalline Quartz	6% cross-linked agarose	Streamline DEAE	
2005	Crystalline Quartz	6% cross-linked agarose	Streamline DEAE	[102]
	Crystalline Quartz	6% cross-linked agarose	Streamline SP	
2006	Stainless Steel	4% cross-linked agarose	Streamline Direct CST-I	[63]
2006	Crystalline Quartz	6% cross-linked agarose	Streamline DEAE	[177]
2007	Zirconium Oxide	Hydrogel-filled	Q/CM HyperZ	[178]
2007	Stainless Steel	Agarose	Streamline Direct HST	[113]
2008	Crystalline Quartz Nickel	6% cross-linked agarose	Streamline Chelating	[179]
2008	Crystalline Quartz	6% cross-linked agarose	Streamline DEAE	[144]
	Zirconium oxide	Hydrogel-filled	CM-HyperZ	
2009	Stainless Steel	Agarose	Streamline Direct HST	[180]
2009	Macroporous acrylic polymer		Amberlite XAD7HP	[181]
2010	Crystalline Quartz	6% cross-linked agarose	Streamline Chelating	[182]
2010	Crystalline Quartz	6% cross-linked agarose	Streamline Phenyl	[183]
2011	Crystalline Quartz	6% cross-linked agarose	Streamline DEAE	[184]
2011	Zirconium Oxide	Hydrogel-filled	CM HyperZ	[185]
2012	Crystalline Quartz	6% cross-linked agarose	Streamline DEAE	[186]
	Crystalline Quartz	6% cross-linked agarose cover with polyvinyl pyrrolidone	Streamline DEAE modified	
2013	Tungsten Carbide	6% cross-linked agarose	Fastline HSA	[87]
	Tungsten Carbide	Agarose	MabDirect MM	
	Zirconium Oxide	Hydrogel-filled	CM HyperZ	
2013	Crystalline Quartz	6% cross-linked agarose	Streamline Q XL	[103]
2013	Tungsten Carbide	Agarose	Rhobust Fastline SP	[85]
2013	Tungsten Carbide	Agarose	MabDirect Protein A	[187]
2013	Tungsten Carbide	Agarose	MabDirect MM	[88]
2014	Crystalline Quartz	6% cross-linked agarose	Rhobust Fastline SP	[188]
	Stainless Steel	Agarose	Streamline Direct HST	
2015	Tungsten Carbide	Agarose	Rhobust Fastline SP	[189]
	Tungsten Carbide	Agarose	Rhobust Fastline DEAE	
	Tungsten Carbide	Agarose	MabDirect Protein A	
2016		Macroporous highly crosslinked polymer	Nuvia cPrime	[190]

Year	Core	Adsorbent	Commercialized Series	Reference
2016		Agarose	Capto MMC	[191]
2017	Tungsten Carbide	Agarose	MabDirect Protein A	[192]
2018	Stainless Steel	Agarose	Streamline Direct HST	[193]

Adsorbents used in EBA have been developed by some major companies as shown in Table 2.4.

Table 2.4 – Commercialized adsorbents by companies.

Manufacturers	Adsorbent		Matrix
GE Healthcare	Streamline Series	Q XL	6% cross-linked agarose containing a quartz core with dextran surface extended.
		XL	
		DEAE	6% cross-linked agarose containing a quartz core.
		SP	
		Phenyl	
		Heparin	
		Chelating	
		rProtein A	4% highly cross-linked agarose containing a quartz core.
		Direct CST-I	4% cross-linked agarose containing stainless steel core.
DSM Biologics	Rhobust Fastline Series		Cross-linked agarose containing a tungsten carbide particles.
	MabDirect Protein A/MM		
Pall BioSepra Corporation	DEAE – Spherodex LS		The porous silica matrix is coated with a continuous layer of ionizable dextran to yield high exchange capacity and improved stability.
	DEAE – Spherodex M		
	CM/S/Q/DEAE – Ceramic HyperD F		Hydrogel polymer with porous ceramic beads.
	Lysine HyperD		Hydrogel polymer within the large pores of rigid beads.
	Heparin HyperD M		Porous rigid mineral bead containing heparin, hydrogel filled pores.
	Q/CM HyperZ		Hydrogel-filled porous with zirconium oxide particles.

The names of the adsorbents are influenced by the ligand used, for example, Diethylaminoethyl (DEAE), Sulphopropyl (SP), Quaternary amine (Q), Recombinant protein A

(r-Protein A), Imino diacetic acid (Chelating), Multi-modal function (Direct CST I and MM), Carboxymethyl (CM) and Polyethyleneimine (PEI) [93, 111, 159].

GE Healthcares (that acquired *Amersham Pharmacia Biotech*) and *DSM Biologics* are examples of companies that already worldwide commercialize and distribute adsorbents. *GE Healthcares* with the Streamline series and *DSM Biologics* with the Rhobust Fastline series (previously owned by *UpFront Chromatography A/S*) are good references for adsorbents in the market.

MabDirect MM is an adsorbent from *Rhobust Fastline series* that is composed by a base matrix of 6% cross-linked agarose with a tungsten carbide particles. The MM ligand have a *pka* near 5.0 and contains some hydrophobic (benzoic acid) regions [87, 88, 194]. MabDirect Protein A adsorbent, also from *Rhobust Fastline series* of *DSM Biologics*, has a binding capacity of Human IgG of 2 - 40 $g.L^{-1}$. Protein A adsorbents present a single polypeptide chain (46.7 kDa) and specific interaction with Immunoglobulin G, making this a very effective ligand for affinity chromatography of this protein from the serum of many species [25].

Mixed mode adsorbents comprise low molecular weight ligands that have both hydrophobic (e.g., aromatic structure) and hydrophilic domains (e.g., amino groups) within the same molecule [65, 195, 196]. At low ionic strength, the charged domain of the ligand implements the ion-exchange adsorption of the target protein, but as the ionic strength increases the hydrophobic domain of the ligand allows hydrophobic interactions to occur in salt-tolerant adsorption. In contrast to ion-exchangers, the binding strength is strongly pH dependent and largely independent of ionic strength in the raw material [146, 195, 197].

The trend is to use a dense solid material to allow processing of higher flow rates and therefore reach a better productivity. In the EBA, it is expected that the adsorbent follows a regular pattern, i.e., the matrix beads will have an appropriate size distribution where the larger or denser particles will be near the bottom of the column while the smaller or less dense particles nearer the top [93, 119, 120].

2.4.6. Adsorbents for HSA and IgG adsorption

Since Human Serum Albumin and Immunoglobulin G are the chosen target proteins to be tested, Table 2.5 and 2.6 show the attention paid to them by the scientific community through the years, where it is specified the adsorbent used, the extraction source and the technique used to do so.

Table 2.5 – Study examples of HSA as the model protein by different techniques.

Year	Source	Adsorbents	Technique	Reference
1989	Protein within a buffer solution	Blue-Sepharose CL-6B	Affinity chromatography	[79]
1992	Blood plasma	Perfluorocarbon affinity emulsion	Affinity chromatography	[198]
1996	HSA solution	Silica- and zirconia-based ion-exchange	Ion Exchange chromatography	[199]
1998	Crude mixture of Human plasma	DEAE Spherodex LS	Mixed-mode chromatography	[161]
1999	High cell density yeast suspensions	Mixed-mode fluoride-modified zirconia particles	Mixed-mode chromatography	[200]
2001	Egg white Commercial HSA solution	Continuous rod of macroporous poly(glycidyl methacrylate-co-ethylene dimethacrylate) with iminodiacetic acid (IDA) chelates.	Immobilized metal affinity chromatography	[201]
2004	Protein within a buffer solution	pHEMA-RY-2 pHEMA/chitosan-RY-2	Affinity membranes	[202]
2007	Human plasma	Cibacron Blue F3GA and Zn(II) derived microporous membranous poly(tetrafluoroethylene) capillaries which are modified by poly(vinyl alcohol) coating	Membranous capillary	[203]
2010	Human plasma	Superdex 75 / Sephadex G25 DEAE Sepharose FF Octyl-Sepharose 4 FF Heparin Sepharose 6 FF	Gel filtration Ion Exchange Hydrophobic interaction Heparin affinity chromatography	[204]
2012	Protein within a buffer solution	DEAE Bestarose 2.5HF, 4FF and 6FF	Ion exchange chromatography	[205]
2014	Protein within a buffer solution	Convective interaction media r-protein A monolithic column	Affinity chromatography	[206]
2014	Protein within a buffer solution	Nuvia cPrime	Mixed-Mode Chromatography	[207]
2015	Protein within a buffer solution	Agarose with tungsten carbide particles (T-MEP and T-ABI)	Hydrophobic charge-induction chromatography	[153]
2016	Protein within a buffer solution	Nuvia cPrime	Mixed-Mode Chromatography	[190]
2017	Protein within a buffer solution	Agarose beads with typtophan analogues	Mixed-Mode Chromatography	[208]
2018	Protein within a buffer solution	Synthesized hydroxide double layer	Ion exchange chromatography	[209]

Table 2.6 – Study examples of IgG as the model protein by different techniques.

Year	Source	Adsorbents	Technique	Reference
1983	Protein within a buffer solution; Sheep serum	Cyanogen bromide-activated Sepharose 4B	Immuno-adsorption chromatography	[210]
1999	Cell culture broth	Streamline rProtein A	Affinity chromatography	[211]
1999	Cell culture broth	Streamline rProtein A	Affinity chromatography	[212]
2005	BSA and the binary mixture of IgG and BSA	DEAE Spharose FF	Ion-exchange electro-chromatography	[213]
2006	Human serum	Glycidiyl methacrylate and methyl methacrylate beads where epoxy groups were converted into amino groups by reaction of ammonia or 1,6-diaminohexane as space-armwith L-histidine ligand	Affinity Chromatography	[214]
2007	Filtered Cell culture supernatant	MabSelect Protein A	Protein A affinity chromatography	[215]
		Q Spharose XL	Anion-exchange chromatography	
		SP Spharose FF	Cation-exchange chromatography	
2009	Protein within a buffer solution	Reactive Green 5 immobilized onto a Streamline adsorbent	Affinity Chromatography	[216]
2010	Human plasma	High-density modified agarose/tungsten carbide beads	Mixed-Mode Chromatography	[148]
2012	Mouse serum	Solid nickel ferromagnetic particles coated with Protein A	Affinity Chromatography	[217]
2012	Human plasma	Concanavalin A (Con A) immobilized magnetic poly(glycidyl methacrylate) (mPGMA) beads in monosize and spherical for (1.62 μm in diameter)	Affinity Chromatography	[218]
2013	IgG, BSA, and the binary mixture of IgG and BSA	4 mixed-mode resin with the following ligands: N-benzyl-N-methyl ethanol amine; 2-benzamido-4-mercaptobutanoic acide; 4-mercapto-ethyl-pyridine; phenylpropylamine	Mixed-Mode Chromatography	[219]
2013	Porcine plasma	Cellulose matrix with divinylsulfone (DVS) with 2-mercaptoimidazole as ligand	Hydrophobic Charge Induction Chromatography	[220]
2014	Crude sweet whey	Fastline SP Streamline Direct CST-I	Mixed-Mode Chromatography	[188]
2014	Protein within a buffer solution	Nuvia cPrime	Mixed-Mode Chromatography	[207]
2015	Protein within a buffer solution	Agarose with tungsten carbide particles (T-MEP and T-ABI)	Hydrophobic charge-induction chromatography	[153]
2016	Protein within a buffer solution	Nuvia cPrime	Mixed-Mode Chromatography	[190]
2017	Protein within a buffer solution	MabDirect	Affinity Chromatography	[192]
2018	Protein within a buffer solution	Synthesized hydroxide double layer	Ion exchange chromatography	[209]

2.5. Conclusions

There is no higher priority than the preservation of Human health. Proteins, among other components, perform an important role to achieve this objective, and therefore, they have great importance in the pharmaceutical industry. Proteins separation and purification became a fundamental prerequisite for any pharmaceutical industry.

When performing proteins separation there is a need to ensure that all impurities from the feedstock are removed and that the sufficient amounts of highly purified protein is efficiently obtained to reduce the production costs. Different techniques were developed through the years; some are still being used (Fixed Bed Adsorption), while others were developed (Expanded bed Adsorption).

Adsorption in expanded bed is an efficient way of proteins purification from a variety of feedstocks that contain particulates. The manufacturing of purpose-designed adsorbents and expanded bed systems enabled the number of separation stages required in a downstream-processing flow sheet to be reduced. The ability of confining 3 different stages (clarification, concentration and purification) in one single step process is the key advantage for costs reduction of proteins recovery [69].

Mixed mode chromatography, i.e. the employment of adsorbents that take advantage of different types of interactions (hydrophobic, electrostatic, hydrogen bonds among others) for binding distinctive target proteins, is a complex process. The understanding of the adsorption mechanism on this type of chromatography is difficult but yet possible. Many researchers already developed models enabling the study of the influence of different factors on adsorption and desorption processes.

Each adsorbate/adsorbent system is unique, i.e., association of different target proteins to the same adsorbent will produce different results (adsorbent capacity); the same happens for the same target protein onto different adsorbents. Across the years, different target proteins have been studied by researchers. Albumin and Immunoglobulin are the main types of proteins on blood serum and by this reason the most studied. On this thesis, Human Serum Albumin and Immunoglobulin G are the model target proteins chosen. There is a wide range of adsorbents that can be used. MabDirect Mixed Mode is the most recent developed among them and by this reason it was selected. To the best of the author knowledge, adsorbate/adsorbent systems using these target proteins and adsorbent were not studied so far.

2.6. Nomenclature

AC	–	Affinity Chromatography
BSA	–	Bovine Serum Albumin
CZE	–	Capillary Zone Electrophoresis
DNA	–	Deoxyribonucleic Acid
EBA	–	Expanded bed Adsorption
FPLC	–	Fast Protein Liquid Chromatography
HIC	–	Hydrophobic Interaction Chromatography
HPLC	–	High-Performance Liquid Chromatography
HSA	–	Human Serum Albumin
IEX	–	Ion Exchange Chromatography
Ig	–	Immunoglobulin
IgG	–	Immunoglobulin G
IMAC	–	Immobilized Metal Ion Affinity Chromatography
mAb	–	Monoclonal Antibody
MMC	–	Mixed Mode Chromatography
RPLC	–	Reverse Phase Liquid Chromatography
RTD	–	Residence Time Distribution
SEC	–	Size Exclusion Chromatography
SDS-PAGE	–	Sodium Dodecyl Sulfate - Polyacrylamide Gel Electrophoresis

2.7. References

[1] P. Li, Protein Separation and Purification by Expanded Bed Chromatography and Simulated Moving Bed Technology, in: Ph.D. Thesis, Department of Chemical Engineering, Faculty of Engineering University of Porto, Portugal, 2006.

[2] Strategies for protein Purification handbook, in, GE Healthcare Bio-Science AB, Sweden, 2010.

[3] The Nobel Prize in Chemistry 1902, http://www.nobelprize.org/nobel_prizes/chemistry/laureates/1902/fischer-bio.html. (Accessed in 15.07.2014)

[4] L.K. James, Nobel laureates in chemistry, 1901-1992, Chemical Heritage Foundation, 1993.

[5] L. Rosenfeld, Origins of Clinical Chemistry: The Evolution of Protein Analysis, Elsevier Science, 2012.

[6] J.B. Sumner, The Isolation and Crystallization of the Enzyme Urease, Journal of Biological Chemistry, 69 (1926) 435-441.

[7] L. Pauling, R.B. Corey, H.R. Branson, The structure of proteins: Two hydrogen-bonded helical configurations of the polypeptide chain, Proceedings of the National Academy of Sciences, 37 (1951) 205-211.

[8] L. Pauling, R.B. Corey, Configurations of polypeptide chains with favored orientations around single bonds: two new pleated sheets, Proceedings of the National Academy of Sciences of the United States of America, 37 (1951) 729.

[9] L. Pauling, R.B. Corey, Atomic coordinates and structure factors for two helical configurations of polypeptide chains, Proceedings of the National Academy of Sciences USA, 37 (1951) 235-240.

[10] M. Sela, F.H. White Jr, C.B. Anfinsen, Reductive cleavage of disulfide bridges in ribonuclease, Science, 125 (1957) 691-692.

[11] C.B. Anfinsen, Studies on the principles that govern the folding of protein chains, Nobel Lecture, Chemistry (1972) 55-71.

[12] J.C. Kendrew, G. Bodo, H.M. Dintzis, R. Parrish, H. Wyckoff, D. Phillips, A three-dimensional model of the myoglobin molecule obtained by x-ray analysis, Nature, 181 (1958) 662-666.

[13] D. Green, V. Ingram, M. Perutz, The structure of haemoglobin. IV. Sign determination by the isomorphous replacement method, Proceedings of the Royal Society of London. Series A. Mathematical and Physical Sciences, 225 (1954) 287-307.

[14] M. Mayani, K. Mohanty, C. Filipe, R. Ghosh, Continuous fractionation of plasma proteins HSA and HIgG using cascade ultrafiltration systems, Separation and Purification Technology, 70 (2009) 231-241.

[15] J.W. Park, J. Smolen, Monoclonal antibody therapy, in: M.S. Edward (Ed.) Advances in Protein Chemistry, Academic Press, 2001, 369-421.

[16] J.G. Elvin, R.G. Couston, C.F. van der Walle, Therapeutic antibodies: Market considerations, disease targets and bioprocessing, International Journal of Pharmaceutics, 440 (2013) 83-98.

[17] Zion-Market-Research, Global Monoclonal Antibody Therapeutics Market Will Reach USD 218.97 Billion by 2023: Zion Market Research, https://goo.gl/gAwqK7. (Accessed in 30.07.2018)

[18] NASA-Spinoff, Health and Medicine: Protein Innovations Advance Drug Treatments, Skin Care, http://spinoff.nasa.gov/Spinoff2011/hm_4.html. (Accessed in 4.6.2014)

[19] D.C. Carter, J.X. Ho, Structure of serum albumin, Advances in Protein Chemistry, 45 (1994) 153-203.

[20] T. Peters Jr, The Albumin Molecule: Its Structure and Chemical Properties, in: T. Peters (Ed.) All About Albumin, Academic Press, San Diego, 1995, 9-11.

[21] G. Fanali, A. di Masi, V. Trezza, M. Marino, M. Fasano, P. Ascenzi, Human serum albumin: From bench to bedside, Molecular Aspects of Medicine, 33 (2012) 209-290.

[22] M. Dockal, D.C. Carter, F. Ruker, The three recombinant domains of human serum albumin. Structural characterization and ligand binding properties, Journal of Biological Chemistry, 274 (1999) 29303-29310.

[23] X.M. He, D.C. Carter, Atomic Structure and chemistry of human serum albumin, Nature Publishing Group, 358 (1992) 209-215.

[24] J. Stadlmann, M. Pabst, D. Kolarich, R. Kunert, F. Altmann, Analysis of immunoglobulin glycosylation by LC-ESI-MS of glycopeptides and oligosaccharides, Proteomics, 8 (2008) 2858-2871.

[25] Antibody Production and Purification Technical Handbook, in, Thermo Scientific Pierce 2010.

[26] L. Rosenfeld, Justus Liebig and animal chemistry, Clinical chemistry, 49 (2003) 1696-1707.

[27] R. Kohler, The background to Eduard Buchner's discovery of cell-free fermentation, Journal of the History of Biology, 4 (1971) 35-61.

[28] J.A. Huntington, P.E. Stein, Structure and properties of ovalbumin, Journal of Chromatography B: Biomedical Sciences and Applications, 756 (2001) 189-198.

[29] E.J. Cohn, L.E. Strong, W. Hughes, D. Mulford, J. Ashworth, M.e. Melin, H. Taylor, Preparation and Properties of Serum and Plasma Proteins. IV. A System for the Separation into Fractions of the Protein and Lipoprotein Components of Biological Tissues and Fluids1a, b, c, d, Journal of the American Chemical Society, 68 (1946) 459-475.

[30] M. Tswett, Physikalisch-chemische Studien über das Chlorophyll. Die Adsorptionen, Berichte der Deutschen Botanischen Gesellschaft, 24 (1906) 316-323.

[31] P.-Å. Albertsson, The contribution of photosynthetic pigments to the development of biochemical separation methods: 1900–1980, Photosynthesis Research, 76 (2003) 217-225.

[32] D. Buzzi, Solid-phase affinity purification of antibodies for the detection of BDNF isoforms, in: Ph.D. Thesis, Università degli studi di Trieste, Italy, 2013.

[33] G. Zhao, X.-Y. Dong, Y. Sun, Ligands for mixed-mode protein chromatography: Principles, characteristics and design, Journal of Biotechnology, 144 (2009) 3-11.

[34] D. Perrett, From ‘protein’ to the beginnings of clinical proteomics, Proteomics: Clinical Applications, 1 (2007) 720-738.

[35] A.D. Sheftel, A.B. Mason, P. Ponka, The long history of iron in the Universe and in health and disease, Biochimica et Biophysica Acta (BBA) - General Subjects, 1820 (2012) 161-187.

[36] J. Porath, P. Flodin, Gel filtration: a method for desalting and group separation, Nature, 183 (1959) 1657-1659.

[37] P. Flodin, J. Porath, B. Ingelman, Fifty years of Sephadex a springboard to innovation, Nature Publishing Group, 183 (1959) 1657-1659.

[38] L. Wide, R. Axén, J. Porath, Radioimmunosorbent assay for proteins. Chemical couplings of antibodies to insoluble dextran, Immunochemistry, 4 (1967) 381-386.

[39] R. Axen, J. Porath, S. Ernback, Chemical coupling of peptides and proteins to polysaccharides by means of cyanogen halides, Nature Publishing Group, 214 (1967) 1302-1304.

[40] P. Cuatrecasas, M. Wilchek, C.B. Anfinsen, Selective enzyme purification by affinity chromatography, Proceedings of the National Academy of Sciences U S A, 61 (1968) 636-643.

[41] J. Kohn, M. Wilchek, The use of cyanogen bromide and other novel cyanylating agents for the activation of polysaccharide resins, Applied Biochemistry and Biotechnology, 9 (1984) 285-305.

[42] A.J. Martin, R.L. Synge, A new form of chromatogram employing two liquid phases: A theory of chromatography. 2. Application to the micro-determination of the higher monoamino-acids in proteins, Biochemical Journal, 35 (1941) 1358-1368.

[43] H. Hjelm, K. Hjelm, J. Sjoquist, Protein A from Staphylococcus aureus. Its isolation by affinity chromatography and its use as an immunosorbent for isolation of immunoglobulins, Federation of European Biochemical Societies Letters, 28 (1972) 73-76.

[44] A. Zider, D. Drakeman, The future of monoclonal antibody technology, mAbs - Landes Bioscience, 2 (2010) 361-364.

[45] M. Mann, P. Højrup, P. Roepstorff, Use of mass spectrometric molecular weight information to identify proteins in sequence databases, Biological Mass Spectrometry, 22 (1993) 338-345.

[46] M.R. Wilkins, J.-C. Sanchez, A.A. Gooley, R.D. Appel, I. Humphery-Smith, D.F. Hochstrasser, K.L. Williams, Progress with proteome projects: why all proteins expressed by a genome should be identified and how to do it, Biotechnology and genetic engineering reviews, 13 (1996) 19-50.

[47] J. Crowther, R. Hartwick, Chemically bonded multifunctional stationary phases for high-performance liquid chromatography, Chromatographia, 16 (1982) 349-353.

[48] R. Bischoff, L.W. McLaughlin, Mixed-Mode chromatographic matrices for the resolution of transfer ribonucleic acids, Journal of Chromatography A, 317 (1984) 251-261.

[49] B.-Y. Zhu, C.T. Mant, R.S. Hodges, Mixed-mode hydrophilic and ionic interaction chromatography rivals reversed-phase liquid chromatography for the separation of peptides, Journal of Chromatography A, 594 (1992) 75-86.

[50] Z. Er-el, Y. Zaidenzaig, S. Shaltiel, Hydrocarbon-coated Sepharoses. Use in the purification of glycogen phosphorylase, Biochemical and Biophysical Research Communications, 49 (1972) 383-390.

[51] R.J. Yon, Chromatography of lipophilic proteins on adsorbents containing mixed hydrophobic and ionic groups, Biochemical Journal, 126 (1972) 765-767.

[52] B.H.J. Hofstee, Hydrophobic affinity chromatography of proteins, Analytical Biochemistry, 52 (1973) 430-448.

[53] B.H.J. Hofstee, Protein binding by agarose carrying hydrophobic groups in conjunction with charges, Biochemical and Biophysical Research Communications, 50 (1973) 751-757.

[54] S. Shaltiel, Z. Er-El, Hydrophobic chromatography: use for purification of glycogen synthetase, National Academy of Sciences U.S.A. , 70 (1973) 778–781.

[55] S. Burton, D. Harding, Hydrophobic charge induction chromatography: salt independent protein adsorption and facile elution with aqueous buffers, Journal of Chromatography A, 814 (1998) 71-81.

[56] M. Schmidt, M. Hafner, C. Frech, Modeling of salt and pH gradient elution in ion-exchange chromatography, Journal of Separation Science, 37 (2014) 5-13.

[57] J.A. Queiroz, C.T. Tomaz, J.M.S. Cabral, Hydrophobic interaction chromatography of proteins, Journal of Biotechnology, 87 (2001) 143-159.

[58] B.K. Nfor, N.N. Hylkema, K.R. Wiedhaup, P.D.E.M. Verhaert, L.A.M. van der Wielen, M. Ottens, High-throughput protein precipitation and hydrophobic interaction chromatography: Salt effects and thermodynamic interrelation, Journal of Chromatography A, 1218 (2011) 8958-8973.

[59] B.L. Johansson, M. Belew, S. Eriksson, G. Glad, O. Lind, J.L. Maloisel, N. Norrman, Preparation and characterization of prototypes for multi-modal separation aimed for capture of positively charged biomolecules at high-salt conditions, Journal of Chromatography A, 1016 (2003) 35-49.

[60] P. Li, G. Xiu, A.E. Rodrigues, Experimental and modeling study of protein adsorption in expanded bed, American Institute of Chemical Engineers Journal, 51 (2005) 2965-2977.

[61] M. Jahanshahi, Y. Sun, E. Santos, A. Pacek, T. Teixera Franco, A. Nienow, A. Lyddiatt, Operational intensification by direct product sequestration from cell disruptates: Application of a pellicular adsorbent in a mechanically integrated disruption-fluidised bed adsorption process, Biotechnology and Bioengineering, 80 (2002) 201-212.

[62] B.K. Nfor, M. Noverraz, S. Chilamkurthi, P.D.E.M. Verhaert, L.A.M. van der Wielen, M. Ottens, High-throughput isotherm determination and thermodynamic modeling of protein adsorption on mixed mode adsorbents, Journal of Chromatography A, 1217 (2010) 6829-6850.

[63] P. Li, G. Xiu, V.G. Mata, C.A. Grande, A.E. Rodrigues, Expanded bed adsorption/desorption of proteins with Streamline Direct CST I adsorbent, Biotechnology and Bioengineering, 94 (2006) 1155-1163.

[64] B.L. Johansson, M. Belew, S. Eriksson, G. Glad, O. Lind, J.L. Maloisel, N. Norrman, Preparation and characterization of prototypes for multi-modal separation aimed for capture of positively charged biomolecules at high-salt conditions, Journal of Chromatography A, 1016 (2003) 35-49.

[65] D. Gao, D.-Q. Lin, S.-J. Yao, Protein adsorption kinetics of mixed-mode adsorbent with benzylamine as functional ligand, Chemical Engineering Science, 61 (2006) 7260-7268.

[66] J. Pezzini, G. Joucla, R. Gantier, M. Toueille, A.-M. Lomenech, C. Le Sénéchal, B. Garbay, X. Santarelli, C. Cabanne, Antibody capture by mixed-mode chromatography: A comprehensive

study from determination of optimal purification conditions to identification of contaminating host cell proteins, Journal of Chromatography A, 1218 (2011) 8197-8208.

[67] M. Du, C.-P. Li, C.-S. Liu, S.-M. Fang, Design and construction of coordination polymers with mixed-ligand synthetic strategy, Coordination Chemistry Reviews, 257 (2013) 1282-1305.

[68] K. Shams, S. Najari, Dynamics of intraparticle desorption and chemical reaction in fixed-beds using inert core spherical particles, Chemical Engineering Journal, 172 (2011) 500-506.

[69] H.A. Chase, Purification of Proteins by Adsorption Chromatography in Expanded Beds, Trends in Biotechnology, 12 (1994) 296-303.

[70] M.A. Fernandez, G. Carta, Characterization of protein adsorption by composite silica-polyacrylamide gel anion exchangers I. Equilibrium and mass transfer in agitated contactors, Journal of Chromatography A, 746 (1996) 169-183.

[71] G. Garke, R. Hartmann, N. Papamichael, W.-D. Deckwer, F.B. Anspach, The Influence of Protein Size on Adsorption Kinetics and Equilibria in Ion-Exchange Chromatography, Separation Science and Technology, 34 (1999) 2521-2538.

[72] A.K. Hunter, G. Carta, Protein adsorption on novel acrylamido-based polymeric ion-exchangers: IV. Effects of protein size on adsorption capacity and rate, Journal of Chromatography A, 971 (2002) 105-116.

[73] S. Zhang, Y. Sun, Ionic strength dependence of protein adsorption to dye-ligand adsorbents, American Institute of Chemical Engineers Journal, 48 (2002) 178-186.

[74] R.O. Owen, H.A. Chase, Modeling of the continuous counter-current expanded bed adsorber for the purification of proteins, Chemical Engineering Science, 54 (1999) 3765-3781.

[75] Q.-Y. Du, D.-Q. Lin, Z.-S. Xiong, S.-J. Yao, One-Step Purification of Lactoferrin from Crude Sweet Whey Using Cation-Exchange Expanded Bed Adsorption, Industrial & Engineering Chemistry Research, 52 (2013) 2693-2699.

[76] N.A. Willoughby, R. Hjorth, N.J. Titchener-Hooker, Experimental measurement of particle size distribution and voidage in an expanded bed adsorption system, Biotechnology and Bioengineering, 69 (2000) 648-653.

[77] M.A. Hashim, K.H. Chu, P.S. Tsan, Modelling of protein adsorption in a Fixed-Bed: Single and Two-solute breakthrough behaviour, Chemical Engineering Communications, 161 (1997) 45-63.

[78] I. Fischer, M. Franzreb, Removal of the nonionic surfactant Eumulgin ES from protein solutions by means of adsorption and ultrafiltration, Separation and Purification Technology, 118 (2013) 217-225.

[79] B.L. Yang, M. Goto, S. Goto, Affinity separation by the combined process of batch adsorption and fixed bed elution, Colloids and Surfaces, 37 (1989) 369-378.

[80] H.A. Chase, Affinity separations utilising immobilised monoclonal antibodies-a new tool for the biochemical engineer, Chemical Engineering Science, 39 (1984) 1099-1125.

[81] W. Somers, K. Van 't Reit, H. Rozie, F.M. Rombouts, J. Visser, Isolation and purification of endo-polygalacturonase by affinity chromatography in a fluidized bed reactor, Chemical Engineering Journal, 40 (1989) B7-B19.

[82] L. Uzun, A. Denizli, Bilirubin removal performance of immobilized albumin in a magnetically stabilized fluidized bed, Journal of Biomaterials Science, Polymer Edition, 17 (2006) 791-806.

[83] J. Mazumder, J. Zhu, A.K. Ray, Optimal design of liquid-solid circulating fluidized bed for continuous protein recovery, Powder Technology, 199 (2010) 32-47.

[84] R. Hjorth, Expanded-bed adsorption in industrial bioprocessing: Recent developments, Trends in Biotechnology, 15 (1997) 230-235.

[85] Q.-Y. Du, D.-Q. Lin, Z.-S. Xiong, S.-J. Yao, One-Step Purification of Lactoferrin from Crude Sweet Whey Using Cation-Exchange Expanded Bed Adsorption, Industrial & Engineering Chemistry Research, 52 (2013) 2693-2699.

[86] J. Thömmes, M. Halfar, H. Gieren, S. Curvers, R. Takors, R. Brunschier, M.-R. Kula, Human Chymotrypsinogen B Production from Pichia pastoris by Integrated Development of Fermentation and Downstream Processing. Part 2. Protein Recovery, Biotechnology Progress, 17 (2001) 503-512.

[87] W. Kelly, P. Garcia, S. McDermott, P. Mullen, G. Kamguia, G. Jones, A. Ubiera, K. Göklen, Experimental characterization of next-generation expanded-bed adsorbents for capture of a recombinant protein expressed in high-cell-density yeast fermentation, Biotechnology and Applied Biochemistry, 60 (2013) 510-520.

[88] W. Kelly, G. Kamguia, P. Mullen, A. Ubiera, K. Göklen, Z. Huang, G. Jones, Using a two species competitive binding model to predict expanded bed breakthrough of a recombinant protein expressed in a high cell density fermentation, Biotechnology and Bioprocess Engineering, 18 (2013) 546-559.

[89] G.L. Skidmore, H.A. Chase, Two-component protein adsorption to the cation exchanger S Sepharose® FF, Journal of Chromatography A, 505 (1990) 329-347.

[90] W.F. Weinbrenner, M.R. Etzel, Competitive adsorption of alpha-lactalbumin and bovine serum albumin to a sulfopropyl ion-exchange membrane, Journal of Chromatography A, 662 (1994) 414-419.

[91] C. Martin, G. Iberer, A. Ubiera, G. Carta, Two-component protein adsorption kinetics in porous ion exchange media, Journal of Chromatography A, 1079 (2005) 105-115.

[92] J. Zhao, S. Yao, D. Lin, Adsorbents for Expanded Bed Adsorption: Preparation and Functionalization, Chinese Journal of Chemical Engineering, 17 (2009) 678-687.

[93] E. Palsson, A. Axelsson, P.O. Larsson, Theories of chromatographic efficiency applied to expanded beds, Journal of Chromatography A, 912 (2001) 235-248.

[94] H.A. Chase, N.M. Draeger, Expanded-Bed Adsorption of Proteins Using Ion-Exchangers, Separation Science and Technology, 27 (1992) 2021-2039.

[95] L.K. McCune, R.H. Wilhelm, Mass and Momentum Transfer in Solid-Liquid System. Fixed and Fluidized Beds, Industrial & Engineering Chemistry Research, 41 (1949) 1124-1134.

[96] F.X. McGarvey, R. Kunin, Mixed bed deionization. US2578937A (1951).

[97] J.B. Noble, G.H. Cowan, W.P. Sweetenham, H.A. Chase, The Application of Modelling to the Prediction of Adsorption in Batch-Stirred Tanks, Packed-Bed and Fluidised-Bed Columns in Biotechnological Separations, in: M.J. Slater (Ed.) Ion Exchange Advances, Springer Netherlands, 1992, 214-221.

[98] F. Fenneteau, H. Aomari, P. Chahal, R. Legros, Modeling of scale-down effects on the hydrodynamics of expanded bed adsorption columns, Biotechnology and Bioengineering, 81 (2003) 790-799.

[99] X.-D. Tong, B. Xue, Y. Sun, Modeling of expanded-bed protein adsorption by taking into account the axial particle size distribution, Biochemical Engineering Journal, 16 (2003) 265-272.

[100] P. Li, G. Xiu, A.E. Rodrigues, Modeling breakthrough and elution curves in fixed bed of inert core adsorbents: analytical and approximate solutions, Chemical Engineering Science, 59 (2004) 3091-3103.

[101] J. Yun, S.-J. Yao, D.-Q. Lin, M.-H. Lu, W.-T. Zhao, Modeling axial distributions of adsorbent particle size and local voidage in expanded bed, Chemical Engineering Science, 59 (2004) 449-457.

[102] J. Yun, D.Q. Lin, S.J. Yao, Predictive modeling of protein adsorption along the bed height by taking into account the axial nonuniform liquid dispersion and particle classification in expanded beds, Journal of Chromatography A, 1095 (2005) 16-26.

[103] C.C. Moraes, M.A. Mazutti, F. Maugeri, S.J. Kalil, Modeling of ion exchange expanded-bed chromatography for the purification of C-phycocyanin, Journal of Chromatography A, 1281 (2013) 73-78.

[104] H.A. Chase, Draeger, N. M., Affinity purification of proteins using expanded beds, Journal of Chromatography A, 597 (1992) 129-145.

[105] N.M. Draeger, Chase, H. A., Liquid fluidized bed adsorption of protein in the presence of cells, Bioseparation, 2 (1991) 67-80.

[106] M. Hansson, Ståhl, S., Hjorth, R., Uhlén, M., Moks, T. , Single–Step Recovery of a Secreted Recombinant Protein by Expanded Bed Adsorption, Nature Biotechnology, 12 (1994) 285-288.

[107] N.M. Draeger, Chase, H. A., Modelling of Protein Adsorption in Liquid Fluidized Beds, in: D.L. Pyle (Ed.) Separations for Biotechnology 2, Springer Netherlands, 1990, 325-334.

[108] Introduction to Expanded bed Adsorption Handbook, in, GE Healthcare.

[109] P.M. Boyer, J.T. Hsu, Experimental studies of restricted protein diffusion in an agarose matrix, American Institute of Chemical Engineers Journal, 38 (1992) 259-272.

[110] L.J. Bruce, H.A. Chase, Hydrodynamics and adsorption behaviour within an expanded bed adsorption column studied using in-bed sampling, Chemical Engineering Science, 56 (2001) 3149-3162.

[111] J. Thommes, A. Bader, M. Halfar, A. Karau, M.R. Kula, Isolation of monoclonal antibodies from cell containing hybridoma broth using a protein A coated adsorbent in expanded beds, Journal of Chromatography A, 752 (1996) 111-122.

[112] Y.-L. Lei, D.-Q. Lin, S.-J. Yao, Z.-Q. Zhu, Preparation and characterization of titanium oxide-densified cellulose beads for expanded bed adsorption, Journal of Applied Polymer Science, 90 (2003) 2848-2854.

[113] Y.-K. Chang, S.-Y. Chou, J.-L. Liu, J.-C. Tasi, Characterization of BSA adsorption on mixed mode adsorbent: I. Equilibrium study in a well-agitated contactor, Biochemical Engineering Journal, 35 (2007) 56-65.

[114] Y.K. Chang, H.A. Chase, Development of operating conditions for protein purification using expanded bed techniques: the effect of the degree of bed expansion on adsorption performance, Biotechnology and Bioengineering, 49 (1996) 512-526.

[115] R.R. Vennapusa, M. Fernandez-Lahore, Effect of chemical additives on biomass deposition onto beaded adsorbents, Journal of bioscience and bioengineering, 110 (2010) 564-571.

[116] J. Hubbuch, J. Thommes, M.R. Kula, Biochemical engineering aspects of expanded bed adsorption, Advances in Biochemical Engineering/Biotechnology, 92 (2005) 101-123.

[117] A. Pai, S. Gondkar, A. Lali, Enhanced performance of expanded bed chromatography on rigid superporous adsorbent matrix, Journal of Chromatography A, 867 (2000) 113-130.

[118] N. Voute, E. Boschetti, Highly dense beaded sorbents suitable for fluidized bed applications, Bioseparation, 8 (1999) 115-120.

[119] F. Asghari, M. Jahanshahi, Fabrication and evaluation of low-cost agarose-zinc nanoporous composite matrix: influence of adsorbent density and size distribution on the performance of expanded beds, Journal of Chromatography A, 1257 (2012) 89-97.

[120] F. Asghari, M. Jahanshahi, A.A. Ghoreyshi, Preparation and characterization of agarose-nickel nanoporous composite particles customized for liquid expanded bed adsorption, Journal of Chromatography A, 1242 (2012) 35-42.

[121] G.E. McCreath, H.A. Chase, C.R. Lowe, Novel affinity separation based on perfluorocarbon emulsions - Use of a perfluorocarbon affinity emulsion for the direct extraction of glucose-6-phosphate dehydrogenase from homogenized bakers' yeast, Journal of Chromatography A, 659 (1994) 275-287.

[122] Y.K. Chang, G.E. McCreath, H.A. Chaset, Development of an expanded bed technique for an affinity purification of G6PDH from unclarified yeast cell homogenates, Biotechnology and Bioengineering, 48 (1995) 355-366.

[123] G.E. McCreath, H.A. Chase, R.O. Owen, C.R. Lowe, Expanded bed affinity chromatography of dehydrogenases from bakers' yeast using dye-ligand perfluoropolymer supports, Biotechnology and Bioengineering, 48 (1995) 341-354.

[124] N. Garg, I. Galaev, B. Mattiasson, Polymer-shielded dye-ligand chromatography of lactate dehydrogenase from porcine muscle in an expanded bed system, Bioseparation, 6 (1996) 193-199.

[125] C.M. Griffith, J. Morris, M. Robichaud, M.J. Annen, A.V. McCormick, M.C. Flickinger, Fluidization characteristics of and protein adsorption on fluoride-modified porous zirconium oxide particles, Journal of Chromatography A, 776 (1997) 179-195.

[126] R.K. Lewus, G. Carta, Binary protein adsorption on gel-composite ion-exchange media, American Institute of Chemical Engineers Journal, 45 (1999) 512-522.

[127] A. Lihme, E. Zafirakos, M. Hansen, M. Olander, Simplified and more robust EBA processes by elution in expanded bed mode, Bioseparation, 8 (1999) 93-97.

[128] S. Gondkar, K. Manudhane, N. Amritkar, A. Pai, A. Lali, Effect of adsorbent porosity on performance of expanded bed chromatography of proteins, Biotechnology Progress, 17 (2001) 522-529.

[129] X.-D. Tong, Y. Sun, Nd-Fe-B alloy-densified agarose gel for expanded bed adsorption of proteins, Journal of Chromatography A, 943 (2001) 63-75.

[130] I. Theodossiou, H.D. Elsner, O.R.T. Thomas, T.J. Hobley, Fluidisation and dispersion behaviour of small high density pellicular expanded bed adsorbents, Journal of Chromatography A, 964 (2002) 77-89.

[131] X.D. Tong, Y. Sun, Particle size and density distributions of two dense matrices in an expanded bed system, Journal of Chromatography A, 977 (2002) 173-183.

[132] M.B. Dainiak, I.Y. Galaev, B. Mattiasson, Polyelectrolyte-coated ion exchangers for cell-resistant expanded bed adsorption, Biotechnology Progress, 18 (2002) 815-820.

[133] X.-D. Tong, X.-Y. Dong, Y. Sun, Lysozyme adsorption and purification by expanded bed chromatography with a small-sized dense adsorbent, Biochemical Engineering Journal, 12 (2002) 117-124.

[134] M. Jahanshahi, A.W. Pacek, A.W. Nienow, A. Lyddiatt, Fabrication by three-phase emulsification of pellicular adsorbents customised for liquid fluidised bed adsorption of bioproducts, Journal of Chemical Technology & Biotechnology, 78 (2003) 1111-1120.

[135] P. Li, G. Xiu, A. E. Rodrigues, Modeling separation of proteins by inert core adsorbent in a batch adsorber, Chemical Engineering Science, 58 (2003) 3361-3371.

[136] X. Zhou, Q.-H. Shi, S. Bai, Y. Sun, Dense pellicular agarose–glass beads for expanded bed application:: Fabrication and characterization for effective protein adsorption, Biochemical Engineering Journal, 18 (2004) 81-88.

[137] Y.-L. Lei, D.-Q. Lin, S.-J. Yao, Z.-Q. Zhu, Preparation of an anion exchanger based on TiO2-densified cellulose beads for expanded bed adsorption, Reactive and Functional Polymers, 62 (2005) 169-177.

[138] Z.-J. Miao, D.-Q. Lin, S.-J. Yao, Preparation and Characterization of Cellulose-Stainless Steel Powder Composite Particles Customized for Expanded Bed Application, Industrial & Engineering Chemistry Research, 44 (2005) 8218-8224.

[139] D.Q. Lin, Z.J. Miao, S.J. Yao, Expansion and hydrodynamic properties of cellulose-stainless steel powder composite matrix for expanded bed adsorption, Journal of Chromatography A, 1107 (2006) 265-272.

[140] H.-F. Xia, D.-Q. Lin, S.-J. Yao, Spherical cellulose–nickel powder composite matrix customized for expanded bed application, Journal of Applied Polymer Science, 104 (2007) 740-747.

[141] H.F. Xia, D.Q. Lin, S.J. Yao, Preparation and characterization of macroporous cellulose-tungsten carbide composite beads for expanded bed applications, Journal of Chromatography A, 1175 (2007) 55-62.

[142] H.F. Xia, D.Q. Lin, S.J. Yao, Chromatographic performance of macroporous cellulose-tungsten carbide composite beads as anion-exchanger for expanded bed adsorption at high fluid velocity, Journal of Chromatography A, 1195 (2008) 60-66.

[143] D. Gao, S.-J. Yao, D.-Q. Lin, Preparation and adsorption behavior of a cellulose-based, mixed-mode adsorbent with a benzylamine ligand for expanded bed applications, Journal of Applied Polymer Science, 107 (2008) 674-682.

[144] M. Jahanshahi, L. Partida-Martinez, S. Hajizadeh, Preparation and evaluation of polymer-coated adsorbents for the expanded bed recovery of protein products from particulate feedstocks, Journal of Chromatography A, 1203 (2008) 13-20.

[145] H.-B. Song, Z.-F. Xiao, Q.-P. Yuan, Preparation and characterization of poly glycidyl methacrylete–zirconium dioxide–β-cyclodextrin composite matrix for separation of isoflavones through expanded bed adsorption, Journal of Chromatography A, 1216 (2009) 5001-5010.

[146] J. Zhao, D.Q. Lin, S.J. Yao, Expansion and hydrodynamic properties of beta-cyclodextrin polymer/tungsten carbide composite matrix in an expanded bed, Journal of Chromatography A, 1216 (2009) 7840-7845.

[147] J. Zhao, D.-Q. Lin, Y.-C. Wang, S.-J. Yao, A novel β-cyclodextrin polymer/tungsten carbide composite matrix for expanded bed adsorption: Preparation and characterization of physical properties, Carbohydrate Polymers, 80 (2010) 1085-1090.

[148] A. Lihme, M.B. Hansen, I.V. Andersen, T. Burnouf, A novel core fractionation process of human plasma by expanded bed adsorption chromatography, Analytical Biochemistry, 399 (2010) 102-109.

[149] F. Shi, D.-Q. Lin, W. Phottraithip, S.-J. Yao, Preparation of cellulose–tungsten carbide composite beads with ionic liquid for expanded bed application, Journal of Applied Polymer Science, 119 (2011) 3453-3461.

[150] D.Q. Lin, H.F. Tong, E.J. van de Sandt, P. den Boer, M. Golubovic, S.J. Yao, Evaluation and characterization of axial distribution in expanded bed. I. Bead size, bead density and local bed voidage, Journal of Chromatography A, 1304 (2013) 78-84.

[151] X.-Y. Zhan, D.-P. Lu, D.-Q. Lin, S.-J. Yao, Preparation and characterization of supermacroporous polyacrylamide cryogel beads for biotechnological application, Journal of Applied Polymer Science, 130 (2013) 3082-3089.

[152] A. Rezvani, M. Jahanshahi, G.D. Najafpour, Characterization and evaluation of the novel agarose–nickel composite matrix for possible use in expanded bed adsorption of bio-products, Journal of Chromatography A, 1331 (2014) 61-68.

[153] W. Shi, D.-Q. Lin, H.-F. Tong, J.-X. Yun, S.-J. Yao, 5-Aminobenzimidazole as new hydrophobic charge-induction ligand for expanded bed adsorption of bovine IgG, Journal of Chromatography A, 1425 (2015) 97-105.

[154] W. Shi, D. Gao, S.-J. Yao, D.-Q. Lin, Integration of Expanded Bed Adsorption and Hydrophobic Charge-Induction Chromatography for Monoclonal Antibody Separation, Industrial & Engineering Chemistry Research, 56 (2017) 765-773.

[155] S. Amiri, M.R. Mehrnia, S. Sobhanifard, F. Pourasgharian Roudsari, S.-N. Hoseini, Evaluation of agarose-entrapped magnetic nanoparticles influence on protein adsorption isotherm and kinetics using nickel-iminodiacetic acid ligand, Separation and Purification Technology, 188 (2017) 423-430.

[156] J. Thömmes, M. Weiher, A. Karau, M.-R. Kula, Hydrodynamics and performance in fluidized bed adsorption, Biotechnology and Bioengineering, 48 (1995) 367-374.

[157] J. Thommes, M. Halfar, S. Lenz, M.R. Kula, Purification of monoclonal antibodies from whole hybridoma fermentation broth by fluidized bed adsorption, Biotechnology and Bioengineering, 45 (1995) 205-211.

[158] Y.K. Chang, H.A. Chase, Ion exchange purification of G6PDH from unclarified yeast cell homogenates using expanded bed adsorption, Biotechnology and Bioengineering, 49 (1996) 204-216.

[159] A. Karau, C. Benken, J. Thommes, M.R. Kula, The influence of particle size distribution and operating conditions on the adsorption performance in fluidized beds, Biotechnology and Bioengineering, 55 (1997) 54-64.

[160] M.P. Smith, An evaluation of expanded bed adsorption for the recovery of protein from crude feedstock, in: Ph.D. Thesis, University College London, UK, 1997.

[161] G.M. Finette, B. Baharin, Q.M. Mao, M.T. Hearn, Optimization considerations for the purification of alpha1-antitrypsin using silica-based ion-exchange adsorbents in packed and expanded beds, Biotechnology Progress, 14 (1998) 286-293.

[162] J. Chi-Wei Lan, G. Hamilton, A. Lyddiatt, Physical and biochemical characterization of a simple intermediate between fluidized and expanded bed contactors, Bioseparation, 8 (1999) 43-51.

[163] A. Pai, S. Gondkar, S. Sundaram, A. Lali, Expanded bed adsorption on supermacroporous cross-linked cellulose matrix, Bioseparation, 8 (1999) 131-138.

[164] L.J. Bruce, R.H. Clemmitt, D.C. Nash, H.A. Chase, Monitoring of adsorbate breakthrough curves within an expanded bed adsorption column, Journal of Chemical Technology & Biotechnology, 74 (1999) 264-269.

[165] J. Thommes, Investigations on protein adsorption to agarose-dextran composite media, Biotechnology and Bioengineering, 62 (1999) 358-362.

[166] R.H. Clemmitt, H.A. Chase, Facilitated downstream processing of a histidine-tagged protein from unclarified E. coli homogenates using immobilized metal affinity expanded-bed adsorption, Biotechnology and Bioengineering, 67 (2000) 206-216.

[167] P.R. Wright, B.J. Glasser, Modeling mass transfer and hydrodynamics in fluidized-bed adsorption of proteins, Aiche Journal, 47 (2001) 474-488.

[168] H.-B. Hu, S.J. Yao, Z.-Q. Zhu, Study on adsorption performance of BSA in Streamline DEAE and DEAE Spharose FF adsorbents, Chinese Journal of Chemical Engineering, 29 (2001).

[169] H.M. Fernández-Lahore, D.-Q. Lin, J.J. Hubbuch, M.-R. Kula, J. Thömmes, The Use of Ion-Selective Electrodes for Evaluating Residence Time Distributions in Expanded Bed Adsorption Systems, Biotechnology Progress, 17 (2001) 1128-1136.

[170] L. J. Bruce, H. A. Chase, The combined use of in-bed monitoring and an adsorption model to anticipate breakthrough during expanded bed adsorption, Chemical Engineering Science, 57 (2002) 3085-3093.

[171] R.H. Clemmitt, H.A. Chase, Direct recovery of glutathione S-transferase by expanded bed adsorption: anion exchange as an alternative to metal affinity fusions, Biotechnology and Bioengineering, 77 (2002) 776-785.

[172] W.D. Chen, X.D. Tong, X.Y. Dong, Y. Sun, Expanded bed adsorption of protein with DEAE Spherodex M, Biotechnology Progress, 19 (2003) 880-886.

[173] Y. Bai, C.E. Glatz, Capture of a recombinant protein from unclarified canola extract using streamline expanded bed anion exchange, Biotechnology and Bioengineering, 81 (2003) 855-864.

[174] P. Li, G. Xiu, A.E. Rodrigues, A 3-zone model for protein adsorption kinetics in expanded beds, Chemical Engineering Science, 59 (2004) 3837-3847.

[175] J. Yun, D.-Q. Lin, S.-J. Yao, Variation of the Axial Dispersion along the Bed Height for Adsorbents with a Density Difference and a Log-Normal Size Distribution in an Expanded Bed, Industrial & Engineering Chemistry Research, 43 (2004) 8066-8073.

[176] J. Yun, D.-Q. Lin, M.-H. Lu, L.-N. Zhong, S.-J. Yao, Measurement and modeling of axial distribution of adsorbent particles in expanded bed: taking into account the particle density difference, Chemical Engineering Science, 59 (2004) 5873-5881.

[177] Y. Chow, B. Tey, M. Ibrahim, A. Ariff, T. Ling, The performance of anion exchange expanded bed adsorption chromatography on the recovery of G6PDH from unclarified feedstock with high biomass concentration, Biotechnology and Bioprocess Engineering, 11 (2006) 466-469.

[178] H.-F. Xia, D.-Q. Lin, S.-J. Yao, Evaluation of new high-density ion exchange adsorbents for expanded bed adsorption chromatography, Journal of Chromatography A, 1145 (2007) 58-66.

[179] F. Poulin, R. Jacquemart, G. De Crescenzo, M. Jolicoeur, R. Legros, A Study of the interaction of HEK-293 cells with streamline chelating adsorbent in expanded bed operation, Biotechnology Progress, 24 (2008) 279-282.

[180] D.-Q. Lin, C.-Q. Chen, Y.-C. Wu, S.-J. Yao, Separation of lactoferrin from whey by expanded bed adsorption with mixed-mode adsorbent, Journal of Zhejiang University (Engineering Science), 43 (2009) 472-476.

[181] J. Li, H.A. Chase, Use of expanded bed adsorption to purify flavonoids from Ginkgo biloba L, Journal of Chromatography A, 1216 (2009) 8759-8770.

[182] W.B. Yap, B.T. Tey, N.B. Alitheen, W.S. Tan, Purification of His-tagged hepatitis B core antigen from unclarified bacterial homogenate using immobilized metal affinity-expanded bed adsorption chromatography, Journal of Chromatography A, 1217 (2010) 3473-3480.

[183] J.-F. Niu, Z.-F. Chen, G.-C. Wang, B.-C. Zhou, Purification of phycoerythrin from Porphyra yezoensis Ueda (Bangiales, Rhodophyta) using expanded bed absorption, Journal of Applied Phycology, 22 (2010) 25-31.

[184] M.H. Shahavi, M. Jahanshahi, G.D. Najafpour, M. Ebrahimpour, A.H. Hosenian, Expanded Bed Adsorption of Biomolecules by NBG Contactor: Experimental and Mathematical Investigation, World Applied Sciences Journal, 13 (2011) 181-187.

[185] M. Alibolandi, H. Mirzahoseini, Purification and Refolding of Overexpressed Human Basic Fibroblast Growth Factor in Escherichia coli, Biotechnology Research International, (2011) 973741.

[186] V. Boeris, I. Balce, R.R. Vennapusa, M. Arevalo Rodriguez, G. Pico, M.F. Lahore, Production, recovery and purification of a recombinant beta-galactosidase by expanded bed anion exchange adsorption, Journal of Chromatography B: Analytical Technologies in the Biomedical and Life Sciences, 900 (2012) 32-37.

[187] P. den-Boer, M. Doeven, J. van der Merwe, A. Lihme, M. Bendix-Hansen, I. Vaarst, M. Pontoppidan, F. Linz, Rhobust EBA Processing high-cell density mammalian cell cultures: process parameters and performance. (2013)

[188] Q.Y. Du, D.Q. Lin, Q.L. Zhang, S.J. Yao, An integrated expanded bed adsorption process for lactoferrin and immunoglobulin G purification from crude sweet whey, Journal of

Chromatography B: Analytical Technologies in the Biomedical and Life Sciences, 947-948 (2014) 201-207.

[189] P.B. Kakarla, R.N. Dsouza, U. Toots, M. Fernández-Lahore, Interactions of Chinese Hamster Ovary (CHO) cell cultures with second generation expanded bed adsorbents, Separation and Purification Technology, 144 (2015) 23-30.

[190] J. Yan, Q.-L. Zhang, D.-Q. Lin, S.-J. Yao, Coadsorption of Human Immunoglobulin G and Bovine Serum Albumin on a p-Aminohippuric Acid Based Mixed-Mode Resin, Journal of Chemical & Engineering Data, 61 (2016) 151-159.

[191] M.d.A. Lima, M.d.F.M.d. Freitas, L.R.B. Gonçalves, I.J.d. Silva Junior, Recovery and purification of a Kluyvermyces lactis β-galactosidase by Mixed Mode Chromatography, Journal of Chromatography B, 1015 (2016) 181-191.

[192] R.N. D'Souza, P.B. Kakarla, V. Yelemane, R. Meyer, P. den Boer, M. Fernández-Lahore, Controlling cell adhesion in antibody purification by expanded bed adsorption chromatography, Separation and Purification Technology, 183 (2017) 270-278.

[193] K.-H. Chen, S.-Y. Chou, Y.-K. Chang, Rapid purification of lysozyme by mixed-mode adsorption chromatography in stirred fluidized bed, Food Chemistry, (2018).

[194] A.O.F. Lihme, M.B. Hansen, Isolation of immunoglobulins. EP1386660A1 (2009).

[195] G.E. Hamilton, F. Luechau, S.C. Burton, A. Lyddiatt, Development of a mixed mode adsorption process for the direct product sequestration of an extracellular protease from microbial batch cultures, Journal of Biotechnology, 79 (2000) 103-115.

[196] D. Gao, D.Q. Lin, S.J. Yao, Mechanistic analysis on the effects of salt concentration and pH on protein adsorption onto a mixed-mode adsorbent with cation ligand, Journal of Chromatography B: Analytical Technologies in the Biomedical and Life Sciences, 859 (2007) 16-23.

[197] K.O. Strætkvern, J.G. Schwarz, D.P. Wiesenborn, E. Zafirakos, A. Lihme, Expanded bed adsorption for recovery of patatin from crude potato juice, Bioseparation, 7 (1998) 333-345.

[198] G.E. McCreath, H.A. Chase, D.R. Purvis, C.R. Lowe, Novel affinity separations based on perfluorocarbon emulsions: Use of a perfluorocarbon affinity emulsion for the purification of human serum albumin from blood plasma in a fluidised bed, Journal of Chromatography A, 597 (1992) 189-196.

[199] G.M.S. Finette, Q.-M. Mao, M.T.W. Hearn, Studies on the expansion characteristics of fluidised beds with silica-based adsorbents used in protein purification, Journal of Chromatography A, 743 (1996) 57-73.

[200] A. Mullick, M.C. Flickinger, Expanded bed adsorption of human serum albumin from very dense Saccharomyces cerevesiae suspensions on fluoride-modified zirconia, Biotechnology and Bioengineering, 65 (1999) 282-290.

[201] Q. Luo, H. Zou, X. Xiao, Z. Guo, L. Kong, X. Mao, Chromatographic separation of proteins on metal immobilized iminodiacetic acid-bound molded monolithic rods of macroporous poly(glycidyl methacrylate-co-ethylene dimethacrylate), Journal of Chromatography A, 926 (2001) 255-264.

[202] M. Yakup Arica, M. Yilmaz, E. Yalçin, G. Bayramoğlu, Surface properties of Reactive Yellow 2 immobilised pHEMA and HEMA/chitosan membranes: Characterisation of their selectivity to different proteins, Journal of Membrane Science, 240 (2004) 167-178.

[203] G. Jin, L. Zhang, Q. Yao, Novel method for human serum albumin adsorption/separation from aqueous solutions and human plasma with Cibacron Blue F3GA-Zn(II) attached microporous affinity membranous capillaries, Journal of Membrane Science, 287 (2007) 271-279.

[204] Y. Kong, X. Li, G. Bai, G. Ma, Z. Su, An automatic system for multidimensional integrated protein chromatography, Journal of Chromatography A, 1217 (2010) 6898-6904.

[205] L. Hui-Li, L. Dong-Qiang, Z. Mi-Mi, Y. Shan-Jing, Protein adsorption on DEAE ion-exchange resins with different ligand densities and pore sizes, Journal of Separation Science, 35 (2012) 3084-3090.

[206] P. Leblebici, M.E. Leblebici, F. Ferreira-da-Silva, A.E. Rodrigues, L.S. Pais, Separation of human immunoglobulin G subclasses on a protein A monolith column, Journal of Chromatography B, 962 (2014) 89-93.

[207] J. Yan, Q.L. Zhang, D.Q. Lin, S.J. Yao, Protein adsorption behavior and immunoglobulin separation with a mixed-mode resin based on p-aminohippuric acid, Journal of Separation Science, 37 (2014) 2474-2480.

[208] Q. Wu, Q. Zhang, S. Xu, C. Ge, S. Yao, D. Lin, Preparation and evaluation of mixed-mode resins with tryptophan analogues as functional ligands for human serum albumin separation, Chinese Journal of Chemical Engineering, 25 (2017) 898-905.

[209] D.R. Gondim, J.A. Cecilia, S.O. Santos, T.N.B. Rodrigues, J.E. Aguiar, E. Vilarrasa-García, E. Rodríguez-Castellón, D.C.S. Azevedo, I.J. Silva, Influence of buffer solutions in the adsorption of human serum proteins onto layered double hydroxide, International Journal of Biological Macromolecules, 106 (2018) 396-409.

[210] J.F. Kennedy, J.A. Barnes, Immunochemical studies of the non-specific interactions of cyanogen bromide-activated macroporous agarose-based immunoadsorbents, Journal of Chromatography A, 281 (1983) 83-93.

[211] J. Feuser, M. Halfar, D. Lutkemeyer, N. Ameskamp, M. Kula, J. Thommes, Interaction of mammalian cell culture broth with adsorbents in expanded bed adsorption of monoclonal antibodies, Process Biochemistry, 34 (1999) 159-165.

[212] D. Lütkemeyer, N. Ameskamp, H. Tebbe, J. Wittler, J. Lehmann, Estimation of cell damage in bench- and pilot-scale affinity expanded- bed chromatography for the purification of monoclonal antibodies, Biotechnology and Bioengineering, 65 (1999) 114-119.

[213] G.M. Tan, Q.H. Shi, Y. Sun, Oscillatory transverse electric field enhances mass transfer and protein capacity in ion-exchange electrochromatography, Journal of Chromatography A, 1098 (2005) 131-137.

[214] G. Bayramoglu, A.U. Senel, M.Y. Arica, Effect of spacer-arm and Cu(II) ions on performance of l-histidine immobilized on poly(GMA/MMA) beads as an affinity ligand for separation and purification of IgG, Separation and Purification Technology, 50 (2006) 229-239.

[215] T. Ishihara, T. Kadoya, Accelerated purification process development of monoclonal antibodies for shortening time to clinic. Design and case study of chromatography processes, Journal of Chromatography A, 1176 (2007) 149-156.

[216] R. Wongchuphan, B.T. Tey, W.S. Tan, F.S. Taip, S.M.M. Kamal, T.C. Ling, Application of dye-ligands affinity adsorbent in capturing of rabbit immunoglobulin G, Biochemical Engineering Journal, 45 (2009) 232-238.

[217] J. Gao, Z. Li, T. Russell, Z. Li, Antibody affinity purification using metallic nickel particles, Journal of Chromatography B: Analytical Technologies in the Biomedical and Life Sciences, 895-896 (2012) 89-93.

[218] B. Akkaya, H. Yavuz, F. Candan, A. Denizli, Concanavalin a immobilized magnetic poly(glycidyl methacrylate) beads for antibody purification, Journal of Applied Polymer Science, 125 (2012) 1867-1874.

[219] R.Z. Wang, D.Q. Lin, H.F. Tong, H.L. Lu, S.J. Yao, Evaluation of mixed-mode chromatographic resins for separating IgG from serum albumin containing feedstock, Journal of Chromatography B: Analytical Technologies in the Biomedical and Life Sciences, 936 (2013) 33-41.

[220] W. Phottraithip, D.Q. Lin, F. Shi, S.J. Yao, New hydrophobic charge-induction resin with 2-mercaptoimidazole as the ligand and its separation characteristics for porcine IgG, Biotechnology and Bioprocess Engineering, 18 (2013) 1169-1175.

Chapter 3: Adsorption of Human Serum Albumin (HSA) on mixed-mode adsorbent: equilibrium and kinetics

"Faith is taking the first step even when you don't see the whole staircase."

- Dr. Martin Luther King, Jr.

The adsorption equilibrium and kinetics of Human Serum albumin (HSA) onto a novel high particle density multimodal adsorbent were studied by batch adsorption experiments in this chapter. MabDirect MM, from Upfront Chromatography A/S, is an agarose-tungsten carbide composite adsorbent with an anionic mixed mode ligand. The effects of ionic strength (by addition of salt) and of pH are assessed. Langmuir isotherms parameters are obtained along with pore diffusivity values by fitting the batch experiments using a pore diffusion model. Furthermore, several experiments were carried out in a fixed bed column with the aim to understand the kinetics and hydrodynamics, and to validate the batch adsorption results.

This chapter is based on the following article:

Gomes, P.F., Loureiro, J.M. & Rodrigues, A.E. Adsorption of Human Serum Albumin (HSA) on a mixed-mode adsorbent: equilibrium and kinetics. Adsorption, 23 (2017), 491-505.

3.1. Introduction

Proteins have great importance for a wide range of applications. The main distinctive properties of proteins are their enzyme activity, specific recognition interactions and other therapeutic actions. Either for academic or industrial purposes, drug discovery initiatives, or high-throughput screening, proteins are the object of study of many researchers worldwide [1].

Human Serum Albumin (HSA) is a globular protein of 585 amino acids with a molecular weight of 66 kDa, which accounts for 60% of the total protein in blood serum. Typically, the concentration of this protein in adults is approximately 40 $g.dm^{-3}$. HSA has binding capacity for a wide range of endogenous and exogenous ligands, and its abundance makes it an important reference of the pharmacokinetics behaviour of many drugs. HSA is a valuable bio-marker of many diseases (such as rheumatoid arthritis, ischemia, post-menopausal obesity and cancer) and diseases that need monitoring of the glycemic levels. Also, this protein is used clinically to treatments like in burns, shocks, surgical blood losses (since it is the major component of Human blood) etc [2-7].

At the end of recombinant protein production process there are several contaminants (dissolved or particulates) along with the desired target protein. In terms of application purposes, protein purity is of utmost priority. There are separation methods that allow the target protein separation and purification from raw materials by downstream processing. It is necessary to ensure that all impurities are removed and highly purified protein is efficiently obtained to reduce the production costs. Proteins separation and purification became a fundamental prerequisite for any pharmaceutical industry [1, 8, 9].

Adsorption techniques are commonly used methods for protein recovery. Adsorption can be carried out in batch or continuous stirred tanks for feedstocks containing particulates, or using fixed bed or expanded bed technologies. Batch adsorption presents an easy setup and it has the capacity to handle particulate contaminants; however, it usually promotes the abrasion of the adsorbent particles and it has poor adsorption and elution efficiency. Fixed bed adsorption is another conventional operating mode. This method is not the most suitable for processing feedstocks that contain particulate material since it becomes trapped in the voids of the bed. Blockage is a common result by the formation of a plug of trapped solids near the bed inlet, increasing, this way, the pressure drop across the bed, which becomes unacceptable and lead to deformation and compression of non-rigid adsorbents. However, when studying the (single or mixture) protein/adsorbent interactions, i.e. without any contaminants from the protein production methods, this method is commonly used [10-14]

Expanded bed adsorption (EBA) has been widely successfully applied as an efficient thecnique for directly capture, separate and purify various products from unclarified source materials. It consists in suspending the adsorbent particles by passing an upwards stream on a column, therefore increasing void fraction, where the unwanted material and contaminants pass through the column unhindered without the risk of any blockage, thus minimizing the pressure drop problems commonly encountered in fixed bed reactors. Specialized adsorbent for EBA is a necessity. Second generation expanded bed adsorption is a technology developed by Upfront chromatography A/S; it consists in the use of tungsten carbide-containing in high density agarose beads that allows high flow rates (300 – 600 cm/h) at a typical expansion bed factor of two. This technology also allow a direct capture of high-value biopharmaceutical products reducing processing time and cost without affecting product quality [1, 13, 14]. Upfront Chromatography developed two types of ligands for this second generation adsorbent, MabDirect MM which possesses a mixed mode ligand while MabDirect Protein A possesses an affinity ligand.

Mixed Mode Chromatography (MMC) is a method of separation that uses more than one form of interactions between the stationary phase and the solutes in a feed stream. Mixed mode consists in complementary charge ligand with additional functional groups that will introduce new cooperative interactions (hydrophobic, electrostatic, thiophilic interactions and hydrogen bonds), which lead to a high capacity, salt-tolerant, facile elution and improvement of adsorption selectivity. The multiple interactions will simultaneously influence the adsorption; being able to understand this interaction is a complex task, although not an impossible one [14, 15].

This work objective is to study a novel multimodal adsorbent exclusively designed for expanded bed adsorption using batch and fixed bed adsorption on a model protein, Human Serum Albumin for later use in EBA. Batch adsorption experiments are conducted in order to determine the adsorption equilibrium isotherms and, at the same time, estimate the diffusivity of the target protein in different conditions. The effects of ionic strength (by addition of salt) and of pH are assessed, since they are the main relevant physical properties that affect protein adsorption. The interaction of these conditions with the target protein are useful to understand the adsorption process. The adsorption kinetics, including film mass transfer and intra-particle diffusion resistances, are modelled with the aim of understanding the mass transfer phenomena. Fixed bed operation is usually used for cleaning and regeneration of the adsorbent, since at these stages, the particulates were already removed. Several experiments are carried out in a fixed bed column with the aim to understand the kinetics and hydrodynamics. In addition, these experiments validate the batch adsorption results, previously obtained. The influence of several operating parameters, such as flow rate, feed concentration and salt concentration are assessed.

3.2. Materials and Methods

3.2.1. Target protein, adsorbent, equipment and buffer solutions

The target protein is Human Serum Albumin (HSA; product number CAS 70024-90-7) with a molecular weight of 66 kDa, 95% purity by Sodium Dodecyl Sulphate-Polyacrylamide Gel Electrophoresis, heavy-metals concentration lower than 20.0 ppm, 6.0% moisture, tested negative for antibodies and conserved between 2 and 8 °C. HSA has a light yellow color and a strong absorbance at 280 nm, like Bovine Serum Albumin (BSA). HSA was purchased from VWR Chemicals.

MabDirect MM is a mixed-mode adsorbent. It is an adsorbent from *Rhobust Fastline series* that is composed by a base matrix of 6% cross-linked agarose with tungsten carbide particles. The mixed-mode ligand has a pKa of 5.0 and contains aromatic ligands with acidic substituents (benzoic acid) (Kelly et al. 2013a and 2013b). Also, this adsorbent has a tested ligand concentration of 35 mmol· $L_{adsorbent}^{-1}$ and adsorbent density of 2.9 g.cm^{-3} according to the users guide. The adsorbent was offered by Upfront Chromatography A/S delivered in an aqueous solution containing 14% NaCl, 0.2M sodium acetate. Due to the adsorbent being commercially available, scarce information is found regarding its ligand. Upfront Chromatography released information regarding one of the ligands used in the mixed mode chromatography (Figure 3.1).

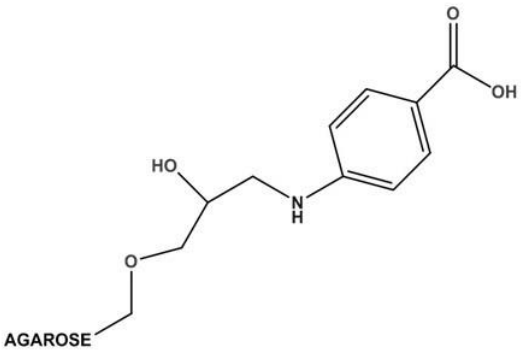

Figure 3.1 – Chemical structure of MabDirect MM by Upfront Chromatography.

A XK 16/20 column (*Amersham Pharmacia Biotech*, Uppsala, Sweden, now *GE Healthcare*) was used for the fixed bed adsorption experiments; this column has an internal diameter of 1.55 cm and a maximum height of 20 cm; moreover, the column height can be adjusted in order to optimize the amount of adsorbent. A Knauer 50 mL pump was used to feed the column. A Jasco 7800 UV detector (Tokyo, Japan) equipped with a flow-cell was used to monitor HSA effluent concentration at 280 nm wavelength in all fixed bed and batch adsorption

experiments, and the absorbance signal was recorded using data-acquisition software in a personal computer.

Regarding the pH and salt concentrations to be tested, the buffer in which the protein is dissolved was changed accordingly. For pH values of 3, 5 and 6 a citrate buffer was used (citric acid, $C_6H_8O_7$, 192.12 g.mol^{-1}, with tri-sodium citrate di-hydrate, $Na_3C_6H_5O_7.2H_2O$, 294.10 g.mol^{-1}, dissolved in deionized water), although acetic buffer could have been used. For pH 7 a phosphate buffer was used (sodium di-hydrogen phosphate di-hydrate, $NaH_2PO_4 \cdot 2H_2O$, 156.01 g.mol^{-1}, with di-sodium hydrogen phosphate, Na_2HPO_4, 141.96 g.mol^{-1}, dissolved in deionized water). A 20 mM concentration were used for all buffers, except for the buffer in which the adsorbent was stored which had 0.2M concentration. When necessary, the final solution pH was adjusted with 1 M NaOH or 1 M HCl. Sodium chloride (NaCl, 58.44 g.mol^{-1}) was added to study the effect of ionic strength. Buffers and solutions were prepared using deionized water.

Sodium di-hydrogen phosphate di-hydrate and di-sodium hydrogen phosphate were purchased from VWR Chemicals, while citric acid, tri-sodium citrate di-hydrate, hydrochloric acid, sodium hydroxide, sodium acetate and sodium chloride were purchased from Reagente5.

3.2.2. Adsorbent conditioning

Before performing adsorption equilibrium and kinetic experiments, the adsorbent was conditioned with the same buffer chosen for protein solutions preparation. This procedure consists in washing 8 mL of adsorbent (bulk volume) in a 250 mL Erlenmeyer flask by adding 240 mL (30 times the adsorbent volume) of deionized water. The flask was introduced in a shaking incubator (GFL 3018, Gesellschaft fur Labortechnik mbH, Burgwedel, Deutschland) for 30 minutes (260 rpm, enough to suspend the adsorbent particles) and the deionized water was changed four times (to a final conductivity near 3 µS/cm). Then, the buffer in which the experiment is to be conducted is added and it is left overnight in the shaking incubator.

3.2.3. Adsorption equilibrium isotherms and kinetics by batch experiments

Adsorbent samples (± 1.26 g – dry weight) are mixed with 100 mL of different protein concentrations for about 4h at room temperature (20 °C) in a shaking incubator (GFL 3018, Gesellschaft fur Labortechnik mbH, Burgwedel, Deutschland) at 230 rpm. Then, 2 mL samples are collected, filtered on 0.45 µm filters, and HSA protein is measured by Jasco 7800 UV detector at 280 nm wavelength in a quartz cuvette. Regarding the kinetic study, the same procedure was used but samples were collected at different times. Moreover, experiments at different stirring

speeds were conducted to study the external mass transfer phenomenon. Also, some experiments were conducted in which the mass of adsorbent was three times the value above referred. At the end of each run, the adsorbent was collected and stored in a stock 0.2 M sodium acetate with 14% NaCl solution, equal to the solution where the adsorbent was supplied.

3.2.4. Fixed bed adsorption

The XK 16/20 column was packed with MabDirect MM adsorbent and used for the frontal analysis of HSA adsorption experiments. The buffer used for equilibration of the column before sample loading, e.g. 20 mM citrate buffer pH 5, was pumped through the column in downward flow to equilibrate the adsorbent, and then the process is switched to feedstock application. The protein concentration in the outlet stream from the bottom of the column was measured by UV absorption at 280 nm. Two possible solutions can be pumped to the column by the Knauer 50 mL pump; for example, the equilibration buffer or the buffer with HSA protein can be chosen. Then, just before the entrance of the column (downward flow) a valve is located that has the purpose of removing any air from the tubes or from the pump when the solution bottles are being exchanged. The XK 16/20 column has the capability of being heated or cooled as wanted. Post-column, the protein concentration in the outlet stream is measured in a Jasco 7800 UV detector at 280 nm wavelength before going to a waste recipient for disposal.

Different steps take place when performing a fixed bed adsorption experiment to study the interaction of HSA protein with MabDirect MM. Before the adsorption step can take place, the adsorbent is conditioned in two solutions; first, the stock solution (0.2 M sodium acetate with 14% NaCl) is pumped through the column in downward flow during 30-45 minutes, with the purpose to attain an initial condition equal to the same adsorbent stored in buffer; second, equilibration buffer (e.g., 20 mM citrate buffer without salt, pH 5) is fed to the column. This second procedure lasts about 30-45 minutes as well. Then, the following steps are conducted:

Adsorption step: When the flow rate is stable and the fixed bed is equilibrated with the equilibration buffer, the process switches to feedstock application (HSA protein dissolved on citrate buffer without salt, pH 5, for example). The flow rate is periodically checked and recorded. The outlet stream from the bottom of the column passes through the flow cell, where the UV absorbance (proportional to the HSA concentration, according to the calibration curve) is monitored online by spectrophotometry at 280 nm, and the signal is logged by the data acquisition software in a personal computer.

Desorption step: When the breakthrough curve reaches the feed protein concentration, the process switches to the washing buffer (the same as the equilibration buffer) to washout the unbound proteins from the column, until the effluent absorbance signal reaches a relative stable

value. After washing, the pump is switched to elution buffer (20 mM citrate buffer with 1M NaCl - pH 5, for example) to elute HSA protein from the adsorbent. At this stage the pH and NaCl concentration can be increased to improve the elution efficiency.

In order to re-use the adsorbent, regeneration solution (1M NaOH with 1M NaCl recommended by the supplier) is pumped through the column for a time period of 30-45 minutes. To finalize the cycle, the stock solution is fed to the fixed bed so that the adsorbent stays stable at the standard conditions.

3.3. Mathematical modelling and numerical solution for the protein adsorption

3.3.1. Batch adsorption model

A pore diffusion model was used to fit the dynamic uptake data of several experiments in order to assess the effective pore diffusivity of proteins at different salt concentrations and pH. It is assumed that diffusion occurs inside the pores with a driving force expressed in terms of pore fluid concentration gradient [13, 16-20]. The mass balance in a volume element of the adsorbent particle is written as

$$\varepsilon_p \frac{\partial C_p}{\partial t} + \rho_\rho \frac{\partial q}{\partial t} = \frac{D_{pe}}{r^2} \frac{\partial}{\partial r}\left(r^2 \frac{\partial C_p}{\partial r} \right) \tag{3.1}$$

where ε_p represents the particle porosity and has a value of 0.237, determined by mercury porosimetry and ρ_ρ represents the particle density. C_p and q are the protein concentration in the pore fluid and the adsorption uptake capacity, respectively, both functions of time (t) and radial position (r). D_{pe} is the adsorbate effective pore diffusivity. On its turn, the global mass balance to the batch adsorber, relating the change in the liquid-phase concentration due to the solid-phase uptake can be written as [19, 21]

$$\frac{dC_b}{dt} = -\frac{3D_{pe}}{r_p} \frac{{}^{w}/_{\rho_\rho}}{V_L} \left(\frac{\partial C_p}{\partial r} \right)_{r=r_p} \tag{3.2}$$

where r_p is the particle radius, w represents the adsorbent mass used in the experiment and V_L is the volume of protein solution in the batch adsorber. In this work the adsorption equilibrium is represented by the Langmuir isotherm,

$$q = \frac{q_{max} \cdot K_L \cdot C_p}{1 + K_L \cdot C_p} \tag{3.3}$$

where q_{max} and K_L represent the maximum adsorption capacity and the equilibrium constant, respectively, both of which are determined by batch adsorption equilibrium experiments.

Boundary conditions

$$r = 0 \quad \rightarrow \quad \frac{\partial C_p}{\partial r} = 0 \tag{3.4}$$

$$r = r_p \quad \rightarrow \quad C_p = C_b \tag{3.5}$$

Initial conditions

$$t = 0 \quad \rightarrow \quad q\,(r) = 0 \quad C_p\,(r) = 0 \quad C_b = C_{b0} \tag{3.6}$$

Adsorption uptake capacity is calculated using the following equation:

$$q = \frac{V_L \cdot (C_{b0} - C_b)}{w} \tag{3.7}$$

where C_{b0} and C_b represent the initial and bulk protein concentrations, respectively.

3.3.2. Frontal analysis in a fixed bed column

To successfully predict a breakthrough curve of a fixed bed adsorption experiment several factors must be taken into account, namely hydrodynamics, adsorption equilibrium and kinetics [22-25]. The following assumptions were considered:

- The process is isothermal.
- The mobile phase velocity is constant.
- The bed is packed with porous particles that are spherical and uniform in size.
- The concentration gradient in the radial direction of the bed is negligible.
- Axial dispersed plug flow is considered for the fluid phase.
- Adsorption equilibrium is described by the Langmuir isotherm equation.
- Adsorption kinetics is described by the linear driving force approximation.

The mass balance for the protein in a volume element of the mobile phase is represented by the following equation:

$$\varepsilon_b \cdot \frac{\partial\, C_b}{\partial\, t} + (1 - \varepsilon_b)\, \rho_\rho \frac{\partial\, \bar{q}}{\partial\, t} + u_i \cdot \varepsilon_b \cdot \frac{\partial\, C_b}{\partial\, z} = \varepsilon_b \cdot D_L \cdot \frac{\partial^2\, C_b}{\partial\, z^2} \tag{3.8}$$

Where $\bar{q}$ is the average adsorbed protein concentration, C_b is the bulk protein concentration, D_L is the axial dispersion coefficient, u_i is the interstitial velocity of the fluid phase, ε_b is the bed external porosity (volume void fraction), *z* is the axial coordinate and *t* is time. The external (bed) porosity of this column was estimated to be $\varepsilon_b = 0.45$, using the stoichiometric time of a breakthrough experiment.

The linear driving force (LDF) approximation was assumed and its equation was used:

$$\frac{\partial \overline{q}}{\partial t} = k_G \cdot (q^* - \bar{q}) \tag{3.9}$$

where k_G is the global mass transfer coefficient and q^* is the adsorbed concentration at the adsorbent surface, supposed in equilibrium (described by the Langmuir isotherm) with the local concentration in the mobile phase.

Boundary conditions

$$z = 0 \quad \rightarrow \quad u_i \cdot C_{bo} = u_i \cdot (C_b)_{z=0} - D_L \cdot \left(\frac{\partial C_b}{\partial z}\right)_{z=0} \tag{3.10}$$

$$z = H \quad \rightarrow \quad \left(\frac{\partial C_b}{\partial z}\right)_{z=H} = 0 \tag{3.11}$$

Initial conditions

$$t = 0 \quad \rightarrow \quad C_b(z, 0) = 0 \tag{3.12}$$

As in the batch adsorption studies, here the adsorption equilibrium is represented by the Langmuir isotherm.

3.3.3. Model parameters

The effective pore diffusivity, D_{pe} in the adsorbent was estimated by independent batch experiments.

The molecular diffusion can be calculated by a correlation provided by Young and co-workers [26] which is based on a wide range of proteins.

$$D_m = 8.34 \times 10^{-12} \cdot \left(\frac{T}{\eta \cdot {M_w}^{1/3}}\right) \tag{3.13}$$

where D_m is the molecular diffusion coefficient ($cm^2.s^{-1}$), T is temperature (K), η is viscosity (cP) and M_w is molecular weight ($g \cdot mol^{-1}$). Additionally, Young indicated that the Wilke-Chang [27] correlation cannot be extrapolated for estimating protein diffusion coefficients in water.

Later, Walters and co-workers [28] suggested that Human Serum Albumin (66 kDa at 20 °C) has a molecular diffusion of 3.84×10^{-5} ($cm^2 \cdot min^{-1}$) [29].

The effective pore diffusion can be estimated by the following equation

$$D_{pe} = \frac{\varepsilon_p \cdot D_m}{\tau} \tag{3.14}$$

$$k_{int} = \frac{15 \cdot D_{pe}}{{r_p}^2} \tag{3.15}$$

The estimation of the global mass transfer coefficient (k_G) to be used in the LDF model (equation 3.9) was done by fitting the model solution to the breakthrough experimental results of packed bed experiments. Also, it can be estimated as function of the external and internal mass transfer coefficients, k_{ext} and k_{int} , respectively.

$$\frac{1}{k_G} = \frac{1}{k_{ext}} + \frac{1}{k_{int}} \tag{3.16}$$

The Wilson-Geankoplis [30] equation, applicable to low Reynolds number is used to estimate the external mass transfer.

$$Sh = \frac{1.09}{\varepsilon_b} \cdot Re^{1/3} \cdot Sc^{1/3} \qquad (0.0015 < Re < 55) \tag{3.17}$$

where Re is the Reynolds number [$= \rho \cdot d_p \cdot u_i / \eta$], Sc represents the Schmidt number [$= \eta / (\rho \cdot D_m)$], Sh is the Sherwood number [$= d_p \cdot k_{ext} / D_m$], and D_m is the molecular diffusion coefficient. However other equations can be used, such as, Ranz and Marshall [31], Wakao and Funazkri [32], or Fan et al. [33].

3.3.4. Numerical solution

The numerical solution of the model equations was obtained by using the commercial software gPROMS (general PROcess Modelling System) version 3.4.0, using a method of orthogonal collocation in finite elements (OCFEM); the axial dimension of the bed was discretized in 51 finite elements with 2 interior collocation points in each finite element and the DASOLV integration solver was used to solve the remaining system of ordinary differential equations in time. Regarding the batch kinetic experiments, the radial dimension was discretized in 100 finite elements with 2 interior collocation points in each finite element. For all simulations a tolerance of 10^{-5} was used.

3.4. Results and discussion

3.4.1. Characterization of Mabdirect MM

MabDirect MM is a mixed mode adsorbent with an anionic mixed mode ligand from *Rhobust Fastline series* that is composed by a base matrix of 6% cross-linked agarose with a tungsten carbide particles. According to Kelly et al. [34, 35] the ligand has a pKa of 5.0 and contains hydrophobic (benzoic acid) regions. Also, this adsorbent has a tested ligand concentration of 35 mmol.$L_{adsorbent}^{-1}$ and adsorbent density of 2.9 g·cm^{-3} according to the users guide.

A particle size distribution experiment (Figure 3.2) was conducted in a Coulter LS230 Laser particle size analyser giving a mean particle size of 94.6 µm. Also the 10%, 50% (median) and 90% of the cumulative volume of the particle size distribution correspond to 69.3, 103.9 and 133.2 µm, respectively.

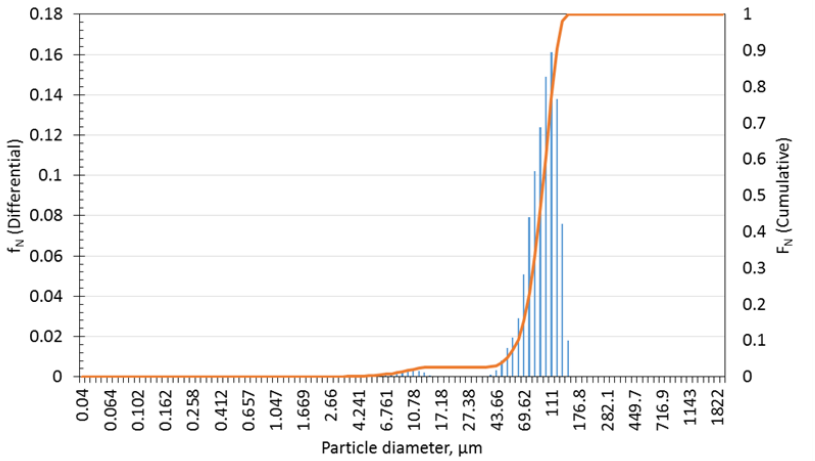

Figure 3.2 – Differential and cumulative particle size distributions for MabDirect MM.

Before characterization of the adsorbent, it was dried at room temperature overnight inside of a desiccator so that the hydrate structure would not be compromised. Mercury porosimetry was conducted over a sample of the adsorbent, and it was obtained an intra-particle (ε_p) porosity of 0.237. Also, helium pycnometry provided a particle porosity of 0.239, confirming the previous value. In order to determine the structure of the adsorbent used, a Scanning Electron Microscopy (SEM) analysis was conducted at the *Centro de Materiais da Universidade do Porto – Portugal*. The results can be observed in Figures 3.3 and 3.4.

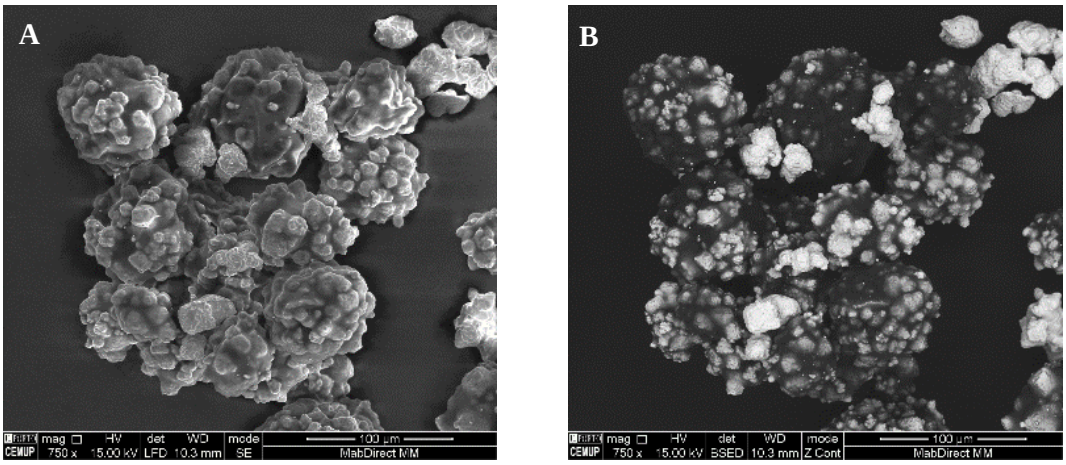

Figure 3.3 – Representation of SEM method from secondary electrons (A) and atomic number of specimen (B).

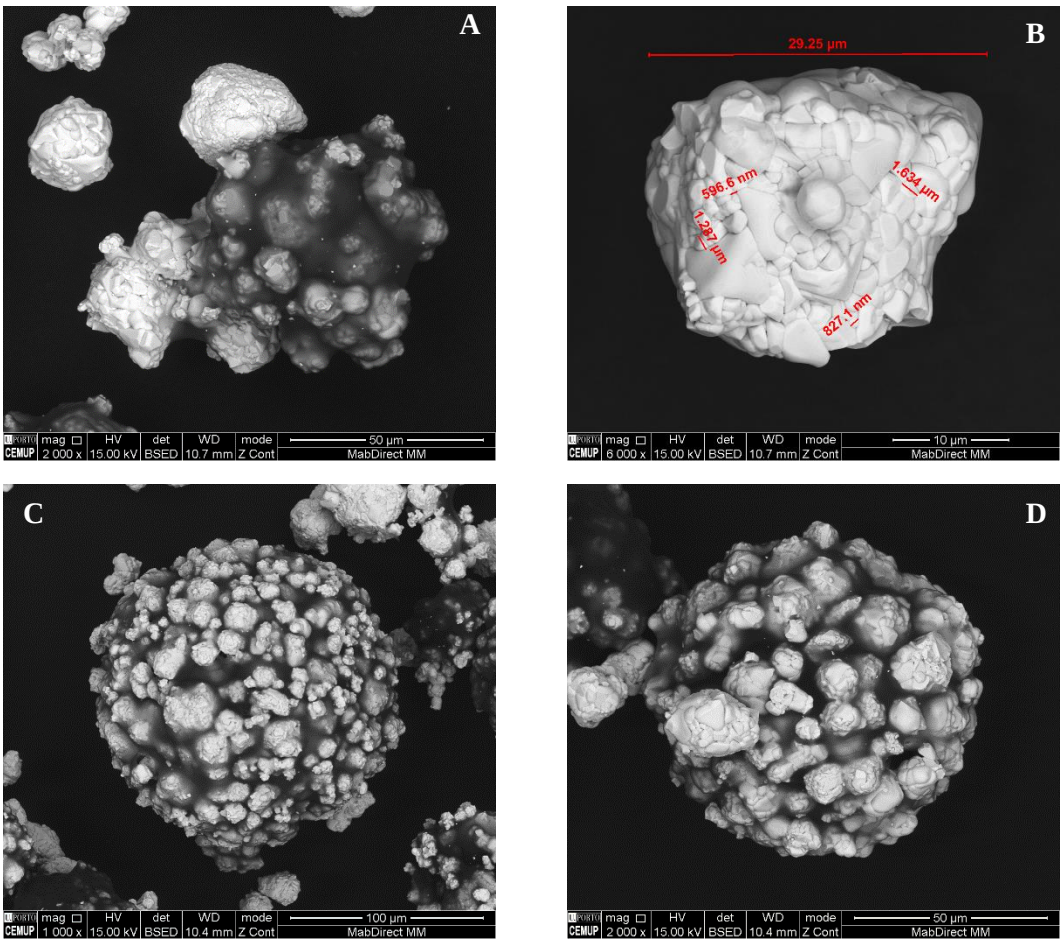

Figure 3.4 – Scanning Electron Microscopy of MabDirect MM adsorbent. (A) 6% cross-linked agarose matrix with tungsten carbide particle and free particle of tungsten carbide; (B) tungsten carbide particle; (C and D) Agarose matrix with tungsten carbide particles in spherical arrangement.

A similar adsorbent structure was observed by Xia et al. [36] and Shi et al. [37] when they prepared cellulose matrix with tungsten carbide composite beads with anion exchange ligand of dextrandiethylaminoethyl (DEAE) for expanded bed application purposes.

3.4.2. Adsorption equilibrium isotherm and HSA effective pore diffusivity

Different HSA protein concentrations (0.2 – 2.0 g.dm^{-3}) were prepared in 100 mL buffer solutions at 20 °C, and 1.26 g of dry adsorbent were added. The effect of ionic strength and of pH were assessed since they are the main relevant physical properties that affect protein adsorption. For the study at pH 3.0, 5.0 and 6.0, a 20 mM citrate buffer was used, while for the study of pH 7.0 it was used a 20 mM phosphate buffer. Different salt concentrations (0 – 1 M) were tested for different pH values. An experiment was conducted to study the adsorption kinetic behaviour by changing the stirring velocity, Figure 3.5.

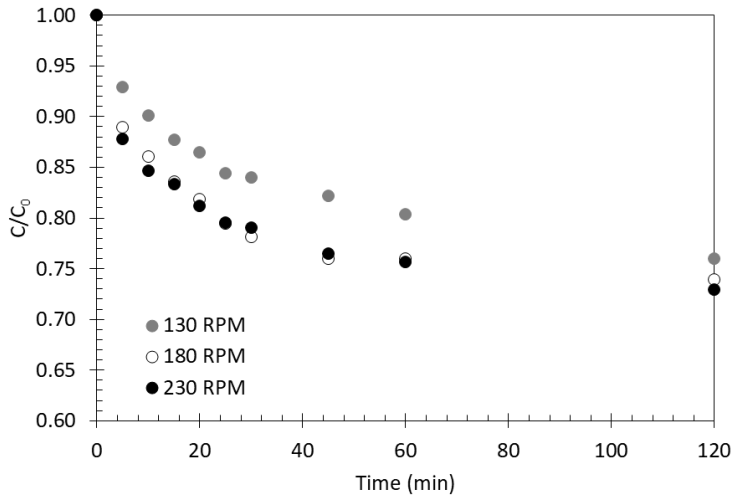

Figure 3.5 – Effect of stirrer speed on the evolution of HSA normalized concentration vs time (min) in batch adsorber. Conditions: C_0= 1g.dm^{-3}, ~ 1.26 g of dry MabDirect MM; 100 mL of HSA solution (20 mM citrate buffer pH 5), 20 °C.

The adsorption kinetics at 180 and 230 rpm showed the same behaviour, and it was chosen to work at 230 rpm, so that the external mass transfer coefficient could be neglected. This result proves that the internal mass transfer is dominant, and the external mass transfer can be neglected.

3.4.2.1. Effect of salt on HSA adsorption

The protein binding showed some typical properties, such as salt-tolerance and pH-dependence. Table 3.1 lists the parameters of HSA adsorption equilibrium on MabDirect MM for the different pH and salt concentrations tested.

Table 3.1 – Parameters of HSA adsorption equilibrium and kinetics of MabDirect MM in 20 mM citrate buffer (pH 5.0) and 20 mM phosphate buffer (pH 7.0), containing different NaCl concentrations.

pH	C_{NaCl}(mol·L^{-1})	q_m(mg·g$_{dry}^{-1}$)	K_L (L·g^{-1})	D_{pe} (×10^{-6} cm^2·min^{-1})
5	0	36.0 ± 3.5	4.62 ± 0.46	2.2 ± 0.1
	0.1	30.7 ± 6.3	3.46 ± 0.42	1.9 ± 0.1
	0.5	29.1 ± 1.1	0.88 ± 0.05	2.4 ± 0.4
	1	13.4 ± 2.5	2.36 ± 0.47	2.2 ± 0.4
7	0	8.6 ± 2.1	10.08 ± 2.48	2.4 ± 0.6
	1	11.8 ± 2.2	1.65 ± 0.34	4.8 ± 0.3

Figure 3.6 and Figure 3.7 show the effect of ionic strength by adding salt to the protein buffer on adsorption isotherms. These figures show that the Langmuir model was able to represent the experimental data for all series of tested conditions.

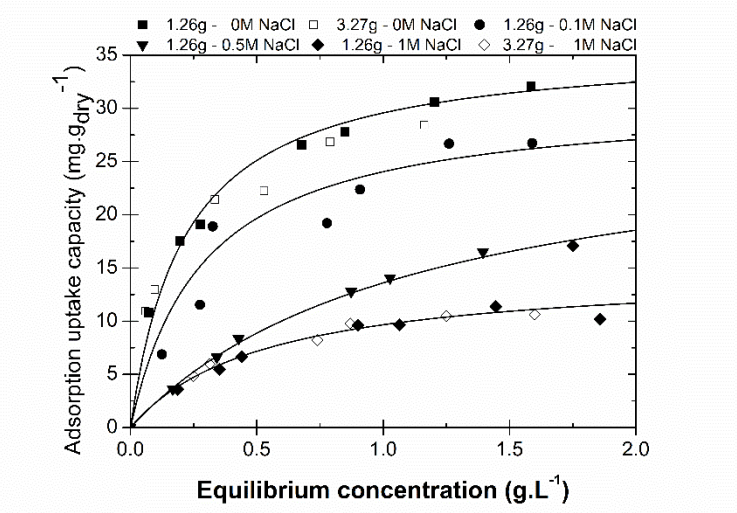

Figure 3.6 – Adsorption isotherms of HSA on MabDirect MM from a 20 mM citrate buffer at pH 5.0 for different NaCl concentrations at 20 °C: experimental data (full points – 1.26g of adsorbent, hollow points – 3.27g of adsorbent) and Langmuir model (curves).

From Figure 3.6 it is possible to conclude that the absence of salt in solution has a positive effect on adsorption, registering the largest maximum adsorption uptake capacity (36.0 ± 3.5 mg·g$_{dry}^{-1}$). In contrast, when 1M of NaCl is added to the protein buffer solution the maximum adsorption capacity was 13.4 ± 2.5 mg.g$_{dry}^{-1}$. It is important to notice that even at high ionic strength, such as 1M NaCl, the adsorbent ligand has a larger binding capacity to the HSA, as

opposed to the classical ion exchangers (Streamline SP and DEAE). Understanding the effect of the ionic strength in the effective pore diffusion coefficient is a complex task. In the work of Li et al. [14] it is referred that when the ionic strength in the protein solution increases, although the electrostatic interaction becomes significantly weak, there still exist hydrogen bonds and hydrophobic interactions between the target protein and the adsorbent ligand that lead to a larger binding capacity even when increasing the salt concentration.

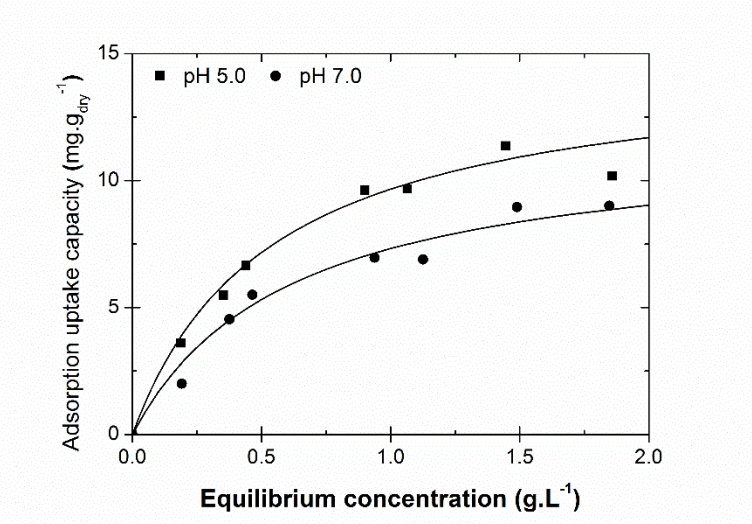

Figure 3.7 – Adsorption isotherms of HSA in 20 mM citrate buffer pH 5 (squares) and HSA in 20 mM phosphate buffer pH 7 (circles): Experimental data (points) and Langmuir model (curves). Conditions: All experiments with 1M NaCl at 20 °C.

Regarding the adsorption equilibrium experiments in which three times the mass of adsorbent were added (3.27 ± 0.16 g), Figure 3.6 also shows that the new experimental data (open symbols) fit with the previously determined batch adsorption isotherms.

It is interesting to note that, contrarily to what happens near the isoelectric point of the adsorbent, i.e., at pH 5.0, for a protein buffer of pH 7.0, a slight increase in the maximum adsorption capacity was observed when adding salt.

Kinetic studies were performed in a batch adsorber in order to determine the uptake rates of the HSA at different conditions for this material. In order to study the transport properties of the adsorbent/protein system, it is important to fit the experiments with a suitable transport model. In this work, the pore diffusion model (PDM) was used, and results (for 20 mM citrate buffer pH 5.0 without and with 0.1, 0.5 and 1M NaCl) are shown in Figure 3.8 as well as for 20 mM phosphate buffer pH 7.0 without and with 1M NaCl as it can be observed in Figure 3.9.

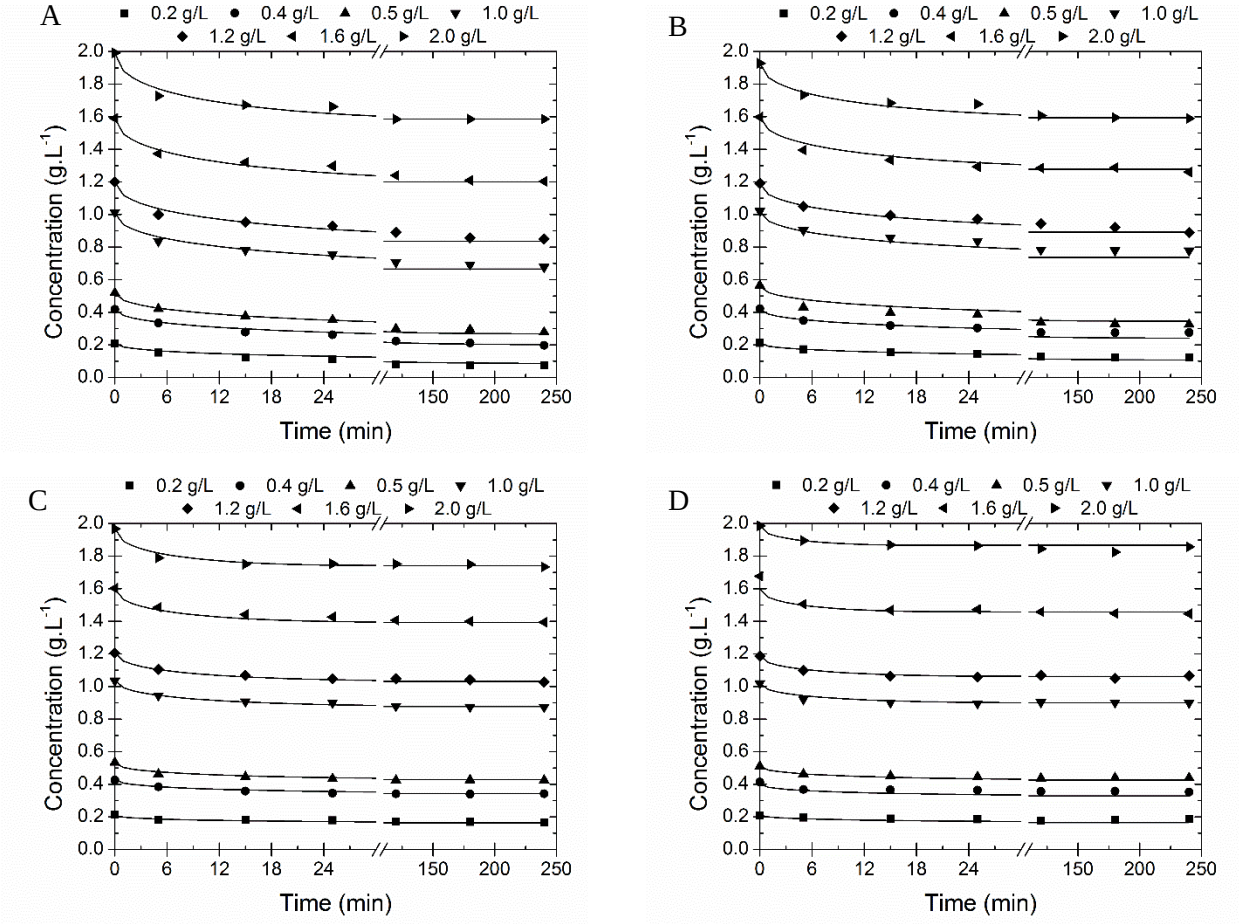

Figure 3.8 – Experimental data and calculated uptake curves of HSA from 20 mM citrate buffer pH 5.0 on MabDirect MM, at 20 °C, with different salt concentrations: A) Without salt; B) 0.1M NaCl; C) 0.5M NaCl; D) 1M NaCl.

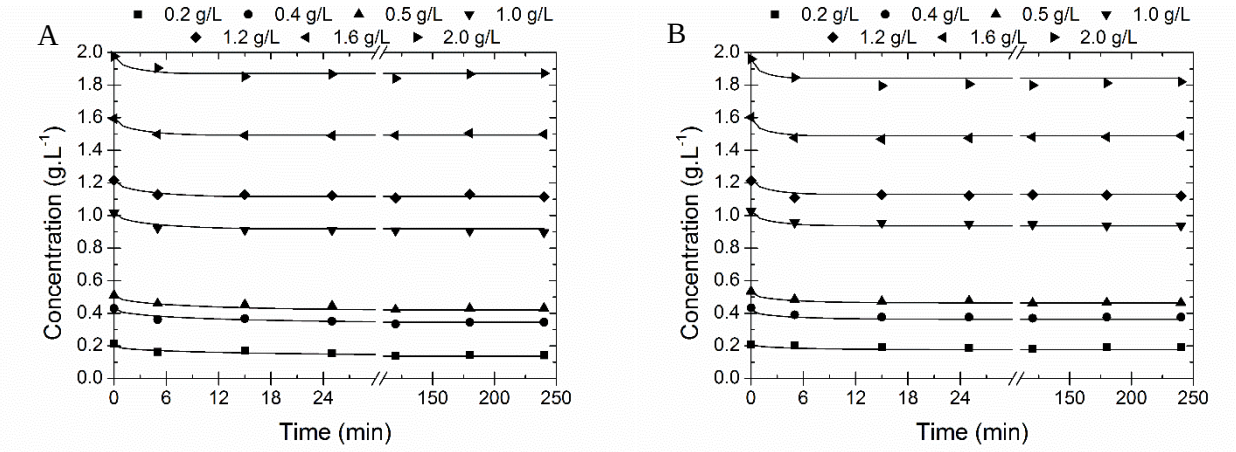

Figure 3.9 – Experimental data and calculated uptake curves of HSA from 20 mM phosphate buffer pH 7.0 on MabDirect MM, at 20 °C, with different salt concentrations: A) Without salt B) 1M NaCl.

It is to be noted that the PDM could describe well the adsorption kinetics under the studied conditions. Reasonable estimations were made for the intra-particle diffusion coefficient. The fitted values of the effective pore diffusion coefficient are also given in Table 3.1. It was obtained a significantly lower D_{pe} value than reported for traditional ion exchanger adsorbents (Streamline DEAE, 1.9 $\times 10^{-5}$ $cm^2 \cdot min^{-1}$).

For 20 mM citrate buffer pH 5.0 without the addition of salt where it was used 3.27g of adsorbent it was estimated a D_{pe} of (2.4 ±0.2) × 10^{-6} $cm^2 \cdot min^{-1}$ comparable with (2.2 ± 0.1) × 10^{-6} $cm^2 \cdot min^{-1}$ previously obtained (see Table 3.1). For pH 5.0 buffer with 1M NaCl the same D_{pe} value (2.2 ± 0.4) × 10^{-6} ($cm^2 \cdot min^{-1}$) was used and proved to fit the experimental results (Figure 3.10).

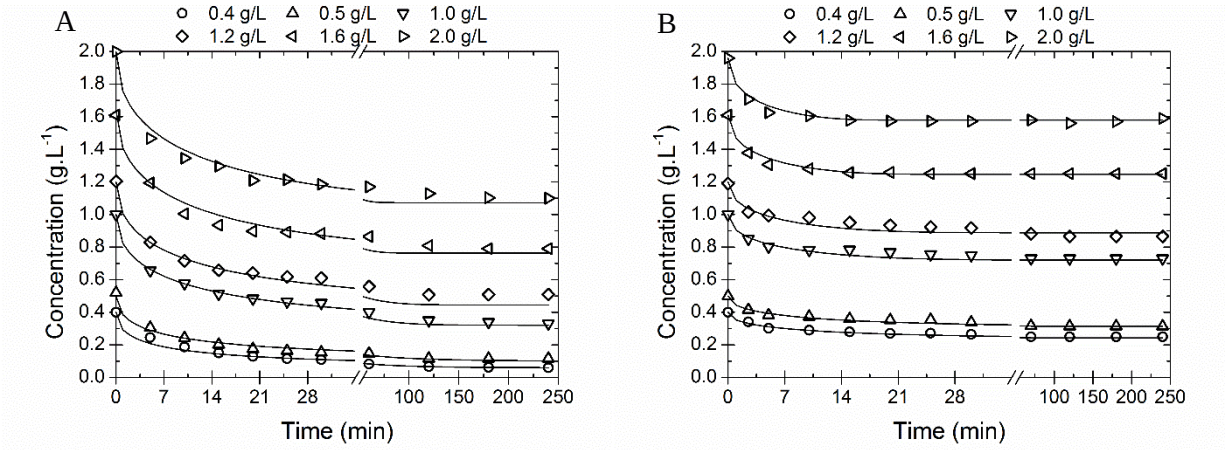

Figure 3.10 – Experimental data and calculated uptake curves of HSA from pH 5.0, at 20 °C, for 3.27g of adsorbent, without (A) and with 1M NaCl (B).

Kelly et al. [34] report similar results when working with two mixed-mode adsorbents (one of which is the MabDirect MM) referring that this result could be due to the additional charge and hydrophobic interactions occurring between the diffusion target protein and the adsorbent surface.

In our work, when studying the effect of ionic strength for two distinctive pH values, it was found that, when the pH (5.0) is near the *pI* of the target protein (4.7), for 0.5M NaCl, the largest D_{pe} value was (2.4 ± 0.4) × 10^{-6} $cm^2 \cdot min^{-1}$, while for a pH where the major protein-adsorbent interaction is the electrostatic repulsion (7.0), the largest D_{pe} value was (4.8 ± 0.3) × 10^{-6} $cm^2 \cdot min^{-1}$, for 1M NaCl. These results agree with those of Kelly and co-workers, who state that changing the salt concentration affects the diffusivity value and variation in the pH and salt concentration affects the interactions between the charges on the target protein and the adsorbent surface.

Nfor and co-workers [38] studied the thermodynamic modeling of protein adsorption on mixed mode adsorbents functionalized with ligand carrying hydrophobic and electrostatic regions. They studied five model proteins, including albumin from bovine serum, lysozyme from chicken egg white, ovalbumin (albumin from chicken egg white), alpha-chymotrypsin from bovine pancreas and amyloglucosidade from *Aspergillus niger* in four different HIC-IEX mixed mode resins from two different suppliers, including PPA HyperCel (phenylpropylamine) and HEA HyperCel (hexylamine) from Pall Life Sciences, Capto MMC (2-Benzamido-4-

mercaptobutanoic acid) and Capto Adhere (N-benzyl-N-methylethanolamine) from *GE Healthcare*. Nfor et al. used a weak anion exchanger mixed mode ligand to explain the effect of pH and salt on mixed mode protein binding strength. They referred that, regarding the study of the ionic strength at low salt concentration, the protein and the ligand present opposite charges, electrostatic protein-ligand interactions dominate, decreasing with the increasing salt concentration until some intermediate salt concentration is reached, where there is a balance of the electrostatic and hydrophobic interactions resulting in a minimal protein binding strength; and as the salt concentration increases, hydrophobic interactions become dominant. This so-called salt-tolerant protein adsorption behaviour [14, 39-41] has been observed even under electrostatic repulsion conditions between protein and the ligand. In this case, the electrostatic protein-ligand interactions are driven by the heterogeneous charge distribution on the surface of the protein which creates oppositely charged regions or patches on the protein with respect to the ligand and irrespective of same sign net charge of protein and the adsorbent, designated in this way a "Patch-controlled" protein adsorption. The results and interaction mechanism described by Nfor and co-workers validate the results obtained. Although Nfor et al. is indicating for anion exchanger mixed-mode resins, they also refer that an opposite effect is possible to be presented for cation exchanger mixed-mode resins.

When studying the effect of ionic strength, increasing the salt concentration to 1M, it is possible to observe a maximum on the effective pore diffusion value at a salt concentration of 0.5M. To summarize, it can be said that adding salt gradually, the D_{pe} value will increase due to a decrease in the ionic interaction with a minimal hydrophobic interaction; however, continuing to increase the solution salt concentration there will be an increase in the hydrophobic interaction which might explain the decrease of D_{pe} at pH 5.0 when the salt concentration goes from 0.5 to 1M (Table 3.1) [34].

3.4.2.2. Effect of pH on HSA adsorption

pH is the other major factor that influences the protein adsorption in a mixed mode adsorbent. The apparent maximum binding capacity and the Langmuir equilibrium constant values for different pH are given in Table 3.2. Also, the estimated effective pore diffusion coefficient values are presented.

Table 3.2 – Parameters of HSA adsorption equilibrium and kinetics to MabDirect MM in 20 mM citrate buffer (pH 3.0, 5.0, 6.0) and 20 mM phosphate buffer (pH 7.0), without salt.

pH	q_m(mg·g$_{dry}^{-1}$)	K_L (L·g^{-1})	D_{pe} ($\times 10^{-6}$ cm^2·min^{-1})
3	30.9 ± 5.7	10.36 ± 1.91	2.9 ± 0.4
5	36.0 ± 3.5	4.62 ± 0.46	2.2 ± 0.1
6	21.5 ± 2.9	1.74 ± 0.28	2.0 ± 0.5
7	8.6 ± 2.1	10.08 ± 2.48	2.4 ± 0.6

Wang and co-workers [42] provided a good insight about the effect of pH on protein adsorption. They studied Immunoglobulin (IgG) and Bovine Serum Albumin (BSA) adsorption in four distinct mixed mode adsorbents, cation and anion exchangers with different bead base (agarose or cellulose). They stated that the hydrophobic interaction is offered by the aromatic rings of the ligands and that, in addition to it and to ionic interactions (electrostatic attraction and repulsion forces), there are secondary interactions, including hydrogen bonding, thiophilic interaction, pi-pi interaction and pi-cation interaction [15, 43]. Moreover, the aromatic moiety of the ligand may interact with the residues that have an aromatic ring (Phe, Tyr, Try and His) or cationic group (Arg, His and Lys) [44, 45]. Wang et al. [42] reported that the zeta potential of the BSA went to zero when the pH was near 4.5, corresponding to the protein isoelectric point. Zeta potential is a parameter used in the colloid science to understand the colloid electrostatic interaction; it is also used to describe the cell surface charge properties and bioadhesion [46]. Therefore, a variety of molecular interactions between the mixed-mode ligand and the protein will confer unique specificity to the adsorbent, and the operating conditions need to be studied for an efficient protein separation. Additionally, the charge of the ligand depends of the type of adsorbent.

Relating to the mixed mode adsorbent (Bestarose Diamond MMC from BestChrom Biotechnology, China) increasing the solution pH from the pI to pH 8.0, BSA could be eluted with a recovery of 83.1% because the adsorbent ligand carries more negative charges since the carboxylic group is not completely dissociated at pH 4; so the protein can be adsorbed at this pH and desorb during a gradient increase of pH which is when the ionic repulsion is high enough and surpasses all attraction forces. In other work, Yan et al. [47] studied the behaviour of Nuvia cPrime resin (mixed-mode resin with *p*-aminohippuric acid as the functional ligand) with bovine

immunoglobulin G and BSA as the model protein and impurity, respectively. They conclude that protein adsorption behaviour is strongly influenced by the pH referring that increasing the pH, the adsorption of BSA decreases; regarding the ionic strength studies they conclude that increasing the concentration of NaCl on solution there was a gradually decrease of the adsorption capacity of BSA.

Nfor and co-workers [38] also referred that when studying the effect of pH in protein adsorption there are two distinctive parameters of interest such as isoeletric point of protein and the pKa of the charger group on the mixed mode ligand. Nfor et al. extended the explanation by stating that by varying the solution pH relative to the pI of the protein and the pKa of the ligand, the net charges on the protein and the ligand can be manipulated. At pH values below the pI, the protein and ligand become similarly charged and so experience electrostatic charge repulsion. At pH values close to or equal to the pI, the protein loses most or all of its net charge and so hydrophobic interactions are expected to be dominant. At pH values above the pI of the protein and below the pKa of the ligand, the strength of electrostatic protein interaction increases with increasing pH. When the pH is increased above the pKa (or below the pKa in the case of a weak cation exchanger mixed mode ligand), the ligand gradually loses its net charge thereby weakening the electrostatic protein interactions. This conclusion achieved by Nfor and co-workers validate the results obtained. In fact, when the buffer pH is below the protein pI, the net charge of protein and the adsorbent ligand are similar and so experience electrostatic charge repulsion. However, continually increasing buffer pH (close to pka of the adsorbent ligand) will make protein lose most of its net charge and so hydrophobic interactions are expected to be dominant. Crossing the pH above the pKa of the adsorbent, electrostatic protein interaction increases, and therefore the protein adsorption is reduced. Regarding our system (adsorbent-protein), we know that the adsorbent has pKa near 5.0 and the HSA has a *pI* near 4.7, making the highest adsorption binding capacity at pH 5.0; also, there is a gradually decrease of binding capacity with an increase in pH, as expected. Therefore, the protein will bind at low pH, near the *pI* since it presents an optimal balance of positive and negative charges and hydrophobic interaction between the adsorbent and the target protein, and will be eluted at high pH by electrostatic repulsion.

Li et al. [40] verified, when working with Streamline CST-I adsorbent (now Streamline HST), that it also had higher adsorbing capacity for the BSA when the pH of the protein solution was near the isoelectric point of the target protein. They refer that, when operating in a pH range of 5-7, BSA has negative charge so the binding takes advantage of hydrogen bonds instead of charge-charge interactions. Also, when working at pH 4.0, the BSA has positive charges, the adsorption of the target protein takes advantage of the charge-charge interactions and hydrogen bonds. Finally, when working at pH 5.0 (near *pI* of BSA), there is a maximum binding capacity which is an evidence of the contribution of hydrophobic interaction.

In this work the largest adsorption capacity (36.0 ± 3.5 $mg_{HSA} \cdot g_{adsorbent,dry}^{-1}$) was observed at pH 5.0, near the isoelectric point of the target protein (4.7), as already referred, due to the hydrophobic interaction and hydrogen bonding. Then, increasing the solution pH, the electrostatic repulsion interaction will increase achieving the lowest adsorption binding capacity (8.6 ± 2.1 $mg_{HSA} \cdot g_{adsorbent,dry}^{-1}$) at the highest pH tested. Regarding the Langmuir adsorption constant there is a minimum value obtained for pH 6.0. In the work of Gao et al. [41], when comparing the values obtained for the Langmuir constant in different pH and salt concentrations, they concluded that when increasing the pH value and decreasing the salt concentration, the Langmuir adsorption constant will decrease. They also refer that this behaviour suggests that the maximum affinity between protein and adsorbent is around the *pI* of the target protein and at low salt concentration. In our case, a minimum value of K_L is found for pH 6.0; this result differs from Gao and co-workers because the target protein and adsorbent are different.

Figure 3.11 presents the adsorption isotherms for the different pH values tested.

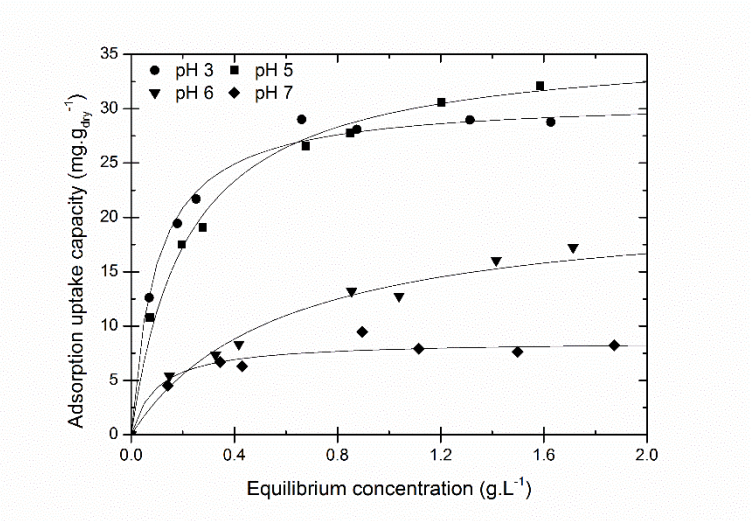

Figure 3.11 – Adsorption isotherms of HSA in different buffer pH: 20 mM citrate buffer pH 3 (circles), pH 5 (squares), pH 6 (triangles); and 20 mM phosphate buffer pH 7 (diamonds): Experimental data (points) and Langmuir model (curves). Conditions: All experiments without salt at 20 °C.

As when studying the effect of ionic strength, experiments were conducted to study the influence of the buffer pH on the adsorption kinetics. Again, the pore diffusion model was used to fit the experimental data along the time (Figure 3.12).

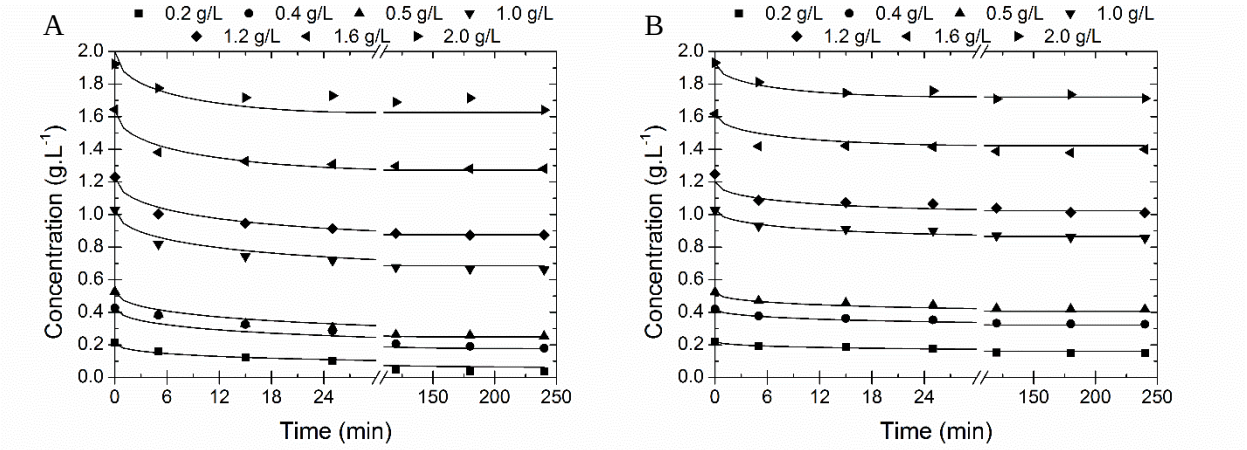

Figure 3.12 – Experimental data and calculated uptake curves of HSA to MabDirect MM under different pH A) 3.0 in 20 mM citrate buffer and B) 6.0 in 20 mM phosphate buffer, 20 °C, 1.26 g of dry adsorbent, 230 rpm.

The fitted values of the effective pore diffusion coefficient are also given in Table 3.2. By observing the obtained results, it is possible to refer that a minimum D_{pe} value is obtained on a buffer pH of 6.0 ($2.0 \pm 0.5 \times 10^{-6}$ cm^2·min^{-1}). This occurrence could be due to the affinity between the target protein and the adsorbent since it was registered also a minimum for the Langmuir coefficient also for this studied condition.

Based on the experimental results, the optimum recommended conditions for HSA protein adsorption in Mabdirect MM would be 20 mM citrate buffer, pH 5.0, without the presence of salt; these optimum conditions will be used in the packed bed experiments. Regarding desorption, it is recommended to use a 20 mM phosphate buffer, pH 7.0, with 1M NaCl, albeit the slight difference observed. Kelly and co-workers [34] also recommended this elution solution and they report an elution recovery in the 91.3-97.1% range.

Although adsorption of HSA in a buffer solution of pH 3.0 was studied, as also in literature [39, 41, 48], below pH 3.0 the hydrodynamic diameter of HSA does not remain stable and for this reason it is not recommended to work in that range, as Lu et al. [39] refer in their work.

An alternative simple method to estimate D_{pe} based on the work of Li et al. [49] is as follows. Equation 3.1 and 3.2, as referred, represent the mass balance in a volume element of the adsorbent particle and the global mass balance to the batch adsorber relating the change in the liquid-phase concentration due to the solid-phase. These model equations using the dimensionless variables $\Theta = {}^{t}/_{\tau_d} = \frac{t \cdot D_{pe}}{{r_p}^2}$ and $x = \frac{r}{r_p}$ were solved leading to $C_b(\Theta)$. For a given concentration C_b, one calculates Θ from the model and the corresponding time from experimental curves $C_b(t)$. In Figure 3.13, Θ from the model is represented versus time for each concentration achieved by batch kinetics experiments.

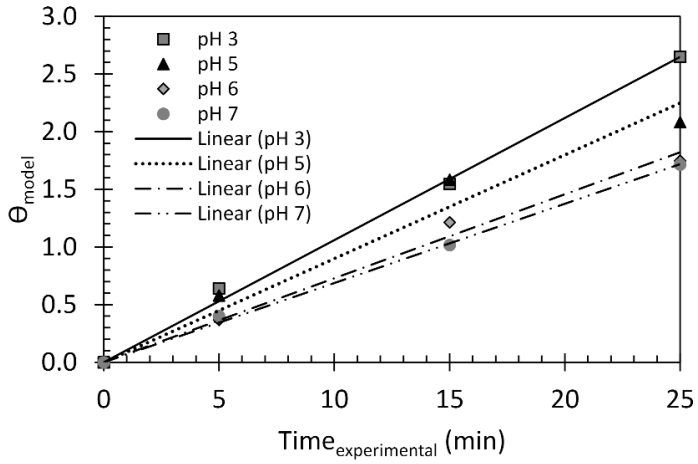

Figure 3.13 – θ vs. time plot for the adsorption kinetics performed in 20 mM citrate buffer, pH 3.0 (squares), 5.0 (triangles), 6.0 (diamonds) and for 20 mM phosphate buffer pH 7.0 (circles), without the addition of salt.

The effective pore diffusion can be calculated from the slope θ vs t plot. For a particle radius of 51.5 µm the D_{pe} obtained for the represented conditions are displayed in Table 3.3.

Table 3.3 – Effective pore diffusion calculated by the slope θ vs. t plot (20 mM citrate buffer, pH 3.0, 5.0, 6.0 and for 20 mM phosphate buffer pH 7.0, without the addition of salt).

pH	D_{pe} ($\times 10^{-6}$ cm^2·min^{-1})
3	2.8
5	2.3
6	1.9
7	1.8

The calculated value of the effective pore diffusion is in reasonable agreement with the estimation provided by the simulations performed by gPROMS (Table 3.2).

3.4.3. Fixed bed adsorption experiments

Frontal analysis experiments were accomplished with HSA as the target protein using MabDirect MM. Several experiments (Table 3.4) were conducted by either changing the feed protein concentration or adding 0.5M NaCl to the feed inlet. Also the efficiency of the regeneration of the adsorbent was studied by packing the column with adsorbent already used.

Table 3.4 – Operating conditions for different breakthrough experiments; adsorption uptake capacity calculated from batch and fixed bed breakthrough experiments at 20 ± 1 °C, using an adsorption 20 mM citrate buffer pH 5.0 solution.

Runs	1	2	3	4
Adsorbent	Cleaned	Fresh	Fresh	Fresh
NaCl (M)	0	0	0.5	0
C_{b0} (g.dm^{-3})	0.92	0.91	0.90	0.22
Q (cm^3.min^{-1})	4.31	4.35	3.70	5.11
H (cm)	4.7	4.4	4.5	4.8
w_{dry} (g)	8.8	8.3	8.4	9.0
$q_{Fixed\text{-}bed}$ (mg·g$_{dry}^{-1}$)	28.26	30.19	12.31	13.31
$q_{Isotherm}$ (mg·g$_{dry}^{-1}$)	29.13	29.03	12.85	18.22
Difference (%)	3	4	4	27

Several experiments with a HSA concentration of near 1 g.dm^{-3} dissolved in a solution of 20 mM citrate buffer, pH 5.0, without salt were conducted. Figure 3.14 presents different adsorption runs using cleaned and fresh adsorbent. Being the terms “cleaned” referred to an adsorbent that went through all the desorption stages; and “fresh” meaning the use of adsorbent that was only conditioned after extracted from the supplier flask. The results show that for the complete cleaning of the adsorbent, four steps are necessary, namely a washing (20 mM citrate buffer pH 5.0, without salt), an elution (20 mM citrate buffer pH 5.0, 1M NaCl), a regeneration (1M NaOH + 1M NaCl) and a final stock solution (200 mM sodium acetate with 14% NaCl) cleaning step. Figure 3.14 shows the differences between the breakthrough curves for a cleaned and a fresh adsorbent.

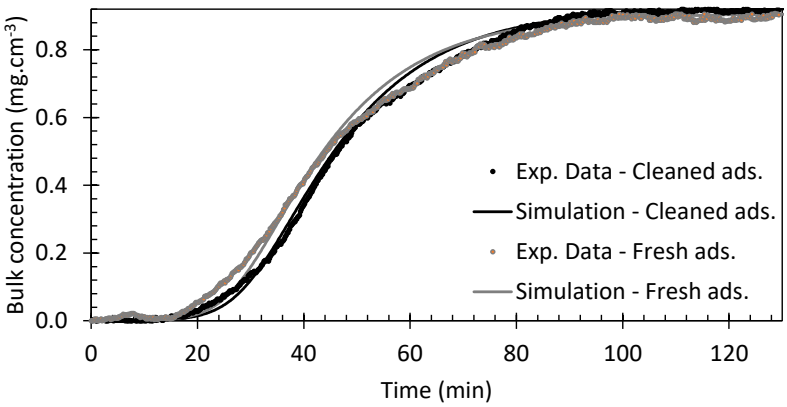

Figure 3.14 – Fixed bed breakthrough experiment for cleaned and fresh adsorbent (black and grey, respectively). Experimental data (points), simulation (curves). Adsorption: 20 mM citrate buffer, pH 5.0, without salt; Operating conditions presented in Table 3.4.

The results show adsorption uptakes of 28.26 and 30.19 $mg_{protein} \cdot g_{adsorbent,dry}^{-1}$ for a protein concentration around 0.92 $g \cdot dm^{-3}$ in 20 mM citrate buffer, pH 5.0, without salt using cleaned and fresh adsorbent, respectively. Note that the equilibrium study gave an adsorption capacity near 29.03 $mg.g_{dry}^{-1}$ in the same conditions. The observed difference of 3-4% is hardly relevant and probably the result of experimental errors. The mathematical model in the present work demonstrated to be able to fit the experimental data (Figure 3.14). The global mass transfer coefficient was determined as 1.28×10^{-4} $cm \cdot min^{-1}$.

An experiment was conducted with a feed solution of 0.22 $g.dm^{-3}$ of HSA in 20 mM citrate buffer, pH 5.0, without salt, flowrate of 5.11 $cm^3 \cdot min^{-1}$, packed bed volume of 9 mL (bed height of 4.8 cm); this experiment was concluded before the saturation of the column and the working capacity cannot be extracted from its results. Nonetheless, the mathematical model used in the present work demonstrated to be able to fit the available experimental data (Figure 3.15). In this instance, the global mass transfer coefficient was determined to be 0.7×10^{-4} $cm \cdot min^{-1}$.

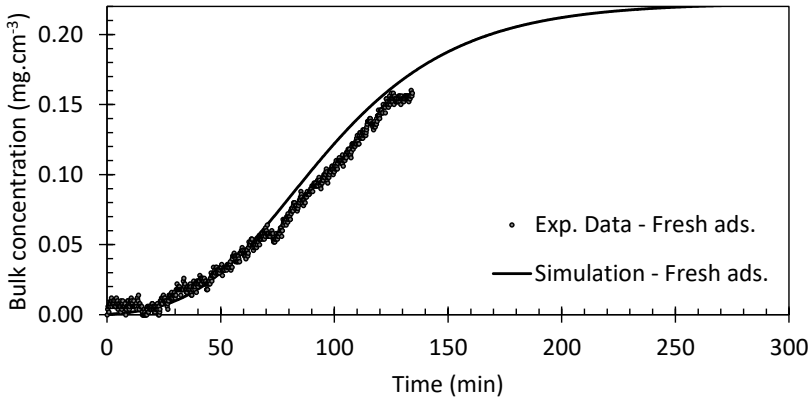

Figure 3.15 – Fixed bed breakthrough experiment for fresh adsorbent with a feed protein concentration of 0.22 $g.dm^{-3}$. Experimental data (points), simulation data (curve). Adsorption conditions: 20 mM citrate buffer, pH 5.0, without salt; Operating conditions presented in Table 3.4.

Another experiment was conducted where salt was added to the feed protein solution. For a feed solution of 0.90 g.dm^{-3} of HSA in 20 mM citrate buffer, pH 5.0, 0.5M NaCl, it was achieved an adsorption uptake capacity of 12.31 $mg_{protein} \cdot g_{adsorbent,dry}^{-1}$. From batch adsorption isotherms it was measured for this protein concentration an adsorption uptake capacity of 12.85 $mg_{protein} \cdot g_{adsorbent,dry}^{-1}$. This result is expected since the electrostatic repulsion is the main force of interaction. The mathematical model demonstrated to reasonably fit the experimental data (Figure 3.16). Global mass transfer coefficient was estimated as 8.0×10^{-4} cm·min^{-1}.

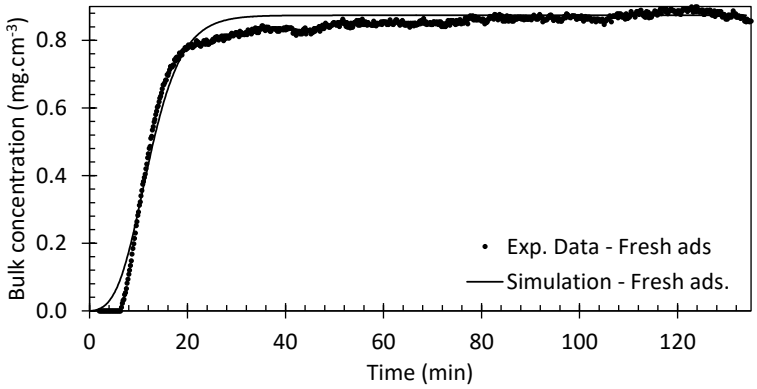

Figure 3.16 – Fixed bed breakthrough experiment for fresh adsorbent with a protein solution of ~ 0.90 g·L^{-1} with salt. Experimental data (points), simulation data (curve). Adsorption: 20 mM citrate buffer, pH 5.0, 0.5M NaCl; Operating conditions presented in Table 3.4.

From the literature, Li et al. [40] reported a 5 % dynamic binding capacity (DBC) of 18.8 mg·g^{-1} for BSA using a mixed-mode adsorbent (Streamline CST-I) at 7.10 cm^3·min^{-1}, determined by the following equation,

$$q_{5\%} = \frac{\int_0^{V_{5\%}} (C_{bo} - C_b) dV}{V_A} \tag{3.18}$$

where V is the effluent liquid volume from the fixed bed, $V_{5\%}$ is the effluent liquid volume at 5% BSA breakthrough point, and V_A is the packed bed volume of adsorbent.

Kelly and co-workers [34] also reported for a globular recombinant protein produced by a proprietary process from a yeast host strain at GlaxoSmithKline using a mixed-mode adsorbent (Fastline HSA) in fixed bed a 10 % DBC of 3.6 - 7.3 mg·g^{-1} and 17-28 mg·g^{-1} for MabDirect MM at 0.3 and 1 cm^3·min^{-1}.

In our work, for HSA using MabDirect MM it was obtained a 10 % DBC of 13.84 and 14.51 $mg \cdot g_{dry}^{-1}$ for cleaned and fresh adsorbent, respectively. The difference of adsorption capacity can be due to the difference of the target protein, since different proteins present distinctive isoelectric points and molecular weight.

3.5. Conclusions

MabDirect MM, a mixed-mode adsorbent, can capture Human Serum Albumin from high ionic strength solutions, as opposed to the ion exchanger sorbents, such as Streamline SP or DEAE.

The maximum adsorption of the protein HSA on the MabDirect MM adsorbent was observed when it is diluted in a 20 mM citrate buffer, pH 5.0, without the presence of salt; a maximum adsorption capacity of 36.0 ± 3.5 $mg \cdot g_{adsorbent,dry}^{-1}$ was experimentally determined in those conditions. In this study, the lowest adsorption capacity was observed when adsorbing from a 20 mM phosphate buffer, pH 7.0, without the presence of salt.

When studying the ionic strength in a pH 5 protein buffer, the largest effective pore diffusion coefficient, $(2.4 \pm 0.4) \times 10^{-6}$ $cm^2 \cdot min^{-1}$, was achieved for the buffer solution with 0.5M NaCl. While for the pH, the largest effective pore diffusion coefficient value, $(2.9 \pm 0.4) \times 10^{-6}$ $cm^2 \cdot min^{-1}$, was estimated for a pH value of 3.0. However, they were nearly one order of magnitude lower than for the first generation adsorbents due to additional charge and/or hydrophobic interactions.

When performing fixed bed breakthrough experiments, it was obtained an adsorbent uptake capacity in agreement with the adsorption equilibrium for all studied conditions. For a feed concentration of 0.92 $g \cdot L^{-1}$, pH 5.0, without salt, the adsorbent removed 30.19 $mg \cdot g_{adsorbent,dry}^{-1}$ from the solution, validating the adsorption equilibrium isotherms (29.03 $mg \cdot g_{adsorbent,dry}^{-1}$). It was obtained a 10 % DBC of 14.51 $mg \cdot g_{adsorbent,dry}^{-1}$ representing near 50% of saturation capacity. For a feed concentration of 0.90 $g \cdot L^{-1}$, pH 5.0, with 0.5M NaCl, it was obtained an adsorption uptake capacity of 12.31 $mg \cdot g_{adsorbent,dry}^{-1}$, also in agreement with the adsorption equilibrium isotherms (12.85 $mg \cdot g_{adsorbent,dry}^{-1}$). A 10% DBC of 2.46 $mg \cdot g_{adsorbent,dry}^{-1}$ was achieved, representing 20% of saturation capacity.

It was possible to estimate a global mass transfer coefficient fitting the experimental data. For the experiments conducted with feed concentration of ± 0.92 $g \cdot L^{-1}$ in pH 5.0, without the presence of salt, the global mass transfer coefficient was estimated as 1.28×10^{-4} $cm \cdot min^{-1}$. For a feed concentration of 0.22 $g \cdot L^{-1}$ in pH 5.0, without the presence of salt, the global mass transfer coefficient was estimated as 0.7×10^{-4} $cm \cdot min^{-1}$ although the experiment was concluded before the saturation of the column. Finally for a feed concentration of 0.90 $g \cdot L^{-1}$ in pH 5.0, with 0.5M NaCl, the global mass transfer coefficient was estimated as 8.0×10^{-4} $cm \cdot min^{-1}$.

3.6. Nomenclature

Bi	–	Biot number
C_{b0}	–	Feed protein concentration
C_b	–	Protein concentration in the bulk phase
C_p	–	Protein concentration in the particle pore
C_{NaCl}	–	Salt (NaCl) concentration
D_L	–	Axial dispersion coefficient
D_m	–	Molecular diffusivity
d_p	–	Particle diameter
D_{pe}	–	Effective pore diffusivity
H	–	Bed height
k_{ext}	–	External mass transfer coefficient
k_G	–	Global mass transfer coefficient
k_{int}	–	Internal mass transfer coefficient
K_L	–	Langmuir adsorption constant
M_w	–	Molecular weight
Q	–	Average adsorption flow rate
$q_{5\%}$	–	Dynamic binding capacity at 5% of breakthrough
q	–	Adsorbed concentration
$\bar{q}$	–	Average adsorbed concentration
q_{max}	–	Maximum adsorption capacity
Re	–	Reynolds number
r_p	–	Particle radios
Sc	–	Schmidt number
Sh	–	Sherwood number
T	–	Temperature
u_i	–	Interstitial velocity
V	–	Effluent liquid volume from the fixed bed
$V_{5\%}$	–	Effluent liquid volume at 5% BSA breakthrough point
V_A	–	Packed bed volume of adsorbent
V_L	–	Volume of protein solution
w	–	Adsorbent mass
t	–	Time
r	–	Radial position
z	–	Axial position

Greek letters

ε_p	–	Particle (solid) porosity
ε_b	–	External (bed) porosity
ε_T	–	Total particle porosity
ρ	–	Density
ρ_ρ	–	Particle density
τ	–	Tortuosity
η	–	Viscosity

Acronyms

HSA	–	Human Serum Albumin
BSA	–	Bovine Serum Albumin
MM	–	Mixed-mode
SEM	–	Scanning Electron Microscopy
SDS-Page	–	Sodium dodecyl sulfate - Polyacrylamide gel electrophoresis
rpm	–	Rotations per minute
pI	–	Protein isoelectric point

3.7. References

[1] H.A. Chase, Purification of Proteins by Adsorption Chromatography in Expanded Beds, Trends in Biotechnology, 12 (1994) 296-303.

[2] NASA Spinoff - Marshall Space Flight Center, Health and Medicine: Protein innovations advance drug Treatments skin Care, https://spinoff.nasa.gov/Spinoff2011/hm_4.html

[3] X.M. He, D.C. Carter, Atomic Structure and chemistry of human serum albumin, Nature Publishing Group, 358 (1992) 209-215.

[4] D.C. Carter, J.X. Ho, Structure of serum albumin, Advances in Protein Chemistry, 45 (1994) 153-203.

[5] T. Peters Jr, The Albumin Molecule: Its Structure and Chemical Properties, in: T. Peters (Ed.) All About Albumin, Academic Press, San Diego, 1995, 9-11.

[6] M. Dockal, D. C. Carter, F. Ruker, The three recombinant domains of human serum albumin. Structural characterization and ligand binding properties, Journal of Biological Chemistry, 274 (1999) 29303-29310.

[7] G. Fanali, A. di Masi, V. Trezza, M. Marino, M. Fasano, P. Ascenzi, Human serum albumin: From bench to bedside, Molecular Aspects of Medicine, 33 (2012) 209-290.

[8] S. Graslund, P. Nordlund, J. Weigelt, B.M. Hallberg, J. Bray, O. Gileadi, S. Knapp, U. Oppermann, C. Arrowsmith, R. Hui, J. Ming, S. dhe-Paganon, H.W. Park, A. Savchenko, A. Yee, A. Edwards, R. Vincentelli, C. Cambillau, R. Kim, S.H. Kim, Z. Rao, Y. Shi, T.C. Terwilliger, C.Y. Kim, L.W. Hung, G.S. Waldo, Y. Peleg, S. Albeck, T. Unger, O. Dym, J. Prilusky, J.L. Sussman, R.C. Stevens, S.A. Lesley, I.A. Wilson, A. Joachimiak, F. Collart, I. Dementieva, M.I. Donnelly, W.H. Eschenfeldt, Y. Kim, L. Stols, R. Wu, M. Zhou, S.K. Burley, J.S. Emtage, J.M. Sauder, D. Thompson, K. Bain, J. Luz, T. Gheyi, F. Zhang, S. Atwell, S.C. Almo, J.B. Bonanno, A. Fiser, S. Swaminathan, F.W. Studier, M.R. Chance, A. Sali, T.B. Acton, R. Xiao, L. Zhao, L.C. Ma, J.F. Hunt, L. Tong, K. Cunningham, M. Inouye, S. Anderson, H. Janjua, R. Shastry, C.K. Ho, D. Wang, H. Wang, M. Jiang, G.T. Montelione, D.I. Stuart, R.J. Owens, S. Daenke, A. Schutz, U. Heinemann, S. Yokoyama, K. Bussow, K.C. Gunsalus, Protein production and purification, Nature Methods, 5 (2008) 135-146.

[9] M. Saraswat, L. Musante, A. Ravida, B. Shortt, B. Byrne, H. Holthofer, Preparative purification of recombinant proteins: current status and future trends, BioMed research international, (2013) 1-18.

[10] M.A. Fernandez, G. Carta, Characterization of protein adsorption by composite silica-polyacrylamide gel anion exchangers I. Equilibrium and mass transfer in agitated contactors, Journal of Chromatography A, 746 (1996) 169-183.

[11] G. Garke, R. Hartmann, N. Papamichael, W.-D. Deckwer, F.B. Anspach, The Influence of Protein Size on Adsorption Kinetics and Equilibria in Ion-Exchange Chromatography, Separation Science and Technology, 34 (1999) 2521-2538.

[12] A.K. Hunter, G. Carta, Protein adsorption on novel acrylamido-based polymeric ion-exchangers: IV. Effects of protein size on adsorption capacity and rate, Journal of Chromatography A, 971 (2002) 105-116.

[13] Giorgio Carta, Alois Jungbauer, Protein Chromatography: Process Development and Scale-Up, Wiley, 2010.

[14] P. Li, Protein Separation and purification by expanded bed chromatography and simulated moving bed technology, in: Ph.D. Thesis, Department of Chemical Engineering, Faculty of Engineering University of Porto, Portugal, 2006.

[15] M.d.A. Lima, M.d.F.M.d. Freitas, L.R.B. Gonçalves, I.J.d. Silva Junior, Recovery and purification of a Kluyvermyces lactis β-galactosidase by Mixed Mode Chromatography, Journal of Chromatography B, 1015–1016 (2016) 181-191.

[16] L.E. Weaver, G. Carta, Protein Adsorption on Cation Exchangers: Comparison of Macroporous and Gel-Composite Media, Biotechnology Progress, 12 (1996) 342-355.

[17] P.R. Wright, F.J. Muzzio, B.J. Glasser, Batch Uptake of Lysozyme: Effect of Solution Viscosity and Mass Transfer on Adsorption, Biotechnology Progress, 14 (1998) 913-921.

[18] K. Kaczmarski, D. Antos, H. Sajonz, P. Sajonz, G. Guiochon, Comparative modeling of breakthrough curves of bovine serum albumin in anion-exchange chromatography, Journal of Chromatography A, 925 (2001) 1-17.

[19] W.-D. Chen, X.-Y. Dong, Y. Sun, Analysis of diffusion models for protein adsorption to porous anion-exchange adsorbent, Journal of Chromatography A, 962 (2002) 29-40.

[20] D. Gao, D.-Q. Lin, S.-J. Yao, Protein adsorption kinetics of mixed-mode adsorbent with benzylamine as functional ligand, Chemical Engineering Science, 61 (2006) 7260-7268.

[21] O. Levenspiel, Chemical reaction engineering, Wiley, 1972.

[22] D.M. Ruthven, Principles of Adsorption and Adsorption Processes, Wiley, 1984.

[23] G. Guiochon, D.G. Shirazi, A. Felinger, A.M. Katti, Fundamentals of Preparative and Nonlinear Chromatography, Academic Press, 2006.

[24] R.P.V. Faria, C.S.M. Pereira, V.M.T.M. Silva, J.M. Loureiro, A.E. Rodrigues, Sorption enhanced reactive process for the synthesis of glycerol ethyl acetal, Chemical Engineering Journal, 258 (2014) 229-239.

[25] G. Guiochon, Preparative liquid chromatography, Journal of Chromatography A, 965 (2002) 129-161.

[26] M.E. Young, P.A. Carroad, R.L. Bell, Estimation of diffusion coefficients of proteins, Biotechnology and Bioengineering, 22 (1980) 947-955.

[27] C.R. Wilke, P. Chang, Correlation of diffusion coefficients in dilute solutions, American Institute of Chemical Engineers Journal, 1 (1955) 264-270.

[28] R.R. Walters, J.F. Graham, R.M. Moore, D.J. Anderson, Protein diffusion coefficient measurements by laminar flow analysis: Method and applications, Analytical Biochemistry, 140 (1984) 190-195.

[29] S. Tarleton, R. Wakeman, Solid / Liquid Separation: Principles of Industrial Filtration, Elsevier Science, 2005.

[30] E.J. Wilson, C.J. Geankoplis, Liquid Mass Transfer at Very Low Reynolds Numbers in Packed Beds, Industrial & Engineering Chemistry Fundamentals, 5 (1966) 9-14.

[31] W. Ranz, W. Marshall, Evaporation from drops, Chemical Engineering Progress, 48 (1952) 141-146.

[32] N. Wakao, T. Funazkri, Effect of fluid dispersion coefficients on particle-to-fluid mass transfer coefficients in packed beds: Correlation of sherwood numbers, Chemical Engineering Science, 33 (1978) 1375-1384.

[33] L.-T. Fan, Y.-C. Yang, C.-Y. Wen, Mass transfer in semifluidized beds for solid-liquid system, American Institute of Chemical Engineers Journal, 6 (1960) 482-487.

[34] W. Kelly, P. Garcia, S. McDermott, P. Mullen, G. Kamguia, G. Jones, A. Ubiera, K. Göklen, Experimental characterization of next-generation expanded-bed adsorbents for capture of a recombinant protein expressed in high-cell-density yeast fermentation, Biotechnology and Applied Biochemistry, 60 (2013) 510-520.

[35] W. Kelly, G. Kamguia, P. Mullen, A. Ubiera, K. Göklen, Z. Huang, G. Jones, Using a two species competitive binding model to predict expanded bed breakthrough of a recombinant protein expressed in a high cell density fermentation, Biotechnology and Bioprocess Engineering, 18 (2013) 546-559.

[36] H.F. Xia, D.Q. Lin, S.J. Yao, Preparation and characterization of macroporous cellulose-tungsten carbide composite beads for expanded bed applications, Journal of Chromatography A, 1175 (2007) 55-62.

[37] F. Shi, D.-Q. Lin, W. Phottraithip, S.-J. Yao, Preparation of cellulose–tungsten carbide composite beads with ionic liquid for expanded bed application, Journal of Applied Polymer Science, 119 (2011) 3453-3461.

[38] B.K. Nfor, M. Noverraz, S. Chilamkurthi, P.D.E.M. Verhaert, L.A.M. van der Wielen, M. Ottens, High-throughput isotherm determination and thermodynamic modeling of protein adsorption on mixed mode adsorbents, Journal of Chromatography A, 1217 (2010) 6829-6850.

[39] L. Hui-Li, L. Dong-Qiang, Z. Mi-Mi, Y. Shan-Jing, Protein adsorption on DEAE ion-exchange resins with different ligand densities and pore sizes, Journal of Separation Science, 35 (2012) 3084-3090.

[40] P. Li, G. Xiu, V.G. Mata, C.A. Grande, A.E. Rodrigues, Expanded bed adsorption/desorption of proteins with Streamline Direct CST I adsorbent, Biotechnology and Bioengineering, 94 (2006) 1155-1163.

[41] D. Gao, D.Q. Lin, S.J. Yao, Mechanistic analysis on the effects of salt concentration and pH on protein adsorption onto a mixed-mode adsorbent with cation ligand, Journal of Chromatography B: Analytical Technologies in the Biomedical and Life Sciences, 859 (2007) 16-23.

[42] R.Z. Wang, D.Q. Lin, H.F. Tong, H.L. Lu, S.J. Yao, Evaluation of mixed-mode chromatographic resins for separating IgG from serum albumin containing feedstock, Journal of Chromatography B: Analytical Technologies in the Biomedical and Life Sciences, 936 (2013) 33-41.

[43] G. Zhao, X.-Y. Dong, Y. Sun, Ligands for mixed-mode protein chromatography: Principles, characteristics and design, Journal of Biotechnology, 144 (2009) 3-11.

[44] W.K. Chung, Y. Hou, M. Holstein, A. Freed, G.I. Makhatadze, S.M. Cramer, Investigation of protein binding affinity in multimodal chromatographic systems using a homologous protein library, Journal of Chromatography A, 1217 (2010) 191-198.

[45] C. Lin, R. Chinnappan, K. Acharya, J.-L. Pellequer, R. Jankowiak, On stabilization of a neutral aromatic ligand by π–cation interactions in monoclonal antibodies, Biophysical Chemistry, 154 (2011) 35-40.

[46] D.-Q. Lin, L.-N. Zhong, S.-J. Yao, Zeta potential as a diagnostic tool to evaluate the biomass electrostatic adhesion during ion-exchange expanded bed application, Biotechnology and Bioengineering, 95 (2006) 185-191.

[47] J. Yan, Q.L. Zhang, D.Q. Lin, S.J. Yao, Protein adsorption behavior and immunoglobulin separation with a mixed-mode resin based on p-aminohippuric acid, Journal of Separation Science, 37 (2014) 2474-2480.

[48] F.Y. Oliva, L.B. Avalle, O.R. Cámara, C.P. De Pauli, Adsorption of human serum albumin (HSA) onto colloidal TiO2 particles, Part I, Journal of Colloid and Interface Science, 261 (2003) 299-311.

[49] P. Li, G. Xiu, A. E. Rodrigues, Modeling separation of proteins by inert core adsorbent in a batch adsorber, Chemical Engineering Science, 58 (2003) 3361-3371.

Chapter 4: Adsorption equilibrium and kinetics of Immunoglobulin G on a mixed-mode adsorbent in batch and packed bed configuration

"All labor that uplifts humanity has dignity and importance and should be undertaken with painstaking excellence."

- Dr. Martin Luther King, Jr.

This chapter presents the adsorption equilibrium isotherms and the adsorption kinetics of Human Immunoglobulin G (IgG) onto a novel second generation high particle density multimodal adsorbent (MabDirect MM) obtained from batch adsorption experiments. The effects of ionic strength (by addition of salt) and of pH are assessed. Langmuir isotherms parameters are obtained along with pore diffusivity values by fitting the batch experiments using a pore diffusion model that take into account the intraparticle effective diffusion and film mass transfer. Furthermore, several experiments were carried out in a fixed bed column with the aim to understand the kinetics and hydrodynamics, and to validate the batch adsorption results. Dynamic binding capacity is also presented.

This chapter is based on the following article:

Gomes, P.F., Loureiro, J.M. & Rodrigues, A.E. Adsorption equilibrium and kinetics of Immunoglobulin G on a mixed-mode adsorbent in batch and packed bed configuration. Journal of Chromatography A, 1524 (2017), 143-152.

4.1. Introduction

Protein purification has been performed for a long time. Monoclonal antibody technology appeared in 1975, involving the establishment of stable cell lines producing a single selected protein. This technique, in association with highly selective chromatographic media, made possible the conception of a large number of applications in research and pharmaceuticals production [1-4].

Immunoglobulin G (IgG) is a complex antibody composed by four peptide chains (with quaternary amine) with two heavy chains and two identical light chains arranged in a Y-shape typical of antibody monomers. IgG represents approximately 75% of immunoglobulins present in human serum. This protein has important functions on the immune system since it is the main antibody found in blood and extracellular fluid, having the function of controlling infection of body tissues. IgG antibodies have a molecular weight of 153 kDa and present four subclasses in humans (IgG1, IgG2, IgG3 and IgG4). IgG can be used for diagnostic purposes, where the measured IgG levels are generally considered to be indicative of an individual immune status to a particular pathogen. Also, it can be used in therapy, where it is extracted from donated blood plasma and used to treat immune deficiencies, autoimmune disorders and infections [5, 6]. This antibody is the only class of Immunoglobulins that can cross the human placenta, and therefore convey protection to the newborn during the first months of life. Considering its abundance and the good specificity towards antigens, IgG became the main antibody to be used in immunological research and clinical diagnostics [5].

Efficient separation and purification of proteins to the desired level of purity is one bottleneck in pharmaceutical industries. Affinity chromatography, using Protein A and Protein G ligands, is commonly used for IgG separations. However, the use of these adsorbents presents potential issues, such as clean-in-place difficulty, ligand leakage and overall sorbent cost [7-10].

Mixed mode chromatography (MMC) appears as an alternative to these costly sorbents. MMC is a method of separation that uses more than one form of interaction between the stationary phase and the solutes in a feed stream. They provide a salt-tolerant, high capacity, easy elution and improvement of adsorption selectivity since they possess additional functional groups that will introduce new cooperative interactions, such as hydrophobic, electrostatic, thiophilic interactions and hydrogen bonds [11-13].

Adsorption techniques are commonly used for protein separation and purification. Adsorption can be carried out in batch or continuous stirred tanks, or using fixed bed or expanded bed technologies. Pros and cons of using each referred method are specified in a previous Chapter 3 [14]. Second generation expanded bed adsorption is a technology developed by Upfront

Chromatography A/S [15, 16]; it consists in the use of a high density material, in this case tungsten carbide particles in agarose matrix (MabDirect MM being an example), that allows high flow rates (300 – 600 $cm \cdot h^{-1}$) at a common expansion factor of two. Using this technology also allows a direct capture of the high-value biopharmaceutical products, reducing process cost and operating time without affecting product purity [11, 17, 18].

The objective of this chapter is to study a novel multimodal adsorbent, especially designed for expanded bed adsorption (EBA) operation, using batch and fixed bed operating modes in the adsorption of a polyclonal antibody protein, Immunoglobulin G (IgG), for a later use in EBA (Chapter 5 and 6) where the influence of different parameters will be investigated. First, batch adsorption experiments are conducted in order to determine the adsorption equilibrium isotherms and the effective diffusivity of the target protein in different conditions. The effects of pH and ionic strength (by addition of salt) are assessed. Fixed bed experiments are then performed in order to validate the batch adsorption results, previously obtained.

4.2. Materials and Methods

4.2.1. Immunoglobulin G

Immunoglobulin G from Human serum (hIgG) was purchased from Sigma–Aldrich, USA. According to the product information sheets, human IgG was purified from pooled normal human serum, and purity was determined to be not less than 95% by sodium dodecyl sulfate polyacrylamide gel electrophoresis (SDS-PAGE) (Product information sheet, Human IgG, Sigma-Aldrich, USA, Product Number I4506). Human IgG was shipped as salt free lyophilized powder. In this work, Human IgG is quantified as total and not its subclasses IgG 1 to 4, so the presence of confounding effects of these multiple subclasses on the protein adsorption and transport are not addressed.

4.2.2. Mixed mode adsorbent

MabDirect MM, from Rhobust Fastline series, is a mixed mode adsorbent composed by a base matrix of 6% cross-linked agarose with tungsten carbide particles [14, 19, 20]. Delivered in an aqueous solution containing 14% NaCl and 0.2M sodium acetate, this adsorbent, with a tested ligand concentration of 35 $mmol \cdot L_{adsorbent}^{-1}$ and adsorbent density of 2.9 $g \cdot mL^{-1}$, according to the manufacturer. The mixed-mode ligand has a pKa of 5.0 and contains aromatic ligands with acidic substituents (benzoic acid) [14, 19, 20]. More details already discussed in Chapter 3.

4.2.3. Equipment

Batch equilibrium experiments were conducted in a Sigma 203 model centrifuge and in a VWR himac CT 15RE centrifuge, while adsorption kinetics experiments were conducted in a Jeio Tech SI-300R shaking incubator. For fixed bed adsorption experiments, an Omnifit 6.6/11 column was used. A Gilson 117 UV detector equipped with a flow-cell was used to monitor IgG concentration at 280 nm wavelength for both batch and packed bed experiments.

4.2.4. Buffer solutions

Target protein is dissolved in different buffer solutions regarding the pH and salt conditions to be tested. A citrate buffer was used for pH values of 5.0 and 6.0 (citric acid, $C_6H_8O_7$, 192.12 $g.mol^{-1}$, with tri-sodium citrate di-hydrate, $Na_3C_6H_5O_7.2H_2O$, 294.10 $g.mol^{-1}$, dissolved in deionized water). A phosphate buffer was used for pH 7.0 (sodium di-hydrogen phosphate di-hydrate, $NaH_2PO_4 \cdot 2H_2O$, 156.01 $g.mol^{-1}$, with di-sodium hydrogen phosphate, Na_2HPO_4, 141.96 $g.mol^{-1}$, dissolved in deionized water) and a Tris-HCl buffer was used for pH value of 8.5 ($C_4H_{11}NO_3HCl$, 157.64 $g.mol^{-1}$, dissolved in deionized water). For all buffer solutions, a 20 mM concentration was used, except for the buffer in which the adsorbent was stored which had a 200 mM concentration. If necessary, the final solution pH was adjusted with 1 M NaOH or 1 M HCl. To study the effect of salt concentration, sodium chloride (NaCl, 58.44 $g.mol^{-1}$) was added [14].

Sodium di-hydrogen phosphate di-hydrate and di-sodium hydrogen phosphate were purchased from VWR Chemicals, while citric acid, tri-sodium citrate di-hydrate, hydrochloric acid, sodium hydroxide, Tris-HCl, sodium acetate and sodium chloride were purchased from Reagente5 [14].

Before performing adsorption equilibrium and kinetics experiments, the adsorbent was conditioned with the same protein buffer solution. This procedure consists in placing some amount of adsorbent in a special glassware equipped with a proper filter connected to a vacuum pump where it will be cleaned with 1L of deionized water before flowing the chosen buffer [14].

4.2.5. Adsorption equilibrium isotherms by Batch experiments

Adsorbent samples (0.050 and 0.127 g – wet weight) are mixed with 1 mL of different protein concentration solutions for about 4h at room temperature (20 °C) in a centrifuge (Sigma 203 model) at 1000 rotations per minute (rpm). After reaching equilibrium, the supernatant is collected by centrifuging (VWR himac CT 15RE) at 4000 rpm for 10 minutes. The equilibrium protein concentration in the liquid phase is measured by a UV spectrophotometer detector at 280

nm. The measurements were repeated three times, and the average value was obtained. The experimental reproducibility was in the range of less than 10%.

4.2.6. Adsorption kinetics by Batch experiments

An adsorbent sample (2 g - wet weight) is mixed with 40 mL of the chosen buffer with an IgG concentration of 0.7 $g \cdot L^{-1}$ at a controlled temperature (20 °C) in a shaking incubator (Jeio Tech SI-300R) at 270 rpm. Periodically, samples (20 µL) were collected and the protein concentration in the liquid phase was measured by a UV spectrophotometer detector at 280 nm. The measurements were repeated three times, and the average value was obtained. The experimental reproducibility was in the range of less than 10%.

4.2.7. Fixed bed Adsorption

Before performing fixed bed adsorption experiments, 3 mL of adsorbent, measured in a graduated cylinder, was drained using a vacuum pump as previously described to account for the wet adsorbent mass. After this step, the wet adsorbent was hydrated in the chosen working buffer and the Omnifit 6.6/11 column was packed and used for the frontal analysis of IgG adsorption experiments. Before the sample loading, the buffer used for equilibration of the packed column was pumped through the column in downward flow. The protein concentration in the outlet stream was measured by UV adsorption at 280 nm.

Different steps take place when performing a fixed bed adsorption experiment as described in previous Chapter 3 [14]. To summarize, the adsorption step, where after the fixed bed column is equilibrated, the process switches to the feedstock application, the desorption step, that starts right after the breakthrough curve reaches the feed protein concentration, after which the process switches to the washing buffer (same as the equilibration buffer) to washout the unbound proteins from the column, and then to elution buffer to elute the IgG protein from the adsorbent at lower flow rate. At this stage the pH and NaCl concentration can be increased to improve the elution efficiency according to the adsorption isotherms. In order to re-use the adsorbent, regeneration solution (1M NaOH with 1M NaCl recommended by the supplier) is pumped through the column. Finally, the stock solution is fed to the fixed bed column so that the adsorbent stays stable at the standard conditions.

4.3. Mathematical Modelling and Numerical Solution for the Protein Adsorption

4.3.1. Batch adsorption model

In order to evaluate the effective pore diffusivity of proteins at studied conditions (pH and salt concentration), a pore diffusion model was used to simulate the dynamic uptake data of several experiments. It is considered that diffusion occurs inside the pores with a driving force expressed in terms of pore fluid concentration gradient [11, 18, 21-23].

The mass balance in a volume element of the adsorbent particle is written as

$$\varepsilon_p \frac{\partial C_p}{\partial t} + \rho_\rho \frac{\partial q}{\partial t} = \frac{D_{pe}}{r^2} \frac{\partial}{\partial r}\left(r^2 \frac{\partial C_p}{\partial r} \right) \tag{4.1}$$

where ε_p is the particle porosity determined by mercury porosimetry (0.237), C_p is the protein concentration in the pore fluid (mg.cm^{-3}), t denotes time (min), ρ_ρ is the particle density (g.cm^{-3}), q is the adsorbed concentration (mg$_{protein}$.g$_{adsorbent}^{-1}$), D_{pe} is the effective pore diffusivity (cm^2.min^{-1}) and r is the radial position (cm).

On its turn, the global mass balance to the batch adsorber, relating the change in the liquid-phase concentration due to the solid-phase uptake can be written as [21, 24]:

$$\frac{dC_b}{dt} = -\frac{3D_{pe}}{r_p} \frac{{}^{W}/_{\rho_\rho}}{V_L} \left(\frac{\partial C_p}{\partial r} \right)_{r=r_p} \tag{4.2}$$

where C_b is the protein concentration in the bulk phase (mg.cm^{-3}), r_p is the particle radius (cm) and V_L is the volume of protein solution in the batch adsorber (cm^3).

Boundary conditions

$$r = 0 \quad \rightarrow \quad \frac{\partial C_p}{\partial r} = 0 \tag{4.3}$$

$$r = r_p \quad \rightarrow \quad D_{pe}\left(\frac{\partial C_p}{\partial r} \right) = k_{ext}\left(C_b - C_p \right) \tag{4.4}$$

where k_{ext} is the external mass transfer coefficient (cm.min^{-1}).

Initial conditions

$$t = 0 \quad \rightarrow \quad q\,(r) = 0 \quad C_p\,(r) = 0 \quad C_b = C_{b0} \tag{4.5}$$

Adsorption equilibrium is represented by the Langmuir isotherm,

$$q = \frac{q_{max} \cdot K_L \cdot C_p}{1 + K_L \cdot C_p} \tag{4.6}$$

where K_L represents the equilibrium constant and q_{max} the maximum adsorption capacity, both determined by adsorption equilibrium batch experiments.

Adsorption capacity is calculated using equation 4.7:

$$q = \frac{V_L \cdot (C_{b0} - C_b)}{w} \tag{4.7}$$

where C_{b0} and C_b represent the initial and bulk protein concentrations, respectively, V_L represents the volume of protein solution and w the adsorbent mass. The calculation of the adsorption capacity does not take into account the amount of liquid in the adsorbent pores since the pore volume is negligible when compared to the solution volume.

4.3.2. Frontal Analysis in a packed bed

Different models can be used to predict the breakthrough curve of a packed bed adsorption experiment, taking into account several factors, such as hydrodynamics, adsorption equilibrium and kinetics [25-28]. The model presented here is the same used in a previous work [14].

Several assumptions were considered:

- The process is isothermal and the mobile phase velocity is constant.
- The bed is packed with porous particles that are spherical and uniform.
- The concentration gradient in the radial direction of the bed is negligible.
- For the fluid phase axial dispersed plug flow is considered.
- Langmuir isotherm equation describes the adsorption equilibrium.
- The linear driving force (LDF) approximation is used to describe the adsorption kinetics.

The mass balance to the protein in a volume element of the mobile phase is described by the following equation:

$$\varepsilon_b \cdot \frac{\partial C_b}{\partial t} + (1 - \varepsilon_b)\, \rho_\rho \frac{\partial \bar{q}}{\partial t} + u_i \cdot \varepsilon_b \cdot \frac{\partial C_b}{\partial z} = \varepsilon_b \cdot D_L \cdot \frac{\partial^2 C_b}{\partial z^2} \tag{4.8}$$

where ε_b is the bed porosity; C_b is the bulk protein concentration; $\bar{q}$ is the average adsorbed protein concentration; u_i is the interstitial velocity of the fluid phase; D_L is the liquid axial dispersion coefficient; *z* is the axial coordinate; *t* is time. The bed porosity of the column was estimated to be $\varepsilon_b = 0.35$, using the stoichiometric time of a breakthrough experiment.

The linear driving force (LDF) approximation was considered and its equation was used:

$$\frac{\partial \overline{q}}{\partial t} = k_G \cdot (q^* - \bar{q}) \tag{4.9}$$

where q^* is the adsorbed concentration at the adsorbent surface and k_G is the global mass transfer coefficient. It is assumed that, at the adsorbent surface, the adsorbed concentration is in equilibrium with the concentration in the mobile phase.

Boundary (BC) and initial conditions (IC) are described as follows

$$BC: \quad z = 0 \quad \rightarrow \quad u_i \cdot C_{bo} = u_i \cdot (C_b)_{z=0} - D_L \cdot \left(\frac{\partial C_b}{\partial z}\right)_{z=0} \tag{4.10}$$

$$z = H \quad \rightarrow \quad \left(\frac{\partial C_b}{\partial z}\right)_{z=H} = 0 \tag{4.11}$$

$$IC: \quad t = 0 \quad \rightarrow \quad C_b(z, 0) = 0 \tag{4.12}$$

4.3.3. Model Parameters

Young and co-workers [29] provided a correlation based on data for a wide range of proteins to calculate the molecular diffusion (D_m). Later, Walters and co-workers [30] suggested that human Immunoglobulin G (153 kDa at 20 °C) has a molecular diffusion of 2.4×10^{-5} ($cm^2 \cdot min^{-1}$). Independent batch experiments allow us to estimate the effective pore diffusion coefficient (D_{pe}) in the adsorbent. However, if the molecular diffusivity of the protein and the intraparticle porosity (ε_p) and tortuosity (τ) of the adsorbent are known or estimated, it can also be estimated by the following equation

$$D_{pe} = \frac{\varepsilon_p \cdot D_m}{\tau} \tag{4.13}$$

Knowing D_{pe}, it is possible to calculate the internal mass transfer coefficient (k_{int}) by equation 4.14, assuming a parabolic concentration profile inside spherical particles.

$$k_{int} = \frac{15 \cdot D_{pe}}{{r_p}^2} \tag{4.14}$$

The global mass transfer coefficient (k_G) was estimated by fitting the model solution to the breakthrough experimental results of packed bed experiments for later use in the LDF model (equation 4.9).

Also, it can be estimated as function of the external (k_{ext}) and internal (k_{int}) mass transfer coefficients, using a resistances-in-series model.

$$\frac{1}{k_G} = \frac{1}{k_{ext}} + \frac{1}{k_{int}} \tag{4.15}$$

Ranz and Marshall [31], Fan et al. [32] or Wakao and Funazkri [33] provided equations to estimate the external mass transfer coefficient for packed bed columns; however, the Wilson-Geankoplis [34] equation, valid for low Reynolds number, was used.

$$Sh = \frac{1.09}{\varepsilon_b} \cdot Re^{1/3} \cdot Sc^{1/3} \qquad (0.0015 < Re < 55) \tag{4.16}$$

where Sh is the Sherwood number $[= d_p \cdot k_{ext} / D_m]$; D_m is the molecular diffusion coefficient; Re is the Reynolds number $[= \rho \cdot d_p \cdot u_i / \eta]$ and Sc is the Schmidt number $[= \eta / (\rho \cdot D_m)]$; d_p is the particle diameter, ρ is the density and η is the viscosity.

4.3.4. Numerical method

Commercial software gPROMS (general PROcess Modelling System), version 3.4.0, allowed us to solve the model equations by employing a method of orthogonal collocation in finite elements (OCFEM); the axial dimension of the bed was discretized in 51 finite elements with 2 interior collocation points in each finite element and the DASOLV integration solver was used to solve the remaining system of ordinary differential equations in time. In the simulation of batch adsorption kinetic experiments, the radial dimension of particles was discretized in 100 finite elements with 2 interior collocation points in each finite element. A tolerance of 10^{-5} was used for all simulations.

4.4. Results and discussion

4.4.1. Mixed mode adsorbent – *MabDirect MM*

Although the adsorbent is commercially available, information published in literature is scarce. In a previous chapter [14], we present some information that can be found in literature [19, 20] as well as some adsorbent characterization. Table 4.1 briefly summarizes the characteristics of this mixed mode adsorbent.

Table 4.1 – Properties of MabDirect MM adsorbent.

Name	Fastline series MabDirect MM		
Manufacturer	Upfront Chromatography A/S (now: Patheon Inc.)		
Matrix structure [a]	6% cross-linked agarose with tungsten carbide particles		
Ligand [a,b]	Cation exchanger mixed mode pKa 5 with hydrophobic (benzoic acid) regions 35 mmol.dm^{-3}		
Bulk density [a,b]	2.9 g.cm^{-3}		
Particle size [c]	94.6 µm (avg.)		
Size distribution [c]	10%	50% (median)	90%
	69.3	103.9	133.2
Porosity (Hg porosimetry) [c]	0.237		
Porosity (He pycnometry) [c]	0.239		

a – from user guide provided by Upfront Chromatography A/S

b – from literature [19-20].

c – from previous work [14].

4.4.2. Adsorption equilibrium isotherm and IgG effective pore diffusivity

Different target protein concentrations (0.2, 0.5, 0.7, 1, 2, 4, 7, 10 g·L^{-1}) were prepared in 1 mL buffer solution at 20 °C, and 0.050 and 0.127g of wet adsorbent mass were added. Two distinctive wet adsorbent masses were used in order to validate the obtained results. pH and ionic strength are the two most studied properties that affect protein adsorption and, for this reason, their effects are accordingly assessed.

The adsorption kinetics was experimentally studied in batch, following the strategy of Li et al. [23]. A model, relating the solute concentration with the dimensionless time $\theta = t/\tau_d =$

$(t \cdot D_{pe})/r_p^2$, was built and solved for several values of the Biot number (Bi); where τ_d is the diffusion time and r_p is the particle radius. For the same experimental and simulated values of the solution concentration, the correct Biot value corresponds to a straight line when θ is represented against t. The slope of this straight line, $1/\tau_d$, gives the value of the effective pore diffusivity, D_{pe}. Knowing the Biot number and the effective pore diffusion it is possible to calculate the external mass transfer.

$$k_{ext} = \frac{D_{pe}}{r_p} Bi \tag{4.17}$$

For cases where $Bi \geq 100$ the external mass transfer can be neglected. One example ($C_b(\theta)$ and θ *vs.* t) is presented in the following figures. Figure 4.1 and 4.2 are examples of plots drawn to test various Bi numbers:

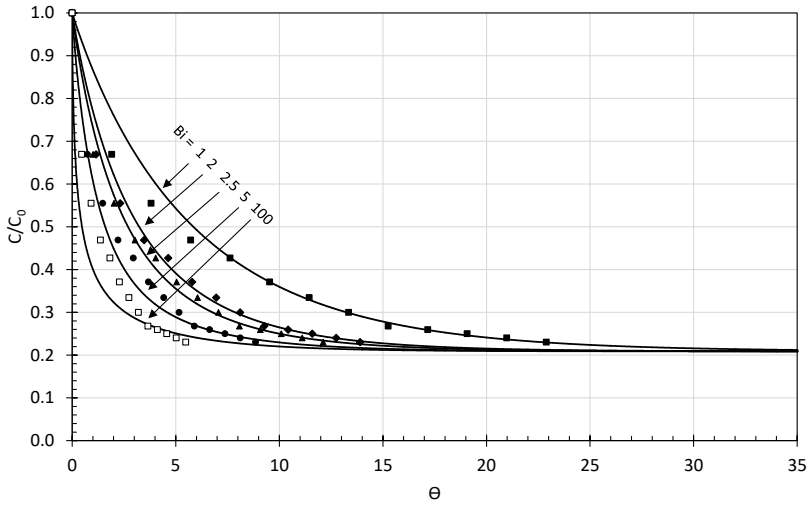

Figure 4.1 – Normalized bulk concentration as a function of dimensionless time Θ. Curves represent simulation while points represent the experimental data for dimensionless time.

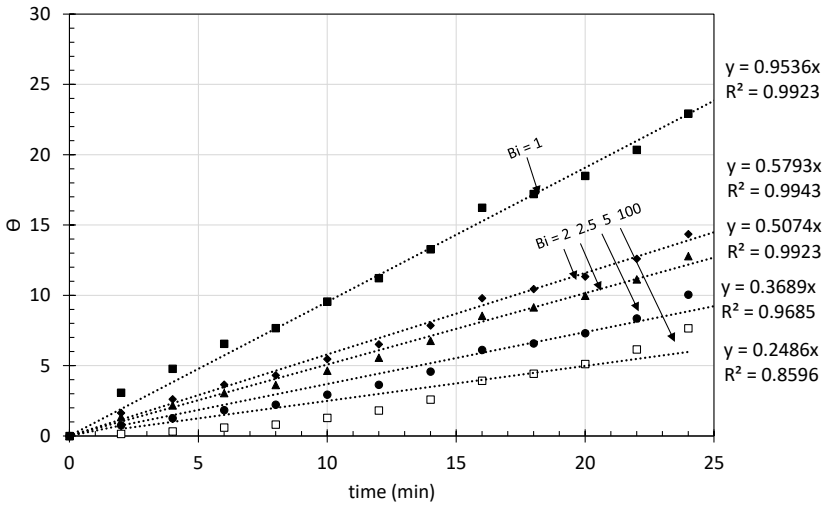

Figure 4.2 – $\Theta_{simulation}$ vs. $t_{experimental}$ curves for various Bi obtained by reading the corresponding $\Theta_{simulation}$ and $t_{experimental}$ at each $C_{b,exp} = C_{b,cal}$ for pH 5.0 without salt concentration.

For a better choice of the Biot number not only the R^2 of the slope of the straight line from the plot Θ *vs. t* but also uncertainty between the Θ_{exp} and Θ_{cal} was calculated using least squares for error propagation.

4.4.2.1. Effect of salt on IgG adsorption

Salt concentration is one of the major studied factors on protein adsorption. Table 4.2 presents the apparent maximum binding capacity, the Langmuir equilibrium constant, and the estimated Biot number, calculated effective pore diffusion coefficient and external mass transfer values.

Table 4.2 – Parameters of IgG adsorption equilibrium and kinetics for MabDirect MM in 20 mM citrate buffer pH 5.0 without and with different salt concentrations.

NaCl (M)	q_m(mg·g$_{dry}^{-1}$)	K_L (L·g^{-1})	Bi	D_{pe} (×10^{-6} cm^2·min^{-1})	k_{ext} (cm·min^{-1})
0	149.7 ± 7.1	0.32 ± 0.02	2	15.36	0.0060
0.1	104.7 ± 5.1	0.31 ± 0.02	5	6.50	0.0063
0.2	62.3 ± 5.0	0.53 ± 0.05	15	3.72	0.0108
0.4	16.3 ± 8.0	3.08 ± 1.51	100	1.04	0.0203

The protein binding showed salt-dependent behaviour at low salt concentration. Figure 4.3 represents the effect of ionic strength on adsorption isotherms, by NaCl addition to the IgG solution buffer.

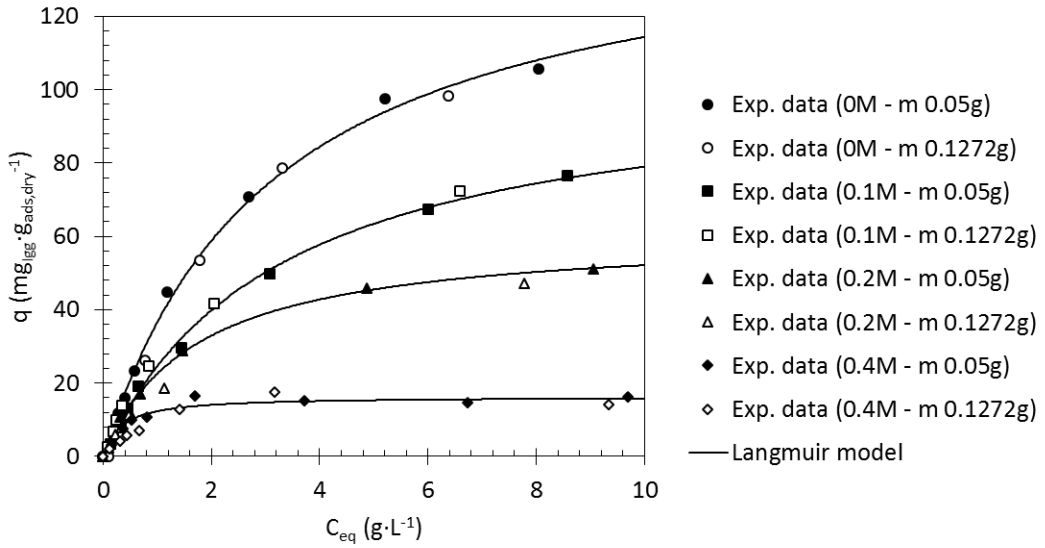

Figure 4.3 – Adsorption isotherms of IgG on MabDirect MM from a 20 mM citrate buffer at pH 5.0 for different NaCl concentrations (circles – without, squares – 0.1M, triangles – 0.2M and diamonds – 0.4M) at 20 °C: Experimental points (closed points – 0.05g of adsorbent, open points – 0.127g of adsorbent) and Langmuir model (curves).

From Figure 4.3 and Table 4.2 it is possible to verify that the Langmuir model was able to represent reasonably the experimental data for all tested conditions. Additionally, it is possible to conclude that the absence of salt in the buffer solution has a positive effect on adsorption, conducing to the largest maximum adsorption capacity (149.7 ± 7.1 $mg_{IgG} \cdot g_{adsorbent,dry}^{-1}$), as it was expected since we are dealing with a cation exchanger mixed-mode adsorbent. The lowest adsorption capacity (16.3 ± 8.0 $mg_{IgG} \cdot g_{adsorbent,dry}^{-1}$) was registered for the condition with high ionic strength, namely 0.4M NaCl.

Very similar trends were observed in the previous chapter [14] where it was used the same adsorbent (MabDirect MM) but a different target protein, Human Serum Albumin (HSA), as well as in literature [11, 35, 36]. Increasing the salt concentration in solution, the adsorption capacity decreases significantly due to weakened electrostatic interaction between the protein and the adsorbent. However, since it is a mixed mode adsorbent, there still exists different interactions, such as hydrophobic interaction and hydrogen bonds, which can possibly lead to larger binding capacity of IgG comparing to HSA adsorption for equal salt concentration study.

Adsorption kinetics studies were performed in a batch adsorber in order to access the uptake rate of the IgG at different salt concentrations for a pH 5.0 buffer solution. Figure 4.4 shows that a pore diffusion model (PDM) fitted reasonably to the experimental data. External mass transfer was not neglected and for these conditions (pH 5.0 with different salt concentration) they should be taken into account. Fitting a suitable transport model is important to study the transport properties of the adsorbent/protein system. Reasonable estimations were made regarding the intra-particle diffusion coefficient. The fitted values of the effective pore diffusion are also given in Table 4.2.

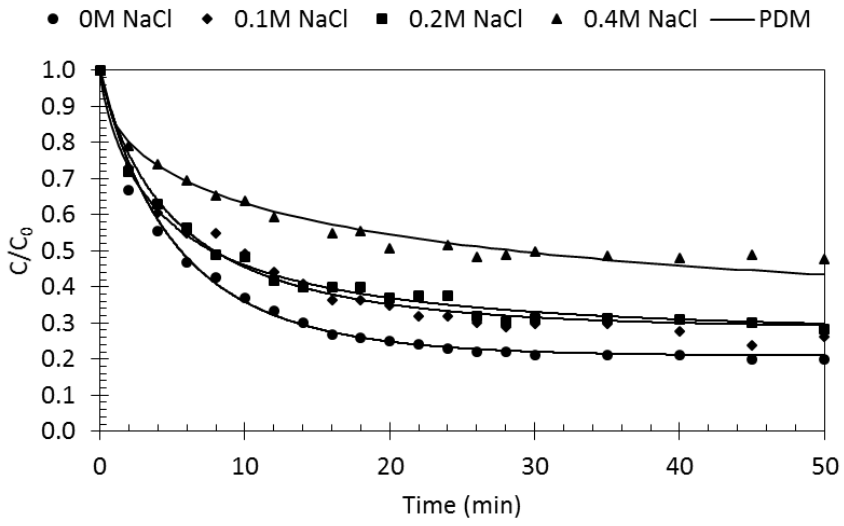

Figure 4.4 – Adsorption kinetics of IgG on MabDirect MM from a 20 mM citrate buffer at pH 5.0 for different NaCl concentrations (circle points – without salt, diamond points – 0.1M NaCl, square points – 0.2M NaCl and triangle points – 0.4M NaCl), at 20 °C and 270 rpm.

The value of D_{pe} at pH 5.0 without and with 0.1, 0.2 and 0.4M NaCl were 15.36, 6.50, 3.72 and 1.04 $\times 10^{-6}$ $cm^2 \cdot min^{-1}$, respectively. When increasing the ionic strength, the D_{pe} from the pore diffusion model decreases. These results agreed with literature [19, 36], who referred that changing the ionic strength present in solution affects the diffusion value, and that the values of this parameter and of pH, affect the interactions between the charges on the target protein and on the adsorbent surface.

Many researchers [35-37] already stated that regarding the study of the ionic strength at low salt concentration, the electrostatic protein/ligand interactions are dominant, and that increasing the salt concentration, the hydrophobic interactions become dominant.

4.4.2.2. Effect of pH on IgG adsorption

The protein adsorption in a mixed mode adsorbent is influenced by several factors, pH being a commonly studied parameter. The apparent maximum binding capacity, the Langmuir equilibrium constant, the Biot number, the calculated effective pore diffusion coefficient and the external mass transfer coefficient values are presented in Table 4.3. The protein binding showed pH-dependence.

Table 4.3 – Parameters of IgG adsorption equilibrium and kinetics for MabDirect MM in 20 mM citrate buffer (pH 5.0 and 6.0) and 20 mM phosphate buffer (pH 7.0) without salt concentrations.

pH	q_m(mg·g_{dry}^{-1})	K_L (L·g^{-1})	Bi	D_{pe} (×10^{-6} $cm^2 \cdot min^{-1}$)	k_{ext} (cm·min^{-1})
5	149.7 ± 7.1	0.32 ± 0.02	2	15.36	0.0060
6	129.0 ± 9.2	0.38 ± 0.03	400	2.34	0.1817
7	90.4 ± 9.1	0.31 ± 0.05	500	1.87	0.1816

Figure 4.5 represents the adsorption isotherms for the different pH values tested.

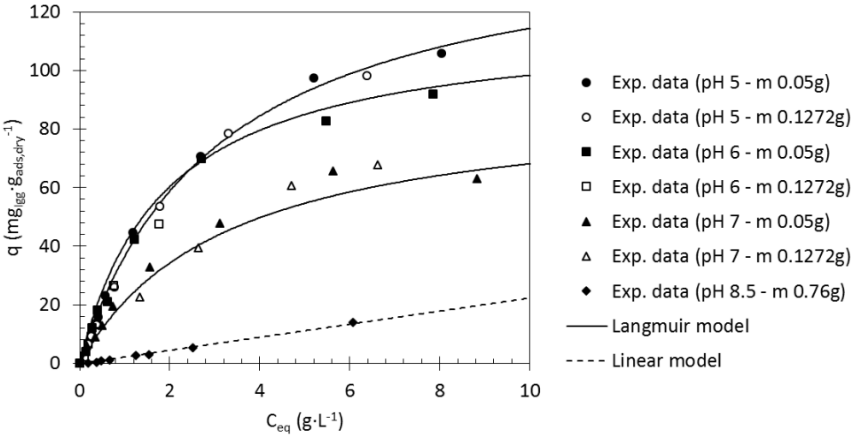

Figure 4.5 – Adsorption isotherms of IgG on MabDirect MM from a 20 mM citrate buffer at pH 5.0 (circles) and pH 6.0 (squares), a 20 mM phosphate buffer at pH 7.0 (triangles) and 20 mM Tris-HCl at pH 8.5 (diamonds) at 20 °C. Closed points represent 0.05g of wet adsorbent mass with exception for pH 8.5 where it was used 0.76g and open points represent 0.127 g of adsorbent. Langmuir model is represented for pH 5.0, 6.0 and 7.0 while linear model is represented for pH 8.5.

The Langmuir model, as in the ionic strength study, fitted reasonably well the experimental data for all tested conditions. As the solution pH increases, there will be a decrease in the adsorption capacity, due to the weakened electrostatic interactions. From Figure 4.5 and Table 4.3, the largest maximum adsorption capacity is 149.7 ± 7.1 $mg_{IgG} \cdot g_{adsorbent,dry}^{-1}$, for pH 5.0, while the lowest adsorption capacity was at pH 8.5. Note that the Langmuir model was used throughout with the exception of pH 8.5 for which a linear model was sufficient to describe equilibrium. For this pH value, 0.76 g of wet adsorbent were used, since a lower adsorption capacity would be achieved.

Two important parameters are necessary to understand the strong influence of the strength of electrostatic protein-ligand interactions which are the isoelectric point of the target protein and the adsorbent pKa. From literature, Du et al. [36], the isoelectric point of IgG is between pH 5.8 and 7.3. Also, earlier to that date, Wang et al. [38] published the zeta potential of IgG as function of pH, providing similar isoelectric point, which means that when the solution pH is below the isoelectric point of hIgG, the protein has positive charge and when above, the hIgG has negative charge. Furthermore, the MabDirect MM adsorbent has a pKa of 5.0, which means that when the solution pH is below the pKa, the adsorbent presents itself neutrally charged while when the solution pH is above the pKa, the adsorbent presents as negatively charged, typical cation exchanger mixed mode adsorbent. The binding behaviour presented in our study is in good agreement with the expectation. Considering a studied solution buffer of 6, 7 and 8.5, the adsorption capacity decreases significantly; this is due to the electrostatic repulsion since the solution pH is above the isoelectric point of the protein, making the protein negatively charged and at the same time the solution pH is above the pKa of the adsorbent, which becomes also negatively charged. For the studied solution pH of 5.0, the target protein presents a positive charge and the adsorbent presents as neutrally charged, occurring electrostatic attraction. In case of a weak anion exchanger mixed-mode adsorbent, Nfor et al. [37] explain the electrostatic behaviour also in detail. Du et al. [36] reported adsorption equilibrium and kinetics of IgG on a cation exchanger mixed-mode adsorbent (Streamline CST-I). Similar behaviours were reported by them for both ionic strength and pH studies. They also refer that their results indicated that IgG could be adsorbed at a pH below 6 (preferably) and eluted with high salt concentration.

Kinetics experiments were also performed in a batch adsorber in order to determine the uptake rate of the IgG at different buffer solution pHs without the addition of salt. Figure 4.6 shows a pore diffusion model (PDM) fitted to the experimental data. Reasonable estimations were made regarding the intra-particle diffusion coefficient.

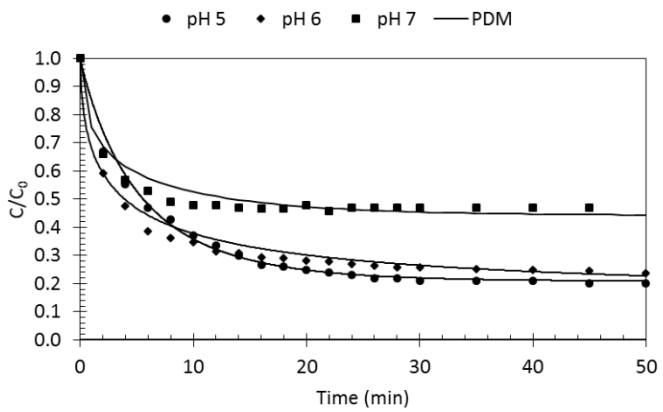

Figure 4.6 – Adsorption kinetics of IgG on MabDirect MM for different buffer solutions, 20 mM citrate buffer pH 5.0 (circles) and pH 6.0 (diamonds) and 20 mM phosphate buffer pH 7.0 (squares) without addition of salt, at 20 °C and 270 rpm. Pore diffusion model is represented by the lines.

The fitted values of the effective pore diffusion are also given in Table 4.3. The D_{pe} value obtained at pH 5.0, 6.0 and 7.0 were 16.36, 2.34 and 1.87 $\times 10^{-6}$ $cm^2 \cdot min^{-1}$, respectively. PDM might not fit the experimental data accurately for pH 7; however, the effective pore diffusivities estimated by PDM could represent the basic trend correctly.

Since the target protein and the adsorbent in this work constitute an unique system, they cannot be compared directly with data from the literature; however, data from similar systems exist. Some examples are presented in the following.

Du et al. [36] studied the effect of salt and pH conditions using IgG as target protein and a cation exchanger mixed mode adsorbent (Streamline CST-I). They stated that at higher pH, IgG carried more negative charges, while CST-I attracted proteins with net positive charge and repelled proteins with net negative charge. They refer that the driving force for intra-particle mass transfer of IgG in CST-I was mainly electrostatic attraction between IgG and the adsorbent ligand, since increasing the pH, the electrostatic attraction decreased and the repulsive force increased which resulted in slow mass transfer rate. They indicate that the diffusion of IgG in CST-I was faster compared to the diffusion reported by Gao et al. [39] and, for this reason, CST-I could be used for the adsorption of IgG under high operating velocity. In our work a similar trend is presented, since a slow mass transfer rate is observed with the increase of pH, probably due to the electrostatic interaction between the target protein and the adsorbent ligand.

Gao and co-workers [39] studied the adsorption kinetics of bovine serum albumin (BSA) on a mixed-mode adsorbent with benzylamine ligand (Cell-SSP-BA-4 with a ligand density of 49 $\mu mol \cdot mL^{-1}$), via stirred-batch uptake experiments. They reported an effective pore diffusion of 1.26, 1.79 and 2.52 $\times 10^{-6}$ $cm^2 \cdot min^{-1}$ for 0, 0.25 and 0.5M NaCl for pH 7.0, respectively. Our results present a slightly faster behaviour for pH 7.0 without salt addition.

Perez-Almodovar and Carta [40] studied the IgG adsorption kinetics on a Protein A adsorbent using a solution of 10 mM Na_2HPO_4, adjusted to pH 7.4 with phosphoric acid with the addition of 0.15M NaCl. They obtained by PDM an effective pore diffusion in the range of 4.50 and 4.26 $\times 10^{-6}$ $cm^2 \cdot min^{-1}$ for an IgG concentration between 0.5 and 1 $g \cdot L^{-1}$. Although these values are slightly different than those presented in this work (D_{pe} = 1.87 $\times 10^{-6}$ $cm^2 \cdot min^{-1}$ for the most similar conditions) it is important to notice that they are in the same order of magnitude and in this way showing that mixed mode adsorbents are similar to higher cost adsorbents like protein A affinity chromatography adsorbent.

Finally, Liu et al. [41] studied the IgG adsorption kinetics in a hydrophobic charge-induction resin with dextran-grafted agarose gel as the matrix and 2-mercapto-1-methyl-imidazole (MMI) as the functional ligand. They studied pH higher than 7 and also the ionic strength for pH 8.5 obtaining a D_{pe} between 0.70 and 2.64 $\times 10^{-6}$ $cm^2 \cdot min^{-1}$. In our work, for the same conditions, a larger value of D_{pe} was obtained indicating that the diffusion of IgG in MabDirect MM was faster than reported by these authors.

After the studied adsorption characteristics, it can be concluded that the best pH for IgG adsorption was pH 5.0 without the addition of salt. In contrast, the best buffer solution to elute the target protein is at higher pH and adding salt. Regarding this last statement, a final adsorption isotherm and kinetics by bath experiments were performed, where it was studied the protein adsorption in a 20 mM phosphate buffer pH 7.0 with 0.4 M NaCl.

Figure 4.7 and Table 4.4 present the adsorption isotherms by batch experiments for these conditions in comparison with the lowest adsorption capacity achieved for pH 5.0 with the same amount of salt concentration.

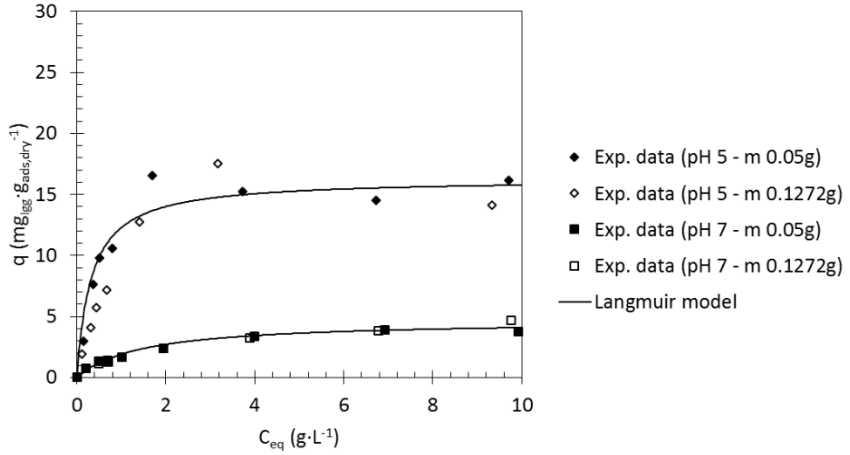

Figure 4.7 – Adsorption isotherms of IgG on MabDirect MM from a 20 mM citrate buffer at pH 5.0 (diamonds) and 20 mM phosphate buffer pH 7.0 (squares) with 0.4M NaCl at 20 °C. Closed points represent 0.05g of wet adsorbent mass and open points represent 0.127 g of adsorbent. Langmuir model is represented for both conditions tested.

Table 4.4 – Parameters of IgG adsorption equilibrium and kinetics for MabDirect MM in 20 mM citrate buffer (pH 5.0) and 20 mM phosphate buffer (pH 7.0) with 0.4M NaCl, 20 °C.

pH	q_m(mg·g_{dry}^{-1})	K_L (L·g^{-1})	Bi	D_{pe} (×10^{-6} cm^2·min^{-1})	k_{ext} (cm·min^{-1})
5	16.3 ± 8.0	3.08 ± 1.51	100	1.04	0.0203
7	4.7 ± 0.4	0.69 ± 0.07	200	0.16	0.0063

Comparing the protein adsorption at pH 7 and pH 5 for this ionic condition strength, it is possible to visualize a significant decrease in the adsorption capacity and also in the estimated effective pore diffusion coefficient. Furthermore, according to Figure 4.8, it is possible to refer that the Pore Diffusion Model fits reasonably well the experimental data.

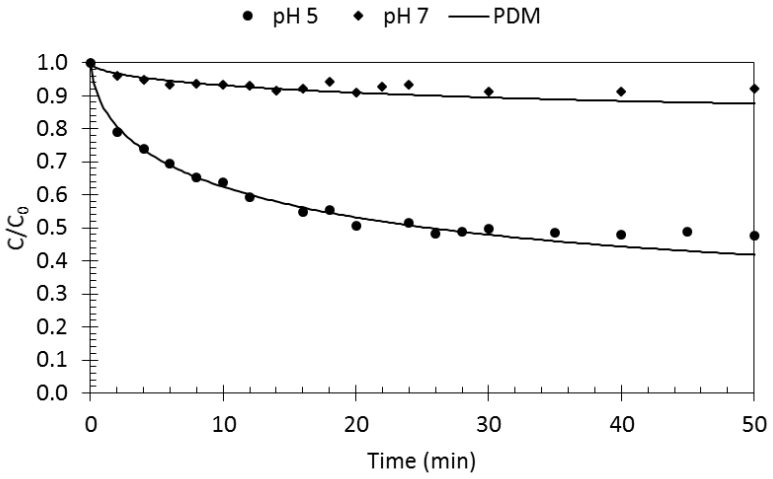

Figure 4.8 – Adsorption kinetics of IgG on MabDirect MM for different buffer solutions, 20 mM citrate buffer pH 5.0 (circles) and 20 mM phosphate buffer pH 7.0 (diamonds) with 0.4M NaCl, at 20 °C and 270 rpm. Pore diffusion model is represented by the lines.

4.4.3. Fixed bed adsorption experiments

Frontal analysis experiments were conducted for this polyclonal antibody using MabDirect MM. Two breakthrough experiments were performed (Table 4.5).

Table 4.5 – Operating conditions for different breakthrough experiments. Adsorption performed in 20 mM citrate buffer pH 5.0 solution at 20 °C without and with 0.4M NaCl.

Run	1	2
NaCl (M)	0	0.4
C_{b0} (g.dm^{-3})	0.68	0.53
Q (cm^3.min^{-1})	1	1
H (cm)	6.2	7.1
w_{wet} (g)	6.1510	7.0438

The second experiment differs from the first in the changed feed concentration of the IgG and salt concentration in buffer solution, in order to achieve the saturation of the column with less amount of protein, as observed in the adsorption batch experiments.

Figure 4.9 shows a fixed bed breakthrough experiment with an IgG feed concentration of 0.68 $g \cdot dm^{-3}$ in a solution of 20 mM citrate buffer pH 5.0 without salt at 1 $cm^3 \cdot min^{-1}$. Due to the protein costs the experiment was stopped before reaching the equilibrium. However, it can be observed that the mathematical model demonstrated to reasonably fit the experimental data.

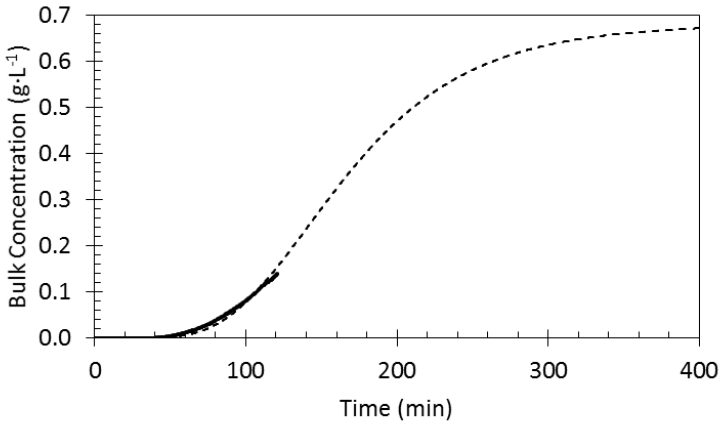

Figure 4.9 – Fixed bed breakthrough experiment with a feed concentration of 0.68 $g \cdot L^{-1}$. Experimental data (points), simulation data (curve). Adsorption conditions: 20 mM citrate buffer pH 5.0, without salt; Operating conditions presented in Table 4.5.

The global mass transfer coefficient was estimated as 3.81×10^{-3} $cm \cdot min^{-1}$. Adsorption capacity from this experiment could not be determined due to the fact that the experiment was not concluded.

A second fixed bed breakthrough experiment was conducted (Figure 4.10), where the feed concentration was changed to 0.53 $g \cdot L^{-1}$ in a pH 5.0 solution with 0.4M NaCl. Table 4.6 provides information regarding the operating conditions.

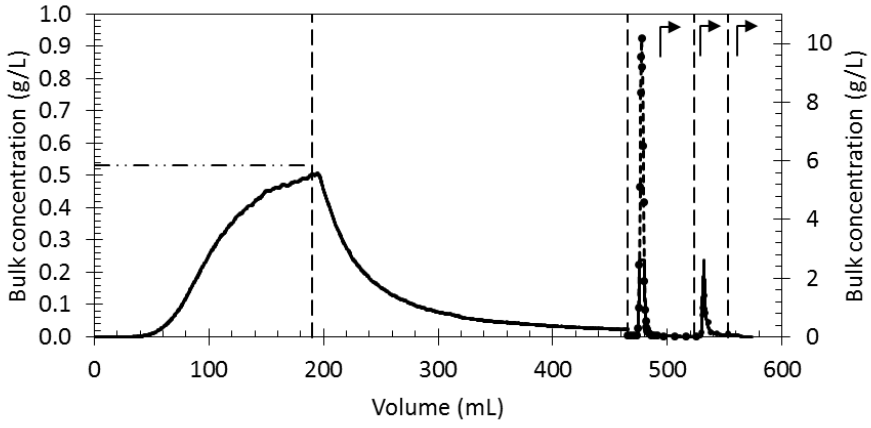

Figure 4.10 – Fixed bed breakthrough experiment with a feed concentration of ~ 0.53 g/L. Experimental data (points); start of each stage (dotted line). Adsorption conditions: 20 mM citrate buffer, pH 5.0 with 0.4M NaCl. Operating conditions presented in Table 4.6.

Table 4.6 – Operating conditions for breakthrough experiment: flow rate, feed concentration, bed height, adsorbent volume and weight and retained protein mass on each stage at 20 °C.

Parameter	Adsorption	Desorption				Difference (%)
		Washing	Elution	Regeneration	Stock	
Q ($cm^3.min^{-1}$)	1	1	0.5	0.5	0.5	
C_{feed} ($g.dm^{-3}$)	0.53	n.a.				
H (cm)	7.1					
V (cm^3)	2.43					
w_{dry} (g)	5.3216					
$m_{protein}$ (mg)	60.72	24.09	36.43	8.86	0.61	13

The measured adsorption capacity from fixed bed experiments was 8.62 $mg_{IgG} \cdot g_{wet}^{-1}$ (11.41 $mg_{IgG} \cdot g_{dry}^{-1}$); the difference between the measured value and the adsorption capacity calculated from batch experiments is probably due to the fact that the breakthrough experiment did not reach the plateau. The dynamic binding capacity (DBC) at 10% of breakthrough calculated by the equation (4.18) was 7.06 $mg_{IgG} \cdot g_{dry}^{-1}$ (15.4 $mg_{IgG} \cdot mL^{-1}$), which represents 62% of the experimental adsorption capacity. The relative low DBC at 10% of breakthrough is due to the buffer solution (pH 5.0 with 0.4M NaCl) tested. It was achieved a recovery of 99.4%.

$$q_{\,10\%} = \frac{\int_0^{V_{10\%}} (C_{b0} - C_b)\, dV}{V_a} \tag{4.18}$$

where V_a is the packed bed volume of adsorbent, V is the effluent liquid volume, $V_{10\%}$ is the effluent liquid volume at 10% IgG breakthrough point.

Figure 4.11 represents the adsorption stage, where an IgG feed concentration of 0.53 $g \cdot L^{-1}$ in 20 mM citrate buffer pH 5.0 with 0.4M NaCl was pumped at a flow rate of 1 $mL \cdot min^{-1}$.

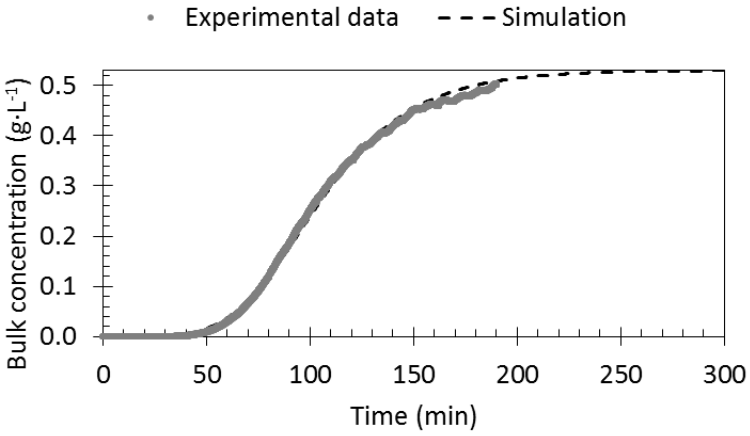

Figure 4.11 – Fixed bed breakthrough experiments. Adsorption stage: 0.53 $g.dm^{-3}$ IgG concentration in 20 mM citrate buffer pH 5.0 with 0.4M NaCl for a flow rate of 1 mL/min. Experimental data (grey points) and simulation (black line).

The numerical simulation of this experiment is also presented in the figure. It is fair to say that the mathematical model in the present work fitted reasonably well to the experimental results. The global mass transfer coefficient was estimated to be 3.81 $\times 10^{-3}$ cm·min^{-1}. When comparing the experimental results to the literature several factors need to be taken into account, such as, solution pH, salt type and concentration, adsorbent, target protein and source, feed concentration and flow rate. Finding in literature experiments that can be compared to ours become a difficult task since each researcher chose different conditions. Some examples are referred for different adsorbent types for adsorption of IgG as the target protein.

In 1999, Färenmark et al. [42] studied IgG adsorption on Streamline Phenyl, a hydrophobic interaction chromatography adsorbent with a macroporous 6% cross-linked agarose containing crystalline quartz core material designed also for expanded bed adsorption. They conducted a packed bed breakthrough experiment with 1 g·L^{-1} of IgG as feed concentration in 20 mM NaH_2PO_4 pH 7.0 with 1M $(NH_4)_2SO_4$ at a flow velocity of 300 cm·h^{-1} in a streamline 25 column achieving a DBC of 10.38 mg·mL^{-1}.

Perez-Almodovar and Carta [40] studied the IgG adsorption on a new protein A adsorbent based on macroporous hydrophilic polymers. They conducted packed bed breakthrough experiments with different feed concentrations dissolved in 10 mM Na_2HPO_4 pH 7.4 with 150 mM NaCl for distinctive bed volumes. Although the conditions were not very similar with ours (1 g·L^{-1} IgG in 20 mM citrate buffer pH 5.0 with 0.4M NaCl at a flow rate 1 mL·min^{-1}), they obtained for an equal feed concentration and flow rate a DBC of 17.1 mg·mL^{-1}, a higher value compared with our adsorbent. It is an expected result when comparing a protein A adsorbent with a mixed mode due to the highly affinity interaction.

Shi et al. [43] studied two new hydrophobic charge-induction ligand coupled onto agarose beads containing tungsten carbide (T-MEP and T-ABI) for the adsorption of bovine IgG. They report that for T-MEP ligand for a feed concentration of 2 g·L^{-1} (pH 5.0 without salt) a DBC of 5.65 and 3.60 mg·mL^{-1} are obtained for flow velocities of 200 and 400 cm·h^{-1}, respectively; while for T-ABI ligand for a feed concentration of 2 g·L^{-1} (pH 5.0 without salt) a DBC of 15.15 and 6.74 mg·mL^{-1} are obtained for flow velocities of 200 and 400 cm·h^{-1}, respectively.

Hahn and co-workers [44] studied the performance of 15 commercially available protein A media, such as rPrA Sepharose FF, PrA Sepharose 4 FF, MabSelect, IPA 500, PrA Hyper D, Prosep-A, Prosep-rA and Poros 50 A for purification of monoclonal and recombinant antibodies. The equilibrium and dynamic binding capacity were determined for a studied solution of 0.4 mg·mL^{-1} IgG in 0.05 M sodium phosphate buffer pH 7.5 with 0.15M NaCl. They presented a dynamic binding capacity at 2.5% breakthrough between 6.4-15.6 mg·mL^{-1} for an adsorbent volume of 0.5 mL and a flowrate 175 cm·h^{-1}, and also a DBC between 13.9-21.2 mg·mL^{-1} for an

adsorbent volume of 2 mL and a flowrate 175 $cm \cdot h^{-1}$. Swinnen et al. [45] also studied the dynamic binding capacity at 10% breakthrough for monoclonal antibody (IgG4) for different protein A adsorbents. They obtained a DBC for a studied condition of 10 mM phosphate buffer pH 7.2 with 0.15M NaCl between 31.1-67.4 $mg \cdot mL^{-1}$ for protein A adsorbents such as Prosep-vA, Prosep-A, PrA Sepharose 4 FF, MabSelect and MabSelect Xtra for an adsorbent column volume of 18.4 mL and a flowrate 175 $cm \cdot h^{-1}$.

Bela Sheth [46] studied MabSelect, MabSelect Xtra and Prosep Ultra achieving a DBC at 10% breakthrough point between 27.1-30.1 $mg \cdot mL^{-1}$ for a feed concentration of 1 $mg \cdot mL^{-1}$ of IgG in phosphate buffer saline pH 7.4 for an adsorbent volume of 2 mL and a flowrate 175 $cm \cdot h^{-1}$. Comparing to the adsorbent studied, a DBC at 10% breakthrough point of 30.7 $mg \cdot mL^{-1}$ was calculated for a feed concentration of 1 $mg \cdot mL^{-1}$ of IgG in 20 mM citrate buffer pH 5.0 without salt for an adsorbent volume of 2.43 mL and a flowrate 175 $cm \cdot h^{-1}$.

Although a lower dynamic binding capacity was achieved compared to the affinity adsorbent, MabDirect MM constitutes an alternative for capture of hIgG. It presents an effective pore diffusion in the same order of magnitude as the protein A adsorbents, and good recovery at a lower cost.

4.5. Conclusions

MabDirect MM proved that can capture Immunoglobulin G effectively. The maximum adsorption of the IgG protein was observed from a buffer solution of pH 5.0 without salt addition; a value of 149.7 ± 7.1 $mg \cdot g_{dry}^{-1}$ was obtained by batch experiments. For a feed concentration of 0.5 $g \cdot L^{-1}$ of human IgG at the same conditions, a dynamic binding capacity at 10% of breakthrough 7.06 $mg \cdot g_{dry}^{-1}$ (15.4 $mg_{IgG} \cdot mL^{-1}$) representing 62% of the saturation capacity by fixed bed experiments validating batch results. The lowest adsorption capacity registered was for high pH values and adding salt to the buffer solution. For the conditions tested (pH 7.0 with 0.4M NaCl), it was registered a low adsorption uptake capacity (4.7 ± 0.4 $mg \cdot g_{dry}^{-1}$).

When studying the adsorption kinetics by changing pH buffer solution, the largest effective pore diffusion coefficient, 15.6 $\times 10^{-6}$ $cm^2 \cdot min^{-1}$ was obtained for pH 5.0 without salt. A similar behaviour was observed when studying the ionic strength. The increase in salt concentration and/or pH will decrease the effective pore diffusion. The lowest effective pore diffusion registered was for pH 7.0 with 0.4M NaCl where a value of 0.16 $\times 10^{-6}$ $cm^2 \cdot min^{-1}$ was obtained.

4.6. Nomenclature

Bi	–	Biot number
C_{b0}	–	Feed protein concentration
C_b	–	Protein concentration in the bulk phase
C_p	–	Protein concentration in the particle pore
D_L	–	liquid axial dispersion coefficient
D_m	–	Molecular diffusivity
d_p	–	Particle diameter
D_{pe}	–	Effective pore diffusivity
H	–	Bed height
k_{ext}	–	External mass transfer coefficient
k_G	–	Global mass transfer coefficient
k_{int}	–	Internal mass transfer coefficient
K_L	–	Langmuir adsorption constant
$m_{protein}$	–	Protein mass adsorbed/desorbed
$q_{10\%}$	–	Dynamic binding capacity at 10% breakthrough point
q	–	Adsorbed concentration
$\bar{q}$	–	Average adsorbed concentration
q_{max}	–	Maximum adsorption capacity
Re	–	Reynolds number
r_p	–	Particle radius
Sc	–	Schmidt number
Sh	–	Sherwood number
u_i	–	Interstitial velocity
V	–	Effluent liquid volume from the fixed bed
$V_{10\%}$	–	Effluent liquid volume at 10% IgG breakthrough point
V_a	–	Packed bed volume of adsorbent
V_L	–	Volume of protein solution
w	–	Adsorbent mass
t	–	Time
r	–	Radial position
x	–	Dimensionless particle radius
z	–	Axial position

Greek letters

ε_b	–	External (bed) porosity
ε_p	–	Particle (solid) porosity
ρ	–	Density
ρ_ρ	–	Particle density
θ	–	Dimensionless time
τ_d	–	Mean residence time
τ	–	Tortuosity
η	–	Viscosity

Acronyms

BSA	–	Bovine Serum Albumin
EBA	–	Expanded bed adsorption
gPROMS	–	general PROcess Modelling System
HSA	–	Human Serum Albumin
hIgG	–	Immunoglobulin G from Human serum
IgG	–	Immunoglobulin G
MM	–	Mixed-mode
MMC	–	Mixed-mode Chromatography
OCFEM	–	Orthogonal collocation in finite elements method
PDM	–	Pore diffusion model
rpm	–	Rotations per minute
SDS-Page	–	Sodium dodecyl sulfate - Polyacrylamide gel electrophoresis

4.7. References

[1] H. Hjelm, K. Hjelm, J. Sjoquist, Protein A from Staphylococcus aureus. Its isolation by affinity chromatography and its use as an immunosorbent for isolation of immunoglobulins, Federation of European Biochemical Societies Letters, 28 (1972) 73-76.

[2] A. Zider, D. Drakeman, The future of monoclonal antibody technology, mAbs - Landes Bioscience, 2 (2010) 361-364.

[3] G. Kronvall, A Surface Component in Group A, C, and G Streptococci with Non-Immune Reactivity for Immunoglobulin G, The Journal of Immunology, 111 (1973) 1401-1406.

[4] Strategies for protein Purification Handbook in, GE Healthcare Bio-Science AB, 2010.

[5] Antibody Production and Purification Technical Handbook in, Thermo Fisher Scientific, 2010.

[6] J. Stadlmann, M. Pabst, D. Kolarich, R. Kunert, F. Altmann, Analysis of immunoglobulin glycosylation by LC-ESI-MS of glycopeptides and oligosaccharides, Proteomics, 8 (2008) 2858-2871.

[7] B. Malm, A method suitable for the isolation of monoclonal antibodies from large volumes of serum-containing hybridoma cell culture supernatants, Journal of Immunological Methods, 104 (1987) 103-109.

[8] W.L. Hoffman, D.J. O'Shannessy, Site-specific immobilization of antibodies by their oligosaccharide moieties to new hydrazide derivatized solid supports, Journal of Immunological Methods, 112 (1988) 113-120.

[9] K.L. Carson, Flexibility - the guiding principle for antibody manufacturing, Nature Biotechnology, 23 (2005) 1054-1058.

[10] S.S. Ranjini, D. Bimal, A.P. Dhivya, M.A. Vijayalakshmi, Study of the mechanism of interaction of antibody (IgG) on two mixed mode sorbents, Journal of Chromatography B, 878 (2010) 1031-1037.

[11] P. Li, Protein Separation and purification by expanded bed chromatography and simulated moving bed technology, in: Ph.D. Thesis, Department of Chemical Engineering, Faculty of Engineering University of Porto, Portugal, 2006.

[12] P. Li, P.F. Gomes, J.M. Loureiro, A.E. Rodrigues, Proteins Separation and Purification by Expanded Bed Adsorption and Simulated Moving Bed Technology, in: G. Subramanian (Ed.) Continuous Processing in Pharmaceutical Manufacturing, John Wiley & Sons, Inc., 2014.

[13] M.d.A. Lima, M.d.F.M.d. Freitas, L.R.B. Gonçalves, I.J.d. Silva Junior, Recovery and purification of a Kluyvermyces lactis β-galactosidase by Mixed Mode Chromatography, Journal of Chromatography B, 1015–1016 (2016) 181-191.

[14] P.F. Gomes, J.M. Loureiro, A.E. Rodrigues, Adsorption of Human Serum Albumin (HSA) on a mixed-mode adsorbent: equilibrium and kinetics, Adsorption, 23 (2017) 491-505.

[15] H.F. Xia, D.Q. Lin, S.J. Yao, Chromatographic performance of macroporous cellulose-tungsten carbide composite beads as anion-exchanger for expanded bed adsorption at high fluid velocity, Journal of Chromatography A, 1195 (2008) 60-66.

[16] N. Clark, Robust solution for downstream processing of biotherapeutics: faced with tremendous cost pressures, the biomanufacturing industry is looking at options to simplify downstream processing. One solution is second-generation EBA purification alongside the development of disposable chromatography columns. (2008)

[17] H.A. Chase, Purification of Proteins by Adsorption Chromatography in Expanded Beds, Trends in Biotechnology, 12 (1994) 296-303.

[18] G. Carta, A. Jungbauer, Protein Chromatography: Process Development and Scale-Up, Wiley, 2010.

[19] W. Kelly, P. Garcia, S. McDermott, P. Mullen, G. Kamguia, G. Jones, A. Ubiera, K. Göklen, Experimental characterization of next-generation expanded-bed adsorbents for capture of a recombinant protein expressed in high-cell-density yeast fermentation, Biotechnology and Applied Biochemistry, 60 (2013) 510-520.

[20] W. Kelly, G. Kamguia, P. Mullen, A. Ubiera, K. Göklen, Z. Huang, G. Jones, Using a two species competitive binding model to predict expanded bed breakthrough of a recombinant protein expressed in a high cell density fermentation, Biotechnology and Bioprocess Engineering, 18 (2013) 546-559.

[21] O. Levenspiel, Chemical reaction engineering, Wiley, 1972.

[22] L.E. Weaver, G. Carta, Protein Adsorption on Cation Exchangers: Comparison of Macroporous and Gel-Composite Media, Biotechnology Progress, 12 (1996) 342-355.

[23] P. Li, G. Xiu, A. E. Rodrigues, Modeling separation of proteins by inert core adsorbent in a batch adsorber, Chemical Engineering Science, 58 (2003) 3361-3371.

[24] W.-D. Chen, X.-Y. Dong, Y. Sun, Analysis of diffusion models for protein adsorption to porous anion-exchange adsorbent, Journal of Chromatography A, 962 (2002) 29-40.

[25] D.M. Ruthven, Principles of Adsorption and Adsorption Processes, Wiley, 1984.

[26] G. Guiochon, Preparative liquid chromatography, Journal of Chromatography A, 965 (2002) 129-161.

[27] G. Guiochon, D.G. Shirazi, A. Felinger, A.M. Katti, Fundamentals of Preparative and Nonlinear Chromatography, Academic Press, 2006.

[28] R.P.V. Faria, C.S.M. Pereira, V.M.T.M. Silva, J.M. Loureiro, A.E. Rodrigues, Sorption enhanced reactive process for the synthesis of glycerol ethyl acetal, Chemical Engineering Journal, 258 (2014) 229-239.

[29] M.E. Young, P.A. Carroad, R.L. Bell, Estimation of diffusion coefficients of proteins, Biotechnology and Bioengineering, 22 (1980) 947-955.

[30] R.R. Walters, J.F. Graham, R.M. Moore, D.J. Anderson, Protein diffusion coefficient measurements by laminar flow analysis: Method and applications, Analytical Biochemistry, 140 (1984) 190-195.

[31] W. Ranz, W. Marshall, Evaporation from drops, Chemical Engineering Progress, 48 (1952) 141-146.

[32] L.-T. Fan, Y.-C. Yang, C.-Y. Wen, Mass transfer in semifluidized beds for solid-liquid system, American Institute of Chemical Engineers Journal, 6 (1960) 482-487.

[33] N. Wakao, T. Funazkri, Effect of fluid dispersion coefficients on particle-to-fluid mass transfer coefficients in packed beds: Correlation of sherwood numbers, Chemical Engineering Science, 33 (1978) 1375-1384.

[34] E.J. Wilson, C.J. Geankoplis, Liquid Mass Transfer at Very Low Reynolds Numbers in Packed Beds, Industrial & Engineering Chemistry Fundamentals, 5 (1966) 9-14.

[35] P. Li, G. Xiu, V.G. Mata, C.A. Grande, A.E. Rodrigues, Expanded bed adsorption/desorption of proteins with Streamline Direct CST I adsorbent, Biotechnology and Bioengineering, 94 (2006) 1155-1163.

[36] Q.Y. Du, D.Q. Lin, Q.L. Zhang, S.J. Yao, An integrated expanded bed adsorption process for lactoferrin and immunoglobulin G purification from crude sweet whey, Journal of Chromatography B: Analytical Technologies in the Biomedical and Life Sciences, 947-948 (2014) 201-207.

[37] B.K. Nfor, M. Noverraz, S. Chilamkurthi, P.D.E.M. Verhaert, L.A.M. van der Wielen, M. Ottens, High-throughput isotherm determination and thermodynamic modeling of protein adsorption on mixed mode adsorbents, Journal of Chromatography A, 1217 (2010) 6829-6850.

[38] R.Z. Wang, D.Q. Lin, H.F. Tong, H.L. Lu, S.J. Yao, Evaluation of mixed-mode chromatographic resins for separating IgG from serum albumin containing feedstock, Journal of Chromatography B: Analytical Technologies in the Biomedical and Life Sciences, 936 (2013) 33-41.

[39] D. Gao, D.-Q. Lin, S.-J. Yao, Protein adsorption kinetics of mixed-mode adsorbent with benzylamine as functional ligand, Chemical Engineering Science, 61 (2006) 7260-7268.

[40] E.X. Perez-Almodovar, G. Carta, IgG adsorption on a new protein A adsorbent based on macroporous hydrophilic polymers, Journal of Chromatography A, 1216 (2009) 8348-8354.

[41] T. Liu, D.Q. Lin, Q.L. Zhang, S.J. Yao, Characterization of immunoglobulin adsorption on dextran-grafted hydrophobic charge-induction resins: Cross-effects of ligand density and pH/salt concentration, Journal of Chromatography A, 1396 (2015) 45-53.

[42] J. Färenmark, J. Gustavsson, I. Lagerlund, L. Sandberg, Characterisation of STREAMLINE phenyl, Bioseparation, 8 (1999) 139 -144.

[43] W. Shi, D.-Q. Lin, H.-F. Tong, J.-X. Yun, S.-J. Yao, 5-Aminobenzimidazole as new hydrophobic charge-induction ligand for expanded bed adsorption of bovine IgG, Journal of Chromatography A, 1425 (2015) 97-105.

[44] R. Hahn, R. Schlegel, A. Jungbauer, Comparison of protein A affinity sorbents, Journal of Chromatography B, 790 (2003) 35-51.

[45] K. Swinnen, A. Krul, I. Van Goidsenhoven, N. Van Tichelt, A. Roosen, K. Van Houdt, Performance comparison of protein A affinity resins for the purification of monoclonal antibodies, Journal of Chromatography B, 848 (2007) 97-107.

[46] B. Sheth, Characterisation of chromatography adsorbents for antibody bioprocessing, in: Ph.D. Thesis, Department of Biochemical Engineering, University College London, 2009.

Chapter 5: Expanded bed adsorption of Albumin and Immunoglobulin G from Human Serum onto MabDirect MM

"The quality, not the longevity, of one's life is what is important."

- Dr. Martin Luther King Jr.

In this chapter expanded bed breakthrough experiments are carried out for both target proteins (HSA and IgG separately) in different columns with different operating conditions and compared to the batch adsorption from previous experiments and literature. Residence time distribution experiments are conducted in order to characterize the hydrodynamics for the three different columns used in EBA experiments. Finally, the experimental EBA breakthrough results are compared to the mathematical model solution.

This chapter is based on the following article:

Gomes, P.F., Loureiro, J.M. & Rodrigues, A.E. Expanded bed adsorption of Albumin and Immunoglobulin G from Human Serum onto a cation exchanger mixed mode adsorbent. Adsorption, 24 (2018), 293-307.

5.1. Introduction

Human Serum Albumin (HSA) and Immunoglobulin G (IgG) are the main proteins components of Human plasma. Human Serum Albumin, major circulating plasma protein, is synthesized in the liver and is present in all body fluids. Due to its high concentration (35 – 50 $g \cdot dm^{-3}$) and great binding capacity, this protein has great responsibility of transport in plasma and in maintaining the colloidal osmotic pressure. Immunoglobulin G is a glycoprotein that is synthesized by plasma cells in bone marrow, lymph nodes and spleen. IgG represents near 75% of the immunoglobulins class present in human serum and it is vital for the protection of human body since it has the function of controlling infection of body tissues.[1-4].

Since these highly interesting target proteins are in contact with non-desired products in blood serum, separation methods need to be implemented. Adsorption techniques are commonly and traditionally applied for the objective of separation and purification. Ion exchange chromatography has been widely applied for the serum albumin separation. Also, affinity chromatography has been used as common separation and purification of monoclonal antibodies (mAb). Protein A and G resins are commonly used; however, there have a few limitations, such as high resin cost, ligand leakage and difficulties on clean-in-place procedures [5-9].

Mixed mode chromatography (MMC) appears as a low-cost new opportunity for separation and purification of a wide range of proteins. MMC is a separation method that uses more than one type of interaction between the resin and the target protein, such as electrostatic, hydrophobic, thiophilic interactions and hydrogen bonds. With multiple interactions taking place, this type of resins possesses a good adsorption selectivity, high capacity and facile elution at a competitive market cost [10-14].

Second generation adsorbents are specially designed for expanded bed purposes. Ufpront Chromatography A/S developed MabDirect MM, a mixed-mode (or multimodal) chromatography adsorbent, constituted of 6% cross-linked agarose with tungsten carbide particles, thus possessing a higher particle density, meeting the necessary characteristics to enable the use of higher flow rates in expanded bed adsorption.

Expanded bed adsorption (EBA) was already described on Chapter 2; however a brief summary is presented. It consists on introducing upward flow at the bottom of the column and therefore allowing adsorbent particles to “free” flow and to gradually be positioned from the biggest adsorbent particle at the bottom of the column to the smallest adsorbent particle at the top of the column, therefore increasing void fraction. This way, the unwanted material and contaminants pass through the column unhindered without the risk of any blockage, thus minimizing the pressure drop problems commonly encountered in fixed bed adsorbers [4].

Expanded bed is a more flexible system than fixed bed since in packed bed the adsorbent is fixed. However, in EBA some restrictions have to be met so that the adsorbent do not leave the column while the non-desired compounds can pass through. These restrictions spurred the exploration of new types of adsorbents [15-20]. Using EBA, it is possible to work at high flow rate with a dense adsorbent allowing the cell debris to pass through without blocking the bed [21, 22]. This technology gives us the ability to operate with the particulates in the feedstock and has a good adsorption and elution efficiency.

In this chapter, residence time distribution experiments in expanded bed were conducted in order to characterize the hydrodynamics for three different columns. Furthermore, EBA breakthrough experiments were carried out for the target proteins (Albumin and Immunoglobulin G from human serum dissolved separately in buffer solutions) in distinctive columns with different operating conditions and compared to the batch adsorption from previous experiments and literature. To finalize, the experimental EBA breakthrough results were compared to the implemented mathematical model solution.

5.2. Materials and Methods

5.2.1. Target proteins

Human Serum Albumin (HSA; product number CAS 70024-90-7) has a molecular weight of 66 kDa, an isoelectric point of 4.7, it also has a molecular diffusion of 3.84×10^{-5} $cm^2.min^{-1}$ according to literature [23]. More information regarding HSA can be found on previous Chapter 3 in subsection 3.2.1.

Immunoglobulin G from Human serum (hIgG; product Number I4506) was purchased from Sigma–Aldrich, USA. According to literature [10], human IgG has isoelectric point between 5.8 – 7.3 and a molecular diffusion of 2.4×10^{-5} $cm^2.min^{-1}$ [23]. More detailed information can be found on previous Chapter 4 in subsection 4.2.1.

5.2.2. Multimodal chromatography adsorbent

Mabdirect MM is a cation exchanger multimodal adsorbent constituted by a 6% cross-linked agarose with tungsten carbide particles. More information regarding this adsorbent can be found in Chapter 3, subsections 3.2.1 and 3.4.1. Before performing experiments, the adsorbent was conditioned with the same protein buffer solution. The protocol consists in placing some amount of adsorbent in a special glassware equipped with a proper filter connected to a vacuum pump where it will be cleaned with 1L of deionized water before flowing the chosen buffer [4, 14].

5.2.3. Equipment

The equipment utilized for the batch adsorption isotherms and kinetics for both target proteins was already described in previous Chapters 3 and 4. Regarding the study of expanded bed adsorption experiments, 3 columns were used, an Omnifit 6.6/11 column, a XK 16/20 column (Amersham Pharmacia Biotech, Uppsala, Sweden, and now GE Healthcare) and a Streamline 50 column (GE Healthcare). Both Omnifit and XK columns were used in a Gilson HPLC system with a 305 model pump, an 805 manometric module and a 117 Gilson UV model detector. The Streamline 50 column was connected with a Cole Parmer Masterflex L/S 7518-60 model pump at the bottom inlet and a Jasco 7800 UV detector (Tokyo, Japan) equipped with a flow-cell to monitor protein effluent concentration at 280 nm wavelength at the top outlet.

5.2.4. Buffer solutions

HSA and IgG were dissolved separately in buffer solutions according to the conditions to be tested. Regarding pH 5.0 and 6.0, a citrate buffer was used; for pH 7.0 and 8.5, a phosphate and Tris-HCl buffer were used, respectively. 20 mM concentration for all buffers were used with the exception for the buffer in which the adsorbent was stored. Sodium chloride (NaCl, 58.44 $g.mol^{-1}$) was the chosen salt. pH was adjusted to final value with 1 M NaOH or 1 M HCl. Reagents for pH 7.0 buffer were purchased from VWR Chemicals, while for pH 5.0, 6.0 and 8.5 buffers along with hydrochloric acid, sodium hydroxide, sodium acetate and sodium chloride were purchased from Reagente5. For residence time distribution experiments, Blue Dextran 2000 was used and purchased also from Reagente5 [4, 14].

5.2.5. Batch adsorption equilibrium isotherms and kinetics

Adsorption equilibrium isotherms and kinetics along with packed bed breakthrough experiments were already conducted and reported in previous chapters and can be found in literature for each target protein [4, 14].

5.2.6. Expanded bed adsorption

Two separate laboratory setups were used regarding the different columns and conditions to be tested as mentioned; however, the same protocol was followed. Before packing the column, the desired amount of adsorbent was measured in a graduated cylinder prior to drain using a vacuum pump to account for the wet mass. Subsequently, the adsorbent was hydrated in the chosen working buffer and the column was packed and used for the residence time distribution

or breakthrough experiments. Before each experiment, stock solution (200 mM sodium acetate buffer with 14% NaCl) was pumped in upward flow in order to attain an initial condition equal to the same adsorbent stored in buffer. Then, equilibration buffer (20 mM citrate buffer pH 5.0 without salt) with the purpose of equilibrating the adsorbent, was used to suspend the adsorbent particles and stabilize the bed during 30 to 45 minutes.

For a complete breakthrough experiment different steps take place: adsorption, washing, elution and regeneration of the adsorbent. When the expanded bed is stable and equilibrated, the process switches to feed stock application (target protein dissolved on the specific buffer solution to be tested) starting the adsorption step. The flow rate is constantly monitored and recorded. At the outlet stream from the top of the column, the protein concentration was measured by UV absorption at 280 nm and logged by the data acquisition software, before going to a waste recipient for disposal. After the outlet protein concentration reaches the feed concentration plateau, the feed inlet solution switches to the washing buffer (equal to the equilibration buffer) to washout the unbound proteins from the expanded bed column. Subsequently, desorption step begins where the elution buffer (buffer solution with NaCl and/or increased pH, according to the adsorption equilibrium isotherms to improve the elution efficiency) flows through the column to elute the target protein from the adsorbent.

Finally, for the purpose of reutilizing the adsorbent, regeneration solution (1M NaOH with 1M NaCl) is fed to the expanded bed column for a time period of no more than 45 minutes. Then, stock solution is fed in order to stabilize the adsorbent and store it in the standard conditions.

When performing residence time distribution experiments on an expanded bed column, a similar protocol is followed but tracer pulses are injected instead of the first step.

5.3. Mathematical Modelling and Numerical Solution for the Protein adsorption

5.3.1. Residence time distribution model

The RTD model is similar to the model mentioned below for the expanded bed adsorption breakthrough experiments without taking into account the adsorption phenomenon.

5.3.2. Expanded bed adsorption model

Li and co-workers [24] developed a mathematical model, based on the work of Wright et al. [25], where they take into account the intraparticle diffusion, film mass transfer, liquid and solid axial dispersion, and include in the model the particle size distribution and bed voidage axial variation in expanded bed columns.

Mass balance equation for liquid bulk phase in an expanded bed is

$$D_L \frac{\partial}{\partial Z}\left(\varepsilon_b(Z)\frac{\partial C_b}{\partial Z}\right) - u_s \frac{\partial C_b}{\partial Z} - \varepsilon_b(Z)\frac{\partial C_b}{\partial t} - \frac{3\,k_{ext}(Z)\left(1-\varepsilon_b(Z)\right)}{R\,(Z)}\left[C_b - \left(C_p\right)_{r=R(Z)}\right] = 0 \tag{5.1}$$

where C_b is the protein bulk concentration; D_L is the axial dispersion coefficient; $\varepsilon_b(Z)$ is the bed voidage at the axial distance Z of the column; Z is the axial distance from the column entrance; u_s is the superficial velocity; t denotes time; $k_{ext}(Z)$ is the film mass transfer coefficient at the axial distance Z of the column; $R\,(Z)$ is the radius of the adsorbent at the axial distance Z of the column; C_p denotes the protein pore concentration and r is the radial position in the adsorbent particle.

Boundary (BC) and initial conditions (IC) are presented below

$$BC \left| \begin{array}{lll} Z = 0 & \rightarrow & D_L\left(\frac{\partial C_b}{\partial Z}\right)_{Z=0} = \frac{u_s}{\varepsilon_b(0)}\left[(C_b)_{Z=0} - C_{b0}\right] \quad (5.2) \\ Z = H & \rightarrow & \left(\frac{\partial C_b}{\partial Z}\right)_{Z=H} = 0 \quad (5.3) \end{array} \right.$$

$$IC \left| \begin{array}{lll} t = 0 & \rightarrow & C_b(Z,0) = 0 \end{array} \right. \quad (5.4)$$

where H denotes the expanded bed height. The mass balance for the adsorbent phase in the expanded bed column is described as

$$\left[1-\varepsilon_b(Z)\right]\frac{\partial \bar{q}}{\partial t} = D_s \frac{\partial^2 \bar{q}}{\partial Z^2} + \left[1-\varepsilon_b(Z)\right]\frac{3}{R\,(Z)}k_{ext}(Z)\left[C_b - \left(C_p\right)_{r=R(Z)}\right] \tag{5.5}$$

where $\bar{q}$ is the mean adsorbent phase concentration and D_s is the solid axial dispersion coefficient in the expanded bed, estimated by the Van Der Meer et al. [26] correlation.

Boundary (BC) and initial conditions (IC) are presented as

$$BC \left| \begin{array}{lll} Z = 0 & \rightarrow & \left(\frac{\partial \bar{q}}{\partial Z}\right)_{Z=0} = 0 \quad (5.6) \\ Z = H & \rightarrow & \left(\frac{\partial \bar{q}}{\partial Z}\right)_{Z=H} = 0 \quad (5.7) \end{array} \right.$$

$$IC \;\Big|\; t = 0 \quad \rightarrow \quad \bar{q}\,(Z, 0) = 0 \tag{5.8}$$

The pore diffusion equation in the adsorbent is described as

$$\varepsilon_p \frac{\partial\, C_P}{\partial\, t} + \frac{\partial\, q}{\partial\, t} = D_{pe}\left(\frac{\partial^2\, C_p}{\partial\, r^2} + \frac{2}{r}\frac{\partial C_p}{\partial r}\right) \tag{5.9}$$

where ε_p is the particle porosity, q is the adsorbed concentration and D_{pe} is the effective pore diffusion coefficient.

Boundary (BC) and initial conditions (IC) are as follows

$$BC \;\Big|\; r = 0 \quad \rightarrow \quad \left(\frac{\partial\, C_p}{\partial\, r}\right)_{r=0} = 0 \tag{5.10}$$

$$r = R(Z) \quad \rightarrow \quad D_{pe}\left(\frac{\partial\, C_p}{\partial\, r}\right)_{r=R(Z)} = \frac{R(Z) D_S}{3[1-\varepsilon_b(Z)]}\frac{\partial^2\, \bar{q}}{\partial\, Z^2} + k_{ext}(Z)\left[C_b - \left(C_p\right)_{r=R(Z)}\right] \tag{5.11}$$

$$IC \;\Big|\; t = 0 \quad \rightarrow \quad C_p(r) = 0, \qquad q(r) = 0 \tag{5.12}$$

Based on previous experimental results for either HSA or IgG protein adsorption on MabDirect MM, the Langmuir isotherm model is assigned as

$$q = \frac{q_{max}\, K_L\, C_P}{1 + \, K_L\, C_P} \tag{5.13}$$

where q_{max} is the maximum adsorption uptake capacity and K_L denotes Langmuir constant, both of which are determined by batch experiments, and in this case estimated in previous works [4, 14].

Li et al. [24] recommended the following correlations to estimate the particle size axial distribution ($R(Z)$) and bed voidage axial variation ($\varepsilon_b(Z)$) in expanded beds packed with first-generation adsorbent; MabDirect MM is a second generation adsorbent but, even so, the following correlations were used to estimate an approximated value.

$$R(Z) = \frac{\overline{d_p}}{2}\left(1.20 - 0.51\,\frac{Z}{H}\right) \tag{5.14}$$

$$\varepsilon_b(Z) = \overline{\varepsilon_b}\left(0.629 + 0.738\,\frac{Z}{H}\right) \tag{5.15}$$

$$\overline{\varepsilon_b} = 1 - \left[(1-\varepsilon_0)\frac{H_0}{H}\right] \tag{5.16}$$

where $\overline{d_p}$ is the mean adsorbent particle diameter; H is the bed height; $\overline{\varepsilon_b}$ is estimated as a function of the whole expanded bed height; H_0 is the settled bed height and ε_0 is the settled bed voidage.

5.3.3. Model Parameters

As referred, the adsorbent axial dispersion coefficient (D_s) is estimated by the Van Der Meer correlation [26] using experimental values for the superficial velocity (u_s), as follows

$$D_s = 0.04\, u_s^{1.8}\ (m^2.s^{-1}) \tag{5.17}$$

The liquid axial dispersion coefficient (D_L) is estimated by the residence time distribution (RTD) method during the expanded stage. The effective pore diffusivities (D_{pe}) in adsorbents for each target protein were determined in previous chapters 3 and 4 by fitting a mathematical model to the adsorption kinetics from batch experiments and validated by an alternative method [27].

The Wilson and Geankoplis correlation [28], applicable to low Reynolds number, is used to estimate the external mass transfer in the expanded bed column.

$$Sh = \frac{1.09}{\varepsilon_b} \cdot Re^{1/3} \cdot Sc^{1/3} \tag{5.18}$$

where Re denotes the Reynolds number [$= \rho \cdot d_p \cdot u_i / \eta$], Sc represents the Schmidt number [$= \eta / (\rho \cdot D_m)$], Sh is the Sherwood number [$= d_p \cdot k_{ext} / D_m$], D_m is the molecular diffusion coefficient, d_p is the particle diameter, ρ is the density and η is the viscosity. Ranz and Marshall [29], Wakao and Funazkri [30], or Fan et al. [31] correlations can be used as an alternative.

5.3.4. Numerical method

Employing the orthogonal collocation in finite elements method (OCFEM) it is possible to obtain the numerical solution of the model equations on commercial software gPROMS (general PROcess Modelling System) version 3.4.0. The axial bed dimension was discretized in 51 finite elements with 2 interior collocation points in each finite element and to solve the remaining system of ordinary differential equations in time the DASOLV integration solver was used. The radial dimension was discretized in 100 finite elements with 2 interior collocation points in each finite element. 10^{-5} tolerance was used for all simulations.

5.4. Results and discussion

5.4.1. Adsorption equilibrium isotherms for HSA and IgG

In order to understand and validate the expanded bed adsorption results, a brief summary of adsorption equilibrium isotherms from previous chapters [4, 14] for both target proteins is presented. As far as literature goes, all researchers agree on that the two most important conditions are the ionic strength of the buffer solution by studying salt concentration and the respective solution pH.

Table 5.1 presents the adsorption equilibrium isotherms and kinetics values for both HSA and IgG adsorption in batch experiments for distinctive pH solutions.

Table 5.1 – Parameters of HSA and IgG adsorption equilibrium and kinetics of MabDirect MM in 20 mM citrate buffer (pH 3.0, 5.0 and 6.0) and 20 mM phosphate buffer (pH 7.0), containing different NaCl concentrations.

pH	NaCl (M)	Protein	q_m(mg·g$_{dry}^{-1}$)	K_L (L·g^{-1})	D_{pe} (10^{-6} cm^2·min^{-1})
3	0	HSA	30.9 ± 5.7	10.36 ± 1.91	2.9
5	0	HSA	36.0 ± 3.5	4.62 ± 0.46	2.2
		IgG	149.7 ± 7.1	0.32 ± 0.02	15.4
	0.1	HSA	30.7 ± 6.3	3.46 ± 0.42	1.9
		IgG	104.7 ± 5.1	0.31 ± 0.02	6.5
	0.2	IgG	62.3 ± 5.0	0.53 ± 0.05	3.7
	0.4		16.3 ± 8.0	3.08 ± 1.51	1.0
	0.5	HSA	29.1 ± 1.1	0.88 ± 0.05	2.4
	1		13.4 ± 2.5	2.36 ± 0.47	2.2
6	0	HSA	21.5 ± 2.9	1.74 ± 0.28	2.0
		IgG	129.0 ± 9.2	0.38 ± 0.03	2.3
7	0	HSA	8.6 ± 2.1	10.08 ± 2.48	2.4
		IgG	90.4 ± 9.1	0.31 ± 0.05	1.9
	0.4	IgG	4.7 ± 0.4	0.69 ± 0.07	0.2
	1	HSA	11.8 ± 2.2	1.65 ± 0.34	4.8

Salt concentration was changed according to the target protein, where for IgG it were used 0.1, 0.2 and 0.4M NaCl while for HSA were used 0.1, 0.5 and 1M in two different buffer pH values (5.0 and 7.0). From Table 5.1 it is also possible to perceive that IgG protein is more sensitive to salt concentration than HSA, since for similar achieved adsorption capacities, the salt concentration on HSA was double that of IgG.

Figures 5.1 – 5.3 show the adsorption isotherms for HSA and IgG on distinctive salt concentrations and buffer pH values. The maximum adsorption capacity was registered at pH 5.0 without salt addition for both proteins adsorption as it can be observed in Figure 5.1 (a and b) for both HSA and IgG, respectively. Table 5.1 and Figure 5.2 (a and b) show that for a buffer solution with salt (1M NaCl for HSA and 0.4M NaCl for IgG) the lower pH will allow a larger adsorption capacity.

Regarding the pH study, also from Table 5.1 and Figure 5.3 (a and b), it is possible to observe that HSA adsorption is more sensitive to pH variations than IgG, since while for HSA for pH buffer solution of 5.0, 6.0 and 7.0 there is a decrease from 36.0 to 21.5 (40% of lost capacity) and to 8.6 mg·g_{dry}^{-1} (76% of lost capacity), respectively, for IgG and for the same buffer solution pH the decrease is from 149.7, to 129.0 (14% of lost capacity) and to 90.4 mg·g_{dry}^{-1} (40% of lost capacity), respectively. Adsorption equilibrium isotherms were already compared to the literature in previous chapters [4, 14].

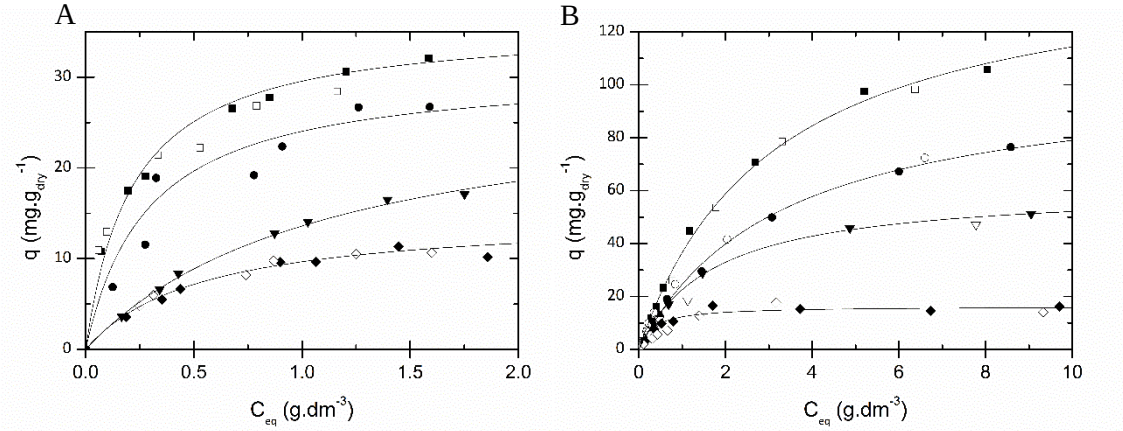

Figure 5.1 – Adsorption isotherms of HSA (A) and IgG (B) on MabDirect MM from a 20 mM citrate buffer at pH 5.0 for different NaCl concentrations (squares – without salt for HSA and IgG; circles – 0.1M NaCl for both HSA and IgG; triangles – 0.5M NaCl for HSA and 0.2M NaCl of IgG; diamonds – 1M NaCl for HSA and 0.4M NaCl for IgG) at 20 °C: experimental data (full symbols – 1.26g (HSA) and 0.050 (IgG) of adsorbent, open symbols – 3.27g (HSA) and 0.127 (IgG) of adsorbent) and Langmuir model (curves) [4, 14].

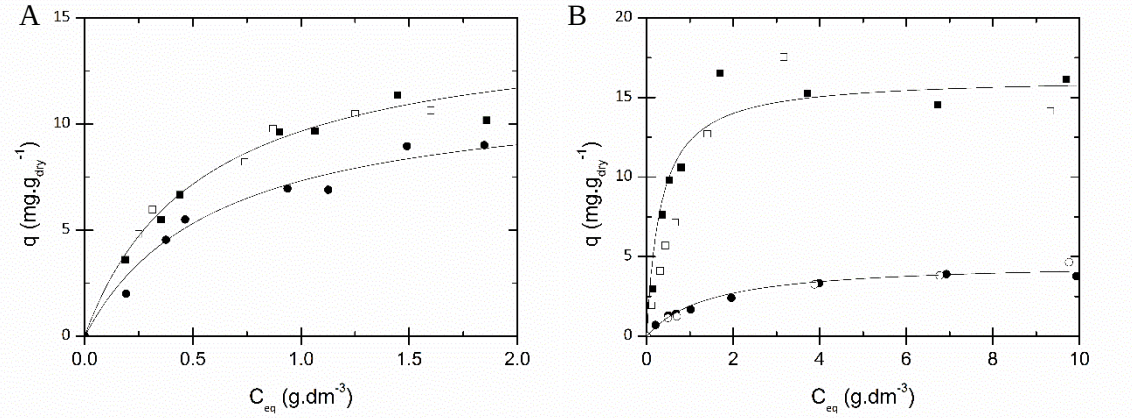

Figure 5.2 – Adsorption isotherms of HSA (A) and IgG (B) in 20 mM citrate buffer pH 5 (squares) and HSA in 20 mM phosphate buffer pH 7 (circles): Experimental data (full symbols – 1.26g (HSA) and 0.050 (IgG) of adsorbent, open symbols – 3.27g (HSA) and 0.127 (IgG) of adsorbent) and Langmuir model (curves). Conditions: All experiments with 1M NaCl for HSA and 0.4M for IgG at 20 °C [4, 14].

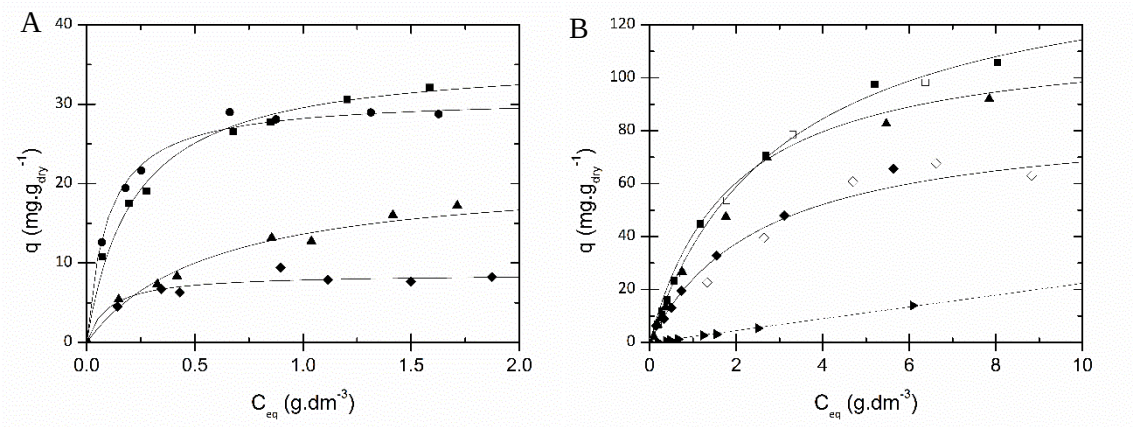

Figure 5.3 – Adsorption isotherms of HSA (A) and IgG (B) in different buffer pH: 20 mM citrate buffer pH 3 (circles), pH 5 (squares), pH 6 (up triangles); 20 mM phosphate buffer pH 7 (diamonds) and 20 mM tris-HCl pH 8.5 (triangles): Experimental data (full symbols – 1.26g (HSA) and 0.050 (IgG) of adsorbent, open symbols – 0.127 (IgG) of adsorbent), Langmuir model (full line) and linear model (dashed line). Conditions: All experiments in solution without salt at 20 °C [4, 14].

5.4.2. Adsorption kinetics for HSA and IgG

Kinetic studies were performed for both target proteins in a batch adsorber in previous chapters concerning the determination of the uptake rate in distinctive conditions. Also, a pore diffusion model (PDM) was fitted to the experiments in order to study the transport properties between the chosen target protein and the adsorbent. For demonstrative purposes, Figures 5.4 and 5.5 present the adsorption kinetics of HSA and IgG on MabDirect MM from a 20 mM citrate buffer without and with 0.1M NaCl, respectively.

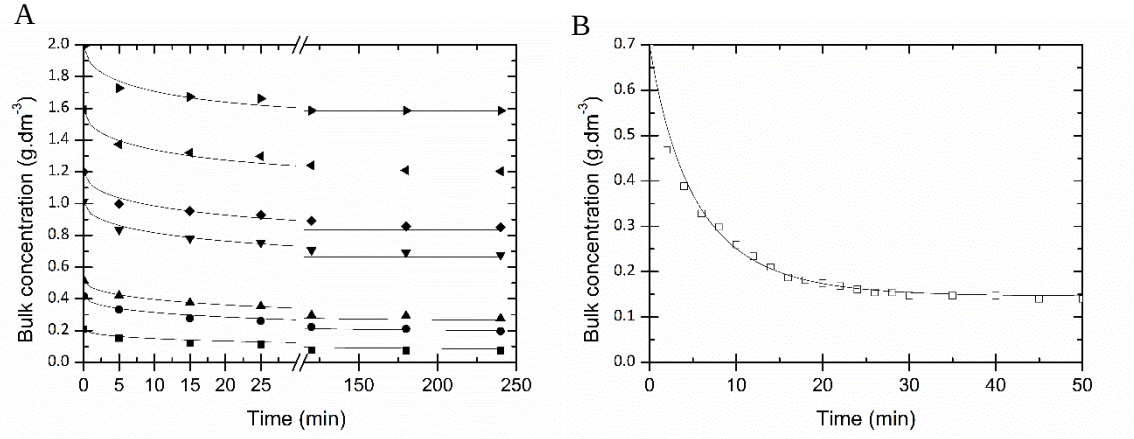

Figure 5.4 – Adsorption kinetics of HSA (A) and IgG (B) on MabDirect MM from a 20 mM citrate buffer at pH 5.0 without NaCl. Experimental data (full symbols : 0.2, 0.4, 0.6, 1.0, 1.2, 1.6 and 2.0 g·dm^{-3} HSA represented by square, circle, up triangle, down triangle, diamond, left triangle and right triangle, respectively; open squares – 0.7 g·dm^{-3} IgG), at 20 °C and 270 rpm [4, 14].

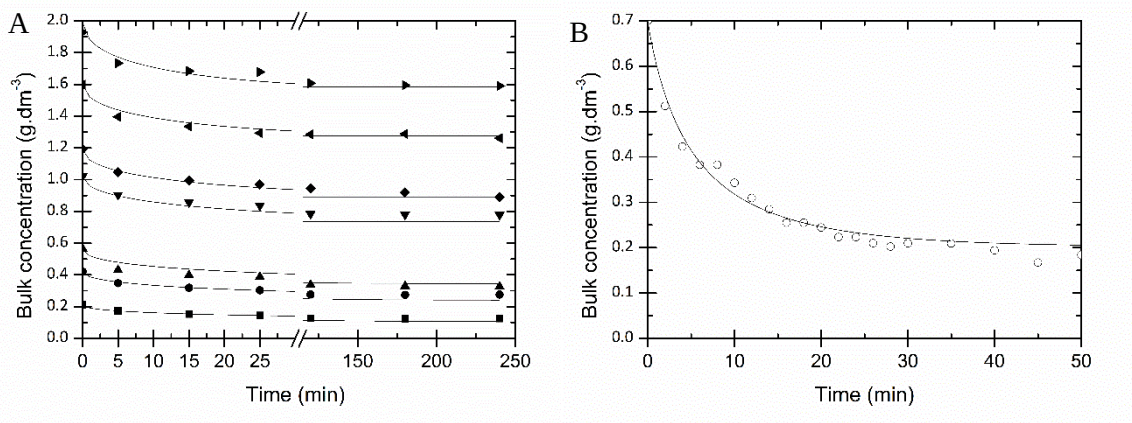

Figure 5.5 – Adsorption kinetics of HSA (A) and IgG (B) on MabDirect MM from a 20 mM citrate buffer at pH 5.0 with 0.1M NaCl. Experimental data (full symbols : 0.2, 0.4, 0.6, 1.0, 1.2, 1.6 and 2.0 g·dm^{-3} HSA represented by square, circle, up triangle, down triangle, diamond, left triangle and right triangle, respectively; open circles – 0.7 g·dm^{-3} IgG), at 20 °C and 270 rpm [4, 14].

Concerning the effective pore diffusion coefficient (D_{pe}) it is possible to visualize from Table 5.1 that for buffers pH 6.0 and 7.0 the D_{pe} values were similar; however, this cannot be stated for buffer pH 5.0. It is believed that for IgG adsorption at pH 5.0 without and with 0.1M NaCl, the batch experiments were not performed at a sufficient stirring speed so that the external mass transfer could be neglected and, for this reason, the D_{pe} value is much higher for this protein since the external resistance is taken into account [14].

Pore diffusion model could describe well the adsorption kinetics under the studied conditions and reasonable estimations were made for the intra-particle diffusion coefficients in Table 5.1. Adsorption kinetics were already compared to the literature in previous chapters [4, 14].

5.4.3. Bed expansion and liquid axial dispersion coefficient in expanded bed

Before performing an expanded bed adsorption breakthrough experiment, some characteristics regarding the column and the adsorbent must be checked. Bed expansion is measured at various superficial flow velocities, as shown in the Figure 5.6, where the streamline 50 column is packed with 100 mL of MabDirect MM for a settled bed height of 5.1 cm. The figure also displays the results of 2 distinctive adsorbents, Streamline DEAE and Streamline Direct CST-I, which are a first and a second generation adsorbents. Streamline DEAE is a low-density base matrix with ligand sensitive to ionic strength and salt concentration (classic ion exchanger), while Streamline Direct CST-I is a high salt-tolerant, multimodal adsorbent, with a matrix structure composed by macroporous cross-linked 4% agarose containing stainless steel materials [24].

From Figure 5.6 it is possible to conclude that this adsorbent presents higher density and allows to operate the expanded bed at higher flow rates which is the purpose of its design.

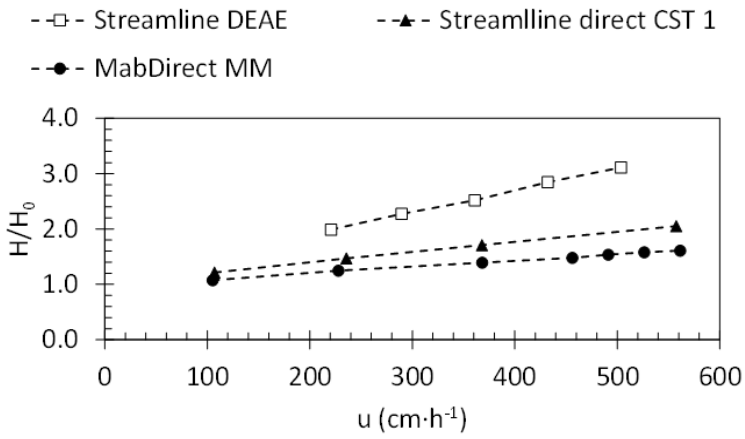

Figure 5.6 – Comparison between bed expansion degree for different flow velocities in expanded bed packed with Streamline DEAE, Streamline direct CST-I and MabDirect MM.

The residence time distribution (RTD) method with a pulse of tracer (Blue Dextran 2000) is utilized to estimate the liquid axial dispersion coefficient in the expanded bed column. The experimental data of RTD for each column are presented in the following subsection.

The mean residence time ($\overline{t_m}$) is calculated by

$$\overline{t_m} = \frac{\int_0^\infty t \cdot C_b \, dt}{\int_0^\infty C_b \, dt} \tag{5.19}$$

While the variance of the distribution (σ^2) is calculated by

$$\sigma^2 = \frac{\int_0^\infty t^2 \cdot C_b \, dt}{\int_0^\infty C_b \, dt} - \bar{t}_m^2 \tag{5.20}$$

On literature there are conventional equations to calculate the liquid axial dispersion coefficient. The first absolute moment of the dispersion model equals to the mean residence time and from the second central moment we can obtain the axial dispersion coefficient.

The following Bruce and Chase [32] equation was chosen to calculate the liquid axial dispersion coefficient.

$$\frac{\sigma^2}{\bar{t}_m^2} = \frac{2\,(\bar{\varepsilon_b}\,D_L/u_s\,H) + 3\,(\bar{\varepsilon_b}\,D_L/u_s\,H)^2}{1 + 2\,(\bar{\varepsilon_b}\,D_L/u_s\,H) + (\bar{\varepsilon_b}\,D_L/u_s\,H)^2} \tag{5.21}$$

5.4.3.1. Streamline 50 column

Table 5.2 presents the streamline 50 expanded bed column characteristics along with conditions of the RTD experiments. Two flow rates and, for each flow rate, three different time pulses (4, 7 and 9 seconds) with 5 g·dm^{-3} of Blue Dextran 2000 were tested. Blue Dextran 2000 was used based on literature [16].

Table 5.2 – Streamline 50 expanded bed column characteristics along with conditions of the RTD experiments.

Parameters	Expanded bed conditions					
d_c (cm)	5					
A_S (cm^2)	19.63					
$H_{settled}$ (cm)	5.1					
$V_{ads,settled}$ (cm^3)	98.2					
Q (cm^3·min^{-1})	160			181		
$H_{expanded}$ (cm)	8.2			9		
$V_{ads,expanded}$ (cm^3)	161.0			176.7		
$\bar{\varepsilon_b}$	0.63			0.66		
τ_d (s)	37.9			38.7		
Pulse time (s)	4	7	9	4	7	9
D_L (10^{-5} m^2·s^{-1})	1.73	3.09	2.99	2.89	2.30	3.28

Figure 5.7 and Figure 5.8 present the outlet concentration history from the moment of time pulse to the end of the experiment at a flow rate of 160 and 181 cm^3·min^{-1}, respectively.

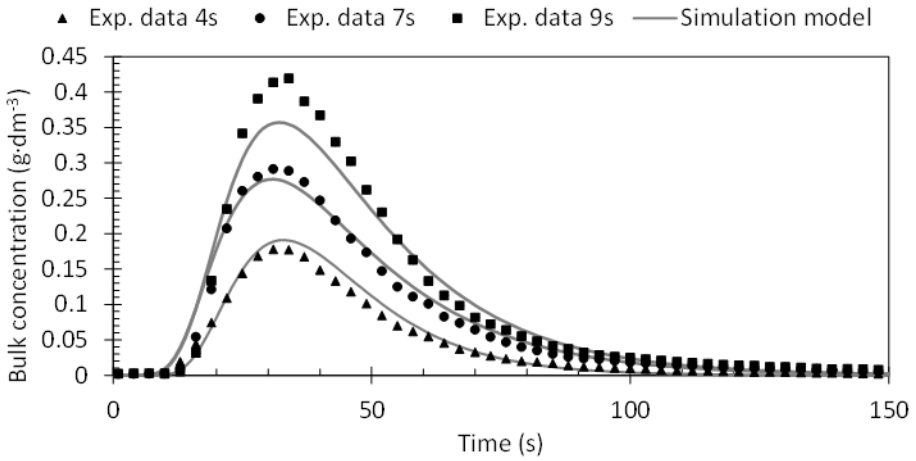

Figure 5.7 – Residence time distribution experimental data points for different time pulses (4, 7 and 9 seconds) for flow rate of 160 cm^3·min^{-1} along with the mathematical model simulations.

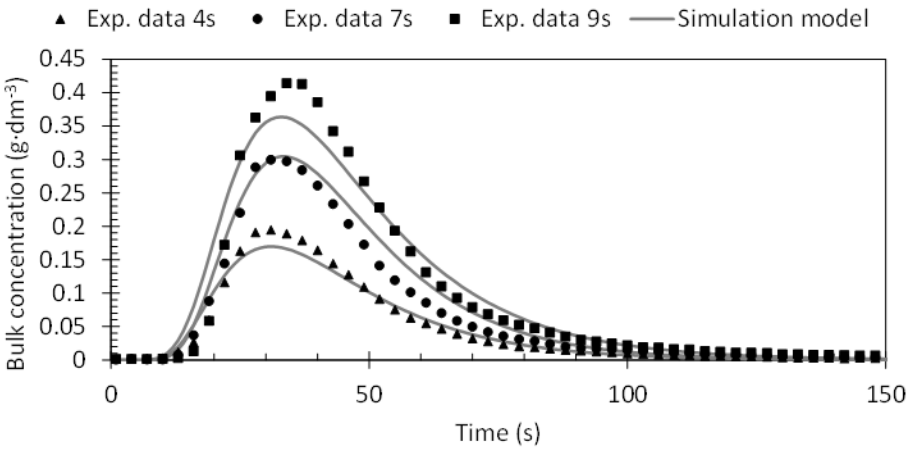

Figure 5.8 – Residence time distribution experimental data points for different time pulses (4, 7 and 9 seconds) for flow rate of 181 $cm^3 \cdot min^{-1}$ along with the mathematical model simulations.

It is possible to visualize that the mathematical model used fits relatively well the experimental data with the exception for the 9 seconds time pulse. The calculated values of the liquid axial dispersion are presented in Table 5.2.

5.4.3.2. Omnifit 66/20 column

Omnifit 66/20 expanded bed column was used to estimate the liquid axial dispersion by residence time distribution experiments. Table 5.3 shows the column characteristics along with the RTD experimental conditions.

Table 5.3 – Omnifit 66/20 expanded bed column characteristics mounted in a Gilson HPLC along with conditions of the RTD experiments.

Parameters	Expanded bed conditions	
d_c (cm)	0.66	
A_S (cm^2)	0.3421	
$H_{settled}$ (cm)	6.9	
$V_{ads,settled}$ (cm^3)	2.4	
Q ($cm^3 \cdot min^{-1}$)	2.0	
$H_{expanded}$ (cm)	10.1	
$V_{ads,expanded}$ (cm^3)	3.5	
V_{loop} (µL)	20	
C_{Tracer} ($g \cdot dm^{-3}$)	5	10
$\overline{\varepsilon_b}$	0.62	
τ_d (s)	60.5	
D_L ($\times 10^{-5}$ $m^2 \cdot s^{-1}$)	1.723	

Figure 5.9 presents the experimental residence time distributions obtained with two different pulses (5 and 10 g·dm^{-3}) at a flow rate of 2 cm^3·min^{-1}.

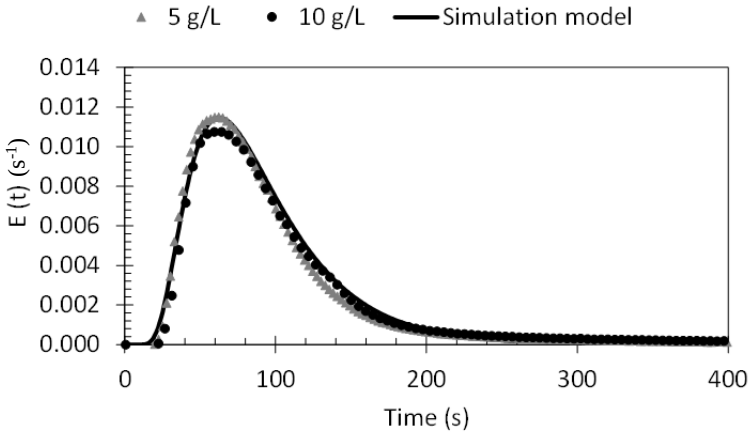

Figure 5.9 – Residence time distribution experimental data points for 20 µL injection for flow rate of 2.0 cm^3·min^{-1} along with the mathematical model simulation.

5.4.3.3. XK 16/20 column

XK 16/20 expanded bed column was used to estimate the liquid axial dispersion by residence time distribution experiments. Table 5.4 shows the column characteristics along with the RTD experimental conditions.

Table 5.4 – XK 16/20 expanded bed column characteristics mounted in a Gilson HPLC along with conditions of the RTD experiments.

Parameters	Expanded bed conditions	
d_c (cm)	1.6	
A_S (cm^2)	2.01	
$H_{settled}$ (cm)	5	
$V_{ads,settled}$ (cm^3)	10	
Q (cm^3·min^{-1})	7	
$H_{expanded}$ (cm)	7.3	
$V_{ads,expanded}$ (cm^3)	14.8	
V_{loop} (µL)	20	
C_{Tracer} (g·dm^{-3})	5	10
$\bar{\varepsilon_b}$	0.60	
τ_d (s)	84.43	
D_L (×10^{-6} m^2·s^{-1})	2.98	

Figure 5.8 presents the experimental residence time distribution curves, for two different pulse concentrations, at a flow rate of 7 $cm^3 \cdot min^{-1}$.

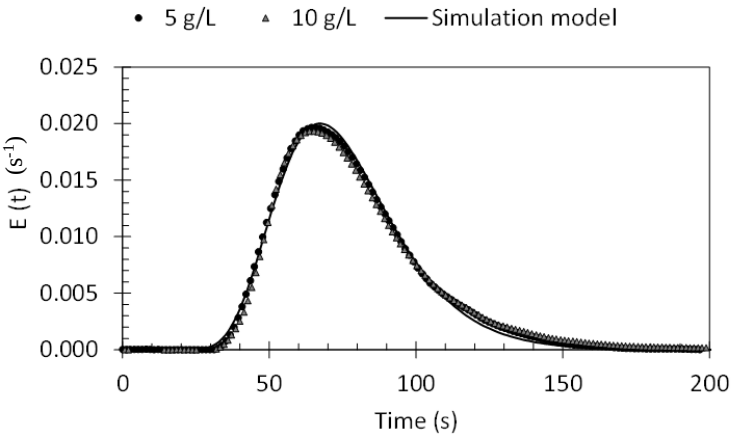

Figure 5.10 – Residence time distribution experimental data points for 20 µL injection for flow rate of 7 $cm^3 \cdot min^{-1}$ for two different Blue Dextran 2000 pulse feed concentrations along with the mathematical model simulation.

5.4.4. HSA protein expanded bed breakthrough behaviour

Several expanded bed breakthrough experiments were performed for HSA protein adsorption. Tables 5.5 and 5.6 show the operating conditions and adsorbed/desorbed protein mass in each stage in different runs. Two experiments, where different flow rates were used (142 and 79 $cm^3 \cdot min^{-1}$ for runs 1 and 2, respectively), are displayed. Then, a third EBA breakthrough experiment was conducted similar to run 1 but with a different flow rate in the elution stage in order to concentrate the desorbed protein. Finally, a fourth experiment was performed where the elution buffer solution was changed in order to allow a better elution according to the adsorption isotherms [4, 14].

Table 5.5 – Operating conditions for all EBA breakthrough experiments along with calculated average bed porosity and Streamline 50 column characteristics.

Parameter \ Run	1	2	3	4
C_{b0} ($g.dm^{-3}$)	0.954	0.950	0.959	0.975
Q_{ads} ($cm^3 \cdot min^{-1}$)	142	79	143	140
$H_{settled}$ (cm)	5.0			
$H_{expanded}$ (cm)	8.5	6.8	8.4	8.3
ε_{b0}	0.40			
$\overline{\varepsilon_b}$	0.65	0.56	0.64	0.64
ε_p	0.2374			
d_c (cm)	5			
A_S (cm^2)	19.63			
R_p (cm)	5.15×10^{-3}			
V (cm^3)	98.2			

Table 5.6 – Flow rates for each adsorption/desorption stage along with the adsorbed/desorbed protein mass obtained for each run conducted for HSA expanded bed adsorption breakthrough in the Streamline 50 column.

Parameter	Run	Adsorption	Desorption				Difference (%)
			Washing	Elution	Regeneration	Stock	
Q ($cm^3 \cdot min^{-1}$)	1	142	142	133	131	130	
	2	79	79	79	79	79	
	3	143	141	34	30	30	
	4	140	136	38	38	38	
$m_{protein}$ (mg)	1	2421.5	493.7	840.6	734.4	108.4	10
	2	2840.9	417.4	1199.4	892.5	54.1	10
	3	2235.6	394.0	1189.0	805.7	0	7
	4	2331.3	563.9	1599.7	163.0	15.1	0.4

The following plots (Figures 5.11 – 5.14) show the outlet protein concentrations during the different stages for each run.

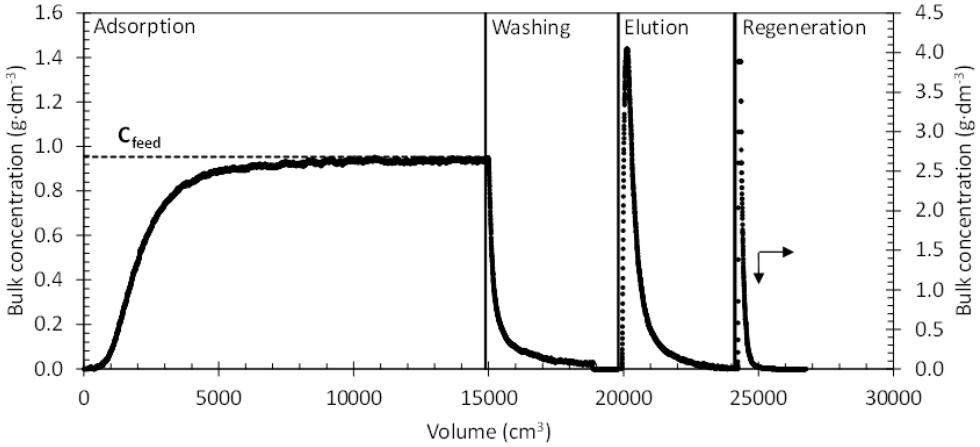

Figure 5.11 – Effluent curves of HSA during adsorption/desorption stages in expanded bed. At the adsorption stage, 0.95 $g \cdot dm^{-3}$ HSA in 20 mM citrate buffer pH 5.0 without salt is applied at 142 $cm^3 \cdot min^{-1}$; at the washing stage, 20 mM citrate buffer pH 5.0 without salt is fed at the same flow rate as adsorption stage; at elution stage, 20 mM citrate buffer pH 5.0 with 1M NaCl is applied at 133 $cm^3 \cdot min^{-1}$, then regeneration solution is fed at 131 $cm^3 \cdot min^{-1}$.

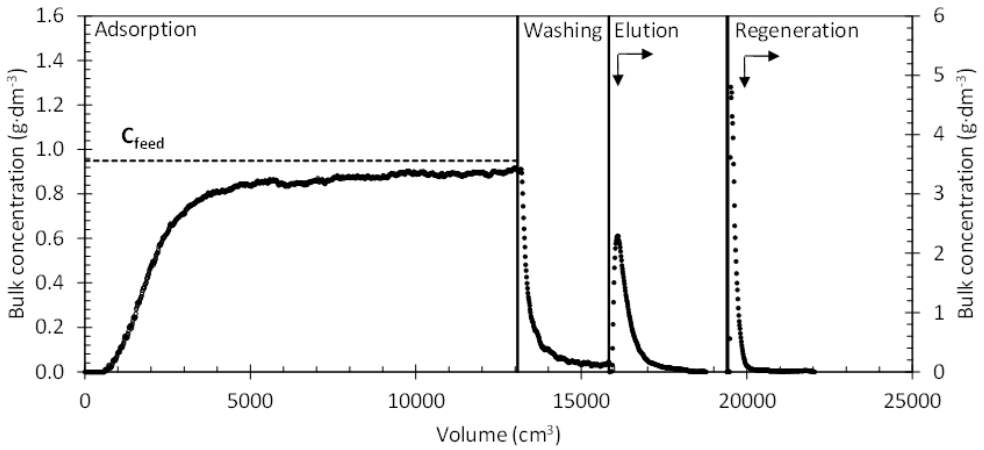

Figure 5.12 – Effluent curves of HSA during adsorption/desorption stages in expanded bed. At the adsorption stage, 0.95 g·dm^{-3} HSA in 20 mM citrate buffer pH 5.0 without salt is fed at 79 cm^3·min^{-1}; at the washing stage, 20 mM citrate buffer pH 5.0 without salt is applied; at elution stage, 20 mM citrate buffer pH 5.0 with 1M NaCl is fed, then regeneration stage solution is applied. Desorption stages (washing, elution, regeneration) flow through the expanded bed column at the same flow rate as adsorption, for this run.

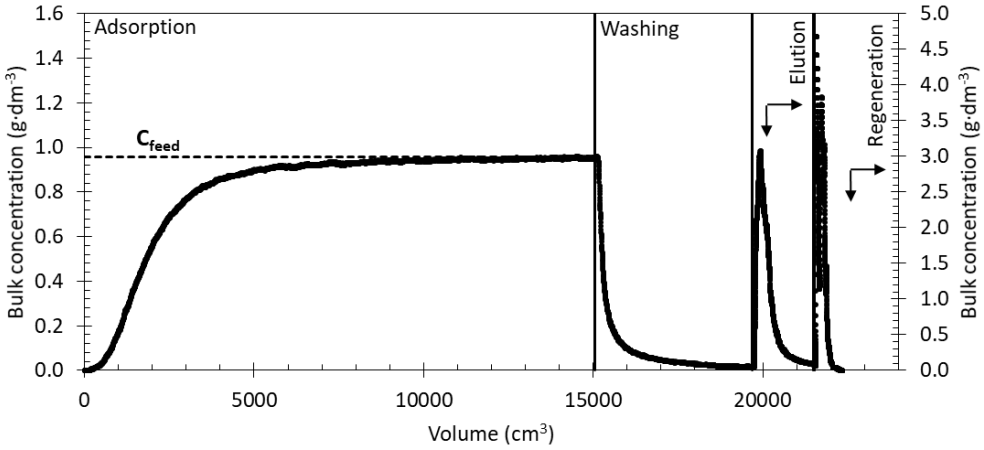

Figure 5.13 – Effluent curves of HSA during adsorption/desorption stages in expanded bed. At the adsorption stage, 0.95 g·dm^{-3} HSA in 20 mM citrate buffer pH 5.0 without salt is applied at 143 cm^3·min^{-1}; at the washing stage, 20 mM citrate buffer pH 5.0 without salt is applied at the same flow rate as adsorption stage; at elution stage, 20 mM citrate buffer pH 5.0 with 1M NaCl is applied at 34 cm^3·min^{-1}, then regeneration stage solution is applied at 30 cm^3·min^{-1}.

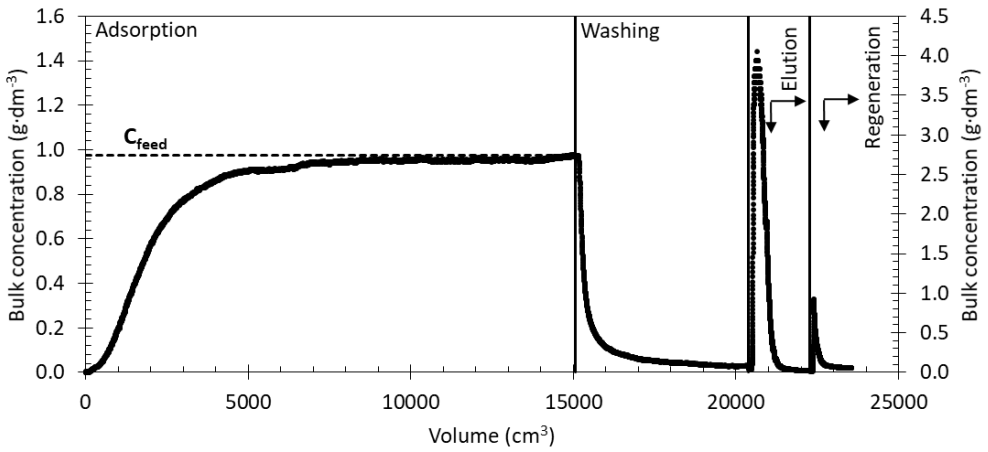

Figure 5.14 – Effluent curves of HSA during adsorption/desorption stages in expanded bed. At the adsorption stage, 0.95 g·dm^{-3} HSA in 20 mM citrate buffer pH 5.0 without salt is applied at 140 cm^3·min^{-1} flow rate; at the washing stage, 20 mM citrate buffer pH 5.0 without salt is applied at the same flow rate as adsorption stage; at elution stage, 20 mM phosphate buffer pH 7.0 with 1M NaCl is applied at 38 cm^3·min^{-1}, then regeneration stage solution is applied at the same flow rate as elution.

Between runs 1 and 3 the flow rate was changed in the elution stage in order to concentrate the eluted HSA protein. From Table 5.6 it is possible to visualize that the desorbed HSA mass goes from 840.6 mg to 1189.0 mg of protein, in agreement with run 2 (1199.4 mg) in which a similar flow rate was used in all stages. Afterwards, another run (4) was performed in order to increase the eluted protein (using a different elution buffer) and decrease the desorbed protein in the subsequently stages (regeneration and stock solution). It was obtained an eluted protein mass of 1599.7 mg, higher than in the previous experiments and, in the regeneration stage, the desorbed protein decreases from 892.5 mg to 163.0 mg, since the regeneration buffer is a solution where the target protein is not stable.

The adsorption stage experiments were compared with the results obtained with the mathematical simulation model. Figure 5.15 shows runs 1 to 4 with the simulation results for only the adsorption stage. Since the two major changes in the four runs are the concentration and the flow rate, the plot was adjusted (normalized concentration) in order to show that the four EBA experiments are in agreement with each other and also with the mathematical model.

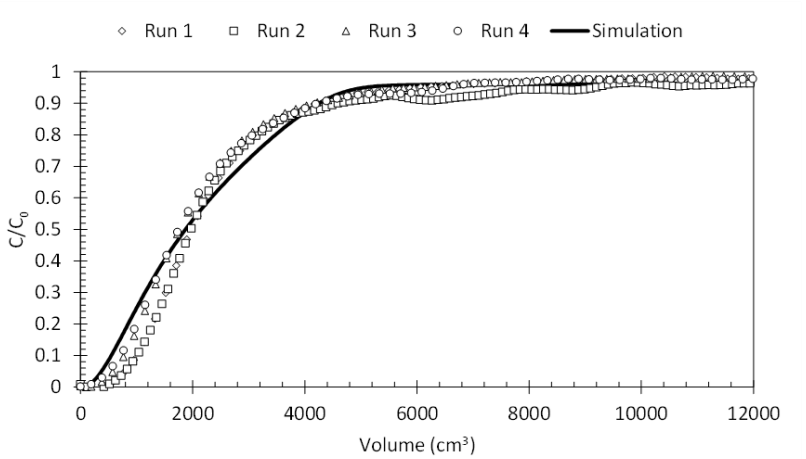

Figure 5.15 – HSA breakthrough curve during adsorption stage. Normalized concentration per eluted volume for all expanded bed experiments with mathematical simulation results.

The experimental data for the four EBA experiments during the adsorption stage were smoothed using the signal processing tool in the OriginPro program in order to neglect the experimental noise. Also, for a better understanding, the volume interval between each pair of collected data points was enlarged due to the excessive data points recorded.

Adsorption equilibrium isotherms allow to calculate the adsorption capacity expected for the feed concentrations of 0.954, 0.950, 0.959 and 0.975 $g \cdot L^{-1}$ of HSA for each run. For the adsorption conditions tested (pH 5.0 without salt) it is obtained an adsorption capacity of 29.34, 29.32, 29.37 and 29.46 $mg \cdot g_{dry}^{-1}$, respectively. The difference between the adsorption capacity calculated from adsorption equilibrium isotherms and the EBA breakthrough experiments (21.91, 25.71, 20.23 and 21.10 $mg \cdot g_{dry}^{-1}$) is due to the fact that the experimental breakthrough experiments were not run until the complete saturation of the adsorbent.

The dynamic binding capacity (DBC) at 10% of the breakthrough is a common calculation coefficient for both fixed bed and expanded bed breakthrough experiments [33]; it is calculated by the following equation

$$q_{10\%} = \frac{\int_0^{V_{10\%}} (C_{b0} - C_b)\, dV}{V_a} \tag{5.22}$$

where V_a is the packed bed volume of adsorbent, V is the effluent liquid volume, $V_{10\%}$ is the effluent liquid volume at 10% protein breakthrough.

For each run it were obtained a DBC at 10% of breakthrough of 8.9, 9.7, 7.5 and 7.0 $mg \cdot g_{dry}^{-1}$ (24.8, 27.0, 21.0 and 19.5 $mg \cdot cm^{-3}$) corresponding to a 41, 39, 38 and 30% of the saturation capacity for runs 1–4, respectively.

Comparing the data with literature, several considerations need to be taken into account, such as, target protein (HSA, BSA, IgG, myoglobin, ovalbumin, etc.) and its source (pure, from

cell growth, hybridoma broth, etc.), adsorbent (ligand structure for different adsorbent type as for example, ion exchange, hydrophobic charge induction, mixed mode, affinity chromatography), feed protein concentration, solution pH, salt type and its concentration and flowrate. Similar experiments found in literature are presented next.

According to literature, Li and co-workers [24] studied the expanded bed adsorption of albumin from bovine serum (BSA) on Streamline CST-I (cation exchanger mixed mode resin) and on Streamline DEAE (anion exchanger). 300 mL of either adsorbent was packed into a streamline 50 column, where a feed concentration of 2 $g.dm^{-3}$ of BSA prepared with 50 mM acetate buffer pH 5.0 without salt at 181 $cm^3.min^{-1}$ for streamline CST-I and 2 $g.dm^{-3}$ of BSA prepared with 20 mM phosphate buffer pH 7.5 without salt at 83.6 $cm^3.min^{-1}$ were pumped from the bottom inlet. They reported a dynamic binding capacity at 5% breakthrough of 34 $mg.cm^{-3}$ of the settled bed volume for Streamline CST-I and 50 $mg.cm^{-3}$ of the settled bed volume for Streamline DEAE.

Xia et al. [34] also studied the adsorption in expanded bed configuration of albumin from bovine serum on a diethylaminoethyl (DEAE) ligand coupled on a macroporous cellulose-tungsten carbide composite beads. 2 $mg.cm^{-3}$ of BSA in 20 mM Tris-HCl pH 8.5 was loaded in a Bio-red column (1 cm diameter, 30 cm length) with a settled bed height of 12 cm (9.42 cm^3). They reported expanded bed adsorption breakthroughs for three different flow velocities, 500, 700 and 900 $cm.h^{-1}$ where it were obtained dynamic binding capacities at 10% breakthrough of 45.1, 44.3 and 38.5 $mg.g^{-1}$ corresponding to 69, 64 and 56% of the saturation capacity.

In 2014, Rezvani et al. [35] performed BSA adsorption on a novel agarose-nickel composite matrix in expanded bed column (0.01 m diameter). For a settled bed height of 6.0 cm (approximately 4.72 mL) and for a BSA feed concentration of 1 $mg.cm^{-3}$ in 10 mM acetate buffer pH 4.0 without salt addition, they obtained dynamic binding capacities at 10% of breakthrough of 9.98 and 7.17 $mg{\cdot}cm^{-3}$ for flow velocities of 170 and 450 $cm.h^{-1}$, respectively. They also studied BSA adsorption in the same concentration and buffer conditions for their novel ligand connected to a Streamline matrix and obtained a DBC at 10% breakthrough of 7.98 $mg{\cdot}cm^{-3}$ for a flow velocity of 170 $cm.h^{-1}$

Although tested in different conditions, MabDirect MM presents an alternative for capturing Human serum albumin; also, as it was demonstrated, it shows good recovery at low cost.

5.4.5. IgG protein expanded bed breakthrough behaviour

Similar breakthrough experiments were conducted in two distinctive expanded bed columns (Omnifit 66/20 and XK 16/20 columns) for IgG adsorption.

5.4.5.1. Omnifit 66/20 expanded bed column

At the adsorption stage, 0.53 g·L^{-1} of IgG on 20 mM citrate buffer pH 5.0 with 0.4M NaCl was fed to the bottom inlet of the column at 2.2 mL·min^{-1} flow rate; then, at the washing stage, the flow rate was maintained to wash the unbound IgG protein. Afterwards, it was switched to elution buffer (20 mM phosphate buffer pH 7.0 with 0.4M NaCl) to elute the bound protein and the flow rate was reduced to concentrate this target protein. Regeneration and stock solution were then performed with each solution already described and it was maintained the same flow rate as during the elution stage. Table 5.7 presents the operating conditions for the expanded bed breakthrough experiment.

Table 5.7 – Operating conditions for expanded bed IgG breakthrough experiment at 20 ± 1 °C, pH 5.0 with 0.4M NaCl, along with Omnifit 66/20 column, adsorbent (MabDirect MM) characteristics, and with the adsorbed/desorbed protein mass obtained in each stage.

Parameter	Adsorption	Desorption				Difference (%)
		Washing	Elution	Regeneration	Stock	
Q (cm3.min^{-1})	2.2		0.6			
C_{b0} (g.dm^{-3})	0.53	n.a.				
d_c (cm)	0.66					
A_S (cm^2)	0.3421					
ε_{b0}	0.4					
$\overline{\varepsilon_b}$	0.63					
ε_p	0.2374					
r_p (cm)	5.15×10^{-3}					
$H_{settled}$ (cm)	6.4					
$H_{expanded}$ (cm)	10.4					
V_{bulk} (mL)	2.19					
w_{dry} (g)	3.3866					
$m_{protein}$ (mg)	56.23	5.30	45.13	8.35	0.65	5

Figure 5.16 shows every stage of the breakthrough experiment. Adsorption until 400 mL, followed by washing, elution, regeneration and stock solution. Adsorption and washing stage are represented in the primary bulk concentration axis (left axis), while elution, regeneration and stock stages are represented in secondary bulk concentration axis (right axis).

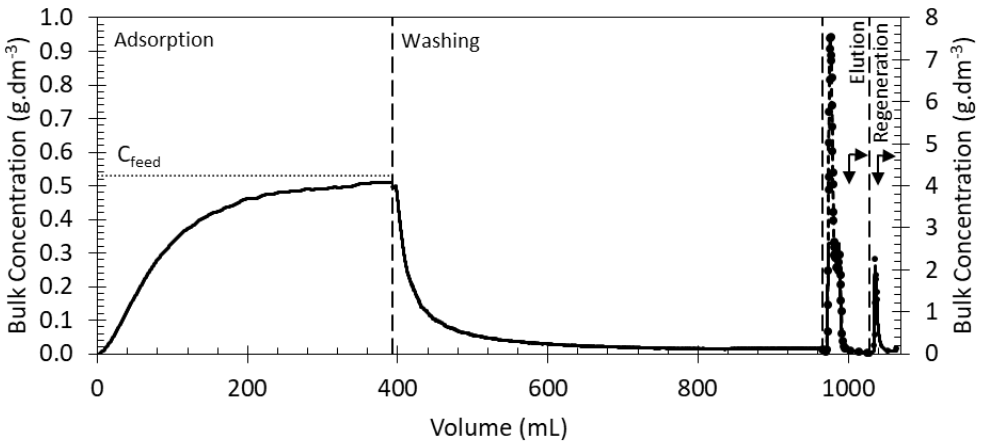

Figure 5.16 – Expanded bed breakthrough experiment with a feed concentration of 0.53 g·dm^{-3}. Experimental data (points); beginning of each stage (dotted line). Adsorption conditions: 20 mM citrate buffer, pH 5.0 with 0.4M NaCl. Operating conditions presented in Table 5.7.

Adsorption equilibrium isotherms allow to calculate the adsorption capacity expected for a feed concentration of 0.53 g·dm^{-3} of IgG. For the adsorption conditions tested (pH 5.0 with 0.4M NaCl) it is obtained an adsorption capacity of 17.2 mg·g_{dry}^{-1}. The difference between the adsorption capacity calculated from adsorption equilibrium isotherms and the EBA breakthrough experiment (15.1 mg·g_{dry}^{-1}) is due to the fact that the experimental breakthrough experiment was not run until the complete saturation of the adsorbent. Figure 5.17 presents the adsorption stage isolated from the desorption stages.

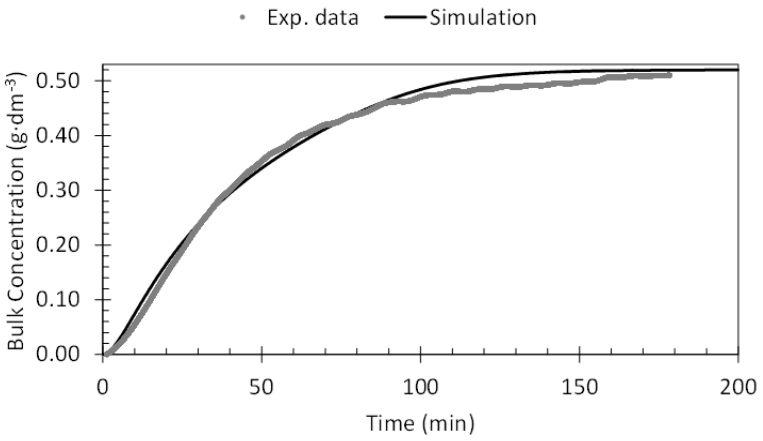

Figure 5.17 – Expanded bed breakthrough experiment. Adsorption stage: 0.53 g·dm^{-3} IgG concentration in 20 mM citrate buffer pH 5.0 with 0.4M NaCl for at 2.2 cm^3.min^{-1}. Experimental data (points); Model (black line – simulation).

It is possible also from this figure to notice that the mathematical model fitted reasonably the experimental data. For a feed concentration of 0.53 g·dm^{-3} of IgG in 20 mM citrate buffer pH 5.0 with 0.4M NaCl, at 2.2 cm^3·min^{-1}, it was obtained a DBC at 10% of breakthrough of 3.3 mg·g_{dry}^{-1} (9.1 mg·cm^{-3}) representing 22% of the saturation capacity. Regarding IgG desorption, for the first run, a protein recovery of 80% was obtained.

5.4.5.2. XK 16/20 expanded bed column

At the adsorption stage, 0.11 g·dm^{-3} of IgG on 20 mM citrate buffer pH 5.0 with 0.4M NaCl was fed to the bottom inlet of the column at 6 mL·min^{-1} flow rate; then, at the washing stage, the flow rate was maintained to wash out the unbound IgG protein. Afterwards, it was switched to elution buffer (20 mM phosphate buffer pH 7.0 with 0.4M NaCl) to elute the bound protein and the flow rate was reduced to concentrate this target protein. Regeneration and stock solution were performed with each solution already described and it was maintained the same flow rate as in the elution stage. Table 5.8 presents the operating conditions for the expanded bed breakthrough experiment.

Table 5.8 – Operating conditions for expanded bed IgG breakthrough experiment at 20 ± 1 °C, pH 5.0 with 0.4M NaCl, along with XK16/20 column, adsorbent (MabDirect MM) characteristics and with the adsorbed/desorbed protein mass obtained for each stage.

Parameter	Adsorption	Desorption				Difference (%)
		Washing	Elution	Regeneration	Stock	
Q (cm^3.min^{-1})	5.9		1.63			
C_{b0} (g.dm^{-3})	0.11	-				
d_c (cm)	1.55					
A_S (cm^2)	1.89					
ε_{b0}	0.4					
$\bar{\varepsilon_b}$	0.52					
ε_p	0.2374					
r_p (cm)	5.15×10^{-3}					
$H_{settled}$ (cm)	5.3					
$H_{expanded}$ (cm)	6.6					
V_{bulk} (mL)	10					
w_{dry} (g)	16.2615					
$m_{protein}$ (mg)	153.71	27.72	95.09	31.21	1.59	1

Figure 5.18 shows every stage of the breakthrough experiment. Adsorption, followed by washing, elution, regeneration and stock solution. Again, adsorption and washing stage are represented in primary bulk concentration axis (left axis), while elution, regeneration and stock stage are represented in secondary bulk concentration axis (right axis).

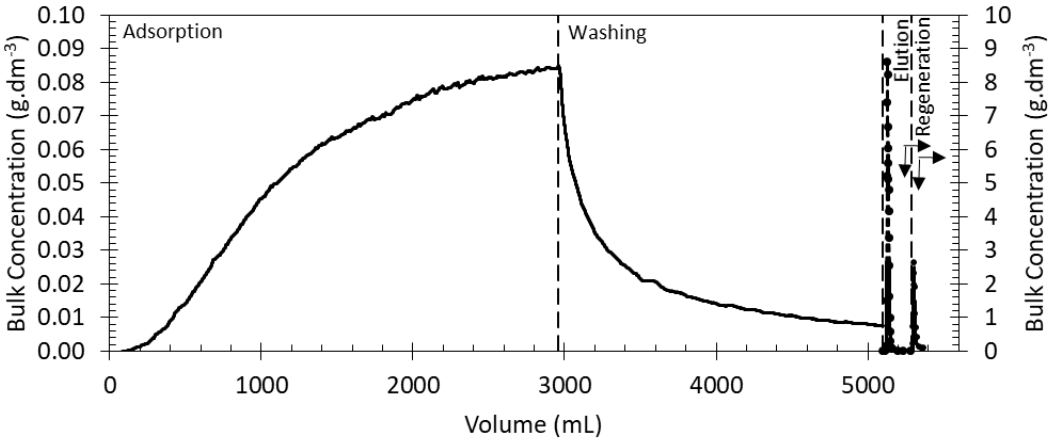

Figure 5.18 – Expanded bed breakthrough experiment with a feed concentration of 0.11 g/L. Experimental data (points), start of each stage (dotted line). Adsorption conditions: 20 mM citrate buffer, pH 5.0 with 0.4M NaCl. Operating conditions presented in Table 5.8.

Adsorption equilibrium isotherms allow to calculate the adsorption capacity expected for a feed concentration of 0.11 g·dm^{-3} of IgG. For the adsorption condition tested (pH 5.0 with 0.4M NaCl) it is obtained an adsorption capacity of 8.2 mg·g_{dry}^{-1}. The difference between the adsorption capacity calculated from adsorption equilibrium isotherms and the EBA breakthrough experiment (7.8 mg·g_{dry}^{-1}) is again due to the fact that the experimental breakthrough experiment was not run until the complete saturation of the adsorbent. Figure 5.19 presents the adsorption stage isolated from the desorption stages. It is possible also from this figure to notice that the mathematical model fitted reasonably with the experimental data.

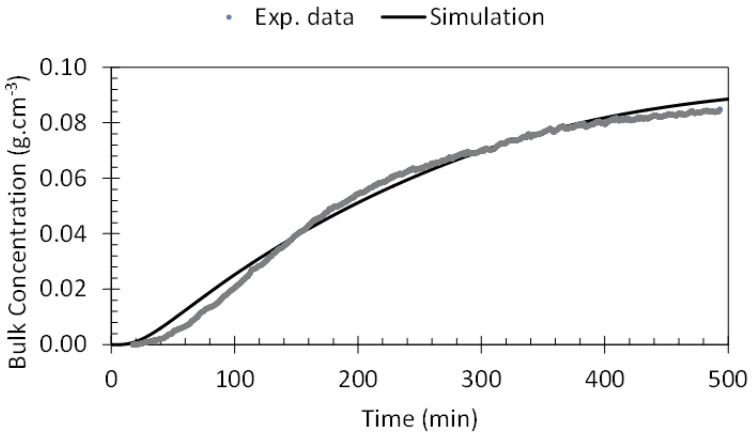

Figure 5.19 – Expanded bed breakthrough experiment. Adsorption stage: 0.11 g.dm^{-3} IgG concentration in 20 mM citrate buffer pH 5.0 with 0.4M NaCl at 5.9 cm^3.min^{-1}. Experimental data (points); Model (black line – simulation).

For run 2, conducted in an XK 16/20 column, for a feed concentration of 0.11 g·dm^{-3} of IgG in 20 mM citrate buffer pH 5.0 with 0.4M NaCl, at 6 cm^3·min^{-1}, it was obtained a DBC at 10% of breakthrough of 2.7 mg·g_{dry}^{-1} (7.4 mg·cm^{-3}) representing 34% of the saturation capacity. The low dynamic binding capacity at 10% of breakthrough is due to the buffer solution (pH 5.0 with

0.4 M NaCl) tested. Regarding IgG desorption, for the second run, a recovery of 89% was obtained.

As mentioned, finding in literature experiments that can be compared to the reported here becomes a difficult task since several conditions need to be similar. Some examples are presented for the target protein IgG adsorption with different adsorbent types.

According to literature, Du et al. [10] studied the expanded bed adsorption of IgG from bovine serum on Streamline CST-I (cation exchanger mixed mode resin). They studied expanded bed adsorption breakthroughs with multiple expansion factors (1.8, 2.0 and 2.2) for a feed concentration of 0.25 $g.dm^{-3}$ of IgG in 20 mM sodium phosphate buffer pH 7.0 on 46.8 cm^3 of Streamline CST-I in an expanded bed column with an internal diameter of 2 cm and 1 m length. They obtained a dynamic binding capacity at 10% of breakthrough of 0.42, 0.55 and 0.48 $mg.cm^{-3}$ for the expansion factors of 1.8, 2.0 and 2.2, respectively, representing between 14.3 and 18.7% of the adsorption capacity. They also referred that their low DBC is due to high flowrate and inappropriate solution pH. Comparing to the results of this work, we achieved a higher dynamic binding capacity due to the fact that we used salt concentration instead of pH as the condition tested. Also, we used significantly less amount of adsorbent.

Shi and co-workers [36] studied the expanded bed adsorption of IgG from bovine serum on a hydrophobic charge-induction chromatography (HCIC) adsorbent which consists in a 5-aminobenzimidazole (ABI) coupled to a tungsten-carbide-densified agarose beads. On a 1 cm dimeter column packed with 13.5 mL of adsorbent, they studied four expansion ratios (1.8, 2.0, 2.2 and 2.4) for a feed with bIgG concentration of 2 $g \cdot dm^{-3}$ in 20 mM sodium phosphate buffer pH 8.0. They obtained a dynamic binding capacity at 10% of breakthrough of 4.53, 5.41, 5.49 and 5.10 $mg.cm^{-3}$ for the expansion factors of 1.8, 2.0, 2.2 and 2.4, respectively, representing 19.3, 23.0, 23.3 and 21.7 % of the adsorption capacity.

Immunoglobulin G adsorption is in general studied by affinity chromatography (adsorbent type in which it is expected a higher dynamic binding capacity); in literature most of the studies use this type of adsorbent for isolation of monoclonal antibodies from cell broth [37-39]. However, a study can be found using pure immunoglobulin G adsorption.

Chase and Draeger [40] studied expanded bed adsorption of hIgG onto Protein A Sepharose Fast Flow. They show a breakthrough curve where a solution of 1 $mg.cm^{-3}$ hIgG in 0.1 M Tris-HCl buffer pH 7.5 without salt addition onto a 2 cm column with a settled bed height of 4 cm and expanded bed height of 12 cm at a linear flow rate of 3 $cm^3.min^{-1}$ was treated. We calculated that they achieved a dynamic binding capacity at 10% breakthrough of 23 $mg.cm^{-3}$ representing 76% of saturation capacity.

Although mixed mode adsorbents (Streamline CST-I and in this work MabDirect MM) have lower dynamic binding capacity when compared to affinity adsorbents, overall they can be considered as an alternative for the capture of Immunoglobulin G in an expanded bed configuration. They also show good recovery at relatively low adsorbent cost.

5.5. Conclusion

MabDirect MM, a novel second generation adsorbent, proved that can capture blood proteins at high flow rates in an expanded bed column, the purpose of its design. Also, it possesses a high particle density when compared with other commonly used adsorbents in EBA.

Residence time distribution experiments in three different expanded bed columns (Streamline 50, Omnifit 66/20 and XK 16/20) were performed in order to estimate the liquid axial dispersion coefficient. The experimental results were compared to a simulation model which proved to be able to represent them with reasonable accuracy.

HSA adsorption breakthrough experiments in a Streamline 50 expanded bed column were performed; for each run it were obtained DBC at 10% of breakthrough of 8.9, 9.7, 7.5 and 7.0 $mg \cdot g_{dry}^{-1}$ corresponding to 41, 39, 38 and 30% of the saturation capacity for runs 1 – 4, respectively. The mathematical simulation model fitted well with the breakthrough experiments.

Regarding the HSA desorption, experiments show that increasing pH and NaCl concentration in the elution buffer along with a decrease in flowrate not only will reduce the desorbed protein in the subsequent regeneration stage but also concentrate the target protein in the elution stage.

Human IgG adsorption breakthroughs in an Omnifit 66/20 and XK 16/20 expanded bed column were performed. For run 1, conducted in an Omnifit 66/20 column, for a feed concentration of 0.53 $g \cdot dm^{-3}$ of IgG in 20 mM citrate buffer pH 5.0 with 0.4M NaCl, at 2.2 $cm^3 \cdot min^{-1}$, it was obtained a DBC at 10% of breakthrough of 3.3 $mg \cdot g_{dry}^{-1}$ representing 22% of the saturation capacity. For run 2, conducted in an XK 16/20 column, for a feed concentration of 0.11 $g \cdot dm^{-3}$ of IgG in 20 mM citrate buffer pH 5.0 with 0.4M NaCl, at 6 $cm^3 \cdot min^{-1}$, it was obtained a DBC at 10% of breakthrough of 2.7 $mg \cdot g_{dry}^{-1}$, representing 34% of the saturation capacity. Regarding IgG desorption, for the first run, a protein recovery of 80% was obtained, while for the second run a recovery of 89% was obtained.

Results show that expanded bed adsorption with a mixed-mode adsorbent can capture blood proteins with high binding capacity; this could possibly be used for the purification of blood plasma in transfusion blood medical centers.

5.6. Nomenclature

A_s	–	Section area
C_{b0}	–	Feed protein concentration
C_b	–	Protein concentration in the bulk phase
C_p	–	Protein concentration in the particle pore
d_c	–	Column diameter
D_L	–	Liquid axial dispersion coefficient
D_m	–	Molecular diffusivity
d_p	–	Particle diameter
$\overline{d_p}$	–	Mean particle diameter
D_{pe}	–	Effective pore diffusivity
D_s	–	Adsorbent axial dispersion coefficient
H	–	Bed height
H_0	–	Settle bed height
$H_{expanded}$	–	Expanded bed height
k_{ext}	–	External mass transfer coefficient
K_L	–	Langmuir adsorption constant
$m_{protein}$	–	Protein mass adsorbed/desorbed
$q_{10\%}$	–	Dynamic binding capacity at 10% breakthrough point
q	–	Adsorbed concentration
$\bar{q}$	–	Average adsorbed concentration
q_{max}	–	Maximum adsorption capacity
Re	–	Reynolds number
r_p	–	Particle radius
Sc	–	Schmidt number
Sh	–	Sherwood number
u_s	–	Superficial velocity
u_i	–	Interstitial velocity
V	–	Effluent liquid volume from the fixed bed
$V_{10\%}$	–	Effluent liquid volume at 10% breakthrough point
V_a	–	Packed bed volume of adsorbent
V_L	–	Volume of protein solution
w	–	Adsorbent mass
t	–	Time
r	–	Radial position
z	–	Axial position

Greek letters

ε_0	–	Settle external (bed) porosity
ε_b	–	External (bed) porosity
$\overline{\varepsilon_b}$	–	Mean external (bed) porosity
ε_p	–	Particle (solid) porosity
ρ	–	Density
η	–	Viscosity

Acronyms

BSA	–	Bovine Serum Albumin
EBA	–	Expanded bed adsorption
gPROMS	–	general PROcess Modelling System
HPLC	–	High performance liquid chromatography
HSA	–	Human Serum Albumin
hIgG	–	Immunoglobulin G from Human serum
IgG	–	Immunoglobulin G
mAb	–	Monoclonal antibody
MM	–	Mixed-mode
MMC	–	Mixed-mode Chromatography
OCFEM	–	Orthogonal collocation in finite elements method
PDM	–	Pore diffusion model
rpm	–	Rotations per minute
SDS-Page	–	Sodium dodecyl sulfate - Polyacrylamide gel electrophoresis

5.7. References

[1] Antibody Production and Purification Technical Handbook in, Thermo Fisher Scientific, 2010.

[2] G. Fanali, A. di Masi, V. Trezza, M. Marino, M. Fasano, P. Ascenzi, Human serum albumin: From bench to bedside, Molecular Aspects of Medicine, 33 (2012) 209-290.

[3] J. Schaller, S. Gerber, U. Kaempfer, S. Lejon, C. Trachsel, Human Blood Plasma Proteins: Structure and Function, Wiley, 2008.

[4] P.F. Gomes, J.M. Loureiro, A.E. Rodrigues, Adsorption of Human Serum Albumin (HSA) on a mixed-mode adsorbent: equilibrium and kinetics, Adsorption, 23 (2017) 491-505.

[5] B. Malm, A method suitable for the isolation of monoclonal antibodies from large volumes of serum-containing hybridoma cell culture supernatants, Journal of Immunological Methods, 104 (1987) 103-109.

[6] W.L. Hoffman, D.J. O'Shannessy, Site-specific immobilization of antibodies by their oligosaccharide moieties to new hydrazide derivatized solid supports, Journal of Immunological Methods, 112 (1988) 113-120.

[7] K.L. Carson, Flexibility - the guiding principle for antibody manufacturing, Nature Biotechnology, 23 (2005) 1054-1058.

[8] S.S. Ranjini, D. Bimal, A.P. Dhivya, M.A. Vijayalakshmi, Study of the mechanism of interaction of antibody (IgG) on two mixed mode sorbents, Journal of Chromatography B, 878 (2010) 1031-1037.

[9] E. Arévalo, M. Rendueles, A. Fernández, M. Díaz, Equilibrium and simulation of the operation for the adsorption of albumin proteins in an iminodiacetic-Cu bounded ion exchange resin (IMAC), Separation and Purification Technology, 18 (2000) 217-225.

[10] Q.Y. Du, D.Q. Lin, Q.L. Zhang, S.J. Yao, An integrated expanded bed adsorption process for lactoferrin and immunoglobulin G purification from crude sweet whey, Journal of Chromatography B: Analytical Technologies in the Biomedical and Life Sciences, 947-948 (2014) 201-207.

[11] P. Li, Protein Separation and purification by expanded bed chromatography and simulated moving bed technology, in: Ph.D. Thesis, Department of Chemical Engineering, Faculty of Engineering University of Porto, Portugal, 2006.

[12] P. Li, P.F. Gomes, J.M. Loureiro, A.E. Rodrigues, Proteins Separation and Purification by Expanded Bed Adsorption and Simulated Moving Bed Technology, in: G. Subramanian (Ed.) Continuous Processing in Pharmaceutical Manufacturing, John Wiley & Sons, Inc., 2014.

[13] M.d.A. Lima, M.d.F.M.d. Freitas, L.R.B. Gonçalves, I.J.d. Silva Junior, Recovery and purification of a Kluyvermyces lactis β-galactosidase by Mixed Mode Chromatography, Journal of Chromatography B, 1015–1016 (2016) 181-191.

[14] P.F. Gomes, J.M. Loureiro, A.E. Rodrigues, Adsorption equilibrium and kinetics of Immunoglobulin G on a mixed-mode adsorbent in batch and packed bed configuration, Journal of Chromatography A, 1524 (2017) 143-152.

[15] M.A. Hashim, K.H. Chu, P.S. Tsan, Modelling of protein adsorption in a Fixed-Bed: Single and Two-solute breakthrough behaviour, Chemical Engineering Communications, 161 (1997) 45-63.

[16] W. Kelly, P. Garcia, S. McDermott, P. Mullen, G. Kamguia, G. Jones, A. Ubiera, K. Göklen, Experimental characterization of next-generation expanded-bed adsorbents for capture of a recombinant protein expressed in high-cell-density yeast fermentation, Biotechnology and Applied Biochemistry, 60 (2013) 510-520.

[17] W. Kelly, G. Kamguia, P. Mullen, A. Ubiera, K. Göklen, Z. Huang, G. Jones, Using a two species competitive binding model to predict expanded bed breakthrough of a recombinant protein expressed in a high cell density fermentation, Biotechnology and Bioprocess Engineering, 18 (2013) 546-559.

[18] G.L. Skidmore, H.A. Chase, Two-component protein adsorption to the cation exchanger S Sepharose® FF, Journal of Chromatography A, 505 (1990) 329-347.

[19] W.F. Weinbrenner, M.R. Etzel, Competitive adsorption of alpha-lactalbumin and bovine serum albumin to a sulfopropyl ion-exchange membrane, Journal of Chromatography A, 662 (1994) 414-419.

[20] C. Martin, G. Iberer, A. Ubiera, G. Carta, Two-component protein adsorption kinetics in porous ion exchange media, Journal of Chromatography A, 1079 (2005) 105-115.

[21] J. Zhao, S. Yao, D. Lin, Adsorbents for Expanded Bed Adsorption: Preparation and Functionalization, Chinese Journal of Chemical Engineering, 17 (2009) 678-687.

[22] E. Palsson, A. Axelsson, P.O. Larsson, Theories of chromatographic efficiency applied to expanded beds, Journal of Chromatography A, 912 (2001) 235-248.

[23] R.R. Walters, J.F. Graham, R.M. Moore, D.J. Anderson, Protein diffusion coefficient measurements by laminar flow analysis: Method and applications, Analytical Biochemistry, 140 (1984) 190-195.

[24] P. Li, G. Xiu, A.E. Rodrigues, Experimental and modeling study of protein adsorption in expanded bed, American Institute of Chemical Engineers Journal, 51 (2005) 2965-2977.

[25] P.R. Wright, B.J. Glasser, Modeling mass transfer and hydrodynamics in fluidized-bed adsorption of proteins, American Institute of Chemical Engineers Journal, 47 (2001) 474-488.

[26] Van Der Meer A.P., C.M.R.J.P. Blanchard, J.A. Wesselingh, Mixing of particles in liquid fluidized beds., Chemical Engineering Research and Design, 62 (1984) 214-222.

[27] P. Li, G. Xiu, A. E. Rodrigues, Modeling separation of proteins by inert core adsorbent in a batch adsorber, Chemical Engineering Science, 58 (2003) 3361-3371.

[28] E.J. Wilson, C.J. Geankoplis, Liquid Mass Transfer at Very Low Reynolds Numbers in Packed Beds, Industrial & Engineering Chemistry Fundamentals, 5 (1966) 9-14.

[29] W. Ranz, W. Marshall, Evaporation from drops, Chemical Engineering Progress, 48 (1952) 141-146.

[30] N. Wakao, T. Funazkri, Effect of fluid dispersion coefficients on particle-to-fluid mass transfer coefficients in packed beds: Correlation of sherwood numbers, Chemical Engineering Science, 33 (1978) 1375-1384.

[31] L.-T. Fan, Y.-C. Yang, C.-Y. Wen, Mass transfer in semifluidized beds for solid-liquid system, American Institute of Chemical Engineers Journal, 6 (1960) 482-487.

[32] L.J. Bruce, H.A. Chase, Hydrodynamics and adsorption behaviour within an expanded bed adsorption column studied using in-bed sampling, Chemical Engineering Science, 56 (2001) 3149-3162.

[33] M. Rendueles de la Vega, C. Chenou, J.M. Loureiro, A.E. Rodrigues, Mass transfer mechanisms in Hyper D media for chromatographic protein separation, Biochemical Engineering Journal, 1 (1998) 11-23.

[34] H.F. Xia, D.Q. Lin, S.J. Yao, Chromatographic performance of macroporous cellulose-tungsten carbide composite beads as anion-exchanger for expanded bed adsorption at high fluid velocity, Journal of Chromatography A, 1195 (2008) 60-66.

[35] A. Rezvani, M. Jahanshahi, G.D. Najafpour, Characterization and evaluation of the novel agarose–nickel composite matrix for possible use in expanded bed adsorption of bio-products, Journal of Chromatography A, 1331 (2014) 61-68.

[36] W. Shi, D.-Q. Lin, H.-F. Tong, J.-X. Yun, S.-J. Yao, 5-Aminobenzimidazole as new hydrophobic charge-induction ligand for expanded bed adsorption of bovine IgG, Journal of Chromatography A, 1425 (2015) 97-105.

[37] J. Thommes, A. Bader, M. Halfar, A. Karau, M.R. Kula, Isolation of monoclonal antibodies from cell containing hybridoma broth using a protein A coated adsorbent in expanded beds, Journal of Chromatography A, 752 (1996) 111-122.

[38] J. Feuser, M. Halfar, D. Lutkemeyer, N. Ameskamp, M. Kula, J. Thommes, Interaction of mammalian cell culture broth with adsorbents in expanded bed adsorption of monoclonal antibodies, Process Biochemistry, 34 (1999) 159-165.

[39] J. Thommes, M. Halfar, S. Lenz, M.R. Kula, Purification of monoclonal antibodies from whole hybridoma fermentation broth by fluidized bed adsorption, Biotechnology and Bioengineering, 45 (1995) 205-211.

[40] H.A. Chase, Draeger, N. M., Affinity purification of proteins using expanded beds, Journal of Chromatography A, 597 (1992) 129-145.

Chapter 6: Co-adsorption of Albumin and Immunoglobulin G from Human Serum onto a cation exchanger mixed mode adsorbent.

"The ultimate measure of a man is not where he stands in moments of comfort and convenience, but where he stands at times of challenge and controversy."

- Dr. Martin Luther King, Jr.

In this chapter, binary mixture adsorption containing Human Immunoglobulin (IgG) and Human Serum Albumin (HSA) on MabDirect MM is assessed by batch, fixed bed and expanded bed adsorption experiments. Competitive adsorption isotherm is measured by batch experiments at the binding condition of pH 5.0 without salt addition. Several experiments are performed in a packed bed column in which the adsorption capacity of the binary mixture is evaluated. Also it is conducted a fixed bed adsorption experiment with the purpose to observe if there is roll up of the less adsorbed protein. Displacement experiments are also ran on a fixed bed column. Afterwards, expanded bed breakthrough experiment is carried out for the target proteins and compared with the batch and fixed bed adsorption from previous experiments and literature.

This chapter is based on the following article:

Gomes, P.F., Loureiro, J.M. & Rodrigues, A.E. Co-adsorption of Albumin and Immunoglobulin G from Human Serum onto a cation exchanger mixed mode adsorbent. Adsorption, (2018), 1-11.

6.1. Introduction

The Human Serum Albumin (HSA) accounts for 60% of the total protein in blood serum. HSA importance is undeniable since it is used clinically to treatments such as burns, shocks, surgical blood losses; it is also a meaningful bio-marker of many diseases and diseases that require the monitoring of the glycemic levels among other functions. Immunoglobulin G (IgG) represents near 75% of immunoglobulins present in human serum. It is used to treat immune deficiencies, autoimmune disorders and infections; IgG controls infection of body tissues and it can be used for diagnostic purposes. Albumin and Immunoglobulin G are present in human plasma [1-3].

In human plasma these highly valuable proteins are present with water (90% of blood plasma), mineral salts and ions (e.g. sodium chloride, buffer salts or metal ions such as calcium, copper, iron, etc), low molecular weight components (such as carbohydrates, amino acids, nucleotides, vitamins, hormones, fatty acids), also with high molecular weight components (polynucleotides among others), gases in soluble form (oxygen, carbon dioxide) and metabolites. The presence of several components can lead to a co-adsorption or competitive adsorption [3]. The study of multicomponent solutions can ease the understanding of protein adsorption mechanisms.

Peula et al. [4], studied the co-adsorption of human IgG and Bovine serum albumin (BSA) onto a sulfonated polystyrene latex with high surface charge density and they found that high amounts of both target proteins could be adsorbed on the surface. Lewus and Carta [5] studied the binary protein adsorption (lysozyme and cytochrome c) on a gel-composite ion exchange media such as S-HyperD-M, a cation exchanger composed of a rigid macroporous silica matrix whose pores are filled with a functionalized polyacrylamide gel. They conclude that at low protein concentration the adsorption is essentially noncompetitive, and the mass transfer is controlled by external film resistance, while at high concentrations, equilibrium becomes competitive. Xu and Lenhoff [6] investigated the binary adsorption of globular proteins on cation exchange media and stated a competitive adsorption dominated by lysozyme and the presence of this protein reduces the adsorption of cytochrome c significantly. Yan et al. [7] studied the separation of bIgG from BSA-containing feedstock on a mixed-mode commercial resin (Nuvia cPrime). They conclude that using an equilibrium buffer of pH 5.0 with 0.8M $(NH_4)_2SO_4$ and eluted with sodium phosphate buffer pH 8.0 with 1M NaCl can be used to effectively purify bIgG from BSA/bIgG mixture with good recovery and purity. Yan et al. [8], more recently measured the adsorption of human IgG and BSA on a p-Aminohippuric acid based mixed mode resin including single and binary component adsorption at different pH and protein mass ratios. They found that the

adsorption capacity of both proteins decreased with the addition of another component and that there was a preferential adsorption and selectivity of IgG over BSA.

Reaching the desired level of purity by efficient protein separation and purification has become one the main challenges of the pharmaceutical industries. Usually, affinity chromatography is used for the separation of monoclonal and polyclonal antibodies such as immunoglobulin G. However, the adsorbent costs, clean-in-place difficulties and ligand leakage create the opportunity for another type of chromatography [9, 10]. Mixed mode chromatography (MMC) is a separation method that uses more than one form of interaction such as electrostatic, hydrophobic, thiophilic interaction and hydrogen bonds. This type of adsorbent provides high capacity, easy elution, salt-tolerance and good adsorption selectivity [11].

Mabdirect MM, developed by Upfront Chromatography A/S, is a cation exchanger mixed mode adsorbent, constituted of 6% cross-linked agarose with tungsten carbide particles and it has a pKa of 5.0 and aromatic ligands with acidic substituents (benzoic acid) [12, 13]. It is an adsorbent classified as second generation specially designed for expanded bed operations. Expanded bed adsorption (EBA), a novel bioseparation technology, is applied to capture proteins directly from crude unclarified feedstocks, such as yeast, fermentation broth. This technology has the objective to capture and concentrate the target protein molecules from source material while removing the bulk impurities, such as cells, cells debris, particulate matter and contaminants. EBA presents the advantage of a being a single pass operation in which the target protein is purified directly from particulate containing feedstocks, without the need of separate clarification, concentration and initial purification; EBA also avoids the risk of blockage thus minimizing the pressure drop problems commonly encountered in the fixed bed adsorbers; however, the need of specialized adsorbents is an issue. EBA is now a cemented field of work where researchers are applying their efforts to better understand its benefits and drawbacks [14-18].

In this chapter, adsorption of a binary mixture containing human IgG and HSA on a new cation exchanger mixed mode adsorbent is assessed. Competitive adsorption isotherm by batch experiments is determined. Frontal analysis and column displacement experiments were conducted for this two-component competitive adsorption system. Finally, binary mixture expanded bed adsorption packed with MabDirect MM adsorbent was investigated.

6.2. Materials and Methods

6.2.1. Target proteins

Human Serum Albumin (HSA, CAS 70024-90-7) has an isoelectric point of 4.7, a molecular weight of 66 kDa, strong absorbance at 280 nm and a molecular diffusion of 3.84 x 10^{-5} $cm^2.min^{-1}$ [19]. HSA has tested negative for antibodies and a measured purity of 95% by Sodium Dodecyl Suphate - Polyacrylamide Gel Electrophoresis (SDS-PAGE). HSA was purchased from VWR Chemicals. More information regarding HSA can be found on previous Chapter 3 in subsection 3.2.1. Immunoglobulin G (IgG; Merck number I4506) was purified from normal human serum, and it has measured purity of not less than 95% by SDS-PAGE, according to the production information sheet. IgG has an isoelectric point between 5.8 and 7.3, according to literature, strong absorbance at 280 nm and a molecular diffusion of 2.4 x 10^{-5} $cm^2.min^{-1}$ [19]. More detailed information can be found on previous Chapter 4 in subsection 4.2.1.

6.2.2. Multimodal chromatography adsorbent

Mabdirect MM is a cation exchanger mixed mode adsorbent initially developed by Upfront Chromatography A/S. It is constituted by a 6% cross-linked agarose with tungsten carbide particles delivered in a 200 mM sodium acetate solution with 14% NaCl. More information regarding this adsorbent can be found in Chapter 3, subsections 3.2.1 and 3.4.1. Before any experiment, the adsorbent is placed in a special glassware equipped with a proper filter connected to a vacuum pump where it will be cleaned with 1L of deionized water before be conditioned with the same protein buffer solution [1, 2].

6.2.3. Equipment and buffer solutions

Figure 6.1 shows the laboratory system set-up.

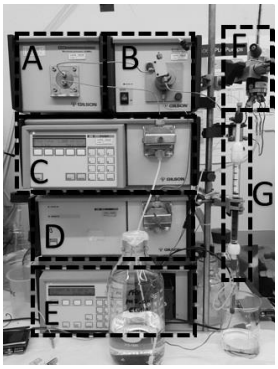

Figure 6.1 – HPLC system set-up with a Gilson 805 manometric module (A), Gilson 811C dynamic mixture (B), Gilson 305 pump (C), Gilson 306 pump (D), Gilson 117 UV detector (E), a Rheodyne 7725i manual injector (F), and packed bed column (G).

When performing fixed bed experiments, it was used an Omnifit 6.6/10 column in a downward flow (Figure 6.1, location G), while for expanded bed experiments, it was replaced with an XK 16/20 column in an upward flow. The system was also used with the SEC column for the determination of protein concentration, as referred in sub section 6.2.4.

HSA and IgG were dissolved together in buffer solutions according to the conditions to be tested. For pH 5.0 a sodium citrate buffer was used, while for pH 7.0 a sodium phosphate buffer was used. pH was adjusted to final value with 1M NaOH or 1M HCl. Citric acid, tri-sodium citrate di-hydrate, along with hydrochloric acid, sodium hydroxide, sodium acetate and sodium chloride were purchased from Reagente5. Sodium di-hydrogen phosphate di-hydrate, di-sodium hydrogen phosphate, methanol, potassium dihydrogen phosphate and potassium chloride were purchased from VWR Chemicals.

6.2.4. Determination of protein concentration

HSA and IgG concentration in the liquid phase were measured by SEC-HPLC. The analytical column (Reprosil 200 SEC 5 µm 300 x 8 mm) and the guard-column (Reprosil 200 SEC guard-column 5 µm 23 x 8 mm) were purchased from I.L.C. – Instrumentos de Laboratório e Científicos, Lda. A sample injection of 20 µm with a mobile phase (50 mM KH_2PO_4 + 150 mM KCl pH 7.0) flowrate of 1 $cm^3.min^{-1}$ was applied in a Gilson HPLC system (Figure 6.1) with a 305 model pump, an 805 manometric module and a 117 Gilson UV model detector at a wavelength of 280 nm.

6.2.5. Adsorption equilibrium isotherm by Batch experiment

Wet adsorbent mass (0.127g) is placed in 1 mL protein solution during 4 h at room temperature (20 °C) in a Sigma 203 centrifuge at 1000 rotations per minute (rpm). Then, the supernatant is collected using a VWR himac centrifuge CT 15RE at 4000 rpm for 10 minutes. The equilibrium protein concentration was determined by the method already mentioned. For each equilibrium concentration, three measurements were performed and the average value was used. The experimental reproducibility was in range of less than 10%.

6.2.6. Frontal analysis in fixed bed

Omnifit 66/10 column is used for breakthrough experiments of HSA and IgG competitive adsorption. Before packing the column, the desired amount of adsorbent was measured in a graduated cylinder prior to drain using a vacuum pump to account for the adsorbent wet mass.

After, the adsorbent is re-hydrated in the chosen binding buffer and packed onto the column. Before adsorption breakthrough the column is equilibrated with binding buffer (20 mM citrate buffer pH 5.0 with 0.4M NaCl) for a period of 30 minutes. Then, adsorption takes place; a binary protein mixture solution (HSA and IgG) is fed until the outlet stream at the bottom of the column reaches the feed concentration plateau, meaning the adsorbent saturation. After this stage, the binding buffer is feeding to washout unbound protein, then elution buffer (20 mM phosphate buffer pH 7.0 with 0.4M or 1M NaCl) is fed to the column to elute the bound protein at a lower flowrate in order to achieve higher target protein concentration in the lowest volume of buffer solution. Regeneration of the adsorbent takes place by feeding to the column a solution of 1M NaOH and 1M NaCl. To store the column, a stock solution (200 mM sodium acetate with 14% NaCl) is fed. The flow rate is constantly monitored and recorded during all stages. The effluent stream from the bottom of the bed column is recorded at 280 nm in a Gilson 117 UV detector. Samples are collected along the experiment in order to quantify the protein concentration by SEC-HPLC.

6.2.7. Column displacement experiments

For displacement adsorption measurements of HSA and hIgG, an Omnifit 66/10 column is used. A given mass of adsorbent is packed in the column and the bed height is measured. First, the packed adsorbent is equilibrated with the binding buffer, then, one of the target proteins (HSA or hIgG in a binding buffer) is loaded to the column in a downward flow until the saturation of the adsorbent is observed. Later on, the column is washed with binding buffer in order to remove the unbound protein in the bed voidage and in the adsorbent pores. After washing stage, the other protein (hIgG or HSA) is fed to the column to displace the bound protein on the MabDirect MM. Furthermore, a washing stage takes place one more time to wash out the unbound proteins before concluding with an elution step. As the frontal analysis experiments, the effluent stream from the bottom of the bed column is recorded at 280 nm in a Gilson 117 UV detector. Samples are collected along the experiment in order to quantify the protein concentration by SEC-HPLC on each stage.

6.2.8. Expanded bed breakthrough experiment

Similarly to the frontal analysis experiments conducted in fixed bed column, an XK 16/20 is used for the experiments of the EBA process. The desired amount of MabDirect MM is conditioned on the binding buffer and measured by the same procedure mentioned above. EBA experiment was described in chapter 5 [20] but is briefly summarized here. First, the equilibration buffer (20 mM citrate buffer pH 5.0 with 0.4M NaCl) is pumped through the column in an upward

flow to the expected expansion degree. The expanded bed is allowed to stabilize during 30-45 minutes. The column plug adapter is positioned 0.2 cm above the bed height in order to reduce dead volume. When the bed is stable, adsorption stage takes place where a binary protein mixture (HSA and IgG) is pumped through the column until the outlet stream at the bottom of the column reaches the feed concentration plateaux. Then, it follows the washing stage, where binding buffer is used to washout the unbound proteins; an elution stage, where elution buffer (20 mM phosphate buffer pH 7.0 with 1M NaCl) is passed through the column to elute the bound proteins at a lower flowrate in order to achieve a higher protein concentration; a regeneration stage, where 1M NaOH and 1M NaCl solution is used in order to regenerate the adsorbent for further experiments, and a stock solution for adsorbent storage.

6.3. Results and discussion

6.3.1. Adsorption equilibrium isotherms for HSA and IgG

HSA and hIgG competitive adsorption isotherm on MabDirect MM is measured by batch experiments at a solution pH of 5.0 without salt addition. Sample solutions are prepared with a mixture of 2 g.dm^{-3} of HSA with different hIgG concentration.

Experimental results are shown in Figure 6.2.

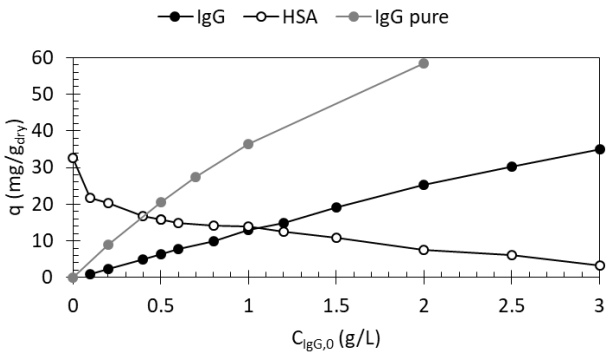

Figure 6.2 – HSA and hIgG competitive adsorption isotherm on MabDirect MM measured by batch experiment at 20 mM citrate buffer (pH 5.0) without salt (NaCl) addition at room temperature (20 °C).

Adsorption capacity is calculated by using the following equation:

$$q = \frac{V_L \cdot (C_{b,0} - C_b)}{w} \tag{6.1}$$

where V_L is the volume of protein solution, $C_{b,0}$ and C_b represent the initial and bulk protein concentration, respectively, and w is the adsorbent mass used in the each experiment.

It is possible to observe that when there is an increase of IgG in the HSA solution there is a significant decrease on the HSA binding capacity as a result of IgG competitive adsorption with HSA on MabDirect MM. Also, from Figure 6.2, it is possible to compare the IgG binding capacity of when there is HSA in solution (black full dots) and when there is not (grey dots). As HSA, it is possible to refer that the IgG binding capacity decreases when there is presence of other target protein, also a result of competitive adsorption. From single component adsorption isotherms (at pH 5.0 without salt) the adsorption capacity at 2 g/L concentration of protein is 32.4 mg/g_{dry} for HSA and 58.4 mg/g_{dry} for IgG. When both proteins are in the mixture in a ratio 1:1 (each with 2 g/L concentration), the capacity of HSA decreases to 7.5 mg/g_{dry} (77% reduction compared to the value of single component adsorption) while IgG decreases to 25.2 mg/g_{dry} (57% reduction). These two factors suggest that the stronger adsorbed protein is IgG. The adsorbed concentration in the binary batch experiment without salt are not the same as those obtained from single adsorption equilibrium isotherms at similar liquid concentrations; this means that the adsorption mechanism is more complex than single protein adsorption in different sites.

Li and co-workers [16] reached similar result when they studied the effect of competitive adsorption of Bovine Serum Albumin (BSA) and Myoglobin (MYO) on a multi modal adsorbent, Streamline Direct CST-I, by static batch experiment at the binding condition of 50 mM acetate buffer pH 5.0. They observed that Streamline Direct CST-I has a high adsorption capacity to BSA without MYO in initial BSA solution; and when there exists MYO, the BSA-binding capacity decreases significantly as a result of MYO competitive adsorption with BSA on the adsorbent.

Yao et al. [8] studied co-adsorption of human IgG and BSA on a p-Aminohippuric acid based mixed mode resin (Nuvia cPrime). They concluded that, for the binary mixture, the adsorption capacity of both proteins decreased with the addition of another component but a preferential adsorption and good selectivity of IgG over BSA could be found.

6.3.2. Fixed bed adsorption and displacement experiments

6.3.2.1. Fixed bed single and binary breakthrough experiments

All fixed bed breakthrough experiments were conducted in an Omnifit column with 0.66 cm of column diameter and 0.342 cm^2 of section area packed with MabDirect MM which possesses a particle porosity of 0.237 and a particle radius of $5.15x10^{-3}$ cm. Table 6.1 shows the operating conditions for the single-component HSA breakthrough experiment.

Table 6.1 – Operating conditions for single-component HSA breakthrough experiment: flow rate; feed concentration, bed height, adsorbent volume and dry weight and adsorbed/desorbed protein mass on each stage at 20 °C.

Conditions	Adsorption	Washing	Elution
Q(cm^3.min^{-1})	2	2	0.5
H(cm)		6.6	
V_{ads}(cm^3)		2.26	
w_{dry}(g)		3.1075	
$C_{F,HSA}$(g.dm^{-3})	1.0	-	-
m_{HSA}(mg)	50.08	4.45	22.54

Figure 6.3 shows the adsorption breakthrough experiment for single-component HSA with 1 g.dm^{-3} feed concentration. When dealing with single protein solutions, it can be used an elution buffer pH greater than 7.0 in order to achieve a higher protein recovery; however, this experiment was a preparation for binary mixture breakthroughs where a SEC column was used to quantify the adsorbed/desorbed protein mass which only allows working a maximum pH of 7.0.

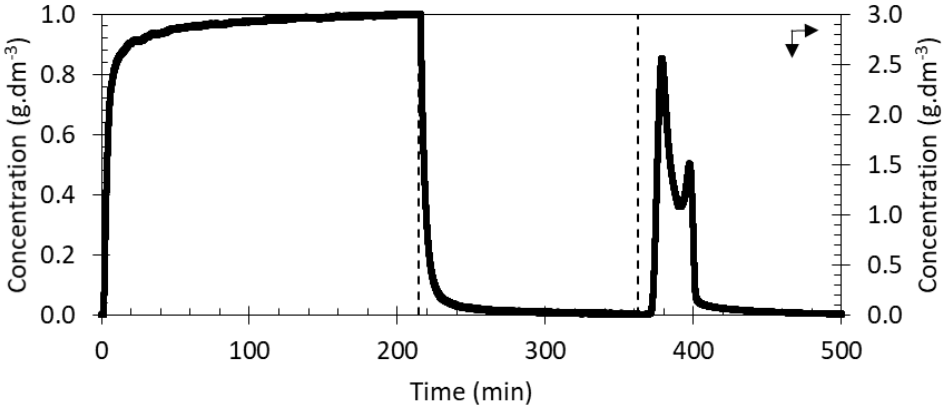

Figure 6.3 – HSA breakthrough experiment in a fixed bed (Omnifit 6.6/11) with a feed concentration of 1 g.dm^{-3} in a 20 mM citrate buffer pH 5.0 with 0.4M NaCl. The same buffer solution was used in the washing stage, while for elution stage it was used a 20 mM phosphate buffer pH 7.0 with 0.4M NaCl. Operating conditions presented in Table 6.1.

Two frontal analysis experiments for two-component HSA 1 g.dm^{-3} and IgG 0.2 g.dm^{-3} were carried out. Figure 6.4 (run 1) shows the breakthrough experiment for this two-component mixture at a flowrate of 2 mL/min. A second frontal analysis experiment (Figure 6.5) for two-component (HSA/IgG) was carried out where we intentionally measured the adsorption stage for a longer timescale by reducing the flowrate from 2.0 to 0.7 cm^3.min^{-1}; also it was increased the salt concentration from 0.4 to 1.0 M NaCl in elution stage. Both figures also show the subsequent stages to the adsorption (washing and elution).

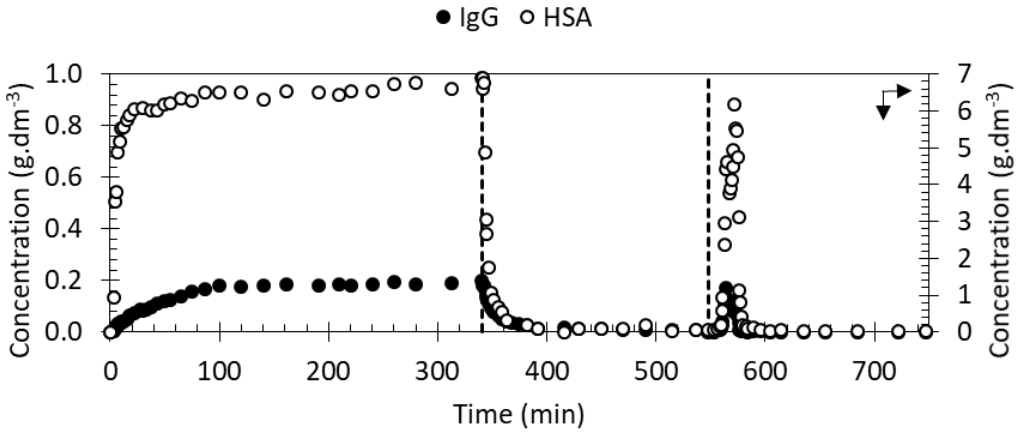

Figure 6.4 – Binary (HSA and IgG) breakthrough experiment in a fixed bed (Omnifit 6.6/11) with a feed concentration of 1 g.dm^{-3} HSA with 0.2 g.dm^{-3} of hIgG in a 20 mM citrate buffer pH 5.0 with 0.4M NaCl at a flowrate for 2.0 mL/min. The same buffer solution was used in the washing stage, while for elution stage it was used a 20 mM phosphate buffer pH 7.0 with 0.4M NaCl. Operating conditions presented in Table 6.2.

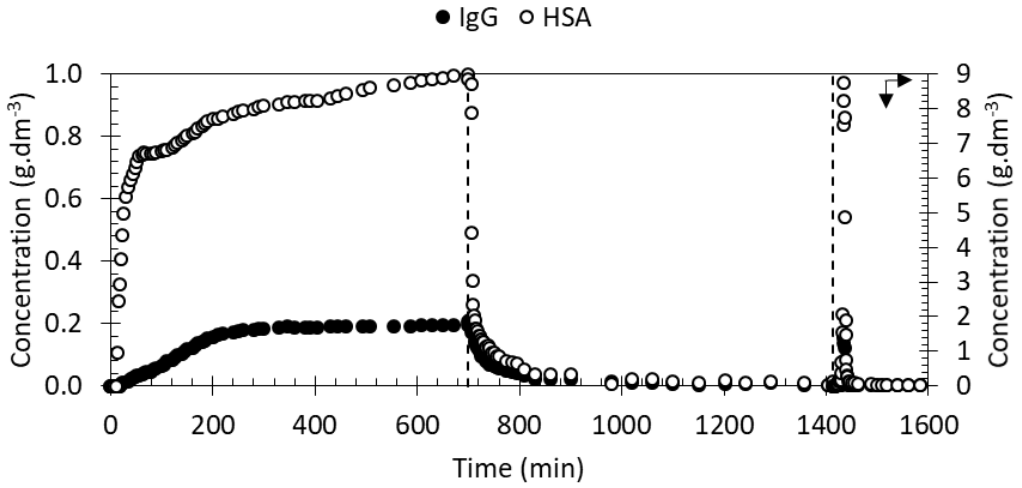

Figure 6.5 – Binary (HSA and IgG) breakthrough experiment in a fixed bed (Omnifit 6.6/11) with a feed concentration of 1 g.dm^{-3} HSA with 0.2 g.dm^{-3} of hIgG in a 20 mM citrate buffer pH 5.0 with 0.4M NaCl at a flowrate for 0.7 mL/min. The same buffer solution was used in the washing stage, while for elution stage it was used a 20 mM phosphate buffer pH 7.0 with 1M NaCl. Operating conditions presented in Table 6.2.

Table 6.2 shows the operating conditions for both binary breakthrough experiments.

Table 6.2 – Operating conditions for binary (HSA and IgG) breakthrough experiments: flow rate; feed concentration, bed height, adsorbent volume and weight and adsorbed/desorbed protein mass on each stage at 20 °C.

Conditions	Run	Adsorption	Washing	Elution
Q(cm^3.min^{-1})	1	2	2	0.5
	2	0.7	0.7	0.7
NaCl (M)	1	0.4	0.4	0.4
	2	0.4	0.4	1
H(cm)	1-2		6.4	
V_{ads}(cm^3)	1-2		2.19	
w_{dry}(g)	1-2		2.7333	
$C_{F,HSA}$(g.dm^{-3})	1-2	1.0	-	-
$C_{F,IgG}$(g.dm^{-3})	1-2	0.2	-	-
m_{HSA}(mg)	1	54.05	15.65	30.83
	2	56.84	19.19	32.61
m_{IgG}(mg)	1	25.30	8.96	5.70
	2	24.70	9.60	5.95

Binding capacity is calculated based on the experimental breakthrough curves for single-component (HSA) and two-component (HSA and IgG) on MabDirect MM packed in a fixed bed column. It was obtained a HSA binding capacity for a single-component breakthrough curve of 14.68 mg.g_{dry}^{-1}, while for two-component breakthrough curve it decreases to 14.05 and 13.77 mg.g_{dry}^{-1} for runs 1 and 2, respectively. Regarding IgG adsorption for two-component breakthrough experiments, it was obtained an IgG adsorption capacity of 5.98 and 5.53 mg.g_{dry}^{-1} for runs 1 and 2, respectively. Either in single or in two-component breakthrough experiments, the adsorption capacity is in good agreement with batch experiments from previous work [1-2].

Dynamic binding capacity (DBC) is also a common used parameter when performing adsorption breakthrough experiments [21]. It is determined by the following equation,

$$q_{10\%} = \frac{\int_0^{V_{10\%}} (C_{bo} - C_b) dV}{V_A} \tag{6.2}$$

where V is the effluent liquid volume from the packed bed, $V_{10\%}$ is the effluent liquid volume at 10% breakthrough point, and V_A is the packed bed volume of adsorbent. In our work, for run 1, a DBC at 10% of breakthrough of 2.52 $mg_{HSA}.g_{dry}^{-1}$ and 0.96 $mg_{IgG}.g_{dry}^{-1}$ were achieved, while for run 2 a DBC at 10% of breakthrough of 3.49 $mg_{HSA}.g_{dry}^{-1}$ and 2.03 $mg_{IgG}.g_{dry}^{-1}$ were obtained.

From run 2, binary breakthrough experiment performed in longer timescale, it is possible to refer that there is no roll-up. Roll-up of the concentration curve is caused by the displacement adsorption between the stronger and the weaker adsorbed component, where the stronger component will replace the already adsorbed (weaker) component originating an increase of concentration compared to the feed stream in the breakthrough experiment. The non-existence of

this phenomenon suggests that the two proteins are adsorbed on different sites at the studied binding condition. From Table 2, it is observed that a small eluted fraction amount of IgG in both runs is 35-39% which can be due to protein steric hindrance.

Regarding HSA and IgG desorption in our work, it was obtained a HSA recovery of 80-87% and an IgG recovery of 35-39% for both experiments. To increase the recovery, the pH solution can be increased in order to elute more protein as shown by adsorption isotherms; however, in the current work we use pH 7.0 with 1M NaCl due to limitation of the size-exclusion column used for quantifying the binary mixture.

Aboudzadeh, et al. [22] studied a binary protein adsorption of HSA and ovalbumin (OVA) on a fixed bed packed with 2 g_{dry} of an anion exchanger DEAE Sepharose FF. For a feed concentration of 2 $g.dm^{-3}$ of each protein, they obtained a 10% dynamic binding capacity of 44.9 and 32.4 $mg.g^{-1}$ for HSA and OVA, respectively.

Li and co-workers [16] also performed a binary (BSA and MYO) breakthrough experiment for a longer time scale in a fixed bed column packed with Streamline Direct CST-I in order to study the roll up phenomenon. They concluded that there was no roll up in breakthrough curves for BSA and MYO competitive adsorption, therefore also suggesting that the two proteins are adsorbed on different sites at the studied binding condition. Regarding the adsorption capacity of Streamline CST-I packed in fixed bed, they obtained a dynamic binding capacity at 5% BSA feed concentration of 27.9 $mg_{BSA}.mL^{-1}$ (15.5 $mg_{BSA}.g_{dry}^{-1}$) and a MYO dynamic binding capacity of 5.58 $mg_{MYO}.mL^{-1}$ (3.1 $mg_{MYO}.g_{dry}^{-1}$) for a feed concentration of 1 $g.dm^{-3}$ of BSA and 0.2 $g.dm^{-3}$ of MYO at 7.1 $cm^3.min^{-1}$.

The difference between the adsorption capacities achieved in the current work and the literature is due to the fact that NaCl was added to feed concentration in order to decrease the amount of protein used, allowing this way to reduce the cost of each experiment performed.

6.3.2.2. Column displacement measurements for HSA and IgG competitive adsorption

Two displacement experiments are performed in order to evaluate the competition between Albumin and Immunoglobulin G on MabDirect MM at a binding condition (20 mM citrate buffer pH 5.0 with 0.4M NaCl) which will allow us to observe if the target proteins are adsorbed on different sites.

Table 6.3 shows the operating conditions for both experiments.

Table 6.3 – Operating conditions for displacement experiments: feed concentrations, column diameter and section area, bed height, adsorbent volume and dry weight, particle radios and particle porosity.

Conditions	*Runs 1 – 2*
Q(cm^3.min^{-1})	0.7
d_c(cm)	0.66
A_s(cm^2)	0.3421
H(cm)	6.4
V_{ads}(cm^3)	2.19
w_{dry}(g)	2.7333
$C_{F,HSA}$(g.dm^{-3})	1.0
$C_{F,IgG}$(g.dm^{-3})	0.2
ε_p	0.2374
r_p(cm)	5.15x10^{-3}

First experiment (run 1 – Figure 6.6) is conducted in which HSA with 1 g.dm^{-3} concentration is fed to the fixed bed column until the adsorbent is saturated, then, the column goes through a washing stage in order to remove the unbound HSA protein in the bed voidage and in the adsorbent pores. After adsorption and washing, a feed concentration of 0.2 g.dm^{-3} of IgG is applied to the column to displace the already bound HSA from the adsorbent.

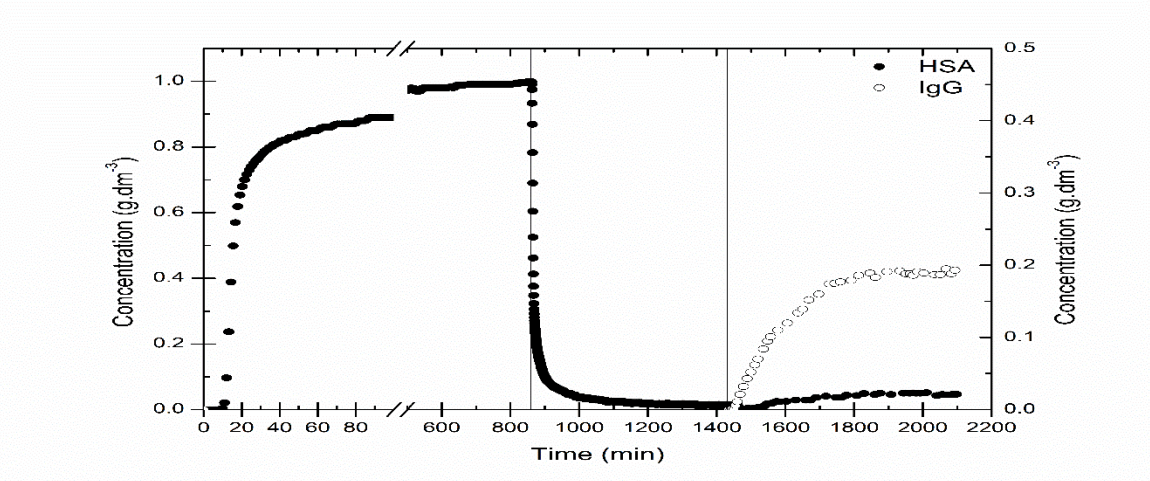

Figure 6.6 – Displacement adsorption experiment (run 1) between HSA and IgG in a fixed bed packed with MabDirect MM. Operating conditions summarized in Table 6.3.

Regarding the second displacement experiment (run 2, Figure 6.7), IgG feed concentration of 0.2 g.dm^{-3} is applied to the column until MabDirect is almost saturated, then the column is washed with binding buffer (20 mM citrate buffer pH 5.0 with 0.4M NaCl) to remove the unbound IgG protein. After the adsorption and washing stage, HSA with 1 g.dm^{-3} is applied to the column for the displacement of the already bound IgG protein.

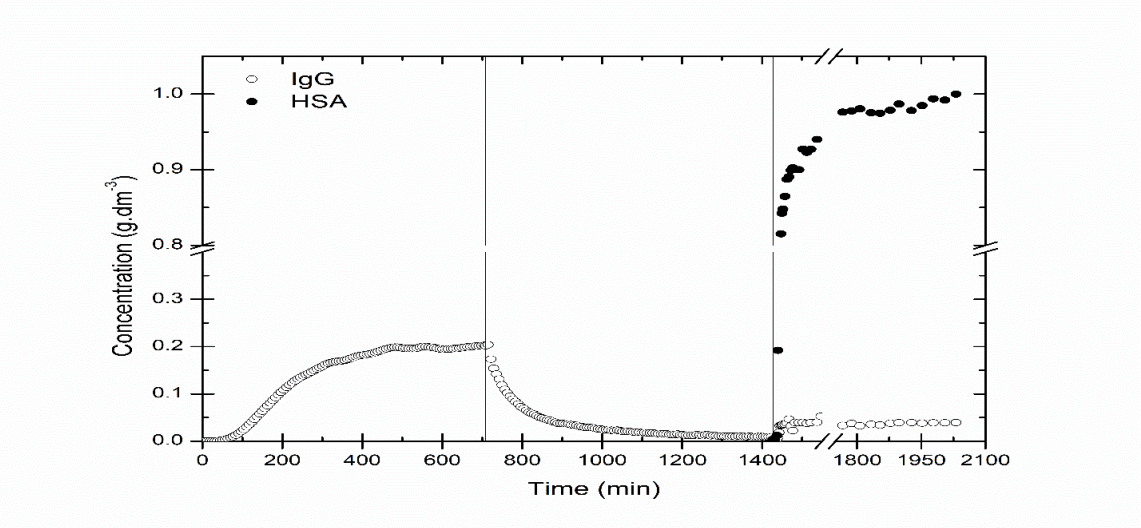

Figure 6.7 – Displacement adsorption experiment (run 2) between IgG and HSA in a fixed bed packed with MabDirect MM. Operating conditions summarized in Table 6.3.

Table 6.4 shows the adsorbed/desorbed protein mass in each stage of both displacement experiments.

Table 6.4 – Adsorbed/desorbed protein mass in each stage of both displacement experiments.

Run	*Protein mass (mg)*	*Adsorption*	*Washing*	*Displacement*	*Washing*	*Elution*
1	HSA	52.09	13.41	6.86	1.81	25.94
	IgG	-	-	22.79	9.62	6.96
2	HSA	-	-	29.98	4.41	21.44
	IgG	31.14	12.94	11.41	1.65	4.78

From run 1, it is obtained a HSA adsorption capacity in adsorption stage of 14.15 $mg.g_{dry}^{-1}$ in agreement to the batch experiments where it was obtained an adsorption capacity of 14.31 $mg.g_{dry}^{-1}$ due to the adsorbent present in column is yet to be saturated. Also for run 1, it is obtained an IgG adsorption capacity of 4.82 $mg.g_{dry}^{-1}$ in the displacement stage; a lower value compared to its batch experiment due to the fact that part of the adsorbent is saturated already with HSA protein. In run 2, it is achieved an IgG adsorption capacity in adsorption stage of 6.66 $mg.g_{dry}^{-1}$ in a good agreement to batch experiments (6.72 $mg.g_{dry}^{-1}$). HSA adsorption capacity, in the displacement stage of run 2, is 9.35 $mg.g_{dry}^{-1}$, a lower capacity compared to the batch experiment since that the adsorbent present is already saturated with IgG protein when a feed concentration of HSA is going through the column.

Figure 6.8 (a, b) represents the HSA and IgG breakthrough curves achieved in both adsorption and displacement stages.

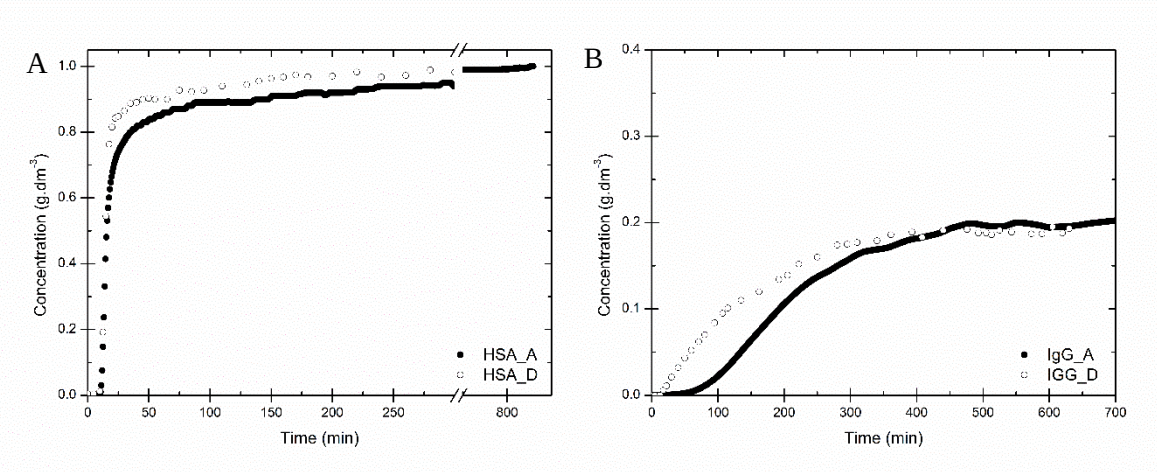

Figure 6.8 – (A) HSA breakthrough curve for both adsorption stage (HSA_A) of run 1 and displacement stage (HSA_D) of run 2. (B) IgG breakthrough curve for both adsorption stage (IgG_A) of run 2 and displacement stage (IgG_D) of run 1.

Li et al. [16] also evaluated the displacement adsorption between BSA and MYO on Streamline Direct CST-I by column displacement experiments at the binding condition 50 mM acetate buffer pH 5.0 where a XK 16/20 column was packed with 10 mL of adsorbent. On their first run, they loaded to the column BSA with 1 $g.dm^{-3}$ until almost saturation then the column is washed with binding buffer. After adsorption and washing stages, MYO with 0.5 $g.dm^{-3}$ is fed to the column to displace the bound BSA. The second run, consisted in feed MYO first and BSA at the displacement stage. They concluded that on first run, MYO cannot displace the bound BSA at the studied pH condition since that the adsorbent possess a higher capacity to BSA, while on the second run BSA slightly displaces the bound MYO; however, the displacement rate is extremely slow as a result of MYO multi-point tightly binding by adsorbent ligand. They concluded by referring that there is a very weak displacement adsorption between BSA and MYO which also suggests that the two proteins are adsorbed on different sites at the binding condition.

In our work, on both runs there is slight displacement of the bound protein on MabDirect MM but at a low displacement rate which also suggests a multi-point binding by the adsorbent ligand. As literature refers, the weak displacement adsorption between the studied proteins suggests that both of them are adsorbed on different sites at the studied binding condition.

6.3.3. Expanded bed breakthrough experiments

First, a single protein (HSA) breakthrough experiment was performed in order to compare data between single and two component breakthrough experiments, such as, adsorption capacity and amount of adsorbed/desorbed protein in each stage; and also to reassure that the EBA system is working properly (constant flowrate throughout all the experiment, monitor pressure during all stages to not damage the EBA column, etc). Then, a second breakthrough experiment with two

component protein (HSA and IgG) was conducted. Column and operating conditions are presented in Table 6.5.

Table 6.5 – Operating conditions for EBA experiments: column diameter, section area, bed height, adsorbent volume and weight, particle radios and particle porosity.

Conditions	*Runs 1-2*
d_c(cm)	1.55
A_s(cm^2)	1.89
H(cm)	5.3
V_{ads}(cm^3)	10
w_{dry}(g)	13.6647
ε_p	0.2374
r_p(cm)	5.15x10^{-3}

Figure 6.9 shows single component expanded bed adsorption curve in a XK 16/20 column packed with MabDirect MM.

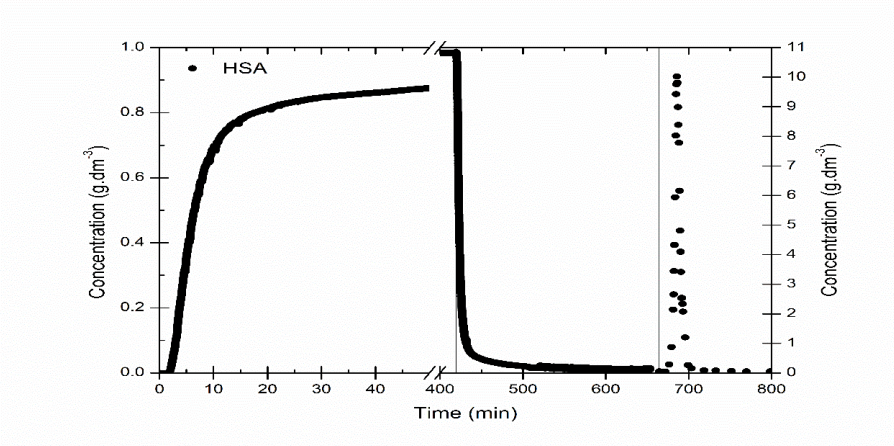

Figure 6.9 – HSA expanded bed breakthrough curve in XK 16/20 column packed with MabDirect MM. Adsorption and washing stages were performed using 20 mM citrate buffer pH 5.0 with 0.4M NaCl, while for elution stage it was used a 20 mM phosphate buffer pH 7.0 with 1M NaCl. Operating conditions in Tables 6.5 and 6.6.

Protein concentration for adsorption and washing stages is represented in left y-axis while for elution stage it is represented on right y-axis. Table 6.6 shows the flowrate and the adsorbed/desorbed protein mass for each stage.

Table 6.6 – Operating conditions: flow rate and adsorbed/desorbed protein mass at 20 °C for expanded bed adsorption breakthrough.

Conditions	**Adsorption**	**Washing**	**Elution**	**Regeneration**	**Stock**	**Difference**
Q(cm^3.min^{-1})	4.5	4.5	1.3	1.3	1.3	-
m_{HSA} (mg)	232.8	40.7	126.0	44.1	2.1	9

At the binding stage with 20 mM citrate buffer pH 5.0 with 0.4M NaCl for a HSA feed concentration of 1.05 g.dm^{-3}, MabDirect MM can capture HSA by expanded bed. It was achieved an adsorption capacity of 14.1 mg.g_{dry}^{-1} which is in good agreement with single HSA protein batch experiment [1] and also from fixed bed experiment in the current work.

Finally, Figure 6.10 presents an EBA breakthrough experiment for a feed concentration of 1.04 g.dm^{-3} of HSA and 0.22 g.dm^{-3} of IgG in a citrate buffer pH 5.0 with 0.4M NaCl at 20 °C.

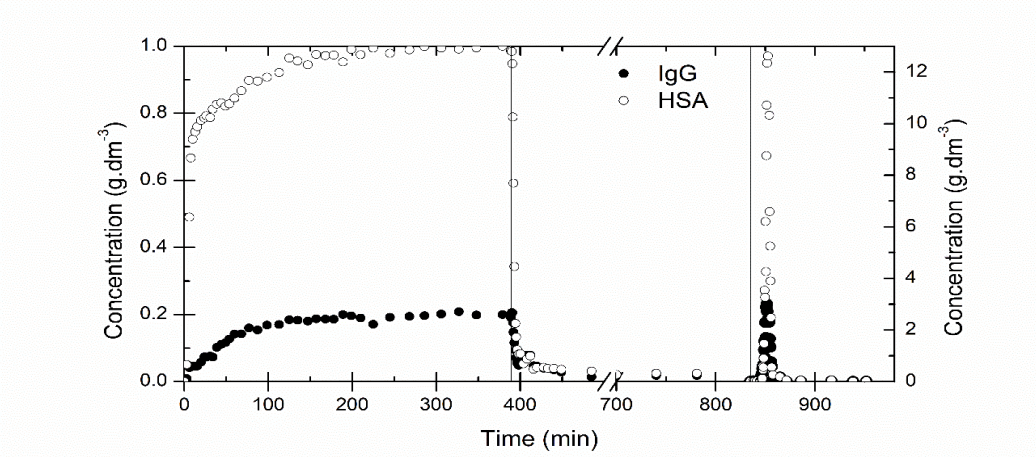

Figure 6.10 – Binary mixture expanded bed breakthrough curve in XK 16/20 column packed with MabDirect MM. Adsorption and washing stages were performed using 20 mM citrate buffer pH 5.0 with 0.4M NaCl, while for elution stage it was used a 20 mM phosphate buffer pH 7.0 with 1M NaCl. Operating conditions in Tables 6.5 and 6.7.

Table 6.7 shows the flowrate and the adsorbed/desorbed protein mass for each stage. Regeneration stage is not displayed when performing binary mixture experiments since the size-exclusion column used can not quantify the amount of released protein due to pH limitation. In order to better quantify the protein adsorbed/desorbed mass, it is recommended to have a SEC column that can withstand higher solution pH and to increase the elution buffer pH in the range of the protein stability.

Table 6.7 – Operating conditions: flow rate and adsorbed/desorbed protein mass for each target protein at 20 °C for expanded bed binary mixture adsorption breakthrough.

Conditions	Adsorption	Washing	Elution
Q(cm^3.min^{-1})	5	5	1.3
m_{HSA}(mg)	210.4	29.7	111.5
m_{IgG}(mg)	101.7	16.2	33.5

At the binding stage, the studied adsorbent can efficiently capture both HSA and IgG protein from the feed solution by expanded bed. It was achieved an adsorption capacity of 14.2 and 6.3 mg.g_{dry}^{-1} for both HSA and IgG, respectively. The achieved adsorption capacity is in good agreement with separate single protein adsorption isotherms by batch experiments. Also, the achieved results are close to the experimental result measured in a fixed bed adsorption process, which suggests that two-component protein competitive adsorption behaviours in a stable

expanded bed are comparable to that in fixed bed. Using Equation 6.2, a dynamic binding capacity at 10% of breakthrough of 1.96 $mg_{HSA}.g_{dry}^{-1}$ and 0.90 $mg_{IgG}.g_{dry}^{-1}$ was calculated. Regarding HSA and IgG desorption, it was obtained a HSA recovery of 62% and an IgG recovery of 39%.

Li et al. [16] conducted an expanded bed adsorption experiment where a feed solution mixture of 1 $g.dm^{-3}$ of BSA and 0.2 $g.dm^{-3}$ MYO is applied at 517 $cm.h^{-1}$ flowrate in a Streamline 50 column packed with 300 mL of Streamline Direct CST-I with an expansion degree about twice settled bed height. They obtained a dynamic binding capacity at 5% BSA feed concentration of 28.5 $mg_{BSA}.mL_{settlebed}^{-1}$ (15.8 $mg_{BSA}.g_{dry}^{-1}$) and a MYO dynamic binding capacity of 5.65 $mg_{MYO}.mL_{settlebed}^{-1}$ (3.14 $mg_{MYO}.g_{dry}^{-1}$). They also refer that the binding capacity of both proteins are close to the experimental results measured in a fixed bed adsorption process and therefore, the two component protein competitive adsorption behaviours in a stable expanded bed are comparable to that in a fixed bed.

6.4. Conclusions

Competitive adsorption between HSA and IgG on MabDirect MM was studied by batch, fixed bed and expanded bed adsorption experiments. It was found that increasing the IgG concentration present in the solution the HSA adsorption capacity decreases progressively as a result of IgG competitive adsorption with HSA on MabDirect MM by batch experiment.

Fixed bed adsorption experiments with binary mixture of HSA and IgG were performed at two distinctive flowrates. There is no roll up in the adsorption breakthrough curves even when it was increased the experiment timescale caused by displacement adsorption between these two proteins which suggests that they are adsorbed on different sites. Displacement experiments were carried out and it showed that some amount of protein is released when other protein is being fed to the column.

Expanded bed breakthrough experiment with binary mixture of HSA and IgG was carried out. It shows an adsorption capacity (14.2 and 6.3 $mg.g_{dry}^{-1}$ for both HSA and IgG, respectively) in good agreement with separate single protein adsorption isotherms by batch experiments. Also, the achieved results are close to the experimental result measured in a fixed bed adsorption process, which suggests that two-component protein competitive adsorption behaviours in a stable expanded bed are comparable to that in fixed bed.

6.5. Nomenclature

A_S	–	Column section area
C_b	–	Protein concentration in the bulk phase
C_F	–	Protein concentration in the feed solution
C_p	–	Protein concentration in the particle pore
d_c	–	Column diameter
H	–	Bed height
K_L	–	Langmuir adsorption constant
$m_{protein}$	–	Protein mass adsorbed/desorbed
$q_{10\%}$	–	Dynamic binding capacity at 10% breakthrough point
q	–	Adsorbed concentration
Q	–	Flow rate
r_p	–	Particle radius
V	–	Effluent liquid volume from the fixed bed
$V_{10\%}$	–	Effluent liquid volume at 10% breakthrough point
V_a	–	Packed bed volume of adsorbent
V_L	–	Volume of protein solution
w	–	Adsorbent mass

Greek letters

ε_p	–	Particle (solid) porosity

Acronyms

BSA	–	Bovine Serum Albumin
EBA	–	Expanded bed adsorption
HPLC	–	High performance liquid chromatography
HSA	–	Human Serum Albumin
hIgG	–	Immunoglobulin G from Human serum
IgG	–	Immunoglobulin G
MM	–	Mixed-mode
MMC	–	Mixed-mode Chromatography
MYO	–	Myoglobin
OVA	–	Ovalbumin
SDS-Page	–	Sodium dodecyl sulfate - Polyacrylamide gel electrophoresis
SEC	–	Size exclusion chromatography

6.6. References

[1] P.F. Gomes, J.M. Loureiro, A.E. Rodrigues, Adsorption of Human Serum Albumin (HSA) on a mixed-mode adsorbent: equilibrium and kinetics, Adsorption, 23 (2017) 491-505.

[2] P.F. Gomes, J.M. Loureiro, A.E. Rodrigues, Adsorption equilibrium and kinetics of Immunoglobulin G on a mixed-mode adsorbent in batch and packed bed configuration, Journal of Chromatography A, 1524 (2017) 143-152.

[3] J. Schaller, S. Gerber, U. Kämpfer, S. Lejon, C. Trachsel, Human Blood Plasma Proteins: Structure and Function, John Wiley & Sons, Ltd, 2008.

[4] J.M. Peula, R. Hidalgo-Alvarez, F.J. De Las Nieves, Coadsorption of IgG and BSA onto sulfonated polystyrene latex: I. Sequential and competitive coadsorption isotherms, Journal of Biomaterials Science, Polymer Edition, 7 (1996) 231-240.

[5] R.K. Lewus, G. Carta, Binary protein adsorption on gel-composite ion-exchange media, American Institute of Chemical Engineers Journal, 45 (1999) 512-522.

[6] X. Xu, A.M. Lenhoff, Binary adsorption of globular proteins on ion-exchange media, Journal of Chromatography A, 1216 (2009) 6177-6195.

[7] J. Yan, Q.L. Zhang, D.Q. Lin, S.J. Yao, Protein adsorption behavior and immunoglobulin separation with a mixed-mode resin based on p-aminohippuric acid, Journal of Separation Science, 37 (2014) 2474-2480.

[8] J. Yan, Q.-L. Zhang, D.-Q. Lin, S.-J. Yao, Coadsorption of Human Immunoglobulin G and Bovine Serum Albumin on a p-Aminohippuric Acid Based Mixed-Mode Resin, Journal of Chemical & Engineering Data, 61 (2016) 151-159.

[9] P. Leblebici, M.E. Leblebici, F. Ferreira-da-Silva, A.E. Rodrigues, L.S. Pais, Separation of human immunoglobulin G subclasses on a protein A monolith column, Journal of Chromatography B, 962 (2014) 89-93.

[10] E. Arévalo, M. Rendueles, A. Fernández, M. Díaz, Equilibrium and simulation of the operation for the adsorption of albumin proteins in an iminodiacetic-Cu bounded ion exchange resin (IMAC), Separation and Purification Technology, 18 (2000) 217-225.

[11] M.d.A. Lima, M.d.F.M.d. Freitas, L.R.B. Gonçalves, I.J.d. Silva Junior, Recovery and purification of a Kluyvermyces lactis β-galactosidase by Mixed Mode Chromatography, Journal of Chromatography B, 1015 (2016) 181-191.

[12] W. Kelly, P. Garcia, S. McDermott, P. Mullen, G. Kamguia, G. Jones, A. Ubiera, K. Göklen, Experimental characterization of next-generation expanded-bed adsorbents for capture of a recombinant protein expressed in high-cell-density yeast fermentation, Biotechnology and Applied Biochemistry, 60 (2013) 510-520.

[13] W. Kelly, G. Kamguia, P. Mullen, A. Ubiera, K. Göklen, Z. Huang, G. Jones, Using a two species competitive binding model to predict expanded bed breakthrough of a recombinant protein expressed in a high cell density fermentation, Biotechnology and Bioprocess Engineering, 18 (2013) 546-559.

[14] V. Yelemane, M. Kangwa, M. Fernández-Lahore, High-Throughput Screening of Cell Repellent Substrate Chemistry for Application in Expanded Bed Adsorption Chromatography,

in: P. B. D, S.N. Gummadi, P.V. Vadlani (Eds.) Biotechnology and Biochemical Engineering: Select Proceedings of ICACE 2015, Singapore, 2016, 145-152.

[15] P. Li, P.F. Gomes, J.M. Loureiro, A.E. Rodrigues, Proteins Separation and Purification by Expanded Bed Adsorption and Simulated Moving Bed Technology, in: G. Subramanian (Ed.) Continuous Processing in Pharmaceutical Manufacturing, John Wiley & Sons, Inc., 2014.

[16] P. Li, G. Xiu, V.G. Mata, C.A. Grande, A.E. Rodrigues, Expanded bed adsorption/desorption of proteins with Streamline Direct CST I adsorbent, Biotechnology and Bioengineering, 94 (2006) 1155-1163.

[17] P. den-Boer, M. Doeven, J. van der Merwe, A. Lihme, M. Bendix-Hansen, I. Vaarst, M. Pontoppidan, F. Linz, Rhobust EBA Processing high-cell density mammalian cell cultures: process parameters and performance. (2013)

[18] H.-F. Xia, D.-Q. Lin, S.-J. Yao, Evaluation of new high-density ion exchange adsorbents for expanded bed adsorption chromatography, Journal of Chromatography A, 1145 (2007) 58-66.

[19] R.R. Walters, J.F. Graham, R.M. Moore, D.J. Anderson, Protein diffusion coefficient measurements by laminar flow analysis: Method and applications, Analytical Biochemistry, 140 (1984) 190-195.

[20] P.F. Gomes, J.M. Loureiro, A.E. Rodrigues, Expanded bed adsorption of albumin and immunoglobulin G from human serum onto a cation exchanger mixed mode adsorbent, Adsorption, 24 (2018) 293-307.

[21] M. Rendueles de la Vega, C. Chenou, J.M. Loureiro, A.E. Rodrigues, Mass transfer mechanisms in Hyper D media for chromatographic protein separation, Biochemical Engineering Journal, 1 (1998) 11-23.

[22] M.R. Aboudzadeh, N. Aboudzadeh, Z. Jiawen, W. Bin, Binary protein adsorption to DEAE sepharose FF, Korean Journal of Chemical Engineering, 24 (2007) 641-647.

Chapter 7: Conclusions and future work

"We must use time creatively."

- Dr. Martin Luther King, Jr.

This final chapter presents an overall conclusion of the work done, future goals and objectives that should be interesting to study.

7.1. Conclusions

MabDirect MM, a new second generation cation exchanger mixed mode adsorbent proved that can capture blood proteins (Human Serum Albumin and Immunoglobulin G) effectively from high ionic strength solution, as opposed to the ion exchanger sorbents, such as Streamline SP and DEAE.

The maximum adsorption of HSA and IgG on the MabDirect MM adsorbent was observed when it is diluted in a 20 mM citrate buffer pH 5.0, without the presence of salt, i.e. it was observed a maximum adsorption of the target protein near its isoelectric point, either for HSA and IgG (36.0 ± 3.5 and 149.7 ± 7.1 $mg \cdot g_{adsorbent,dry}^{-1}$, respectively). It was also observed that increasing pH would negatively affect protein adsorption; for pH of 7.0 it was observed a decrease of adsorption capacity of HSA to 8.6 ± 2.1 $mg \cdot g_{dry}^{-1}$ (76% of lost capacity) while for IgG it was noticed a decrease to 90.4 ± 9.1 $mg \cdot g_{dry}^{-1}$ (40% of lost capacity), indicating this way that HSA adsorption is more sensitive to pH variations than IgG.

Regarding the ionic strength, increasing salt concentration (up to 1M NaCl for HSA and 0.4M NaCl for IgG) in a pH 5.0 buffer solution would decrease the adsorption capacity to 13.4 ± 2.5 and 16.3 ± 8.0 $mg \cdot g_{dry}^{-1}$ (63 and 89% of lost capacity) for HSA and IgG, respectively. Since it was added less salt to IgG study and it is observed a larger percentage of lost capacity, it is safe to say that IgG is more sensitive to NaCl presence in solution than HSA, for the studied pH. Langmuir model is used and fitted well in all studied conditions for both proteins.

In the adsorption kinetics study, the largest effective pore diffusion coefficient determined by PDM model was obtained for a 20 mM citrate buffer pH 5.0 without salt for both target proteins (2.2 and 15.4 $x10^{-6}$ $cm^2.min^{-1}$, for HSA and IgG, respectively).

The effect of feed flowrate, feed concentration and salt concentration on fixed bed and expanded bed adsorption was addressed. Fixed bed adsorption and Expanded bed adsorption experiments were simulated with a general rate model including axial dispersion, film mass transfer and intraparticle mass transfer and fitted well in all studied conditions. Also, it is obtained an adsorbent uptake capacity in agreement with the adsorption equilibrium isotherm from batch experiments.

Two fixed bed breakthrough experiments were conducted and for a feed concentration of 0.9 g/L of HSA dissolved in a pH 5.0 citrate buffer with two different NaCl concentrations (without and with 0.5M), it were obtained a DBC at 10% breakthrough point of 14.51 and 2.46 $mg.g_{dry}^{-1}$ representing near 50% and 20% of saturation capacity, respectively. It was possible to estimate a global mass transfer coefficient fitting the experimental data. While for a feed concentration of 0.5 g/L of IgG dissolved in a pH 5.0 citrate buffer with 0.4M NaCl, it was

obtained a dynamic binding capacity at 10% of breakthrough of 5.3 $mg.g^{-1}$, representing 62% of the saturation capacity.

In order to estimate the liquid axial dispersion coefficient, residence time distribution experiments in three different expanded bed columns (Streamline 50, Omnifit 66/20 and XK 16/20) were performed. The experimental results were compared to a simulation model which proved to be able to represent them with reasonable accuracy.

HSA adsorption breakthrough experiments were performed in a Streamline 50 expanded bed column; for each run it were obtained DBC at 10% of breakthrough of 8.9, 9.7, 7.5 and 7.0 $mg \cdot g_{dry}^{-1}$ corresponding to 41, 39, 38 and 30% of the saturation capacity for runs 1–4, respectively. The mathematical simulation model fitted well with the breakthrough experiments. EBA experiments also show that increasing pH and NaCl concentration in the elution buffer along with a decrease in flowrate not only will reduce the desorbed protein in the subsequent regeneration stage but also concentrate the target protein in the elution stage.

Human IgG adsorption breakthroughs were performed in an Omnifit 66/20 and XK 16/20 expanded bed column. In an Omnifit 66/20 column, for a feed concentration of 0.53 $g \cdot dm^{-3}$ of IgG in 20 mM citrate buffer pH 5.0 with 0.4M NaCl, at 2.2 $cm^3 \cdot min^{-1}$, it was obtained a DBC at 10% of breakthrough of 3.3 $mg \cdot g_{dry}^{-1}$ representing 22% of the saturation capacity. While for the breakthrough experiment conducted in an XK 16/20 column, for a feed concentration of 0.11 $g \cdot dm^{-3}$ of IgG in 20 mM citrate buffer pH 5.0 with 0.4M NaCl, at 6 $cm^3 \cdot min^{-1}$, it was obtained a DBC at 10% of breakthrough of 2.7 $mg \cdot g_{dry}^{-1}$, representing 34% of the saturation capacity. Regarding IgG desorption, a protein recovery of 80-89% was obtained.

Competitive adsorption between HSA and IgG on MabDirect MM was studied by batch, fixed bed and expanded bed adsorption experiments. Competitive adsorption isotherm was conducted by batch experiments at the binding condition of pH 5.0 without salt addition where it was found that increasing the IgG concentration present in the solution, the HSA adsorption capacity decreases progressively as a result of IgG competitive adsorption with HSA on MabDirect MM.

Fixed bed adsorption experiments with binary mixture of HSA and IgG were performed at two different flowrates. There is no roll up in the adsorption breakthrough curves, even when it was increased the experiment timescale, caused by displacement adsorption between these two proteins, which suggests that they are adsorbed on different sites at the binding condition, 20 mM citrate buffer pH 5.0 with 0.4M NaCl. Displacement experiments were carried out and showed that some amount of protein is released when other protein is being fed to the column.

Expanded bed breakthrough experiment with binary mixture of HSA and IgG was carried out. It shows an adsorption capacity (14.2 and 6.3 $mg.g_{dry}^{-1}$ for both HSA and IgG, respectively)

in good agreement with separate single protein adsorption isotherms by batch experiments. Also, the achieved results are close to the experimental result measured in a fixed bed adsorption process, which suggests that two-component protein competitive adsorption behaviour in a stable expanded bed is comparable to that in fixed bed.

Results show that expanded bed adsorption with a mixed-mode adsorbent can capture blood proteins with high binding capacity; this could possibly be used for the purification of blood plasma in transfusion blood medical centres.

7.2. Future work

Science is an ongoing investigation and therefore there are some new perspectives of research that can be explored. The following sub sections present some ideas that can be used for the next possible steps on this research ladder.

7.2.1. Adsorbents

Although mixed mode adsorbent appears as a possible alternative to the affinity adsorbents used for antibodies purification, it should be interesting and, as far as the author knowledge, a new approach, the study of second generation affinity chromatography adsorbents (e.g. MabDirect Protein A) using expanded bed adsorption technology.

Also, studying the target protein in an even higher ionic strength solution. According to some researchers, “salt-tolerance” is a term used for mixed-mode adsorbents that can capture the target protein at high ionic strength. For IgG solution up to 0.4M NaCl or HSA up to 1M NaCl it was only observed a decrease in adsorption capacity. Arguably, it was not used sufficient NaCl concentration to check if the present studied adsorbent has “salt tolerance” capability and for this reason, higher concentration can be studied.

Recently, some studies appear in literature where modifications made to the adsorbent ligand structure can provide better adsorption capacity. It would be interesting to verify if it would be possible to increase the adsorption capacity of older adsorbent. Also, to avoid the dependency of very few adsorbent suppliers, modifications should be introduced on “conventional adsorbents” for their use in EBA systems, e.g., introducing a densifier in order to use these first generation adsorbents at higher flow rates.

7.2.2. Source material

Using source material such as Human serum to directly capture the target protein instead of pure protein in order to better show the practical application. Also, it can be used Cell broth to capture the desired recombinant protein (e.g. Albumin).

7.2.3. Adsorption technique

Sodium chloride is not the only salt used on proteins separation. Influence of pure and mixed salts (such as ammonium sulfate, ammonium chloride, sodium sulfate with sodium chloride) in protein chromatography is a compelling new area where new studies of mathematical modelling of this influence are starting to surface on the scientific community.

Simulated moving bed (SMB) chromatography is a continuous process that can replace the discontinuous elution chromatography. By countercurrent contact between the fluid and the stationary phase, there is a maximisation of the mass transfer leading to a reduced consumption of both phases. SMB technology applied to the separation and purification of biomolecules (proteins, antibodies, nucleosides, etc.) is an area in development. Literature indicates that, based on theoretical analysis, salt gradient ion-exchange SMB chromatography can be performed effectively for the separation and purification of proteins suggesting that further experimental validation is still necessary.

New hybridisation between Expanded Bed Adsorption and Simulated Moving Bed (EBA-SMB) has recently been applied on commercial scale. Mathematical model development and the study of experimental limitations (such as cell adhesion) should be an interesting field of study.

Annex A: Data Acquisition Hardware

"Almost always, the creative dedicated minority has made the world better."

- Dr. Martin Luther King, Jr.

Not always the day-by-day equipment works in our favor. At any time, the equipment can break and the maintenance becomes expensive. During the 4 years, the connection between the Gilson HPLC system and a personal computer damaged and the computer which run 3.1 windows software with a 50 MB 4.5'' hard drive broke. Due to high costs of maintenance, a creative Arduino system was used with the purpose of acquiring the signal from Gilson HPLC system. Also, with time an ADS converter was introduced to the Arduino system in order to improve the maximum limit of bit resolution. This annex is introduced with the solo purpose of helping those who need a creative method of data acquisition and are not willing to pay 4 000 € for a new one.

A.1. General

High Performance Liquid Chromatography (HPLC) is a separation technique in which high pressure is used as driving force to get the a sample through a packed column for the purpose of identify or quantify the components.

In this work, it was used a Gilson HPLC system with a 305 model pump, an 805 manometric module and a 117 Gilson UV model detector. The UV detector is connected to a personal computer with data acquisition software in order to capture the signal. However, not always the equipment works in our favor. Due to high cost maintenance and repair of the connection between the HPLC system and the old computer, Arduino appeared as a creative low-cost alternative.

A.2. Data Acquisition Hardware – Arduino

Arduino is an open-source electronic platform with easy-to-use hardware and software. Arduino board can read input signals and turn it into useful data. In order to achieved this goal, one must use the Arduino programming language and the Arduino software (IDE), based on processing. Arduino was used due to being a low cost, and cross-platform data acquisition system, using a clear and simple programming environment and also due to open source and extensible software and hardware.

In our work the goal was simple, to connect the Arduino to the Gilson UV detector and convert the analog signal into digital. The following sections will demonstrate the software and hardware modifications so that the HPLC signal would be registered in a csv/txt file stored on a SD card for later processing.

A.3. Arduino – Code

Figure A.1 shows the code that must be introduced in Arduino hardware for the capture of HPLC signal.

```
#include "SPI.h"
#include "Adafruit_GFX.h"
#include "Adafruit_ILI9341.h"
#include "HX711.h"
#include <Wire.h>
#include <SPI.h>
#include <SD.h>
#include <inttypes.h>
#define TFT_DC 9
#define TFT_CS 10

Adafruit_ILI9341 tft = Adafruit_ILI9341 (TFT_CS, TFT_DC);

int16_t i = 0, gridx = 0, pix = 20, adc = 0, minutes = 0, height = 0;
float seconds = 0.0, minn = 0.0, gridxfloat = 0.0;
int32_t adc0, adc1, adc2, signalmax=0;

HX711 scale(A2, A1);

void setup() {
 signalmax=10000;
 signalmax=signalmax*1;

 minutes=15;
 pinMode(A0,OUTPUT);// for the UNO_SHIELD_1IN1
 digitalWrite(A0,HIGH);
 SD.begin(4);

 tft.begin();
 tft.setRotation(1);
 tft.fillScreen(ILI9341_GREEN);
 tft.fillScreen(ILI9341_WHITE);
 tft.setCursor(0, 1);
 tft.setTextColor(ILI9341_BLACK);  tft.setTextSize(1);
 tft.println("Iteration   Time (s)  Time (min)  adc0     pix  v2");
 //tft.println("Iteration   Time (s)  Time (h)  Abs (AU)  Signal (mV)");

adc1 = scale.read(); //raw reading from the ADC which will serve as reference for setting values close to
zero
}
void loop(void) {

String dataString = "";
```

```
adc2 = scale.read();
adc0 = adc2 - adc1;  //raw reading from the ADC

pix = (int) (235-((adc0)/(signalmax/240)));

gridxfloat = seconds * (319/(minutes*60.0));
gridx= (int) gridxfloat;

tft.drawPixel(gridx,pix,ILI9341_BLACK);

tft.fillRect(0,  10, 319, 8,ILI9341_YELLOW);
tft.setCursor(2, 10); tft.println(i);

seconds=millis()/1000.0;
tft.setCursor(80, 10); tft.println(seconds);

minn=seconds/60.0;

tft.setCursor(150, 10); tft.println(minn);
tft.setCursor(200, 10); tft.println(adc0);

tft.setCursor(260, 10); tft.println(pix);

dataString = String(seconds) + "," + String(adc2) + "," + String(adc0);

File dataFile = SD.open("peter.txt", FILE_WRITE);
dataFile.println(dataString);
dataFile.close();

i=i+1;
}
```

Figure A.1 – Software code introduced in Arduino Uno.

A.4 Schematics

Figure A.2 represents the hardware connections between Arduino Uno (left blue) and the 2.4'' TFT LCD Shield (right orange) with a later improvement of the Arduino system, 16 Bit ADS converter (blue down). Green, red and blue lines represent physical connections cables.

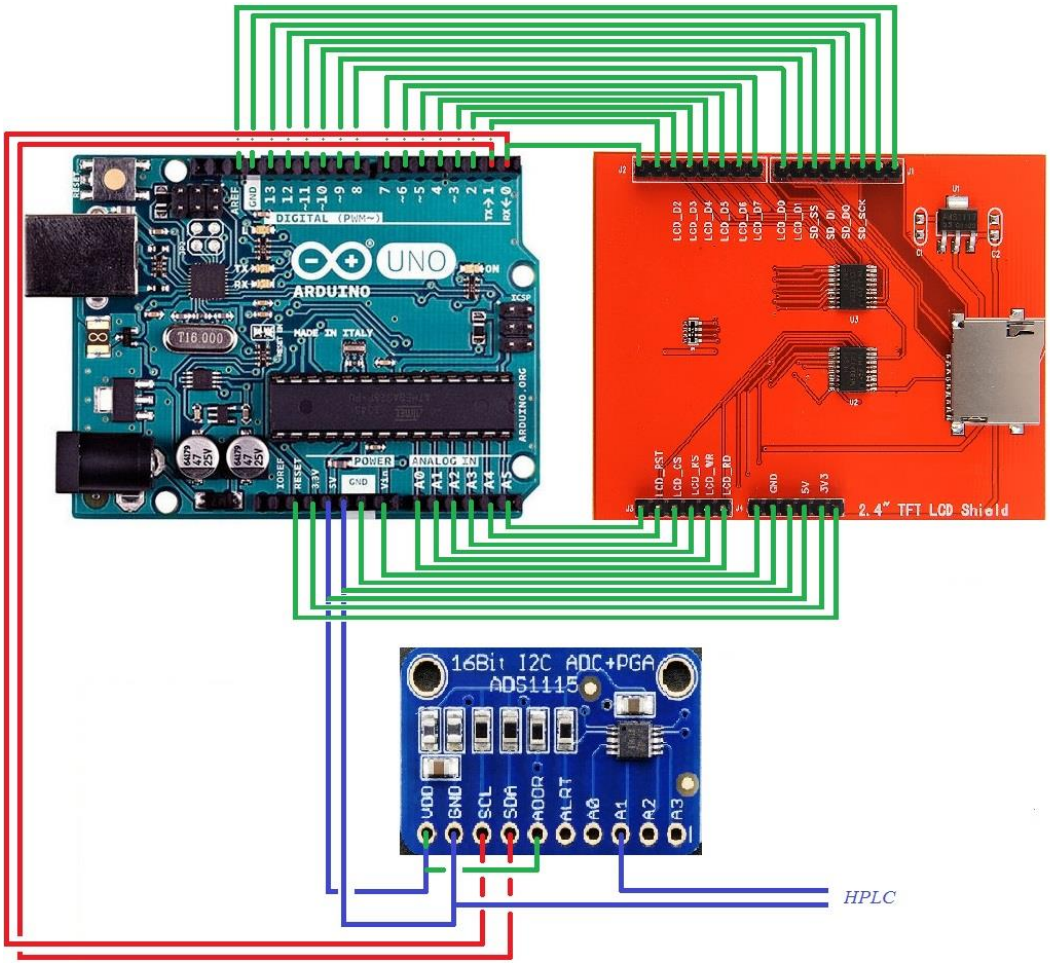

Figure A.2 – Connection between Arduino Uno, 2.4'' TFT LCD Shield and 16 Bit ADS converter.

A.4. Nomenclature

ADC	–	Analog to digital converter
$HPLC$	–	High Performance Liquid Chromatography
LCD	–	Liquid crystal display
TFT	–	Thin film transistor

A.5. Acknowledgement

The author would like to thank friend and colleague Ph.D. student *Elson Dinis Gomes* for the essential help to make this improvement.

A.6. References

Blum, J. (2013) Exploring Arduino: Tools and Techniques for Engineering Wizardry, John Wiley & Sons, Inc.